Evidence-Based Complementary and Alternative Medicine

Antitoxic Effects of Natural Antioxidant Therapies for Novel Therapeutics

Lead Guest Editor: Salah M. El Sayed
Guest Editors: Rabab M. Abou El-Magd

Antitoxic Effects of Natural Antioxidant Therapies for Novel Therapeutics

Evidence-Based Complementary and Alternative Medicine

Antitoxic Effects of Natural Antioxidant Therapies for Novel Therapeutics

Lead Guest Editor: Salah M. El Sayed
Guest Editors: Rabab M. Abou El-Magd

Contents

GC-MS Profiling, *In Vitro* Antioxidant, Antimicrobial, and *In Silico* NADPH Oxidase Inhibition Studies of Essential Oil of *Juniperus thurifera* Bark

Soufyane Lafraxo, Abdelfattah El Moussaoui, Yousef A Bin Jardan, Azeddin El Barnossi, Mohamed Chebaibi, Soukayna Baammi, Aziz Ait Akka, Khalid Chebbac, Mohamed Akhazzane, Tarik Chelouati, Hiba-Allah Nafidi, Khallouki Farid, Mohammed Bourhia, and Amina Bari

Research Article (13 pages), Article ID 6305672, Volume 2022 (2022)

Hindawi
Evidence-Based Complementary and Alternative Medicine
Volume 2023, Article ID 8535139, 12 pages
https://doi.org/10.1155/2023/8535139

Research Article

Phenolic Profile, Antioxidant, Antidiabetic, and Antigout Potential of Stem Extracts of Four Sweet Cherry Cultivars

Younes Aqil,[1] Souad El Hajjaji,[1] Walid Belmaghraoui,[1] Yassine Mourabit,[1] Douae Taha,[1] Mohammed Merae Alshahrani,[2] Ahmed Abdullah Al Awadh,[2] Abdelhakim Bouyahya,[3] Issam Gaamoussi,[4] and Ilhame Bourais[3]

[1]*Laboratory of Spectroscopy, Molecular Modelling Materials, Nanomaterials, Water and Environment Faculty of Sciences, Mohammed V University in Rabat, Rabat, Morocco*
[2]*Department of Clinical Laboratory Sciences, Faculty of Applied Medical Sciences, Najran University, Najran 61441, Saudi Arabia*
[3]*Laboratory of Human Pathologies Biology, Department of Biology, Faculty of Sciences, Mohammed V University in Rabat, Rabat, Morocco*
[4]*Laboratory of Research and Development, AROMI Sarl, 197 BD, Casablanca, Morocco*

Correspondence should be addressed to Souad El Hajjaji; souad.elhajjaji@ufsr.um5.ac.ma, Abdelhakim Bouyahya; a.bouyahya@um5r.ac.ma, and Ilhame Bourais; i.bourais@um5r.ac.ma

Received 6 September 2022; Revised 26 December 2022; Accepted 5 April 2023; Published 5 May 2023

Academic Editor: Salah M El Sayed

In order to highlight the activities of bioactive compounds present in the stem of sweet cherries, four different cultivars (*Van*, *Burlat*, *Napoleon*, and *Cœur pigeon*) were collected in Sefrou city in Morocco and were studied. Several assays were performed for this purpose, such as the quantification of phenolic compounds (TPC, TFC, and CTC) and the evaluation of the antioxidant activity using DPPH, ABTS, and FRAP assays. The phenolic profile of each extract was characterized by UHPLC-DAD/MS analysis. The antidiabetic (α-amylase inhibition) and antigout (xanthine oxidase inhibition) activities were also investigated. The results showed high levels of phenolic compounds, with the values of 340 ± 12.06, 244 ± 10.20, 232 ± 5.07, and 19 ± 3.10 mg gallic acid equivalent/g extract for the cultivars *Napoleon*, *Coeur de pigeon*, Van, and *Burlat*, respectively. According to the same order, the flavonoids showed amounts of 34.31 ± 2.08, 23.75 ± 1.02, 24.37 ± 1.20, and 23.31 ± 0.90 mg (rutin equivalent) RE/g extract. These values were correlated with the results of the antioxidant assays, where the *Napoleon* cultivar proved to be the most potent using the DPPH ($IC_{50} = 2.51\ \mu g/mL$) and ABTS ($IC_{50} = 55.38\ \mu g/mL$) assays. The phenolic profile of each extract resulted in the identification of twenty-two compounds belonging to five distinct groups. The major phenolic compounds identified were sakuranetin and dihydrowgonin with their glucosides. Antidiabetic activity assays showed that only stem extracts from *Burlat* and *Napoleon* cultivars were able to inhibit the α-amylase enzyme with values of $85.57 \pm 1.09\%$ and $68.01 \pm 3.52\%$, respectively. All stem extracts proved their ability to inhibit the xanthine oxidase enzyme which is directly linked to the gout disease, with a high value for *Van* cultivar ($40.63 \pm 2.37\%$). These new findings could provide new opportunities for the valorization of cherry stems for the pharmaceutical application of their active phytochemicals.

1. Introduction

In recent years, many research studies proved the importance of fruits and vegetables in promoting human health for their unique beneficial nutrients and antioxidants, encouraging their increasing consumption both nationally and internationally [1–3]. Cherries, from the Rosaceae family, Prunodea subfamily, are one of the most commercially important species in the world and the most consumed. *Prunus avium* L. (sweet cherry) is geographically distributed worldwide, with greatest predominance in temperate climates, encompassing much of Europe (Mediterranean and

Central), the Near and Far East, the southern Australia and New Zealand, North Africa, and the temperate zones of the American continent [4].

In Morocco, sweet cherry was introduced before 1920 by the French protectorate, and it was extended to the regions of the Moroccan Middle Atlas. Actually, the cultivation covers 4000 ha of the area with the production of about 14,100 tons each year, and the most popular sweet cherry cultivars are "*Bigarreau Van*," "*Bigarreau Burlat*," "*Bigarreau Napoleon*," and "*Cœur pigeon*," [5, 6].

Sweet cherry fruits are one of the most studied by the scientific community for their nutritional and bioactive properties. Many beneficial effects have been recognized, especially the control of diabetes, the prevention of cardiovascular disease, cancer, gout, and other diseases related to oxidative stress [7].

It is noted that little research was conducted on sweet cherry stems, as well as their chemical composition and bioactive properties [5, 7–14].

Sweet cherries are also renowned for their use by food industries for the manufacture of jams, jellies, compotes, and several types of beverages, subsequently generating important waste in the form of stems or kernels. In this context, this study aims to investigate the total content of phenolic compounds, flavonoids, and tannins of cherry stem extracts from different cultivars, as well as their antioxidant properties using DPPH, ABTS, and FRAP methods, with the characterization of the phenolic compounds present in the extracts by the UHPLC-DAD/MS technique [12]. Furthermore, the antidiabetic and antigout activities were evaluated with a comparative approach of four cultivars. Sweet cherry cultivars have not been analyzed in this sense until now.

2. Materials and Methods

2.1. Raw Materials. The harvest area is located in the Middle Atlas region, specifically Laanoceur (Sefrou). The "Laanoceur" locality is known for its continental climate with cold winters and hot summers, with annual average rainfall varying between 400 and 600 mm and an annual average temperature of 10.6°C [5].

Fruit from four sweet cherry (*Prunus avium*) cultivars (*Burlat*, *Napoleon*, *Coeur de pigeon*, and *Van*) were collected at the optimum fruiting period, based on fruit maturity and bright red color (Figure 1). The stems were removed from the cherry fruits, washed with distilled water, and dried in the shade at room temperature. Then, these stems were ground into a fine powder and stored in hermetic bags at 4°C until further use.

2.2. Extraction Method. The hydromethanolic extracts were obtained from the powdered stems of each cultivar. Each of these stems (5 g) was extracted using an ultrasonic sonotrode (Hielscher UP100H) applying 30 kHz for 30 minutes using 50 mL of methanol/water (80 : 20, v/v) as solvent and then filtered using Whatman No. 4 paper. The extracts were then concentrated using a vacuum rotary evaporator (R-100, BUCHI) at 40–55°C under vacuum, and the dried residues

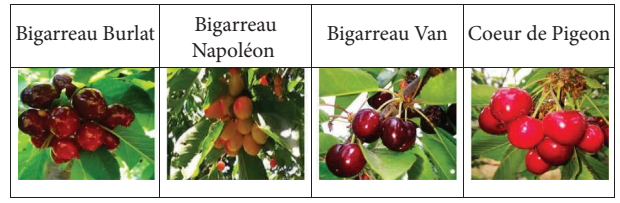

Figure 1: Pictures of the different cherry fruits varieties before harvest.

were stored in Eppendorf tubes at −4°C for further studies. Yields obtained from the starting material were 17.25 ± 0.90 g, 16.90 ± 0.41 g, 18.34 ± 1.01 g, and 22.18 ± 1.12 g for *Burlat*, *Napoleon*, *Coeur de pigeon*, and *Van* cultivars, respectively. Extractions were performed in triplicate.

2.3. Determination of the Total Phenolic Content. The phenol content test was performed using the Folin–Ciocalteu technique as detailed in previous investigations [15, 16].

Thus, 0.5 mL of the sample solution was mixed with 2.5 mL of Folin–Ciocalteu reagent diluted with distilled water in a ratio of 1 : 10, and then 4 mL of Na_2CO_3 (7.5%, w/v) was added. Afterwards, a 45°C water bath was used to heat the mixture for half an hour and absorbance measurements were made at 765 nm using a UV-Vis spectrophotometer in comparison with the blank solution. Under the same conditions, the standard curve of gallic acid was obtained over a concentration range of 0–300 mg/L. The values of phenolic contents were expressed as gallic acid equivalent (mg GAE/g extract). The test was carried out in triplicate for all the samples as well as for the standards and the blank (distilled water).

2.4. Determination of the Flavonoids Content. The flavonoid content was determined according to the method described in the literature with slight modifications [15, 17]. The total flavonoid content was determined using 0.50 mL of each extract stock solution (1 mg/mL) and each dilution of rutin standard solution (10–100 μg/mL) taken separately in test tubes. To each test tube, 1.50 mL methanol, 0.10 mL aluminum chloride solution, 0.10 mL potassium acetate solution, and 2.80 mL distilled water were added and shaken. Blank samples for all extracts and standard rutin dilutions were prepared similarly by replacing the aluminum chloride solution with distilled water. All the prepared solutions were filtered on Whatman No. 1 filter paper before measuring their absorbance at 510 nm against the appropriate blank. From a rutin calibration curve, the total flavonoid content was calculated, and the result was expressed in mg of rutin equivalent per gram of the dry extract (mg RE/g extract). The test was carried out in triplicate for all the samples as well as for the standards and the blank.

2.5. Determination of the Proanthocyanidins Content. The CTC content was performed as described in the previous research studies [15, 18]. Thus, 3 mL of 4% vanillin-methanol

solution was added to 0.05 mL of the extract with the addition of 1.5 mL hydrochloric acid. Subsequently, the mixture is left to stand for 15 minutes. Absorbance was measured at a wavelength of 500 nm, and the results were reported in mg catechin equivalent (CE)/g extract. The assay was carried out in triplicate for all the samples as well as for the standards and the blank.

2.6. Antioxidant Activity. The assays were carried out in triplicate for all the samples as well as for the standards and blank as indicated below:

2.6.1. Free Radical Scavenging Activity. The free radical scavenging activity of the extracts was measured by 1.1-diphenyl-2-picryl-hydrazyl (DPPH) [15, 19]. Thus, 0.5 mL of a 0.2 mM DPPH solution was mixed with 2.5 mL of the extract. The obtained solution was left at 25°C for about 30 minutes, and absorbance was recorded at 517 nm against blank samples. The radical-scavenging activity (RSA) was expressed as a percentage of discoloration. Equation (1) was used to calculate percent inhibition from the obtained absorbance:

$$\%\,\mathrm{RSA} = \frac{A_D - A_E}{A_D} \times 100, \tag{1}$$

where A_D is the recorded value of the blank sample and A_E is the value of the test solution. A_E was determined as the difference between the value of the test solution and the obtained value of its blank.

The IC_{50} value was determined from the graph of the scavenging activity against a range of extract concentrations and is defined as the concentration of antioxidants required to decrease the initial concentration of DPPH radicals by 50%.

2.6.2. ABTS Radical Cation Decolorization Assay. The ABTS radical cation decolorization test was performed as described in [15, 20]. A stock solution of 2 mM ABTS was mixed with 70 mM potassium persulphate stock solution (v/v), and the obtained solution was stored in the dark for 24 h at 25°C. Methanol was carefully added to reach 0.7 ± 0.2 units at 734 nm. Afterwards, 2 mL of the resulting solution was added to 200 μL of the extract, the whole solution was mixed, and the absorbance was recorded at 734 nm at an interval of 1 minute. The results were determined using equation (2) and reported as a percentage of the inhibition of free radical scavenging relative to the blank solution.

$$\text{ABTS radical scavenging activity } (\%) = (1 - \text{Abs sample} - \text{Abs blank}) \times 100, \tag{2}$$

where Abs blank is the value of the blank solution, and Abs sample is the value of the test sample.

2.6.3. Evaluation of Ferric Reducing Antioxidant Power (FRAP). This method is designed around the capacity of the extract to reduce ferric ion (Fe^{3+}) to the corresponding ferrous ion (Fe^{2+}). The remaining Fe^{2+} ions form a blue complex with the reagent 2,4,6-tris(2-pyridyl)-s-triazine (TPTZ), which reaches the absorption maximum at 700 nm. The assessment of the ferric reducing antioxidant power (the FRAP test) was carried out as described by Ouerghemmi and coauthors in [21].

In brief, a volume of 0.25 mL of each sample (1 mg/mL) was added to 1.25 mL of sodium dihydrogen phosphate buffer (0.2 M, pH 6.6) with 1.25 mL of potassium ferricyanide solution (1%), and the mixture was incubated at 50°C for 20 min, followed by the addition of 1.25 mL of trichloroacetic acid (10%), and after centrifugation at 3000 tr/min for 10 min, the supernatant of the solution (1.25 mL) was added to 0.25 mL of iron (III) Chloride (0.1%). The absorbance was measured after a 30 min incubation period at room temperature at 700 nm. An increasing absorbance value means a high reduction capacity. Trolox was used as a standard for the calibration curve (20–400 μg/mL). Finally, the reducing power was represented as Trolox equivalent (μg·TE/g of extract).

2.7. Phytochemical Analysis by UHPLC-DAD/MS. The extracts were analyzed using a Hewlett-Packard 1100 chromatograph (Agilent Technologies) with a quaternary pump and a diode array detector (DAD) coupled to an HP Chem Station (rev. A.05.04) data-processing station. A Waters Spherisorb C18, 5 μm (2.1 mm × 150 mm) column thermostated at 35°C was used. The solvents used were (A) 0.1% formic acid in water and (B) acetonitrile. The elution gradient established was isocratic 15% for 5 min, 15% B to 20% B over 5 min, 20–25% B for 10 min, 25–35% B for 10 min, 35–50% for 10 min, and reequilibrate the column using a flow rate of 0.5 mL/min. The double online detection was carried out in the DAD using 280 nm and 370 nm as preferred wavelengths and in a mass spectrometer (MS) connected to the HPLC system via the DAD cell outlet.

MS detection was performed in an API 3200 Qtrap (Applied Biosystems, Darmstadt, Germany) equipped with an ESI source and a triple quadrupole-ion trap mass analyzer controlled by the Analyst 5.1 software. Zero-grade air served as the nebulizer gas (30 psi) and turbo gas for solvent drying (400°C, 40 psi). Nitrogen served as the curtain (20 psi) and collision gas (medium). The Quadrupols were set to unit resolution. The ion spray voltage was set at −4500 V in the negative mode.

2.8. Assessment of Bioactive Properties

2.8.1. Antidiabetic Activity (the α-Amylase Inhibitory Activity). The α-amylase inhibitory activity was performed according to the protocol of Kusano and colleagues with some modifications [22].

The substrate was prepared by dissolving 200 mg of starch in 25 mL of sodium hydroxide (0.4 M) by heating at 100°C for 5 min. After cooling, the pH was adjusted to 7.0 and the volume was made up to 100 mL with distilled water. Acarbose was used as a positive control. Sample solutions were prepared by dissolving each sample in phosphate buffer (pH 6.5) to obtain 1 mg/mL solutions. 100 μL of α-amylase 3 U/mL (20 mM phosphate buffer with 6.7 mM NaCl, pH 6.9) was preincubated at 37°C for 15 min with 100 μL of acarbose at different concentrations and extract solutions, followed by 500 μL of the substrate solution and incubated at 37°C for 15 min. The reaction was terminated by the addition of 400 μL of HCl (0.1 M), followed by the addition of 400 μL of iodine reagent (2.5 mM). The absorbance was measured at 630 nm. The inhibition percentage of each sample was calculated using the following equation:

$$\mathrm{PI}(\%) = 100 - \left[\frac{(B-A)-(D-C)}{(B-A)} \times 100\right]. \quad (3)$$

A is the absorbance of the enzyme with the substrate. B is the absorbance of the phosphate buffer solution with the substrate. C is the absorbance of the enzyme with the inhibitor and the substrate. D is the absorbance of the phosphate buffer solution with the substrate and enzyme.

2.8.2. Assessment of the Xanthine Oxidase Inhibitory Activity. The inhibitory activity of individual extracts towards xanthine oxidase (XOD) was assessed by adjusting the method used by EL Euch and coauthors with a slight modification [23]. In this method, xanthine oxidase was used as the enzyme catalysing the formation of reactive oxygen species (ROS) and produces uric acid. In brief, 250 μL of the test sample was mixed with 385 μL of 50 mM sodium phosphate buffer (pH = 7.5) and 35 μL of enzyme solution (0.2 units/mL). After preincubation for 15 min at 37°C, 330 μL of xanthine (150 μM) was added as a reaction substrate, and after 15 min of incubation at 37°C, the absorbance of the reaction mixture was measured with a spectrophotometer at 295 nm. Allopurinol was used as a positive control (0.5; 1; 2.5; 5 μg/mL). The inhibition percentage of each sample was calculated using the following formula:

$$\mathrm{PI}(\%) = \left[\frac{(A-B)-(C-D)}{(A-B)}\right] \times 100. \quad (4)$$

A is the absorbance of the enzyme with the substrate. B is the absorbance of the phosphate buffer solution with the substrate. C is the absorbance of the enzyme with the inhibitor and the substrate. D is the absorbance of the phosphate buffer solution with the substrate and the enzyme.

3. Results

3.1. Total Phenolics, Total Flavonoids, and Condensed Tannins Contents. Significant differences were noted in the parameters analyzed, except for the total flavonoid content where the *Napoleon* showed a high value compared to the other cultivars (Table 1). The total phenolic content ranged from 340 mg/g in *Napoleon* to 191 mg/g recorded in the *Burlat* stem extract. Compared to previous works, our result showed a higher amount of the total phenolic content [8, 11, 13, 14]. Interestingly, in another study focusing on fruit quality, the highest total phenolic content value was obtained for the *Napoleon* cultivar, with a value of 306.67 mg/100 g dry weight [5].

For flavonoids, the highest value recorded was for *Napoleon* with 34.31 mg/g. This observation is also true for tannins (9.25 mg/g). On the other hand, *Burlat* seems to be the poorest in all compounds, with 23.31 mg RE/g of flavonoids and no tannin detected. Furthermore, the amount of flavonoids is higher than those reported by some previously reported studies [8, 11, 14].

3.2. Antioxidant Activities

3.2.1. DPPH Scavenging Activity. In this study, four cherry cultivars were evaluated. The free radical scavenging activity was expressed using IC_{50} values (concentration of the extract required to inhibit 50% of the initial DPPH free radical) (Table 2). The results showed that the percentage values of the free radical scavenging activity (% RSA) increased with increasing concentrations of the stem extracts. *Napoleon* extracts showed the most potent DPPH scavenging activity, while *Burlat* extracts showed the weakest activity. These results indicate that the level of phenolic compounds in the cultivars examined correlates with the values obtained by the DPPH test.

Additionally, all extracts exhibited a lower activity than the Trolox positive control ($IC_{50} = 2.95 \pm 0.12$ μg/mL) except for the *Napoleon* extract where the activity was the highest ($IC_{50} = 2.51 \pm 0.15$ μg/mL).

3.2.2. Radical Cation $ABTS^{\bullet+}$ Scavenging Activity. As shown in Table 2, antioxidant activities by the DPPH method produce lower IC_{50} values (2.51 ± 0.15 to 7.78 ± 0.70 μg/mL) than the ABTS assay, which appears to be a good method to express the antioxidant capacity of phenolic compounds in sweet cherry stems. IC_{50} values ranged from 55.38 ± 5.08 to 128.95 ± 16.18 μg/mL, using the ABTS method (Table 2). All extracts exhibited lower activity than the Trolox positive control ($IC_{50} = 30.86 \pm 1.90$ μg/mL).

These results are consistent with those obtained for the phenolic compounds, flavonoids, condensed tannins contents, and DPPH values in which *Napoleon* has the highest dose of these compounds and explain the concentration related efficacy observed in the antioxidant experiments.

3.2.3. Ferric Reducing Antioxidant Power (FRAP). The presence of antioxidants in the samples would reduce Fe^{3+} to Fe^{2+} by donating an electron. The ferric reducing power of

Table 1: Total phenolic, total flavonoid, and condensed tannins contents of the studied cherry stem extracts.

Cultivars	TPC (mg GAE/g extract)	TFC (mg RE/g extract)	TTC (mg CE/g extract)
Burlat	191 ± 3.10	23.31 ± 0.90	—
Napoleon	340 ± 12.06	34.31 ± 2.08	9.25 ± 1.50
Coeur de pigeon	244 ± 10.20	23.75 ± 1.02	1.13 ± 0.90
Van	232 ± 5.07	24.37 ± 1.20	4.07 ± 1.28

Table 2: IC_{50} values of the DPPH, ABTS, and FRAP tests for the different extracts.

Cultivars	DPPH (IC_{50} (μg/mL))	ABTS (IC_{50} (μg/mL))	FRAP (μg·TE/g extract)
Burlat	7.78 ± 0.70	128.95 ± 16.18	34.34 ± 1.17
Napoleon	2.51 ± 0.15	55.38 ± 5.08	29.23 ± 2.91
Coeur de pigeon	5.09 ± 1.02	126.26 ± 14.37	35.13 ± 1.09
Van	4.77 ± 0.80	85.4 ± 8.76	45.63 ± 4.20
Trolox	2.95 ± 0.12	30.86 ± 1.90	—

the samples is expressed as concentration equivalent μg Trolox per gram of the extract, and the results are presented in Table 2. The reducing powers of the samples decreased as follows: *Van* (45.63) > *Coeur de pigeon* (35.13) > *Burlat* (34.31) > *Napoleon* (29.23) μg TE/g of the extract.

3.3. Phytochemical Analysis by UHPLC-DAD/MS. In this study, the analysis of phenolic compounds of cherry stems from four cultivars was performed by UHPLC-DAD/MS, and the chromatograms of each extract are shown in Figure 2. A significant difference was observed in the chromatograms of *Napoleon* cultivars compared to others. Additionally, regarding the high relative intensity of the peaks in most compounds detected in the *Napoleon* cultivar compared to the other cultivars and considering this semiquantitative method, this may explain the results obtained for *Napoleon* stem extracts in TPC, TFC, DPPH, and ABTS assays.

Tentative identification was suggested based on the information provided by the MS data and related information in the literature. The UHPLC-DAD/MS analysis of cherry stem extracts tentatively identified twenty-two compounds, which can be divided into five groups: six hydroxycinnamic acids (1, 3-4, 6, and 8-9), eight flavonols (2, 7, 10–13 and 16-17), one flavan-3-ols (5), five flavanones (15, 18–20 and 22), and two flavones (14 and 21). Table 3 lists the tentatively identified phenolic compounds in the negative ionization mode, together with their retention time (min), their experimental m/z for the deprotonated molecular ion ($[M-H]^-$), and their families.

The peak area of each compound was obtained from the UHPLC data, and the results obtained are presented in Table 4, together with the relative percentage of phenolic acids and flavonoids, which are also subdivided into the relative percentage of each of the four identified classes. Although it was not possible to quantify each phenolic compound individually due to the scarcity of standards, the relative percentage of each phenolic family (calculated based on the chromatographic peak areas) can provide us with an estimate of the relative abundance of each family of compounds in the sample. Nevertheless, it should be noted that this is a semiquantitative method, as compounds may exhibit different sensitivities in UHPLC-MS.

Table 4 aims to present the different concentrations of the different compounds identified. Generally, hydroxycinnamic acids were the only class of phenolic acids identified in all cultivars, with a high relative percentage of this class in *Napoleon* and *Burlat* cultivars. However, other works have identified hydroxybenzoic acids and their glucosides in addition to classes of hydroxycinnamic acids [10, 14].

Regarding the hydroxycinnamic acids, compounds 1, 3-4, 6, 8, and 9 were identified according to MS data and the previous studies [9, 10, 12–14].

Finally, with the respect to the large family of flavonoids, two compounds were distinguished by the high relative intensity of their peak; compound 19 can be either dihydrowogonin or sakuranetin-O-pentosylhexoside and compound 20 may correspond to either dihydrowogonin 7-O-glucoside or sakuranetin 5-O-glucoside (Figure 3), as both compounds are described as being the main compounds detected in cherry stems, as also observed in this case [10, 12].

3.4. Assessment of Bioactive Properties

3.4.1. α-Amylase Inhibitory Activity. In this study, the ability of the 80% methanol extract of sweet cherry stems from different cultivars to inhibit the α-amylase enzyme was investigated. Three of the analyzed extracts inhibited this enzyme at a dose of 1 mg/mL (Table 5).

The most active stem extracts were *Burlat* (85.57 ± 1.09%) and *Napoleon* (68.01 ± 3.52%) cultivars, while stem extract from *Coeur de pigeon* cultivar was the least active. These values are difficult to compare, given the lack of studies carried out in this field. However, the α-amylase inhibitory activity of stem extracts for *Burlat* and *Napoleon* cultivars can be considered comparable to that of green tea, oolong tea, and guava leaf extracts (% I = 21.0 ± 3.7, 10.9 ± 2.7, and 32.4 ± 9.5, respectively, at 250 μg/mL) [24].

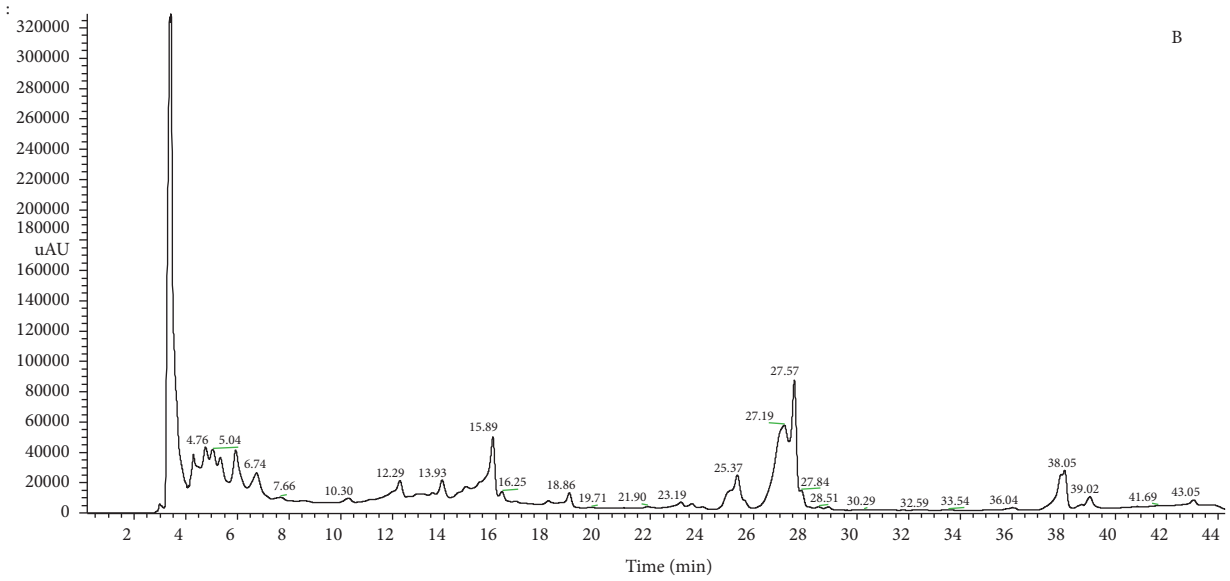

(a)

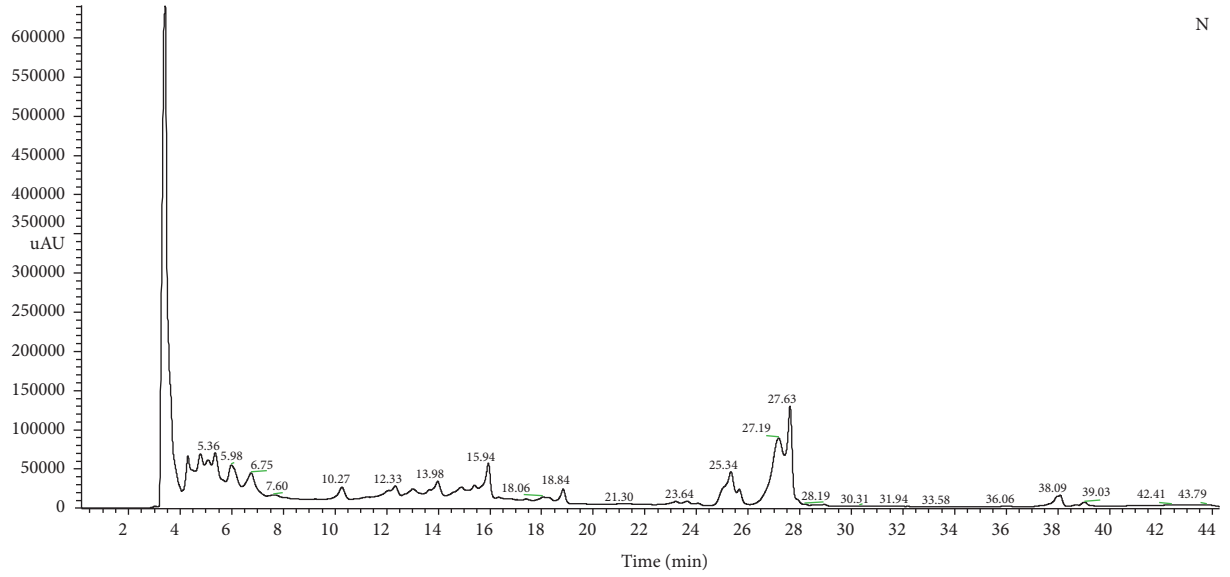

(b)

Figure 2: Continued.

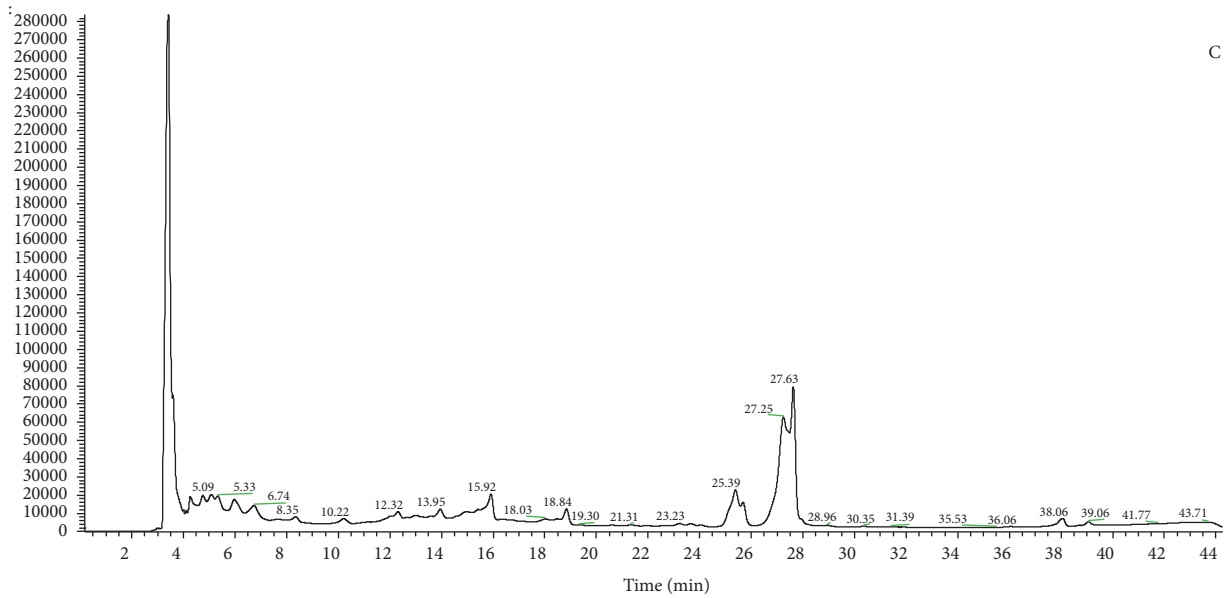

(c)

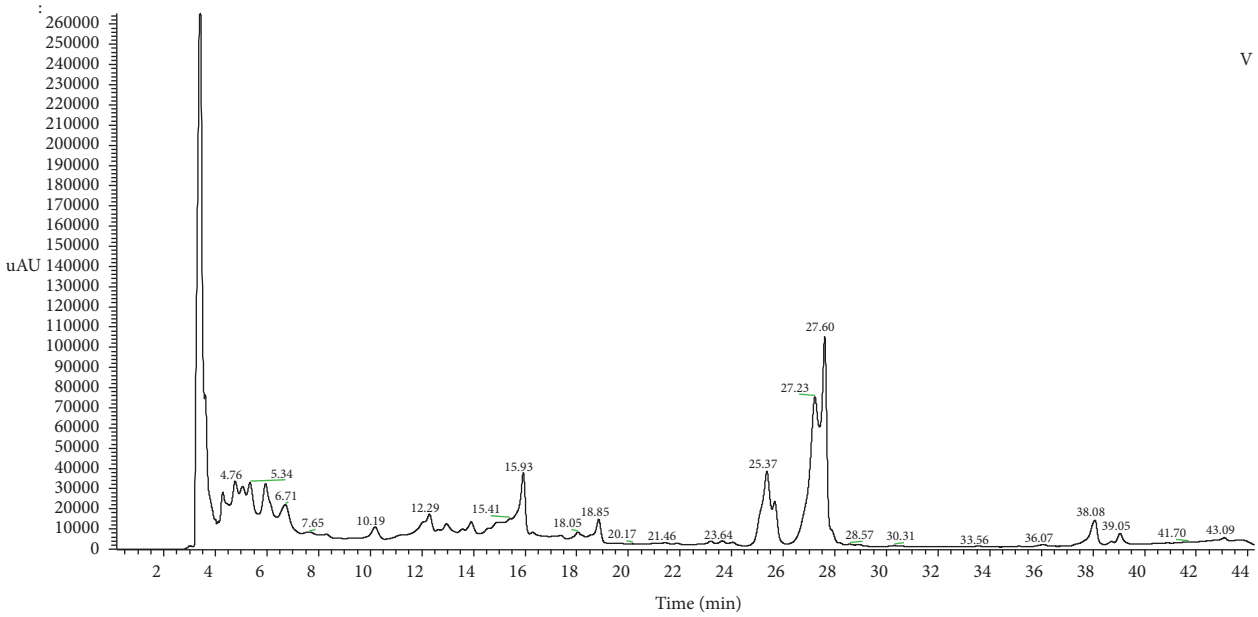

(d)

Figure 2: UHPLC chromatograms of phenolic compounds detected in sweet cherry stem's extracts recorded at 280 nm for different cultivars: (a) *Burlat* (B). (b) *Napoleon* (N). (c) *Coeur de pigeon* (C). (d) *Van* (V).

Our stem extracts showed significantly higher inhibition than those obtained with *Techlovan*, *Sumhit*, and *Rivan* sweet cherry extracts with IC_{50} values of 46.7 ± 0.4, 74.4 ± 1.6, and 78.3 ± 1.4 mg/mL, expressed as dried hydromethanolic and hydrochloric acid extracts, respectively) [25].

3.4.2. Anti-Xanthine Oxidase Inhibitory Activity. XOD catalyses the transformation of purine bases into uric acid and H_2O_2. Underexcretion and/or overproduction of this acid lead to the incidence of hyperuricemia in the form of gout [26]. Consequently, the use of XOD inhibitors is considered as a hypouricemic treatment of gout by stopping the production of uric acid.

In this study, sweet cherry stem's extracts for all cultivars were tested for the XOD inhibitory activity at 1 mg/mL in the final reaction mixture. The results were expressed as inhibition percentage (%) and shown in Table 6. A more potent XOD activity of the extract is indicated by a higher percentage inhibition.

The inhibition percentages varied from $26.25 \pm 0.90\%$ to $40.63 \pm 2.37\%$ according to the cultivar. *Van* cultivar exhibited the highest activity ($40.63 \pm 2.37\%$) compared to

Table 3: Main phenolic compounds identified by UHPLC-MS in cherry stem's extracts of four cultivars: *Burlat* (B), *Napoleaon* (N), *Coeur de pigeon* (C), and *Van* (V).

Peaks	Retention times (min)				Molecular ions	Family	Compounds
	B	N	C	V	$[M-H]^-(m/z)$		
1	4.29	4.30	4.26	4.29	353	Hydroxycinnamic acid	3-O-caffeoylquinic acid
2	4.76	4.78	4.75	4.76	465	Flavonol	Taxifolin-7-O-hexoside
3	5.04	5.09	5.09	5.05	337	Hydroxycinnamic acid	p-Coumaroyl quinic acid
4	ni	5.36	5.33	ni	341	Hydroxycinnamic acid	Caffeic acid hexoside
5	5.93	5.9	5.98	5.94	289	Flavan-3-ols	Catechin
6	6.74ni	6.75	6,74	ni	179	Hydroxycinnamic acid	Caffeic acid
7	7.66	7.60	8.35	ni	449	Flavonol	Aromadendrin-7-O-hexoside
8	10,3	10.27	10.22	10.19	325	Hydroxycinnamic acid	*p*-coumaricacidhexoside
9	12.29	12.33	12.31	12.29	355	Hydroxycinnamic acid	Ferulic acid hexoside
10	ni	13.02	ni	ni	449	Flavonol	Aromadendrin-O-hexoside
11	13.93	13.98	13.95	13.91	463	Flavonol	Methyl-aromadendrin-O-hexoside
12	14.86	14.90	14.99	14.92	609	Flavonol	Quercetin-3-O-rutinoside
13	15.89	15.94	ni	15.93	463	Flavonol	Quercetin-3-O-glucoside
14	ni	18.06	18.03	18.05	431	Flavone	Genistein-7-O-glucoside
15	18.86	18.84	18.48	18.85	433	Flavanone	Naringenin-7-O-glucoside
16	ni	23.21	23.23	23.20	593	Flavonol	Kaempferol-3-O-rutinoside
17	23.61	23.64	23.66	23.64	447	Flavonol	Kaempferol-3-O-glucoside
18	25.37	25.34	25.39	25.37	549	Flavanone	Pinocembrin-O-pentosyl-hexoside
19	27.19	27.19	27.25	27.23	579	Flavanone	Dihydrowogonin/sakuranetin-O-pentosylhexoside
20	27.57	27.63	27.63	27.60	447	Flavanone	Dihydrowogonin7-O-glucoside/sakuranetin5-O-glucoside
21	38.05	38.09	38.06	38.07	415	Flavone	Chrysin-7-O-glucoside
22	39.02	39.03	ni	39.05	285	Flavanone	Dihydroxymethoxyflavanone

ni: not identified.

Table 4: Peak areas ($*10^4$) and average of each family obtained by HPLC/MS analysis of different cultivars: *Burlat* (B), *Napoleaon* (N), *Coeur de pigeon* (C), and *Van* (V).

Peaks	Compounds	Peak areas			
		B	N	C	V
1	3-O-caffeoylquinic acid	72.4	130.9	11.6	11.4
2	Taxifolin-7-O-hexoside	71.2	115.5	14.6	17.01
3	*p*-coumaroyl quinic acid	64	86.2	16.9	16.7
4	Caffeic acid hexoside	—	140.1	18.3	—
5	Catechin	91.5	128.7	22.01	35.02
6	Caffeic acid	64.8	109.5	18.2	—
7	Aromadendrin-7-O-hexoside	9.4	14.06	4.5	—
8	*p*-coumaric acid hexoside	4.7	27.9	4.8	11.1
9	Ferulic acid hexoside	29.9	28.4	7.2	22.5
10	Aromadendrin-O-hexoside	—	40.7	—	—
11	Methyl-aromadendrin-O-hexoside	14.6	42.2	6.2	6.2
12	Quercetin-3-O-rutinoside	20.4	48.9	2	1.1
13	Quercetin-3-O-glucoside	77.8	77.5	—	44.2
14	Genistein-7-O-glucoside	—	4.8	1.3	7.8
15	Naringenin-7-O-glucoside	10.9	23.5	1.8	19.2
16	Kaempferol-3-O-rutinoside	—	7.3	1.5	1.6
17	Kaempferol-3-O-glucoside	3.3	7.3	1.2	1.7
18	Pinocembrin-O-pentosyl-hexoside	71.4	113.3	45.9	84.9
19	Dihydrowogonin/sakuranetin 5-O-pentosylhexoside	206.3	278.3	170.9	188.3
20	Dihydrowogonin 7-O-glucoside/sakuranetin 5-O-glucoside	126.02	196.6	103.9	154.8
21	Chrysin-7-O-glucoside	28.9	36.3	6.8	27.8
22	Dihydroxy methoxyflavanone	13.4	8.1	—	8.4
	Total peak areas	980.92	1666.06	459.61	659.73
	% phenolic acids	24.04	31.39	16.75	9.35
	% hydroxycinnamic acid	24.04	31.39	16.75	9.35
	% flavonoids	75.96	68.61	83.25	90.65
	% flavan-3-ol	9.32	7.73	4.79	5.31
	% flavonol	20.06	21.21	6.53	10.89
	% flavanone	43.64	37.21	70.17	69.06
	% flavone	2.94	2.46	1.76	5.39

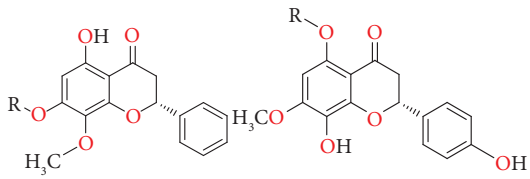

R= H : DihydrowgoninR= Pentosylhexoside: Sakuranetin 5-O- Pentosylhexoside

R= Glucoside Dihydrowgonin-7-O-glucoside R= Glucoside: Sakuranetin5-O-glucoside

Figure 3: Chemical structure of sakuranetin and dihydrowgonin with their glucosides.

Table 5: Enzymatic in vitro α-amylase inhibition of hyperglycaemic of sweet cherry stem extracts from four cultivars.

	Burlat	*Napoleon*	*Coeur de pigeon*	*Van*
% Inhibition	85.57 ± 1.09	68.01 ± 3.52	3.87 ± 0.18	—
mg EAC/g of extract	190.40	143.17	29.38	—

Table 6: Xanthine oxidase inhibitory activity of sweet cherry stem extracts from four cultivars.

	Burlat	*Napoleon*	*Coeur de pigeon*	*Van*
PI (%)	27.94 ± 0.09	30.70 ± 1.80	26.25 ± 0.90	40.63 ± 2.37

the others. This result may be explained by the high relative percentage of flavonoids in *Van* cultivar (90.65% shown in Table 4). Flavonoids are antioxidants that inhibit XOD [27]. Additionally, all stem extracts exhibited a lower activity than the pure compound allopurinol which showed inhibitory effects of 20%, 44.38%, 89.11%, and 90.88% at 0.5, 1, 2.5, and 5 μg/mL, respectively.

4. Discussion

4.1. Radical Cation ABTS$^{\bullet+}$ Scavenging Activity. The ABTS assay is an excellent approach to study the antioxidant activity of hydrogen-donating agents and chain breakers. It is available for both hydrophilic and lipophilic antioxidant media; while the DPPH assay uses a radical dissolved in an organic medium and is, consequently, applicable to hydrophobic media [28].

Regarding the tests in which the total contents of phenolic compounds, flavonoids, and tannins were evaluated (Table 1), as well as for the method of antioxidant activities (Table 2), the results were similar to those obtained by the FRAP method, with the exception of the *Napoleon* extract. This may be because the compounds reacting with DPPH radicals may not be the same as those reacting with the TPTZ-Fe^{3+} complex. According to the DPPH method, the radical is neutralized when it receives H^+ and/or electrons from the antioxidants, but for the FRAP assay, the TPTZ-Fe^{3+} complex was reduced to TPTZ-Fe^{2+} only by an electron transfer mechanism by compounds with a redox potential below 0.7 V [29, 30].

Additionally, the measure of reducing power seems to be related to the degree of hydroxylation of the benzene ring and its possible modification by secondary reactions as well as to the extent of conjugation to the phenolic compound [31].

In the present study, the reducing power ability of our extracts was found to be more potent than that revealed by the hydromethanolic stem extracts from sweet cherry cultivars, namely, *Burlat, Early Bigi NC, Lapins, and Van* (15.15 ± 1.40 μg·TE/g, 18.15 ± 2.24 μg·TE/g, 26.66 ± 2.26 μg·TE/g, and 18.21 ± 2.19 μg·TE/g extract, respectively) [14].

4.2. Phytochemical Analysis by UHPLC-DAD/MS. The analysis of phenolic compounds is of great interest to scientists, manufacturers, and consumers for their impact on product quality and for their protective and preventive functions in the pathogenesis of certain types of cancer and several other chronic diseases. There are many reports in the literature on the identification and quantification of phenolic compounds in *Prunus avium* (L.) fruits. The most commonly identified compounds are phenolic acids (neochlorogenic, chlorogenic, and *p*-coumaroylquinic acids), anthocyanins, flavonols (rutin), and flavan-3-ols (catechin and epicatechin) [10, 16, 31, 32].

To date, few publications have been devoted to the chemical composition of sweet cherry stem. Bursal et al. (2013) studied phenolic acids in ethanolic and aqueous extracts of cherry stems by LC-MS/MS [11]. They have identified pyrogallol, ferulic acid, *p*-coumaric acid, gallic acid, *p*-glucosidic acid, ascorbic acid, and *p*-hydroxybenzoic acid. Bastos et al. compared the HPLC phenolic profile of fruits and stems of *P. avium* L. They detected more phenolic compounds in the stem than in the fruit [10]. Ademović et al. identified phenolic compounds in the alcoholic and aqueous extracts of wild cherry stem [8]. They found that quercetin and (+)-catechin were the two main compounds detected in the alcoholic extract, followed by chlorogenic acid and rutin. Aires et al. analyzed glycosylated flavonoids extracted from sweet cherry stems [9]. They found a high content of sakuranetin, ferulic acid, *p*-coumaric acid, *p*-coumaroylquinic acid, chlorogenic acid, and its isomer neochlorogenic acid. In 2020, Peixoto et al. explored the phenolic profile of infusions prepared with four distinct commercial brands of cherry stems (*Prunus avium* L.) by UHPLC-q-TOF-MS/MS, and they identified eight distinct

classes of phenolic compounds [13]. To our knowledge, only one publication has reported the phenolic composition by HPLC-DAD of stem extracts from four sweet cherry cultivars, with the identification of seventeen compounds [14].

4.3. Assessment of Bioactive Properties

4.3.1. α-Amylase Inhibitory Activity. Diabetes mellitus type 2 (DMT2) is a common chronic metabolic disease. It is caused by abnormalities in carbohydrate metabolism associated with low blood insulin levels or impaired sensitivity of target organs to insulin. The α-amylase enzyme is heavily involved in the digestion of carbohydrates. Therefore, its inhibition will be a contemporary therapeutic approach of DMT2 [33]. To the best of our knowledge, this is the first report on the inhibitory effect of sweet cherry stem extracts from different cultivars against the α-amylase enzyme. However, sweet cherries have already been shown to be a potential inhibitor of this enzyme, mainly due to their high content of phenolic compounds [7, 25]. In the current study, the α-amylase inhibitory activity was not correlated with total phenolic compounds (expressed as % of the peak area in Table 4) in the analyzed extracts; however, some subclasses of the phenolic compound were correlated with this activity, especially for *Burlat* cultivar with a high estimate of the relative abundance of flavan-3-ol (catechin) (9.32%) compared to the other cultivars. This correlation was still not satisfactory. Some poor correlations have also been reported previously [34, 35]. They considered that the specific type (number, type, and position of OH groups) of phenolic compounds is more significant for inhibitory effects on digestive enzymes than the total amounts of phenolic compounds.

4.3.2. Anti-Xanthine Oxidase Inhibitory Activity. XOD catalyses the transformation of purine bases into uric acid and H_2O_2. Underexcretion and/or overproduction of this acid lead to the incidence of hyperuricemia in the form of gout [26]. Consequently, the use of XOD inhibitors is considered as a hypouricemic treatment of gout by stopping the production of uric acid. No previous research has been conducted on the inhibitory activity of the sweet cherry stem extract against XOD; however, some studies have shown that the consumption of sweet cherries reduces serum urate levels in healthy women and suggests a potential application of cherries for the treatment of gout [24, 36, 37].

5. Conclusion

This study was conducted on the stem of four sweet cherry cultivars. The results showed that the extracts obtained from this plant material are rich in polyphenols with a content of 340 ± 12.06, 244 ± 10.20, 232 ± 5.07, and 191 ± 3.10 mg GAE/g extract for the *Napoleon*, *Coeur de pigeon*, *Van*, and *Burlat* cultivars, respectively. In terms of flavonoids and tannins, again, the *Napoleon* cultivar was the most abundant with values of 34.31 ± 2.08 mg RE/g extract and 9.25 ± 1.50 mg CE/g extract, while *Burlat* was low in tannins. These results explain the low IC_{50} values observed for *Napoleon* (2.51 μg/mL for DPPH and 55.38 μg/mL for ABTS) close to those obtained by Trolox. The UHPLC-DAD/MS analysis of cherry stem extracts resulted in the tentative identification of twenty-two compounds belonging to five distinct groups. The *Napoleon* cultivar had the highest amount of all compounds based on their high peak intensity. The major phenolic compounds identified in all cultivars were sakuranetin and dihydrowgonin with their glucosides. Only stem extracts from *Burlat* and *Napoleon* cultivars were able to inhibit the α-amylase enzyme with values of $85.57 \pm 1.09\%$ and $68.01 \pm 3.52\%$, respectively. Some subclasses of the phenolic compounds correlated with this activity, especially for *Burlat* cultivar with a high estimated relative abundance of flavan-3-ols (catechin) (9.32%) compared to the other cultivars. All stem extracts have proved their ability to inhibit the XOD enzyme with a high value for *Van* cultivar $40.63 \pm 2.37\%$. This work shows that the treatment of certain diseases, such as DMT2 and gout, can be based on the choice of some stem cultivars. However, these stems need to be more investigated, and further studies are required to explore nutraceutical and pharmacological formulations or antioxidant preservatives for the food industry and their impacts on human health.

Data Availability

The data used to support the findings of this study are included within the article.

Conflicts of Interest

The authors declare that they have no conflicts of interest.

References

[1] M. Ekor, "The growing use of herbal medicines: issues relating to adverse reactions and challenges in monitoring safety," *Frontiers in Pharmacology*, vol. 4, p. 177, 2014.

[2] C. L. Gorlenko, H. Y. Kiselev, E. V. Budanova, A. A. Zamyatnin Jr, and L. N. Ikryannikova, "Plant secondary metabolites in the battle of drugs and drug-resistant bacteria: new heroes or worse clones of antibiotics?" *Antibiotics*, vol. 9, no. 4, p. 170, 2020.

[3] M. Erb and D. J. Kliebenstein, "Plant secondary metabolites as defenses, regulators, and primary metabolites: the blurred functional trichotomy," *Plant Physiology*, vol. 184, no. 1, pp. 39–52, 2020.

[4] M. F. Basanta, M. F. De Escalada Plá, M. D. Raffo, C. A. Stortz, and A. M. Rojas, "Cherry fibers isolated from harvest residues as valuable dietary fiber and functional food ingredients," *Journal of Food Engineering*, vol. 126, pp. 149–155, 2014.

[5] M. El Baji, O. Kodad, H. Hanine, S. En-nahli, and A. Oubahou, "Phenotypic and biochemical parameters of four sweet cherry (Prunus Avium L.) cultivars grown in agro-ecological conditions of middle Atlas of Morocco," *Lebanese Science Journal*, vol. 20, no. 3, pp. 363–379, 2019.

[6] M. El Baji, H. Hanine, S. En-Nahli, R. Socias I Company, and O. Kodad, "Morphological and pomological characteristics of sweet cherry (Prunus avium L.) grown in-situ under south mediterranean climate in Morocco," *International Journal of Fruit Science*, vol. 21, no. 1, pp. 52–65, 2021.

[7] A. C. Gonçalves, C. Bento, B. M. Silva, and L. R. Silva, "Sweet cherries from Fundão possess antidiabetic potential and protect human erythrocytes against oxidative damage," *Food Research International*, vol. 95, pp. 91–100, 2017.

[8] Z. Ademović, S. Hodžić, Z. Halilić Zahirović et al., "Phenolic compounds, antioxidant and antimicrobial properties of the wild cherry (Prunus avium L.) stem," *Acta Periodica Technologica*, vol. 48, no. 48, pp. 1–13, 2017.

[9] A. Aires, C. Dias, R. Carvalho, and M. J. Saavedra, "Analysis of glycosylated flavonoids extracted from sweet-cherry stems, as antibacterial agents against pathogenic *Escherichia coli* isolates," *Acta Biochimica Polonica*, vol. 64, no. 2, pp. 265–271, 2017.

[10] C. Bastos, L. Barros, M. Dueñas et al., "Chemical characterisation and bioactive properties of Prunus avium L.: the widely studied fruits and the unexplored stems," *Food Chemistry*, vol. 173, pp. 1045–1053, 2015.

[11] E. Bursal, E. Köksal, I. Gülçin, G. Bilsel, and A. C. Gören, "Antioxidant activity and polyphenol content of cherry stem (Cerasus avium L.) determined by LC-MS/MS," *Food Research International*, vol. 51, no. 1, pp. 66–74, 2013.

[12] F. Jesus, A. C. Gonçalves, G. Alves, and L. R. Silva, "Exploring the phenolic profile, antioxidant, antidiabetic and antihemolytic potential of Prunus avium vegetal parts," *Food Research International*, vol. 116, pp. 600–610, 2019.

[13] J. Peixoto, G. Álvarez-Rivera, R. C. Alves et al., "Cherry stem infusions: antioxidant potential and phenolic profile by UHPLC-ESI-QTOF-MS," *Food and Function*, vol. 11, no. 4, pp. 3471–3482, 2020.

[14] S. Afonso, I. V. Oliveira, A. S. Meyer, A. Aires, M. J. Saavedra, and B. Gonçalves, "Phenolic profile and bioactive potential of stems and seed kernels of sweet cherry fruit," *Antioxidants*, vol. 9, no. 12, pp. 1295–1317, 2020.

[15] F. Bouhlal, Y. Aqil, I. Chamkhi et al., "GC-MS analysis, phenolic compounds quantification, antioxidant, and antibacterial activities of the hydro-alcoholic extract of spent coffee grounds," *Journal of Biologically Active Products from Nature*, vol. 10, no. 4, pp. 325–337, 2020.

[16] V. Usenik, J. Fabčič, and F. Štampar, "Sugars, organic acids, phenolic composition and antioxidant activity of sweet cherry (Prunus avium L.)," *Food Chemistry*, vol. 107, no. 1, pp. 185–192, 2008.

[17] A. Kumaran and R. Joel Karunakaran, "In vitro antioxidant activities of methanol extracts of five Phyllanthus species from India," *LWT - Food Science and Technology*, vol. 40, no. 2, pp. 344–352, 2007.

[18] B. Sun, J. M. Ricardo-da-Silva, and I. Spranger, "Critical factors of vanillin assay for catechins and proanthocyanidins," *Journal of Agricultural and Food Chemistry*, vol. 46, no. 10, pp. 4267–4274, 1998.

[19] B. Huang, H. Ke, J. He, X. Ban, H. Zeng, and Y. Wang, "Extracts of Halenia elliptica exhibit antioxidant properties in vitro and in vivo," *Food and Chemical Toxicology*, vol. 49, no. 1, pp. 185–190, 2011.

[20] R. Re, N. Pellegrini, A. Proteggente, A. Pannala, M. Yang, and C. Rice-Evans, "Antioxidant activity applying an improved ABTS radical cation decolorization assay," *Free Radical Biology and Medicine*, vol. 26, no. 9–10, pp. 1231–1237, 1999.

[21] S. Ouerghemmi, H. Sebei, L. Siracusa et al., "Comparative study of phenolic composition and antioxidant activity of leaf extracts from three wild Rosa species grown in different Tunisia regions: rosa canina L., Rosa moschata Herrm. and Rosa sempervirens L," *Industrial Crops and Products*, vol. 94, pp. 167–177, 2016.

[22] R. Kusano, S. Ogawa, Y. Matsuo, T. Tanaka, Y. Yazaki, and I. Kouno, "A-amylase and lipase inhibitory activity and structural characterization of Acacia bark proanthocyanidins," *Journal of Natural Products*, vol. 74, no. 2, pp. 119–128, 2011.

[23] S. K. El Euch, J. Bouajila, and N. Bouzouita, "Chemical composition, biological and cytotoxic activities of Cistus salviifolius flower buds and leaves extracts," *Industrial Crops and Products*, vol. 76, pp. 1100–1105, 2015.

[24] R. A. Jacob, G. M. Spinozzi, V. A. Simon et al., "Consumption of cherries lowers plasma urate in healthy women," *The Journal of Nutrition*, vol. 133, no. 6, pp. 1826–1829, 2003.

[25] A. Wojdyło, P. Nowicka, I. P. Turkiewicz, and K. Tkacz, "Profiling of polyphenols by LC-QTOF/ESI-MS, characteristics of nutritional compounds and in vitro effect on pancreatic lipase, α-glucosidase, α-amylase, cholinesterase and cyclooxygenase activities of sweet (Prunus avium) and sour (P. cerasus) cherries leaves and fruits," *Industrial Crops and Products*, vol. 174, Article ID 114214, 2021.

[26] J. M. Lü, Q. Yao, and C. Chen, "3,4-Dihydroxy-5-nitrobenzaldehyde (DHNB) is a potent inhibitor of xanthine oxidase: a potential therapeutic agent for treatment of hyperuricemia and gout," *Biochemical Pharmacology*, vol. 86, no. 9, pp. 1328–1337, 2013.

[27] A. G. González, I. L. Bazzocchi, L. Moujir, A. G. Ravelo, M. D. Correa, and M. P. Gupta, "Xanthine oxidase inhibitory activity of some Panamanian plants from Celastraceae and Lamiaceae," *Journal of Ethnopharmacology*, vol. 46, no. 1, pp. 25–29, 1995.

[28] D. O. Kim, H. J. Heo, Y. J. Kim, H. S. Yang, and C. Y. Lee, "Sweet and sour cherry phenolics and their protective effects on neuronal cells," *Journal of Agricultural and Food Chemistry*, vol. 53, no. 26, pp. 9921–9927, 2005.

[29] A. S. G. Costa, R. C. Alves, A. F. Vinha et al., "Optimization of antioxidants extraction from coffee silverskin, a roasting byproduct, having in view a sustainable process," *Industrial Crops and Products*, vol. 53, pp. 350–357, 2014.

[30] R. L. Prior, X. Wu, and K. Schaich, "Standardized methods for the determination of antioxidant capacity and phenolics in foods and dietary supplements," *Journal of Agricultural and Food Chemistry*, vol. 53, no. 10, pp. 4290–4302, 2005.

[31] M. Serrano, F. Guillén, D. Martínez-Romero, S. Castillo, and D. Valero, "Chemical constituents and antioxidant activity of sweet cherry at different ripening stages," *Journal of Agricultural and Food Chemistry*, vol. 53, no. 7, pp. 2741–2745, 2005.

[32] S. Pacifico, A. Di Maro, M. Petriccione et al., "Chemical composition, nutritional value and antioxidant properties of autochthonous Prunus avium cultivars from Campania Region," *Food Research International*, vol. 64, pp. 188–199, 2014.

[33] G. Zdunić, A. A. Aradski, D. Gođevac et al., "In vitro hypoglycemic, antioxidant and antineurodegenerative activity of chokeberry (Aronia melanocarpa) leaves," *Industrial Crops and Products*, vol. 148, Article ID 112328, 2020.

[34] Z. Bingol, H. Kızıltaş, A. C. Gören et al., "Antidiabetic, anticholinergic and antioxidant activities of aerial parts of shaggy bindweed (Convulvulus betonicifolia Miller subsp.) – profiling of phenolic compounds by LC-HRMS," *Heliyon*, vol. 7, no. 5, Article ID e06986, 2021.

[35] V. Spínola, J. Pinto, E. J. Llorent-Martínez, and P. C. Castilho, "Changes in the phenolic compositions of Elaeagnus umbellata and Sambucus lanceolata after in vitro

gastrointestinal digestion and evaluation of their potential anti-diabetic properties," *Food Research International*, vol. 122, pp. 283–294, 2019.

[36] M. F. Faienza, F. Corbo, A. Carocci et al., "Novel insights in health-promoting properties of sweet cherries," *Journal of Functional Foods*, vol. 69, Article ID 103945, 2020.

[37] A. C. Gelber and D. H. Solomon, "If life serves up a bowl of cherries, and gout attacks are 'the pits': implications for therapy," *Arthritis and Rheumatism*, vol. 64, no. 12, pp. 3827–3830, 2012.

Hindawi
Evidence-Based Complementary and Alternative Medicine
Volume 2023, Article ID 5643861, 12 pages
https://doi.org/10.1155/2023/5643861

Research Article

Dietary Thymoquinone Alone or Combined with Swimming Exercise Protect against Microcystin-LR-Induced Oxidative Injury in Mice

Ahmed E. Altyar,[1,2] Amira Hassan Bekhet,[3] Mohamed Kamel,[4] Ghadeer M. Albadrani,[5] Osama A. Kensara,[6] and Mohamed M. Abdel-Daim[7,8]

[1]*Department of Pharmacy Practice, Faculty of Pharmacy, King Abdulaziz University, P.O. Box 80260, Jeddah 21589, Saudi Arabia*
[2]*Pharmacy Program, Batterjee Medical College, P.O. Box 6231, Jeddah 21442, Saudi Arabia*
[3]*Faculty of Physical Therapy, Cairo University, Cairo, Egypt*
[4]*Department of Medicine and Infectious Diseases, Faculty of Veterinary Medicine, Cairo University, Giza 12211, Egypt*
[5]*Department of Biology, College of Science, Princess Nourah bint Abdulrahman University, P.O. Box 84428, Riyadh 11671, Saudi Arabia*
[6]*Department of Clinical Nutrition, Faculty of Applied Medical Sciences, Umm Al-Qura University, P.O. Box 7067, Makkah 21955, Saudi Arabia*
[7]*Department of Pharmaceutical Sciences, Pharmacy Program, Batterjee Medical College, P.O. Box 6231, Jeddah 21442, Saudi Arabia*
[8]*Pharmacology Department, Faculty of Veterinary Medicine, Suez Canal University, Ismailia 41522, Egypt*

Correspondence should be addressed to Ahmed E. Altyar; aealtyar@kau.edu.sa and Mohamed M. Abdel-Daim; abdeldaim.m@vet.suez.edu.eg

Received 13 August 2022; Accepted 19 September 2022; Published 22 February 2023

Academic Editor: Salah M. El Sayed

Microcystin-leucine-arginine (MCLR) is the most abundant cyanotoxin produced by cyanobacteria. It induces potent cytotoxicity through oxidative stress and DNA damage. Thymoquinone (TQ) is a natural nutraceutical antioxidant derived from black cumin (Nigella sativa). Physical exercise (EX) improves whole-body metabolic homeostasis. Therefore, this study examined the protective role of swimming exercise and TQ against MC-induced toxicity in mice. Fifty-six healthy adult male albino mice (25–30 g) were randomized into seven groups; group (I) was the negative control and received oral physiological saline for 21 days; group (II) received water EX for 30 min daily; group (III) was intraperitoneally injected with TQ (5 mg/kg daily, for 21 days); group (IV) was intraperitoneally administered MC (10 μg/kg daily, for 14 days) and acted as the positive toxic control; group (V) was treated with MC and water EX; group (VI) was injected with MC and TQ; finally, group (VII) was treated with MC with TQ and water EX. In comparison with the control group, the results showed hepatic, renal, and cardiac toxicity in the MCLR-treated group, indicated by a significant increase ($p < 0.05$) in serum levels of alkaline phosphatase (ALP), aspartate aminotransferase (AST), alanine transferase (ALT), cholesterol, lactate dehydrogenase (LDH), creatine kinase (CK), creatine kinase-myocardial band (CK-MB), urea, creatinine, interleukin-6, interleukin -1β, and tumor necrosis factor-α levels. In addition, there were significant elevations ($p < 0.05$) in malondialdehyde (MDA) and nitric oxide (NO) levels and a significant decrease in reduced glutathione (GSH), glutathione peroxidase (GPx), catalase (CAT), and superoxide dismutase (SOD) in hepatic, cardiac, and renal tissues. Treatment with either TQ or water EX significantly improved ($p < 0.05$) the MC-induced toxicity with superiority of the TQ group in the restoration of normal ranges; however, cotreatment with both TQ and swimming EX showed the most improvement and restoration to normal ranges as a result of increasing EX clinical efficacy by TQ.

1. Introduction

Microcystin (MCs) is a cyclic heptapeptide compound produced by species of *Microcystis* in fresh water and is considered the largest class of cyanotoxins [1]. Exposure to MCs has been proven to result in various adverse health outcomes in animals and humans through cytotoxicity induction. Microcystin-LR (MCLR) is the most toxic variant among the microcystin group. MCLR has a chemically stable formula with multiple routes of exposure, including inhalation, ingestion, or dermal contact with toxin-contaminated waters [2]. One milligram per liter (mg/L) of MC was the recommended limit by the World Health Organization (WHO) in 2020. However, this limit has been exceeded in many aquatic bodies [3]. MC toxicity has grown to be a significant global health issue. Wei et al. reported that MC pollution had been found in various lakes and reservoirs in the waters of 15 Chinese cities. The maximum mean MC concentrations for lakes were reported in Taihu Lake (1.00 μg/L) and Dianchi Lake (23.06 μg/L). For reservoirs, the maximum mean MC concentrations were measured in Yanghe Reservoir (0.98 μg/L) and Guanting Reservoir (4.31 μg/L) [4]. MCLR affects the structure and function of the liver, kidney, brain, and thyroid gland in animals through inhibition of both protein serine/threonine phosphatases-1 and 2A [5–7]; This causes the hyperphosphorylation of proteins, which alters the cytoskeleton causing cell disruption, including cell lysis. Additionally, MCLR induces oxidative stress, which triggers apoptosis, pyroptosis, and tumor promotion [8–11]. Oxidative stress is the imbalance between the synthesis and removal of reactive oxygen species (ROS) that is frequently characterized by alterations in lactate dehydrogenase leakage, lipid peroxidation, and GSH depletion [12].

MCLR exposure at high doses decreases the antioxidant enzyme activities and is accompanied by increased lipid peroxidation. The increased ROS production associated with MCLR toxicity exceeds the capacity of the antioxidant system, which leads to oxidative stress and dysfunction [13]. Antioxidants have a role in decreasing oxidative stress associated with microcystins toxicity. Several studies investigated many antioxidants as protective agents, including piperine, vitamin E, silymarin, or GSH [12, 14, 15]. Moreover, pretreatment with oral antioxidants, including vitamin C or vitamin E, reduced ROS generation and liver injury [16]. However, the exact protection mechanisms from MC-induced toxicity remain questionable. Accordingly, investigating novel antioxidants that offer a high protection level against MC would significantly influence animal and human health.

Thymoquinone (TQ) (2-isopropyl-5-methyl-1,4-benzoquinone) is the principal active component (30% to 48%) of *Nigella* sativa (black cumin) seeds essential oil. TQ has therapeutic effects as anti-inflammatory properties reported in *in-vivo* and *in-vitro* studies [17, 18], in addition to antioxidant properties represented through scavenging ROS and preventing cell damage by various pro-oxidants [19, 20]. TQ's antioxidant properties account for the majority of its health advantages. TQ was reported to decrease oxidative damage in hepatocytes by reducing enzyme activities, including SOD, CAT, and GSH-Px [19, 21, 22].

Regular exercise is a promising nonpharmacological therapeutic strategy impacting mitochondrial metabolism and intracellular signaling processes to enhance renal and hepatic antioxidant activity [23]. Many preclinical and clinical studies have proved the importance of physical activity and exercise training in metabolic improvement. The oxidative stress and inflammatory condition are affected by exercise positively and negatively depending on the exercise type; aerobic (e.g., walking, swimming, cycling, and running) and resistance training are the two main types of exercise [24–28]. Regular aerobic exercise induces adaptations that occur at cellular as well as systemic levels. Aerobic exercise improves the cardiovascular system, significantly lowers ROS, and enhances antioxidant enzyme expression in organs such as the liver, heart, kidney, and brain [24, 25]. Aerobic exercise increases oxygen consumption, affecting the oxidant/antioxidant status [28]. It also helps improve hepatic mitochondrial function, increase fat utilization, and reduce hepatic steatosis [26, 29]. Although exercise's proven antioxidant activity, skeletal muscle is the primary source of ROS during contraction due to the increased metabolic and physical demands associated with exercise. Accordingly, we hypothesize that TQ may improve aerobic exercise's anti-inflammatory and antioxidant efficacy by enhancing its clinical effectiveness and reducing exercise-induced oxidative stress. According to our search, no reports have been published on the effects of TQ and swimming exercises against MCLR toxicity. The current study aimed to evaluate the protective effects of TQ, aerobic swimming exercise, and their combination against MC-oxidative injury in the kidney, liver, and heart tissue.

2. Materials and Methods

2.1. Chemicals. Microcystin -LR; (CAS No 101043-37-2, molecular weight 995.189 g/mol; purity ≥ 98.5%) and TQ-(2-isopropyl-5-methylbenzo-1,4-quinone, CAS № 490-91-5, molecular weight 2164.204 g/mol; purity ≥ 98.5%) were purchased from Sigma–Aldrich (Saint Louis, MO, USA). Biochemical kits used were procured from the Laboratory Bio Diagnostics Company (Cairo, Egypt), except for lactate dehydrogenase (LDH) kits obtained from (Randox Laboratories Ltd., UK). Interleukin-1β (IL-1β) and interleukin-6 (IL-6) were purchased from Glory Science Co. Ltd. (Del Rio, TX, USA), and tumor necrosis factor-α (TNF-α) was obtained from Bio Source International Inc. (Camarillo, CA, USA) for inflammatory reaction assessment.

2.2. Animals. Fifty-six healthy male albino mice, weighing 25–30 g, were kept in wire-mesh metallic cages and housed using controlled conditions, temperature (25±2°C) with 12 h light/ dark cycle. They were acclimatized to the surrounding conditions for seven days before the study, and water and

food were served ad libitum. The Institutional Animal Care and Use Committee, Faculty of Science, Cairo University, Egypt, revised and approved the study protocols and mice investigations. All experimental procedures, sampling methods, animal dealing, and scarification occurred according to international guidelines for the use and care of experimental animals.

2.3. Experimental Groups and Design. Animals were equally distributed into seven experimental groups ($n = 8$/group).

Group I(control): animals were given oral physiological saline. Group II: animals (water exercise group) [27] training program consisted of swimming for 30 min daily in (30 x30 × 40 cm) filled tank using warm water with 25 cm depth to inhibit the mice from supporting themselves using tails touching the bottom of the tank. Group III (TQ group): animals were given thymoquinone (5 mg/kg BW/day for 21 days i.p; Talib (2017)) [30]. Group IV (MCLR group): animals received microcystin(10 μg/kg BW/day, i.p) [31] for 14 days, followed by distilled water for the rest of seven days. Group V (MCIR-TQ): animals were given TQ alone for seven days, followed by TQ and MCIR simultaneously for the rest of 14 days. Group VI (MCIR-swimming Ex): animals trained with the same swimming exercise regimen for seven days, followed by MCLR and swimming exercise for the rest of 14 days. Group VII (MCIR-TQ-swimming EX): animals had TQ and exercise program for seven days, then received MCIR-TQ and swimming exercise for the remaining 14 days.

2.4. Blood Sampling and Tissue Preparation. Twenty-four hours after the last treatment, the animals of all groups were euthanized using an overdose of sodium pentobarbital then blood samples were gathered through heart puncture. The collected samples were left for clotting, then centrifuged at 1200 g for 10 min and stored at −20°C until the assessment of the biochemical parameters. Hearts, kidneys, and livers were excised and homogenized using ice-cold 0.2 M Tris-HCl buffer, pH 7.4, followed by refrigerated centrifugation at 10,000 × g. (4°C), the resulting supernatant was collected and stored at −80°C to determine oxidative cascade markers within the tissue.

2.5. Serum Biochemical Assay. Serum hepatic and renal specific markers were estimated as aspartate transferase (AST), serum alanine transferase (ALT) using Reitman and Frankel [32] method, alkaline phosphatase (ALP) was measured using the technique of Tietz et al. [33], while serum cholesterol and lactate dehydrogenase (LDH) levels were estimated using the method of Babson and Babson; Allain et al. [34, 35]. Moreover, urea and creatinine levels were calculated using the techniques described by Coulombe and Favreau; Larsen [36, 37], respectively. Proinflammatory cytokines, IL-1β, IL-6, and TNF-α, were evaluated using a commercially available ELISAs Kit according to the manufacturer's instructions; absorbance values are determined using an automated ELISA reader at 450 nm. Creatine Kinase (CK) was evaluated according to the method developed by Szasz et al. [38]. While CK-MB was measured according to Wurzburg et al. [39].

2.6. Lipid Peroxidation and Antioxidant Assays. Assessment of lipid peroxidation biomarker malondialdehyde (MDA) was made in hepatic, renal, and cardiac tissue according to Uchiyama and Mihara [40] and nitric oxide (NO) concentration according to the method of Green et al. [41] to indicate the oxidant/antioxidant status in addition to measuring the tissue level of GSH using Beutler et al. [42] method, glutathione peroxidase (GSH-PX) using Paglia and Valentine [43], catalase (CAT) using Aebi [44], and superoxide dismutase (SOD) using Nishikimi et al. method [45].

2.7. Data Analysis. Data were statistically reported in terms of mean and standard deviation (SD). The normality of data was checked using Shapiro–Wilk's test and for homogeneity using Levene's test, then, compared using the one-way analysis of variance (ANOVA) test with Tukey's test for the significance of difference evaluation between means. p values less than 0.05 was considered statistically significant. The computer program IBM SPSS Statistical Package for the Social Science was used in all statistical calculations; IBM Corp, Armonk, NY, USA version 22 for Microsoft Windows.

3. Results

3.1. Serum Biochemical Analysis. Compared to the control group, the MCLR-intoxicated group presented significant elevation ($p < 0.05$) in serum concentrations of hepatic ALT (143%), AST (119%), ALP (125%), renal urea (136%), and creatinine biomarkers (1236%), in addition to elevation of serum LDH (70%), cholesterol (130%), CK (178%), CK-MB (313%) (Table 1), IL-1β (271%), IL-6 (268%), and TNF-α (by 265%) (Figure 1).

MCLR-intoxicated group with TQ, swimming exercise, or both presented improvement in all serum biochemical changes by presenting a significant decrease in ALT by 35%, 32%, and 54.9%, respectively; AST by 41%, 22%, and 48%, respectively; ALP by 37%,30%, and 52%, respectively; renal urea by 41%,28%, and 54%, respectively; and creatinine biomarkers by 58%, 48%, and 85%, respectively, in addition to elevation of serum LDH by 24.6%, 21.3%, and 37.9%, respectively; cholesterol by 32.6%, 24.6%, and 53.8%, respectively; CK by 44%,40%, and 60, respectively; CK-MB by 51%, 45%, and 73%, respectively; (Table 1), IL-1β by 50%, 47%, and 69%, respectively; IL-6 (by 51%, 44%, and 67%, respectively; and TNF-α by 56%, 48%, and 70%, respectively, MCLR-treated group with TQ showed more improvement compared to MCLR-treated group with exercise. Treatment of the MCLR-intoxicated group with TQ and swimming exercise had more restoration of normal control ranges with an insignificant difference($p > 0.05$) with the control group in all serum biochemical changes.

Table 1: The biochemical effects of thymoquinone (TQ 5 mg/kg BW once daily for 21 days orally) and water exercise for 30 min daily during microcystin treatment (10 μg/kg BW/day for 14 days) on serum hepatorenal function biomarkers.

	Control	EX Group	TQ Group	MCLR Group	MCLR-EX Group	MCLR-TQ Group	MCLR-TQ-EX Group
AST (U/L)	43.1 ± 4.5(a)	40.2 ± 5.1(a)	40.1 ± 4.8(a)	94.2 ± 9.3(b)	73.2 ± 11.6(c)	55.4 ± 6.8(d)	48.9 ± 2.5(ad)
ALT (U/L)	24.9 ± 2.9(a)	23.7 ± 2.0(a)	23.7 ± 1.9(a)	60.6 ± 7.3(b)	41.2 ± 4.0(c)	39.2 ± 4.0(c)	27.3 ± 5.3(a)
ALP (U/L)	67.6 ± 6.3(a)	62.2 ± 6.6(a)	62.2 ± 6.6(a)	152.3 ± 13.9(b)	106.6 ± 11.5(c)	95.7 ± 10.3(c)	73.4 ± 15.9(a)
Cholesterol (mg/dl)	106.2 ± 9.3(a)	105.0 ± 8.8(a)	100.7 ± 9.5(a)	243.8 ± 22.0(b)	184.1 ± 11.6(c)	164.1 ± 11.6(c)	112.6 ± 13.5(a)
LDH (U/L)	214.8 ± 29.1(a)	211.5 ± 29.6(a)	205.3 ± 29.6(a)	364.6 ± 41.9(b)	286.8 ± 27.6(c)	274.5 ± 27.3(c)	226.3 ± 17.1(a)
CK (U/L)	106.2 ± 14.5(a)	103.4 ± 18.9(a)	101.7 ± 17.0(a)	295.6 ± 20.2(b)	177.7 ± 12.7(c)	164.8 ± 9.5(c)	118.5 ± 13.2(a)
CK-MB (U/L)	35.5 ± 4.5(a)	34.4 ± 6.6(a)	33.9 ± 6.1(a)	146.5 ± 6.8(b)	80.2 ± 6.7(c)	71.3 ± 3.4(d)	40.3 ± 4.9(a)
Urea (mg/dl)	28.6 ± 3.5(a)	27.9 ± 3.3(a)	26.9 ± 3.3(a)	67.4 ± 6.5(b)	48.6 ± 7.5(c)	40.1 ± 7.5(d)	30.9 ± 3.7(a)
Creatinine (mg/dl)	0.3 ± 0.1(a)	0.2 ± 0.1(a)	0.3 ± 0.1(a)	3.6 ± 0.5(b)	1.9 ± 0.2(c)	1.5 ± 0.2(d)	0.5 ± 0.1(a)

Values are presented as means ± SD ($n = 8$), and different superscripts show significant differences ($p < 0.05$) between groups. ALT: alanine transferase; AST: aspartate transferase; ALP: alkaline phosphatase; LDH: lactate dehydrogenase; CK: creatine kinase.

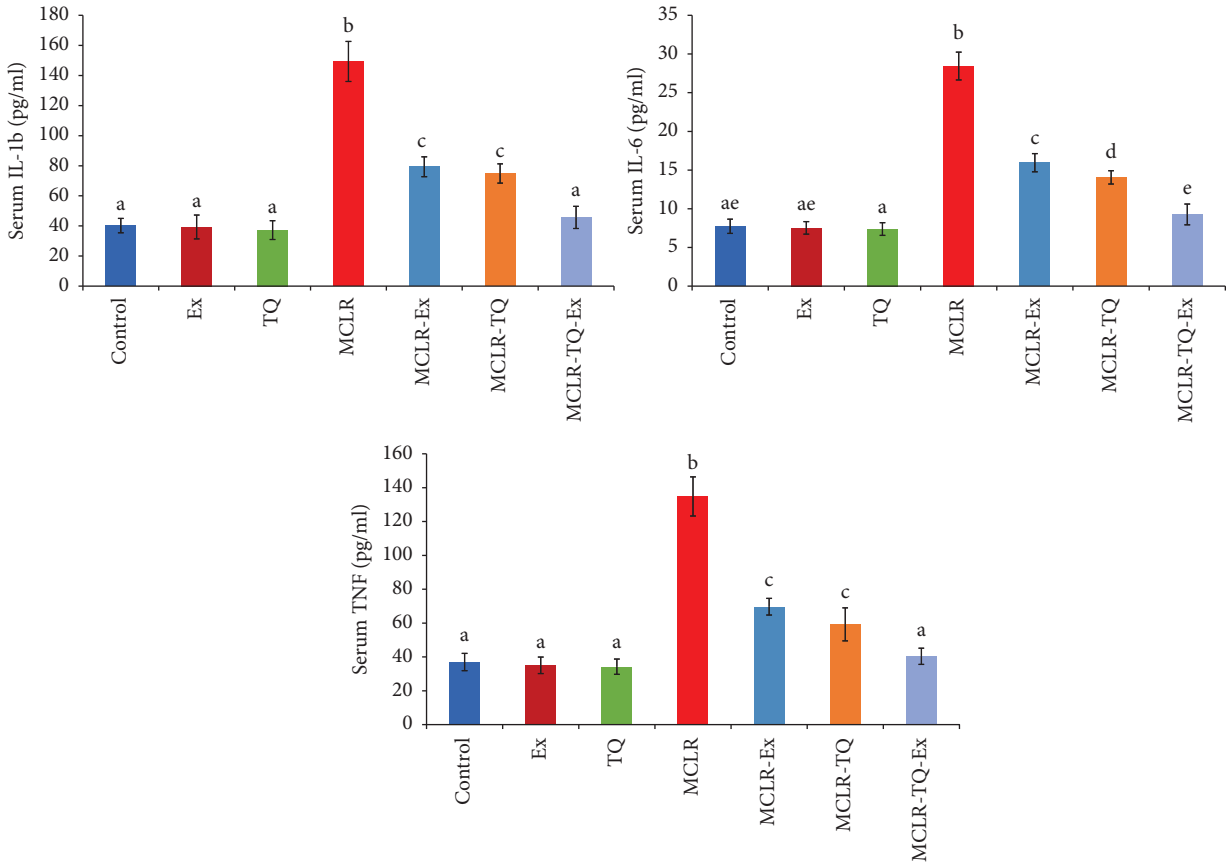

Figure 1: The biochemical effects of swimming exercise and thymoquinone (5 mg/kg BW) against microcystin-LR (10 μg/kg BW/day) on inflammatory markers, Columns (means ± SD) with different superscripts show significant differences ($p < 0.05$) between groups.

3.2. Antioxidant Activity in the Hepatic Tissue. Compared to the control group, the MCLR-intoxicated group exhibited a significant decrease ($p < 0.05$) in hepatic tissue concentrations of GSH by 54%, GSH-PX by 72%, SOD by 72%, and CAT by 70%. Moreover, MDA and NO concentrations in the hepatic tissue were significantly increased ($p < 0.05$) after MCLR- intoxication (by 117% and 138%), respectively. Treatment of MCLR-intoxicated group by TQ, swimming exercise, or both was associated with a significant decrease in MDA by 22.9%, 15.5%, and 50.9%, respectively, and NO by 32%, 25%, and 54%, respectively; when compared to the MCLR group. While there is a significant increase observed in the MCLR-treated groups by TQ, swimming exercise, or both in GSH concentration by 77%, 62.6%, and 110%, respectively, in addition to the antioxidant enzymes activities (GSH-PX by 162%, 146.6%, and 321%, SOD by 141%, 118%, and 200%, and CAT by 130%, 107%, and 215%, respectively) compared to MCLR-treated group, improving these parameters to the normal ranges (Figure 2).

3.3. Antioxidant Activity in the Renal Tissue. The MCLR-intoxicated group expressed a significant increase ($p < 0.05$) in renal tissue MDA and NO concentrations (by 147% and 133%, respectively) compared to the normal group. At the same time, there were significant drops in renal tissue GSH concentrations and activities of GSH-PX, SOD, and CAT by 53%, 65%, 56%, and 70%, respectively, compared to the control group. Treatment of MCLR-intoxicated groups with TQ or swimming exercise significantly reduced MDA and NO concentrations (MCLR-TQ: 33.5%, 32.4% and MCLR-swimming exercise: 27.9%, and 16.18%, respectively) and increased GSH concentrations and activities of GSH-PX, SOD, and CAT (MCLR-TQ: 69%, 93%, 78%, 105% and MCLR-swimming exercise: 49.8%, 55%, 44.6%, and 77%, respectively) in comparison to MCLR group. A combination of TQ and swimming exercise expressed more improvement in the renal antioxidant status of MCLR-intoxicated groups, where there was a reduction in MDA and NO by 56.7% and 54.8%, respectively, and elevations in GSH, GSH-PX, SOD, and CAT by 97%, 163%, 111%, and 169%, respectively, when compared to the MCLR group (Figure 3).

3.4. Antioxidant Activity in the Cardiac Tissue. Microcystin intoxication triggers oxidative damage in the heart, expressed in a significant elevation ($p < 0.05$) in MDA and NO concentrations by 88% and 132%, respectively, and drops in GSH, GSH-PX, SOD, and CAT by 60%, 54%, 62%, and 64%, respectively, in comparison to the normal group. Moreover, treatment of MCLR-intoxicated group with TQ or swimming exercise improved the MC-LR- induced cardiac oxidative damage by significant reductions ($p < 0.05$) in MDA by 21.9%, and

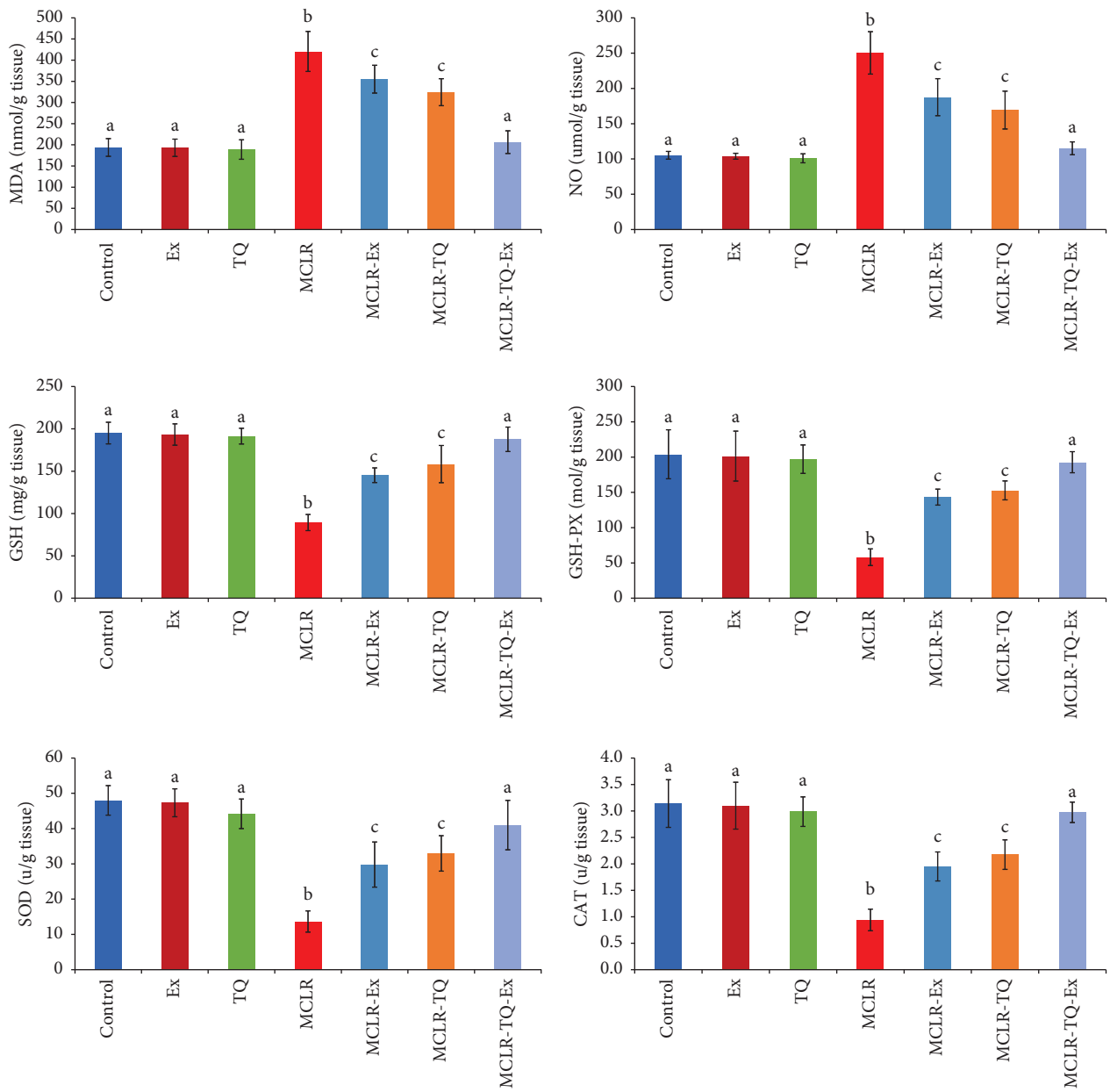

Figure 2: The protective effects of swimming exercise and thymoquinone (5 mg/kg BW) against microcystin-LR (10 μg/kg BW/day) on hepatic tissue MDA malondialdehyde, NO nitric oxide, GSH reduced glutathione, GSH-PX glutathione peroxidase, and SOD superoxide dismutase, CAT catalase. Columns (means ± SD) with different superscripts show significant differences ($p < 0.05$) between groups.

16.7%, respectively, and NO by 36.6%, and 31.26%, respectively, and elevation in GSH levels, GSH-PX, SOD, and CAT (MCLR-TQ: 59%, 79.8%, 88%, and 119.8%, respectively, and MCLR-swimming exercise: 36.9%, 50%, 66%, and 105.6%, respectively) compared to MCLR-intoxicated rats. The treatment combination of TQ and swimming exercise improved the induced cardiac oxidative stress more than every single treatment, expressed by decreasing cardiac MDA and NO (by 35.7% and 50.7%) and increasing cardiac GSH, GSH-PX, SOD, and CAT by 157.7%, 113.4%, 150%, and 165%, respectively compared to the MCLR-intoxicated group (Figure 4).

4. Discussion

In the current study, we examined the anti-inflammatory and antioxidant properties of TQ alone or combined with swimming exercise against MCLR-induced oxidative

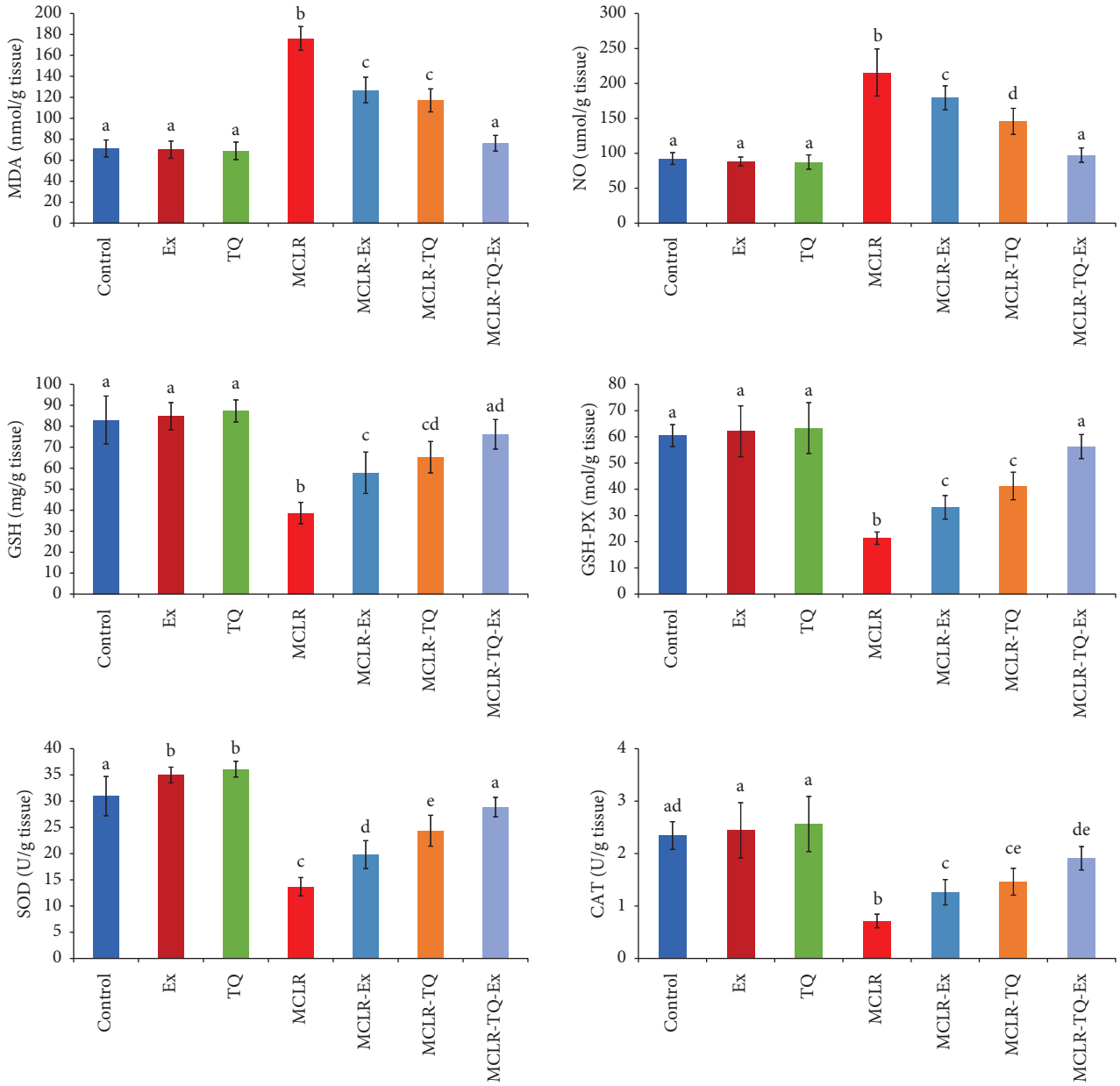

Figure 3: The protective effects of swimming exercise and thymoquinone (5 mg/kg BW) against microcystin-LR (10 μg/kg BW/day) on renal tissue MDA malondialdehyde, NO nitric oxide, GSH reduced glutathione, GSH-PX glutathione peroxidase, SOD superoxide dismutase, and CAT catalase. Columns (means ± SD) with different superscripts show significant differences ($p < 0.05$) between groups.

damage in hepatic, renal, and cardiac tissues. Our data presented MC-induced hepatotoxicity, nephrotoxicity, and cardiotoxicity indicated by significantly elevated serum AST, ALT, ALP, LDH, CK, and CK-MB enzyme activities. Moreover, cholesterol, urea, and creatinine were elevated. In addition to oxidative stress, significant increases in MDA and NO levels are observed with the depletion of cellular antioxidants in the liver, kidney, and heart tissues.

The microcystins are the most abundant toxins found in fresh water, causing hepatorenal injuries as potent acute hepatotoxicity due to inhibition of serine/threonine protein phosphatases (PPs) as PP1 and PP2A 1 through strong covalent bond formation leading to excessive phosphorylation to many cellular proteins, cytoskeleton alterations and loss of integrity. Significant negative impact on cell homeostasis resulted from uncontrolled PPs inhibition and kinases hindering the balance of protein phosphorylation/dephosphorylation, leading to overflow of liver marker enzymes into blood and elevation of ALT, AST, and ALP levels [12, 46, 47]. Our results were in accordance with the data of previous studies [15, 46, 48].

Despite the robust defense system, an increase in the formation of ROS or a reduction in the antioxidant capacity can result in gradual cell damage and a deterioration in physiological performance. The homeostatic balance is interrupted, in addition to shifting the redox state toward

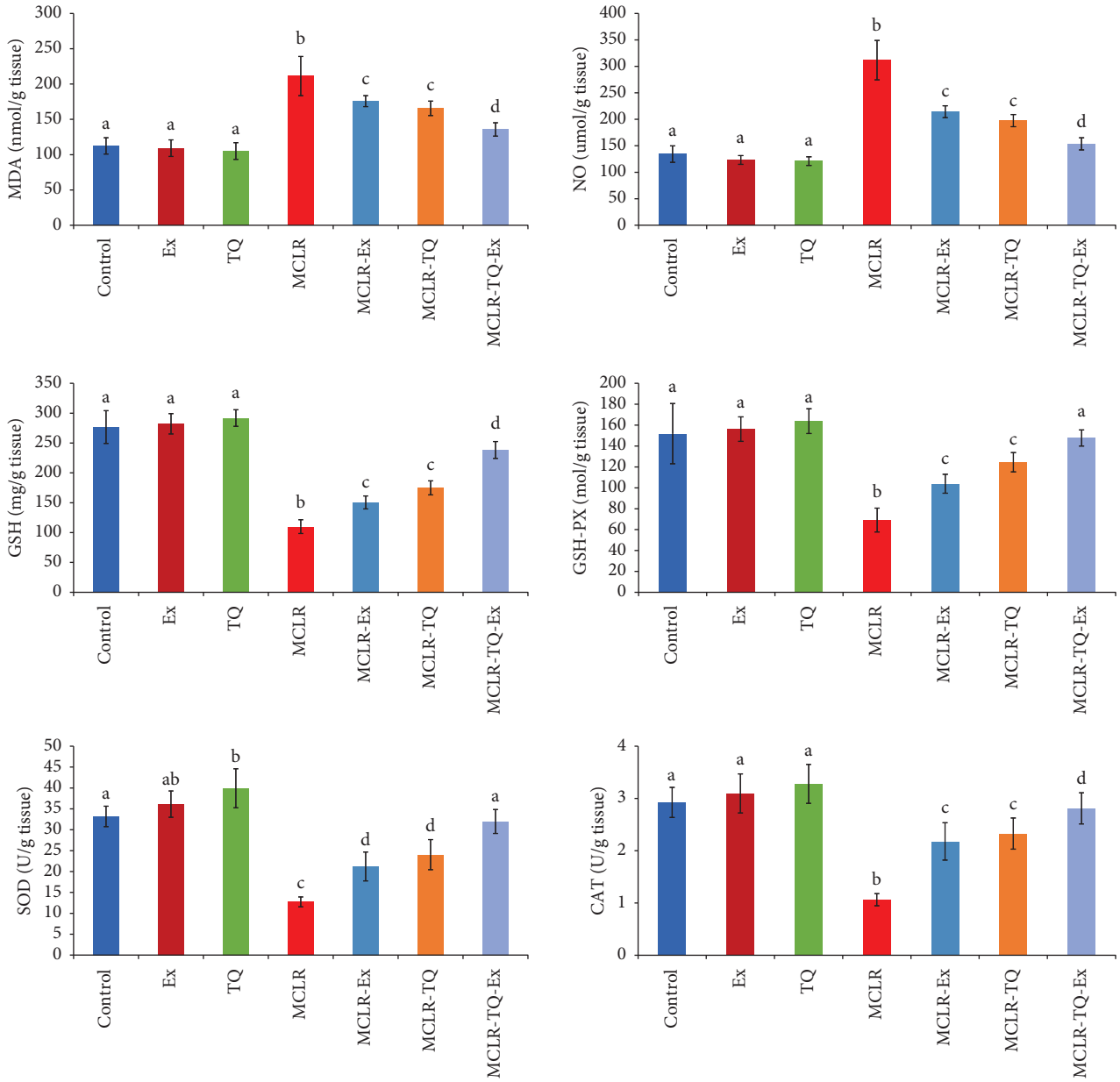

Figure 4: The protective effects of swimming exercise and thymoquinone (5 mg/kg BW) against microcystin-LR (10 μg/kg BW/day) on cardiac tissue MDA malondialdehyde, NO nitric oxide, GSH reduced glutathione, GSH-PX glutathione peroxidase, SOD superoxide dismutase, and CAT catalase. Columns (means ± SD) with different superscripts show significant differences ($p < 0.05$) between groups.

more pro-oxidizing when the oxidant capacity exceeds the antioxidant capacity.

The main function of antioxidant defensive systems is to counter the effect of reactive species through nonenzymatic and enzymatic addition to dietary antioxidants. Glutathione, uric acid, bilirubin, coenzyme Q10, and lipoic acid are nonenzymatic antioxidant agents that originate from endogenous sources and are frequently by-products of cellular metabolism. At the same time, the main enzymatic antioxidants are glutathione peroxidase (GPX), superoxide dismutase (SOD), and catalase.

Similar to the findings of Lowe et al. [48], there is a significant deterioration in renal physiological parameters expressed as elevation of urea and creatinine in the MCLR-treated group; they reported an increase in glomerular filtration rate, proteinuria, renal index, and sodium excretion in addition to the structural changes in renal tissue. Several studies have linked MC-induced hepatotoxicity to the high affinity of MCLR to form strong covalent bonds with hepatic serine/threonine-specific PPs leading to their inhibition. In addition, we observed a significant increase in serum cholesterol and LDH levels, which may be due to the MCLR-induced hepatic injury.

Inhibition of protein phosphatases caused by MCLR leads to overphosphorylation of many proteins associated with hepatic, renal, and cardiac oxidative injuries. It raises

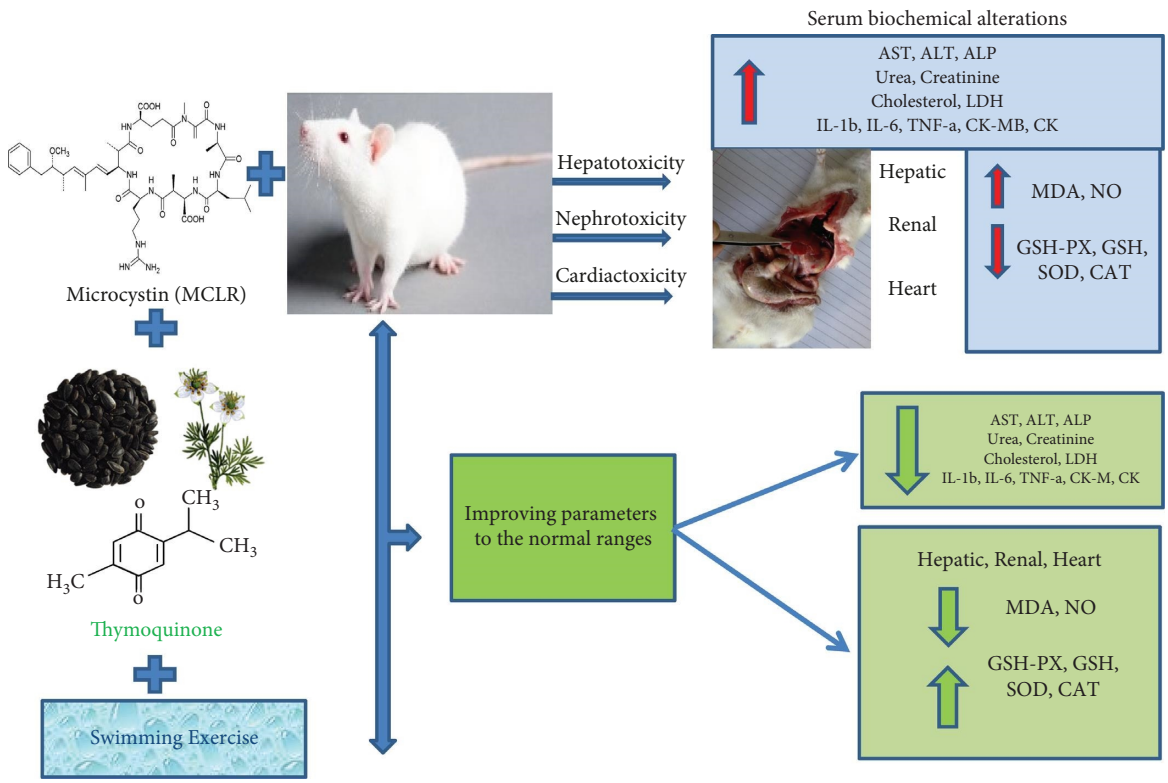

Figure 5: A summary figure for the protective effects of swimming exercise and thymoquinone (5 mg/kg BW) against microcystin-LR(10 μg/kg BW/day).

the intracellular lipid peroxidation, producing the oxidation products that represent the cornerstone of oxidative signaling. MC-induced oxidative stress is expressed as an increase in the production of ROS, such as O2•−, H2O2, and OH•. This overproduction indicates a disturbance in the body's normal redox state, leading to cellular lipids injury, ATP reduction, DNA oxidative damage, and mitochondrial dysfunction [46, 47].

By the findings of Abdel-Daim et al. [15], we observed a significant elevation in MDA and NO levels and a significant reduction in antioxidant enzymes, such as GSH, GPx, SOD, and CAT, acting as defense mechanisms through hydrolysis of H_2O_2 into H_2O. The depletion of antioxidant enzymes could be explained by overutilization in overcoming free radicals produced during MC metabolism.

The present study reported a significant elevation in IL-1β, IL-6, and TNF- α. These findings were in agreement with Cao et al., who noted that MCLR low dose concentration stimulates the production of the proinflammatory factors mRNA of TNF-α, IL-1β, and IL-6 [49]. However, as a result of a high dose, in addition to the prolonged stress of MCLR, the mice's immune systems are severely damaged, and cell secretion of inflammatory factors deteriorates as a result of its apoptosis or necrosis [50].

Our data revealed that TQ and exercise reduce oxidative injuries and improve biochemical alterations induced by MCLR. TQ action may be an antioxidant agent that prevents the peroxidation of membrane lipids in hepatic cells through acting as general free radical scavengers, ROS due to MC toxicity, attacks cellular membrane lipids resulting from lipid peroxidation leading to MDA level elevation as the final product of lipid peroxidation. It acts as an index indicating lipid peroxidation. In our study, the height of MDA in hepatic, renal, and cardiac tissues has ameliorated after the mice's exposure to TQ and exercise.

The effects of one bout of exercise and regular physical activity are dissimilar in cell adaptation to the elevated ROS production to be more resistant to the negative impact of oxidative stress. Regular physical activity has various advantages, and the body adapts to the increased oxidant levels; conversely, acute exercise increases only a minimal amount of adaptation [23, 24, 51]. Although skeletal muscle is relatively resistant to exercise-induced oxidative damage, it is clear that prolonged and/or intense exercise has negative effects. Antioxidant supplementation is widely used with high levels of physical activity. It has a role in preventing exercise-induced oxidative damage [52].

Several studies support a positive association between regular aerobic exercise and decreasing oxidative stress [24, 26, 53]. It has been reported that regular aerobic exercise causes an increase in maximal oxygen consumption (VO2max) and increases ROS production. However, if aerobic exercise intensities do not exceed 50% of VO2max, ROS production is decreased to the minimum values, as demonstrated in studies by Ashton et al. [54] or Chevron et al. [55]. These findings indicate that TQ and exercise are effective in lipid peroxidation prevention and the anti-inflammatory and immunomodulatory effects of TQ [56–58]. Our results

are in accordance with the conclusions of previous reports that investigated the antioxidant and anti-inflammatory effects of TQ [15, 59]. In our study, the swimming exercise was effective against MC-induced metabolic changes. Exercise suppresses endotoxin-induced TNF-a through normalizing overexpression of TNF-a, and the exercise's anti-inflammatory effects protect against chronic systemic low-grade inflammation induced by toxicity [53, 60]. Our data are in accordance with those presented by Booth et al. [61], they showed beneficial results of physical exercise on the liver and kidneys.

Swimming exercise was associated with significant amelioration of MCLR-induced elevation of AST, ALP, and ALT, in addition to reducing the circulating levels of proinflammatory cytokines in intoxicated mice [62]. The combined therapy of TQ with swimming exercise elicited beneficial effects and restored all parameters to normal ranges more than each treatment. Regarding the hepatic and renal function markers, the cotherapy was effectual in returning plasma activities of AST, ALT, ALP, urea, and creatinine to normal levels. Our proposed mechanism for improving and restoring normal levels in this study is referred to improve lipid peroxidation of TQ in addition to anti-inflammatory and immunomodulatory effects and to enhance cellular antioxidant defense mechanisms by TQ and exercise.

Treatment with exercise or TQ reduced the MC-induced hepatotoxicity, renal toxicity, and cardiotoxicity, indicated through improved oxidative/antioxidant state and attenuation of cytokines and the biochemical serum parameters (Figure 5).

5. Conclusion

The data from this study suggest that MC induces hepatic toxicity, renal toxicity, and cardiotoxicity by elevation of serum hepatic and renal biomarkers in addition to proinflammatory cytokines with the reflection of oxidative state disruption. Treatment with TQ or swimming exercise improved the MC-LR-induced hepatorenal and cardiac injuries in mice; a combination of both treatments showed more improvement than each treatment alone. This enhancement may be explained by improving the tissue's antioxidant defensive mechanisms.

Abbreviations

ALT: Alanine aminotransferase
ALP: Alkaline phosphatase
AST: Aspartate aminotransferase
CAT: Catalase
GSH: Reduced glutathione
GSH-Px: Glutathione peroxidase
IL-1β: Interleukin-1β
IL-6: Interleukin-6
LDH: Lactate dehydrogenase
MDA: Malondialdehyde
SOD: Superoxide dismutase
TNF-α: Tumor necrosis factor-α
TQ: Thymoquinone
MCLR: Microcystin-LR
EX: Exercise.

Data Availability

The data used to support the findings of this study are available from the corresponding author upon reasonable request.

Conflicts of Interest

The authors declare that there are no conflicts of interest.

Authors' Contributions

MMA-D and AA conceived the original idea and designed the experiment. MMA-D, AA, MK, GA, and OAK conducted the experiments. AHB, AA, MK, GA, and OAK wrote the draft of the manuscript. AHB, AA, and MMA-D analyzed the data and prepared the figures and tables of the manuscript. AA, AHB, and MMA-D performed the literature review, provided critical feedback, and revised the manuscript. All listed authors contributed to the article and approved the manuscript submission.

Acknowledgments

This research was supported by Princess Nourah bint Abdulrahman University Researchers Supporting Project number: (PNURSP2023R30), Princess Nourah bint Abdulrahman University, Riyadh, Saudi Arabia.

References

[1] D. Dietrich and S. Hoeger, "Guidance values for microcystins in water and cyanobacterial supplement products (blue-green algal supplements): a reasonable or misguided approach," *Toxicology and Applied Pharmacology*, vol. 203, no. 3, pp. 273–289, 2005.

[2] J. Patocka, "The toxins of Cyanobacteria," *Acta medica*, vol. 44, pp. 69–75, 2001.

[3] World Health Organization, "Cyanobacterial Toxins: Microcystins. Background Document for Development of WHO Guidelines for Drinking-Water Quality and Guidelines for Safe Recreational Water Environments," 2020.

[4] H. Wei, Y. Jia, and Z. Wang, "Microcystin pollution in lakes and reservoirs: A nationwide meta-analysis and assessment in China," *Environ Pollut*, vol. 309, Article ID 119791, 2022.

[5] Q. Wu, W. Yan, C. Liu et al., "Microcystin-LR exposure induces developmental neurotoxicity in zebrafish embryo," *Environmental Pollution*, vol. 213, pp. 793–800, 2016.

[6] J. Liu and Y. Sun, "The role of PP2A-associated proteins and signal pathways in microcystin-LR toxicity," *Toxicology Letters*, vol. 236, no. 1, pp. 1–7, 2015.

[7] Y. Zhao, Q. Xue, X. Su, L. Xie, Y. Yan, and A. D. Steinman, "Microcystin-LR induced thyroid dysfunction and metabolic disorders in mice," *Toxicology*, vol. 328, pp. 135–141, 2015.

[8] I. Mrdjen, J. Lee, C. M. Weghorst, and T. J. Knobloch, "Impact of cyanotoxin ingestion on liver cancer development using an at-risktwo-staged model of mouse hepatocarcinogenesis," *Toxins*, vol. 14, no. 7, p. 484, 2022.

[9] M. Puerto, S. Pichardo, and Á Jos, "Differential oxidative stress responses to pure Microcystin-LR and Microcystin-containing and non-containing cyanobacterial crude extracts on Caco-2 cells," *Toxicon*, vol. 55, pp. 514–522, 2010.

[10] G. Meng, J. Liu, S. Lin, Z. Guo, and L. Xu, "Microcystin-LR-Caused ROS generation involved in p38 activation and tau hyperphosphorylation in neuroendocrine (PC12) cells," *Environmental Toxicology*, vol. 30, no. 3, pp. 366–374, 2015.

[11] A. Campos and V. Vasconcelos, "Molecular mechanisms of microcystin toxicity in animal cells," *International Journal of Molecular Sciences*, vol. 11, no. 1, pp. 268–287, 2010.

[12] W.-X. Ding and C. Nam Ong, "Role of oxidative stress and mitochondrial changes in cyanobacteria-induced apoptosis and hepatotoxicity," *FEMS Microbiology Letters*, vol. 220, pp. 1–7, 2003.

[13] A. Campos and V. Vasconcelos, "Molecular Mechanisms of Microcystin Toxicity in Animal Cells," *International Journal of Molecular Sciences*, vol. 8, 2010.

[14] K. A. Mereish, D. L. Bunner, D. R. C. D. Ragland, and D. A. Creasia, "Protection against microcystin-LR-induced hepatotoxicity by Silymarin: biochemistry, histopathology, and lethality," *Pharmaceutical Research*, vol. 8, no. 2, pp. 273–277, 1991.

[15] M. M. Abdel-daim, A. A. Sayed, and A. Abdeen, "Piperine Enhances the Antioxidant and Anti-inflammatory Activities of Thymoquinone against Microcystin-LR-Induced Hepatotoxicity and Neurotoxicity in Mice," 2019, https://www.hindawi.com/journals/omcl/2019/1309175/.

[16] D. Weng, Y. Lu, Y. Wei, Y. Liu, and P. Shen, "The role of ROS in microcystin-LR-induced hepatocyte apoptosis and liver injury in mice," *Toxicology*, vol. 232, no. 1-2, pp. 15–23, 2007.

[17] F. Vaillancourt, P. Silva, Q. Shi, H. Fahmi, J. C. Fernandes, and M. Benderdour, "Elucidation of molecular mechanisms underlying the protective effects of thymoquinone against rheumatoid arthritis," *Journal of Cellular Biochemistry*, vol. 112, no. 1, pp. 107–117, 2011.

[18] U. S. Topaloğlu, M. H. Sipahioğlu, and İ Güntürk, "Effects of Thymoquinone in Prevention of Experimental Contrast-Induced Nephropathy in Rats," 2019, https://pubmed.ncbi.nlm.nih.gov/32133061/.

[19] S. Darakhshan, A. Bidmeshki Pour, and A. Hosseinzadeh Colagar, "Thymoquinone and its therapeutic potentials," *Pharmacol Res*, vol. 95, 2015.

[20] R. B. Kassab and R. E. El-Hennamy, "The role of thymoquinone as a potent antioxidant in ameliorating the neurotoxic effect of sodium arsenate in female rats," 2017, http://linkinghub.elsevier.com/retrieve/pii/S2314808X17302312.

[21] A. Ragheb, A. Attia, and W. S. Eldin, "The protective effect of thymoquinone, an anti-oxidant and anti-inflammatory agent, against renal injury: a review," 2009, http://www.sjkdt.org/text.asp?2009/20/5/741/55356.

[22] O. A. Badary, R. A. Taha, A. M. Gamal El-Din, and M. H. Abdel-Wahab, "Thymoquinone is a potent superoxide anion scavenger," *Drug and Chemical Toxicology*, vol. 26, no. 2, pp. 87–98, 2003.

[23] J. C. Campos, K. M. S. Gomes, and J. C. B. Ferreira, "Impact of exercise training on redox signaling in cardiovascular diseases," *Food and Chemical Toxicology*, vol. 62, pp. 107–119, 2013.

[24] V. R. Muthusamy, S. Kannan, K. Sadhaasivam et al., "Acute exercise stress activates Nrf2/ARE signaling and promotes antioxidant mechanisms in the myocardium," *Free Radical Biology and Medicine*, vol. 52, no. 2, pp. 366–376, 2012.

[25] M. Cai, H. Wang, J. Li et al., "The signaling mechanisms of hippocampal endoplasmic reticulum stress affecting neuronal plasticity-related protein levels in high fat diet-induced obese rats and the regulation of aerobic exercise," *Brain, Behavior, and Immunity*, vol. 57, pp. 347–359, 2016.

[26] K. D. Kistler, E. M. Brunt, J. M. Clark, A. M. Diehl, J. F. Sallis, and J. B. Schwimmer, "Physical activity recommendations, exercise intensity, and histological severity of nonalcoholic fatty liver disease," *American Journal of Gastroenterology*, vol. 106, no. 3, pp. 460–468, 2011.

[27] M. H. Muhammad and M. M. Allam, "Resveratrol and/or exercise training counteract aging-associated decline of physical endurance in aged mice; targeting mitochondrial biogenesis and function," *The Journal of Physiological Sciences*, vol. 68, no. 5, pp. 681–688, 2018.

[28] C. A. Williams, "Horse species symposium: the effect of oxidative stress during exercise in the horse," *Journal of Animal Science*, vol. 94, no. 10, pp. 4067–4075, 2016.

[29] M. A. Linden, J. A. Fletcher, E. M. Morris et al., "Treating NAFLD in OLETF rats with vigorous-intensity interval exercise training," *Medicine & Science in Sports & Exercise*, vol. 47, no. 3, pp. 556–567, 2015.

[30] R. Bargi, F. Asgharzadeh, and F. Beheshti, "The effects of thymoquinone on hippocampal cytokine level, brain oxidative stress status and memory deficits induced by lipopolysaccharide in rats," *Cytokine*, vol. 96, pp. 173–184, 2017.

[31] Y. Lone, M. Bhide, and R. K. Koiri, "Amelioratory effect of coenzyme Q10 on potential human carcinogen Microcystin-LR induced toxicity in mice," *Food and Chemical Toxicology*, vol. 102, pp. 176–185, 2017.

[32] S. Reitman and S. Frankel, "A colorimetric method for the determination of serum glutamic oxalacetic and glutamic pyruvic transaminases," *American Journal of Clinical Pathology*, vol. 28, no. 1, pp. 56–63, 1957.

[33] N. W. Tietz, C. A. Burtis, P. Duncan et al., "A reference method for measurement of alkaline phosphatase activity in human serum," *Clinical Chemistry*, vol. 29, no. 5, pp. 751–761, 1983.

[34] C. C. Allain, L. S. Poon, C. S. G. Chan, W. Richmond, and P. C. Fu, "Enzymatic determination of total serum cholesterol," *Clinical Chemistry*, vol. 20, no. 4, pp. 470–475, 1974.

[35] A. L. Babson and S. R. Babson, "Kinetic colorimetric measurement of serum lactate dehydrogenase activity," *Clinical Chemistry*, vol. 19, no. 7, pp. 766–769, 1973.

[36] J. J. Coulombe and l Favreau, "A new simple semimicro method for colorimetric determination of urea," *Clinical Chemistry*, vol. 9, no. 1, pp. 102–108, 1963.

[37] K. Lausen, "Creatinine assay in the presence of protein with LKB 8600 reaction rate Analyser," *Clinica Chimica Acta*, vol. 38, no. 2, pp. 475-476, 1972.

[38] G. Szasz, J. Waldenström, and W. Gruber, "Creatine kinase in serum: 6. Inhibition by endogenous polyvalent cations, and effect of chelators on the activity and stability of some assay components," *Clinical Chemistry*, vol. 25, no. 3, pp. 446–452, 1979.

[39] U. Wurzburg, N. Hennrich, and H. Lang, "Determination of creatine kinase-MB in serum using inhibiting antibodies (author's transl)," *Klin Wochenschr*, vol. 54, pp. 357–360, 1976.

[40] M. Uchiyama and M. Mihara, "Determination of malonaldehyde precursor in tissues by thiobarbituric acid test," *Analytical Biochemistry*, vol. 86, no. 1, pp. 271–278, 1978.

[41] L. C. Green, D. A. Wagner, J. Glogowski, P. L. Skipper, J. S. Wishnok, and S. R. Tannenbaum, "Analysis of nitrate,

nitrite, and [15N]nitrate in biological fluids," *Analytical Biochemistry*, vol. 126, no. 1, pp. 131–138, 1982.

[42] E. Beutler, O. Duron, and B. Kelly, "Improved method for the determination of blood glutathione," *The Journal of Laboratory and Clinical Medicine*, vol. 61, pp. 882–888, 1963.

[43] D. E. Paglia and W. N. Valentine, "Studies on the quantitative and qualitative characterization of erythrocyte glutathione peroxidase," *The Journal of Laboratory and Clinical Medicine*, vol. 70, no. 1, pp. 158–169, 1967.

[44] H. Aebi, "Catalase in vitro," *Methods in Enzymology*, vol. 105, pp. 121–126, 1984.

[45] M. Nishikimi, N. Appaji Rao, and K. Yagi, "The occurrence of superoxide anion in the reaction of reduced phenazine methosulfate and molecular oxygen," *Biochemical and Biophysical Research Communications*, vol. 46, no. 2, pp. 849–854, 1972.

[46] H. Sies, C. Berndt, and D. P. Jones, "Oxidative stress," *Annual Review of Biochemistry*, vol. 86, no. 1, pp. 715–748, 2017.

[47] J. Cadet, S. Loft, R. Olinski et al., "Biologically relevant oxidants and terminology, classification and nomenclature of oxidatively generated damage to nucleobases and 2-deoxyribose in nucleic acids," *Free Radical Research*, vol. 46, no. 4, pp. 367–381, 2012.

[48] J. Lowe, J. Souza-Menezes, and D. S. Freire, "Toxicon Single sublethal dose of microcystin-LR is responsible for different alterations in biochemical, histological and physiological renal parameters," *Toxicon*, vol. 59, 2012.

[49] L. Cao, F. Huang, and I. Y. Massey, "E Ff Ects of Microcystin-LR on the Microstructure and Inflammation-Related Factors of Jejunum in Mice," 2019, https://www.ncbi.nlm.nih.gov/pmc/articles/PMC6783826/.

[50] C. Pan, Y. Chen, T. Xu, J. Wang, D. Li, and X Han, "Chronic exposure to microcystin-leucine-arginine promoted proliferation of prostate epithelial cells resulting in benign prostatic hyperplasia," *Environmental Pollution*, vol. 242, pp. 1535–1545, 2018.

[51] S. K. Powers, J. Duarte, A. N. Kavazis, and E. E Talbert, "Reactive oxygen species are signalling molecules for skeletal muscle adaptation," *Experimental Physiology*, vol. 95, no. 1, pp. 1–9, 2010.

[52] T.-T. Peternelj and J. S. Coombes, "Antioxidant supplementation during exercise training," *Sports Medicine*, vol. 41, no. 12, pp. 1043–1069, 2011.

[53] A. W. Marie Petersen and B. Klarlund Pedersen, "The anti-inflammatory effect of exercise Evidence for Anti-Inflammatory Effects of Exercise in CKD," *Journal of Applied Physiology*, vol. 1154, pp. 1154–1162, 2014.

[54] T. Ashton, C. C. Rowlands, E. Jones et al., "Electron spin resonance spectroscopic detection of oxygen-centred radicals in human serum following exhaustive exercise," *European Journal of Applied Physiology*, vol. 77, no. 6, pp. 498–502, 1998.

[55] S. Chevion, D. S. Moran, Y. Heled et al., "Plasma antioxidant status and cell injury after severe physical exercise," *Proceedings of the National Academy of Sciences*, vol. 100, no. 9, pp. 5119–5123, 2003.

[56] I. Ö Aycan, A. Tüfek, O. Tokgöz et al., "Thymoquinone treatment against acetaminophen-induced hepatotoxicity in rats," *International Journal of Surgery*, vol. 12, no. 3, pp. 213–218, 2014.

[57] M. A. Mansour, M. N. Nagi, A. S. El-Khatib, and A. M Al-Bekairi, "Effects of thymoquinone on antioxidant enzyme activities, lipid peroxidation and DT-diaphorase in different tissues of mice: a possible mechanism of action," *Cell Biochemistry and Function*, vol. 20, no. 2, pp. 143–151, 2002.

[58] M. L. Salem, "Immunomodulatory and therapeutic properties of the Nigella sativa L. seed," *International Immunopharmacology*, vol. 5, pp. 1749–1770, 2005.

[59] H. Zeinvand-Lorestani, A. Nili-Ahmadabadi, and F. Balak, "Protective role of thymoquinone against paraquat-induced hepatotoxicity in mice," *Pestic Biochem Physiol*, vol. 148, pp. 16–21, 2018.

[60] F. W. Booth, C. K. Roberts, and M. J. Laye, *Lack of Exercise Is a Major Cause of Chronic Diseases*, Compr Physiol [Internet, Hoboken, NJ, USA, 2012.

[61] S. O. Heck, B. C. W. Fulco, C. B. Quines et al., "Combined therapy with swimming exercise and a diet supplemented with diphenyl diselenide is effective against age-related changes in the hepatic metabolism of rats," *Journal of Cellular Biochemistry*, vol. 118, no. 6, pp. 1574–1582, 2017.

[62] C. Keller, P. Keller, M. Giralt, J. Hidalgo, and B. K. Pedersen, "Exercise normalises overexpression of TNF-α in knockout mice," *Biochemical and Biophysical Research Communications*, vol. 321, no. 1, pp. 179–182, 2004.

Hindawi
Evidence-Based Complementary and Alternative Medicine
Volume 2023, Article ID 5068304, 15 pages
https://doi.org/10.1155/2023/5068304

Research Article

Rutin and Hesperidin Alleviate Paclitaxel-Induced Nephrocardiotoxicity in Wistar Rats *via* Suppressing the Oxidative Stress and Enhancing the Antioxidant Defense Mechanisms

Yasmine A. Ali,[1] **Osama M. Ahmed**,[2] **Hanan A. Soliman**,[1] **Mohamed Abdel-Gabbar**,[1] **M. Al-Dossari**,[3] **N. S. Abd El-Gawaad**,[4] **El-Shaymaa El-Nahass**,[5] **and Noha A. Ahmed**[2]

[1]*Biochemistry Department, Faculty of Science, Beni-Sued University, P.O. Box 62521, Beni-Suef, Egypt*
[2]*Physiology Division, Zoology Department, Faculty of Science, Beni-Suef University, P.O. Box 62521, Beni-Suef, Egypt*
[3]*Research Center for Advanced Materials Science (RCAMS), King Khalid University, P.O. Box 9004, Abha 61413, Saudi Arabia*
[4]*Department of Physics, Faculty of Science, King Khalid University, P.O. Box 9004, Abha 62529, Saudi Arabia*
[5]*Department of Pathology, Faculty of Veterinary Medicine, Beni-Suef University, P.O. Box 62521, Beni-Suef, Egypt*

Correspondence should be addressed to Noha A. Ahmed; drnohascience@science.bsu.edu.eg

Received 28 August 2022; Revised 5 October 2022; Accepted 27 January 2023; Published 22 February 2023

Academic Editor: Salah M. El Sayed

Paclitaxel is a primary chemotherapy agent that displays antitumor activity against a variety of solid tumors. However, the clinical effectiveness of the drug is hampered by its nephrotoxic and cardiotoxic side effects. Thus, this investigation aimed at assessing the protective effects of rutin, hesperidin, and their combination to alleviate nephrotoxicity caused by paclitaxel (Taxol), cardiotoxicity in male Wistar rats, as well as oxidative stress. Rutin (10 mg/kg body weight), hesperidin (10 mg/kg body weight), and their mixture were given orally every other day for six weeks. Rats received intraperitoneal injections of paclitaxel twice weekly, on the second and fifth days of the week, at a dose of 2 mg/kg body weight. In paclitaxel-treated rats, the treatment of rutin and hesperidin decreased the elevated serum levels of creatinine, urea, and uric acid, indicating a recovery of kidney functions. The cardiac dysfunction in paclitaxel-treated rats that got rutin and hesperidin treatment also diminished, as shown by a substantial reduction in elevated CK-MB and LDH activity. Following paclitaxel administration, the severity of the kidney and the heart's histopathological findings and lesion scores were markedly decreased by rutin and hesperidin administration. Moreover, these treatments significantly reduced renal and cardiac lipid peroxidation while markedly increased GSH content and SOD and GPx activities. Thus, paclitaxel likely induces toxicity in the kidney and the heart by producing oxidative stress. The treatments likely countered renal and cardiac dysfunction and histopathological changes by suppressing oxidative stress and augmenting the antioxidant defenses. Rutin and hesperidin combination was most efficacious in rescuing renal and cardiac function as well as histological integrity in paclitaxel-administered rats.

1. Introduction

Taxanes are natural compounds produced by members of the genus *Taxus*. These compounds are used to treat various cancers and are preliminary therapies for earlier stages of cancer [1–4]. Paclitaxel is a key taxane and an effective antitumor agent [5]. The Food and Drug Administration (FDA) initially approved paclitaxel in 1992 to treat ovarian cancer [6]. Subsequently, the drug was frequently tested for use in the treatment of other cancers, such as breast, prostate, bladder, cervical, and brain [7–10]. However, the clinical use of paclitaxel is considerably restricted because of its limited solubility, recrystallization after dilution, and cosolvent-induced toxicity [11]. Further, cancer cells become resistant to paclitaxel chemotherapy, and the use of the drug causes numerous adverse effects, including neuropathy,

cardiac toxicity, and hepatotoxicity [12–14]. Paclitaxel lowers levels of glutathione (GSH) and increases malondialdehyde (MDA) concentrations, suggesting oxidative stress [15], and may have caused renal injury due to induction of oxygen radicals in the reaction, which was a trigger of renal oxidative stress [16]. Furthermore, paclitaxel may cause cardiotoxic effects [17, 18]. According to several studies, different antioxidants can prevent deoxyribonucleic acid (DNA) oxidative stress damage [19–21].

Citrus species are an important biological resource from an economic perspective; these plants produce a diversity of phytonutrients and phytochemicals with promising therapeutic properties [22]. Flavonoids exhibit varied bioavailability and biological efficacy. These chemicals may confer health benefits *via*anti-inflammatory, antioxidant, antimicrobial, antiproliferative, proapoptotic, and hormone regulatory properties [23–25]. Combining rutin with other drugs can reduce drug resistance and the side effects of chemotherapy [26]. Rutin eliminated oxidative/nitrosative stress, inflammation, and apoptosis in rat kidney [27]. Also, it significantly inhibited myocardial oxidative insults by modulating ROS levels [28–31]. Hesperidin is a strong candidate phytocompound that displays antimicrobial, anticancer, antioxidant, anti-inflammatory, antidiabetic, and cardiovascular protective properties [32]. The compound also counteracts acute nephrotoxicity *via* antioxidant activity [33]. Further, hesperidin exhibits chemopreventive and chemotherapeutic effects against various carcinomas [34].

Chemotherapeutic drugs such as paclitaxel have several deleterious side effects, including kidney and heart damage, and we intend to reduce these effects by employing plant constituents with antioxidant and anti-inflammatory properties. Thus, this study assessed the renal and cardiac protection by rutin and hesperidin against the toxicity caused by paclitaxel in male Wistar rats. The study also focused on evaluating the functions of the heart and kidneys as well as the histological integrity, architecture, and defenses against oxidative stress and antioxidants.

2. Materials and Methods

2.1. Chemicals. The formulation vehicle of Cremophor® EL* (CrEL) contains paclitaxel, often known as Taxol or paclitaxel by trade (polyoxyethylated castor oil) (batch number: 7E05628), was obtained from Bristol–Myers Squibb global biopharmaceutical company (Princeton, USA). Rutin (batch number: 501) was obtained from Oxford Laboratory Company (Mumbai, India). From the Sigma-Aldrich Company, hesperidin (lot number: # SLBT3541) was obtained (St. Louis, MO, USA). Creatinine reagent kit (catalog number: M11502c-18) and urea reagent kit (catalog number: M11536c-16) were bought from Biosystem S.A. (Spain), respectively. Uric acid, creatine kinase-MB (CKMB), and lactate dehydrogenase (LDH) reagent kits were purchased from Spin React (Spain); these kits have catalog numbers: MD41001, MD41254, and MX41214, respectively. Chemicals of oxidative stress including trichloroacetic acid (TCA) (batch number: 5O011689) was obtained from PanReac AppliChem ITW Companies (Spain); thiobarbituric acid (TBA) (batch number: L 16A/1916/1212/13) was obtained from Sd Fine Chem Limited (SDFCL) Company (India); 1,1,3,3-tetramethoxypropane or malondialdehyde (MDA) (catalog number: T9889) was obtained from Sigma-Aldrich (MO, USA); metaphosphoric acid (batch number: M 21519) was obtained from ALPHA CHEMIKA Company (India); 5,5'-dithiobis (2-nitrobenzoic acid) (DTNB or Ellman's reagent) (batch number: 40K3652) was obtained from Sigma-Aldrich (MO, USA); GSH (batch number: 3W010085) was obtained from PanReac AppliChem ITW Companies (Spain); pyrogallol (batch number: 1280B251114) was obtained from ResearchLab Company (India). The highest purity and analytical grade reagents were used throughout the investigations.

2.2. Physiochemical Properties of Rutin and Hesperidin. Rutin has a molecular weight of 610.5 and the empirical formula C27H30O16. It is a light-yellow crystalline powder that tastes slightly bitter. It has low solubility in water (125 mg/L), while highly soluble in polar solvents, and melts at around 176–178°C.

Hesperidin is a light yellow crystalline powder with the empirical formula C28H34O15 and a molecular weight of 610.6; it is odorless and tasteless. It demonstrated poor pH-independent aqueous solubility; however, it is soluble in formamide and dimethyl formamide at 60°C, slightly dissolve in other polar solvents, and melts at around 258–262°C.

2.3. Experimental Animals. Thirty mature male Wistar rats weighing 130–150 g and aging 8–9 weeks were provided as the experimental rats. Rats were taken from the animal house of the National Research Center in Dokki, Giza, Egypt. For avoiding intercompetitive infection, the animals were observed for 15 days prior to the experiment. Rats were maintained in stainless steel-covered, ventilated polypropylene cages that were kept at room temperature (25 ± 5°C) and subjected to 12-hour light/dark cycles every day. Animals received unrestricted water availability but were also nourished with a well-balanced meal *ad libitum* on a daily basis. The Faculty of Science at the University of Beni-Suf in Egypt followed all guidelines and directions issued by the Experimental Animal Ethics Committee (Ethical Approval Number: BSU/FS/2017/8). All efforts have been made to mitigate animal suffering, anxiety, and discomfort.

2.4. Experimental Approach. Male adult Wistar rats had been subdivided into 5 groups in this study (6 rats per group) (Figure 1)

(1) Negative control group: this group of rats received 5 mL of 1% carboxymethylcellulose orally (CMC) (vehicle used to dissolve rutin and hesperidin)/kg body weight (b. wt) on an alternate day and 2 mL of isotonic saline (0.9% NaCl) (vehicle in which paclitaxel is dissolved)/kg b. wt twice per week *via* the intraperitoneal (i.p.) route for 6 weeks.

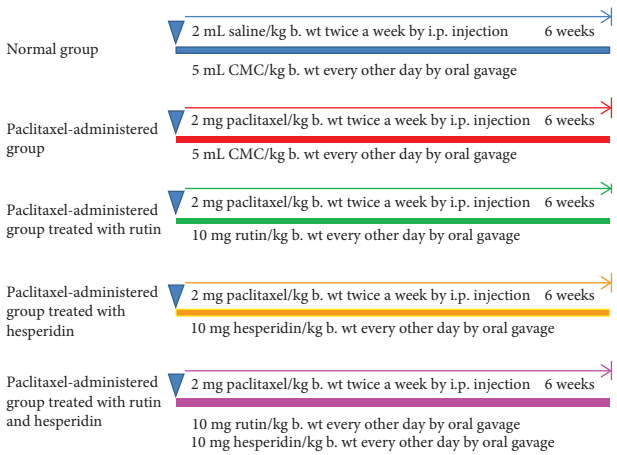

Figure 1: Animal grouping and experimental design.

(2) Paclitaxel-administered control group: paclitaxel was given to this group of rats at a dose of 2 mg/kg body weight (in 2 mL 0.9% NaCl) by i.p. injection [35] twice a week at the 2nd and 5th days of each week for 6 weeks; every other day an oral equivalent dose from 1% CMC (5 mL/kg body weight) was also administered.

(3) Paclitaxel-administered group treated with rutin: this group of rats received paclitaxel as in the paclitaxel-administered control group, as well as rutin at a dose of 10 mg/kg b. wt [36] (dissolved in 5 mL of 1% CMC) taken orally on an alternate day for six weeks.

(4) Paclitaxel-administered group treated with hesperidin: Paclitaxel was administered to this group of rats in the same manner as it was to the paclitaxel-treated control group, along with hesperidin, orally twice weekly in a dose of 10 mg/kg body weight [37] (dissolved in 5 mL of 1% CMC).

(5) Paclitaxel-administered group treated with rutin as well as hesperidin combination: paclitaxel was delivered to this group of rats in the same manner as it was in the paclitaxel control group, along with rutin and hesperidin at a dose of 10 mg/kg b. wt. (dissolved in 5 mL of 1% CMC) on an alternate day for six weeks.

2.5. Blood and Tissue Sampling. Rats were slaughtered under diethyl ether anesthesia [38] after receiving the prescribed dosages for six weeks. Jugular vein blood samples were drawn into gel and clot activating tubes, which were then centrifuged for 15 minutes at 3000 rounds per minute after allowing the clots to form at room temperature (rpm). For biochemical analysis, the sera were rapidly collected, divided into four sections, and kept at 30°C. Following decapitation and dissection, the kidneys and heart were rapidly resected and weighed. Tissue samples from the kidney and heart were removed for biochemical analysis and histopathology analysis. A piece of tissue was excised and transferred to 70% alcohol after being fixed in phosphate buffered formalin (10%) for 24 hours for histology. Using a Teflon homogenizer, 0.5 g of tissue was homogenised in 5 ml of saline (0.9% NaCl) (made by Glas-Col, Terre Haute, USA). The homogenates were then centrifuged for 15 minutes at 3000 rpm, and the supernatants were collected and stored in the refrigerator at −20°C until employed to measure biochemical parameters of antioxidant defenses and oxidative stress markers.

2.6. Determination of Serum Kidney Function Parameters. Urea and creatinine levels were detected as previously described, respectively, by Fabiny and Ertingshausen [39] and Tabacco et al. [40]. Uric acid had been measured using a method previously reported by Fossati et al. [41].

2.7. Evaluation of Serum Heart Function Parameters. So according to the respective methods belonging to Young [42] and Pesce [43], the CK-MB and LDH activities were assessed.

2.8. Assessing the Parameters of the Antioxidant Defense System and Oxidative Stress. Utilizing chemical reagents made in the lab, the heart and kidney oxidative stress and antioxidant defense parameters were evaluated. Lipid peroxidation (LPO) was determined as stated earlier by Preuss et al. [44]. In brief, protein was precipitated by mixing 1 mL of homogenate with 0.15 mL of 76% TCA. Next, 0.35 mL of TBA, a color-enhancing substance, was added to the separated supernatants. After 30 minutes of incubation in a water bath at 80°C, the produced light pink colour was observable at 532 nm. The benchmark was MDA. Based on Beutler et al. [45], the GSH content was evaluated by adding 0.5 mL of DTNB or Ellman's reagent to the homogenate supernatant after protein precipitation (as a color-developing agent). The yellow colour of the samples and GSH standards had been contrasted with a blank at 412 nm. Matkovics et al. [46] procedure was used to determine GPx activity with some modifications. The method works by identifying any remaining GSH and deducting it from the total amount of GSH converted by the enzyme to oxidized glutathione (GSSG). In a Wasserman tube, 350 μl of Tris buffer (pH 7.6), 50 μl of GSH solution (2 mM), and 50 μl of hydrogen peroxide (H_2O_2) (3.38 mM) were combined with 50 μl of homogenate supernatant (3.38 mM). The remaining GSH content was then evaluated using the aforementioned procedure for GSH measurement at 430 nm following a 10-minute incubation period. Standard tests were prepared by substituting 50 μl of distilled water for 50 μl of the sample, and a blank test tube was prepared by substituting 100 μl of distilled water for 50 μl each of the sample and GSH solution. The sample's residual GSH concentration may then be detected, and GSH can then be transformed to GSSG to measure the activity of the enzyme. Using the Marklund and Marklund [47] method, SOD activity was evaluated. The suppression of pyrogallol autooxidation by SOD is the basis of the mechanism. Superoxide ions are necessary for the

process to take place. The amount of enzyme that results in 50% suppression in extinction changes in comparison to the control after one minute is referred to as one unit of enzyme activity.

2.9. Histological Investigations. All animals were immediately decapitated by cervical dislocation and dissection, and their kidneys and hearts were removed. They were subsequently transferred to the pathology department of the faculty of veterinary medicine at Beni-Suef University in Egypt for additional processing, wax blocking, sectioning, and staining with hematoxylin and eosin after being stored in 10% neutral buffered formalin for 24 hours (H&E) [48]. Five random fields were estimated for each section. The number of sections in each group is six. Sections of tissues were examined under light microscopy. The methodology outlined by El-Far et al. [49] was used to determine the histopathological lesion scores. Score scale 0 = normal, $1 \leq 25\%$, 2 = 26–50%, 3 = 51–75%, and 4 = 76–100%. The lesions were graded in a blinded manner.

2.10. Statistical Analysis. The mean and standard error of the mean were used to reveal all the data SEM ± Mean. The statistical analyses were carried out using the IBM software, USA, Statistical Package for the Social Sciences (SPSS) computer software (version 22). To determine the significance of group means, a one-way analysis of variance (ANOVA) test was conducted. Tukey's posthoc test was then used to compare pair averaged results. Differences were deemed significant at $p < 0.05$ [50]:

$$\%\ \text{change} = \frac{\text{Final value} - \text{Initial value}}{\text{initial value}} \text{x}100. \quad (1)$$

3. Results

3.1. Effects of Toxicity Studies on the Kidney Function-Related Serum Parameters. Rats receiving paclitaxel intraperitoneally for six weeks revealed a significant rise ($p < 0.05$) in their serum levels of urea, uric acid, and creatinine with respective percentage changes +111.90, +68.94, and + 361.67%, compared with corresponding normal controls. Rutin and its combination with hesperidin significantly restored increased creatinine, urea, and uric acid levels to normal in paclitaxel-induced rat models. Treatment with hesperidin indicated a nonsignificant decrease ($p \geq 0.05$) in serum creatinine and urea levels but significant improvement in serum uric acid levels. The combination of rutin and hesperidin treatment of paclitaxel-administered rats was the most efficacious in lowering high creatinine, urea, and uric acid levels, with respective percentage decreases −43.82, −38.03, and −60.65% (Figure 2).

3.2. Effects of Toxicity Studies on the Heart Function Related to Serum Biomarkers. Rats receiving paclitaxel intraperitoneally for six weeks reported significant alleviation in their serum levels of CK-MB and LDH, with percentage changes of +433.33, +311.85, and +53.31%, respectively, in comparison to the corresponding normal controls. Rutin, hesperidin, and their combination all significantly reduced the increased CK-MB and LDH activity in paclitaxel-induced rats. Treatment with rutin and hesperidin mixture treatmen was most efficacious in reducing high levels of CK-MB and LDH, with percentage decreases of −45.83, −57.54, and −28.92% (Figure 3).

3.3. Effects of Toxicity Studies on the Kidney and Heart Oxidative Stress and Antioxidant Defense System Indicators. Following paclitaxel administration, kidney GSH content, SOD, and GPx activities all significantly decreased, while renal LPO significantly increased. Rats that received paclitaxel then treated with rutin, hesperidin, as well as their mixture showed a significant diminished kidney LPO. Hesperidin seemed to be the best in depleting elevated kidney LPO product. Additionally, compared to paclitaxel-administered controls, these treatments dramatically ameliorated decreased kidney GSH content and SOD activity. Only rutin plus hesperidin significantly increased kidney GPx activity (Figure 4).

Rats receiving paclitaxel for six weeks showed highly significant increases in the heart LPO and significant decreases in the heart GSH content, in addition to SOD and GPx activity. This was similar to what was seen in the kidney. Rats receiving paclitaxel and treated with rutin, hesperidin, and their mixture indicated significantly lower heart LPO. Hesperidin seemed to be the most effective in lowering elevated heart LPO product. Moreover, all three treatments significantly restored decreased heart SOD and GPx activities; only rutin caused a significant rise in cardiac GSH content (Figure 5).

3.4. Correlation between Kidney and Heart Function Biomarkers and Oxidative Stress Bio Indicators. The serum creatinine, urea, and uric acid levels showed positive correlation with LPO while they exhibited negative correlation with GSH content and SOD and GPx activities (Table 1).

In addition, the serum CK-MB and LDH activities showed positive correlation with LPO while they exhibited negative correlation with GSH content and SOD and GPx activities (Table 2).

3.5. Effects of the Toxicity Studies on the Kidney Histological Changes. Pathological lesions in the kidneys are summarized in Table 3 and illustrated in Figure 6. Normal histological architecture was observed in tissues from normal rats (Figure 6(a)). Paclitaxel-administered animals showed severe pathological lesions, including degenerative changes and nuclear pyknosis of the lining epithelium of the renal tubules associated with glomerulonephrosis in most glomeruli. Focal interstitial nephritis was also observed. Further, congestion was found in the glomerular tuft and interstitial blood capillaries (Figure 6(b)). Paclitaxel/rutin-treated group showed mild to moderate degenerative changes in the renal lining epithelium associated with focal leucocytic infiltration, mainly lymphocytes in the interstitial area (Figure 6(c)). Paclitaxel/hesperidin-treated group

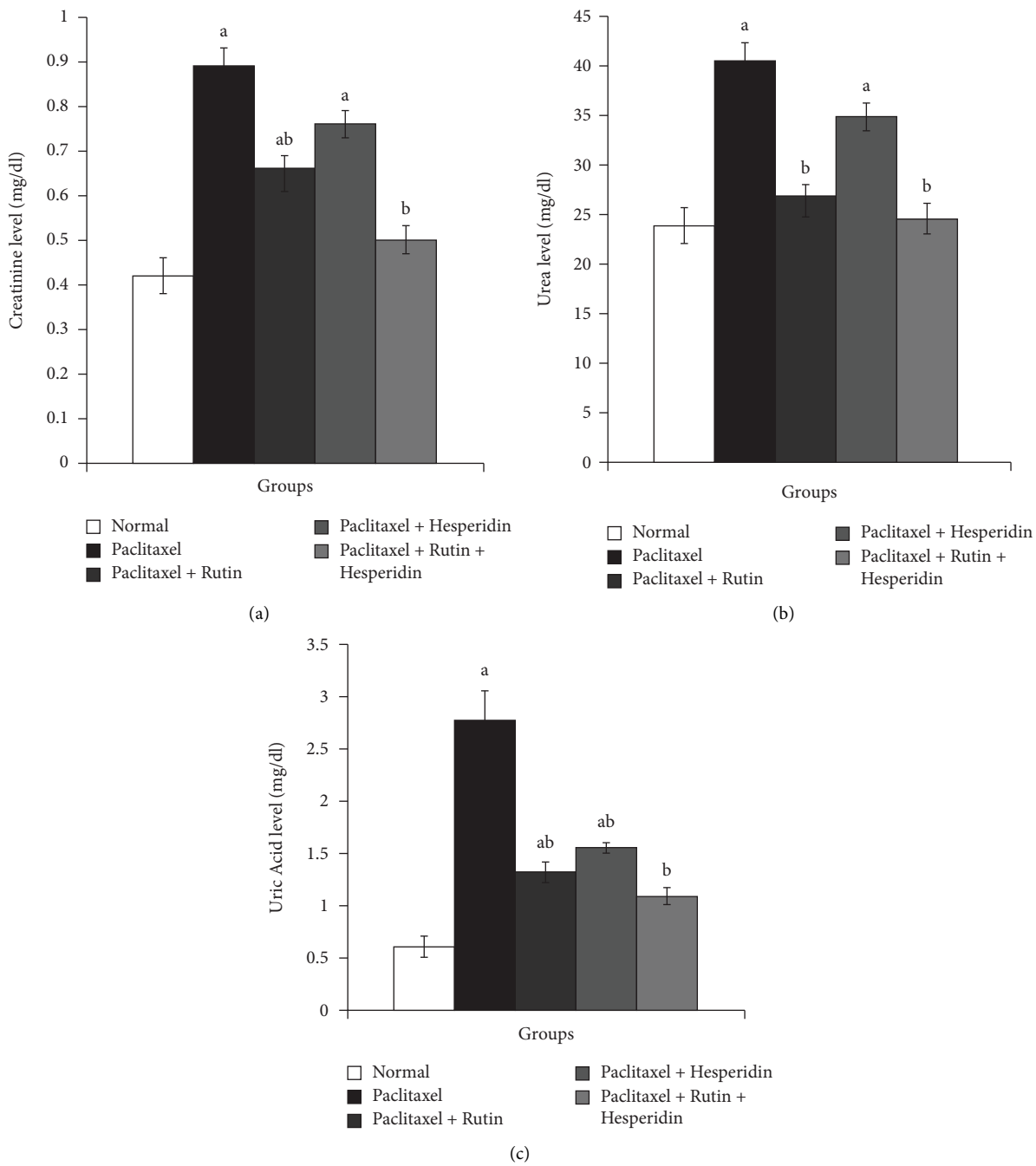

Figure 2: Graphs show the effects of rutin and hesperidin on, serum creatinine (a), urea (b), and uric acid (c) levels in paclitaxel-administered group. [a] $p < 0.05$: significant compared with normal group. [b] $p < 0.05$: significant compared with paclitaxel-administered group.

suffered from moderate glomerulonephrosis and mild necrosis of lining epithelium of renal tubules (Figure 6(d)). Paclitaxel/rutin/hesperidin-treated group exhibited mild degenerative changes of the glomerular tuft and lining renal epithelium (Figure 6(e)).

3.6. Effects of the Toxicity Studies on the Heart Histological Changes. Detailed pathological lesions are briefly summarized in Table 4 and illustrated in Figure 7. Primary lesions were hyalinosis and lymphocytic myocarditis. Normal histological structure of cardiac muscles was found in normal animals (Figure 7(a)). In contrast, severe hyalinosis associated with focal leucocytic infiltration was seen in paclitaxel-administered control group (Figure 7(b)). Mild lesions were observed in paclitaxel/rutin-treated animals (Figure 7(c)). Paclitaxel/hesperidin-treated group was characterized by an absence of focal lymphocytic myocarditis; however, moderate hyalinosis was seen (Figure 7(d)). Mild degenerative changes of cardiac muscles were seen in tissues from paclitaxel/rutin/hesperidin-treated animals (Figure 7(e)).

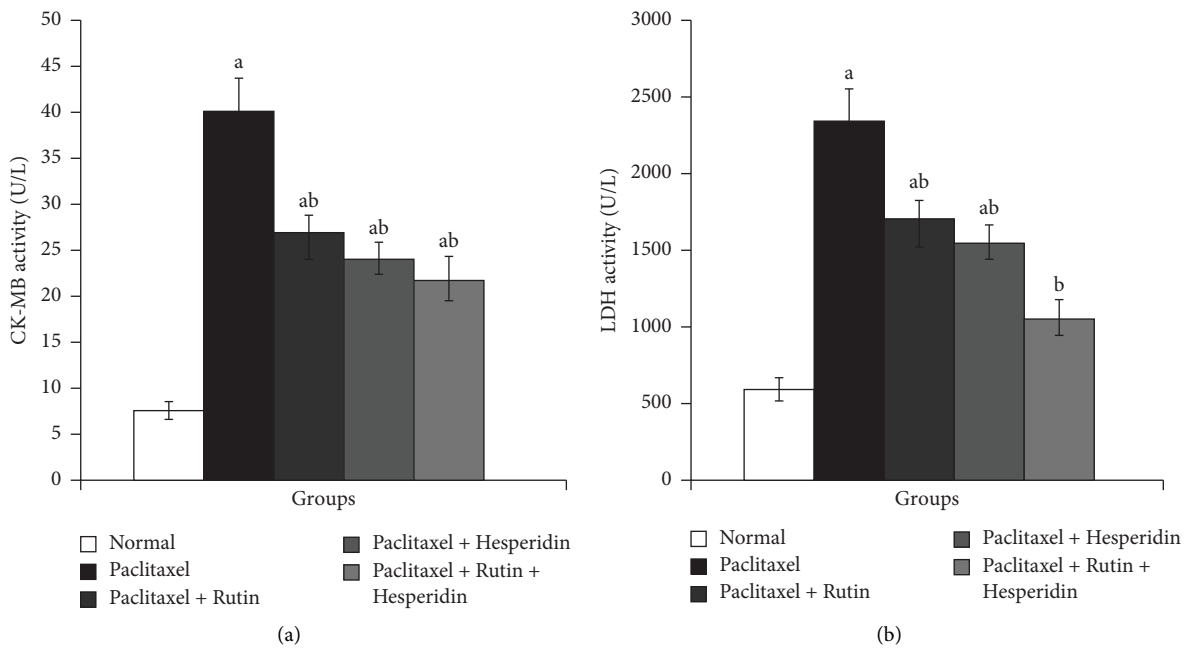

Figure 3: Graphs show the effects of rutin and hesperidin on serum, CK-MB (a) and LDH (b) activities in paclitaxel-administered group. [a]$p < 0.05$: significant compared with normal group. [b]$p < 0.05$: significant compared with paclitaxel-administered group.

4. Discussion

Numerous tumours are treated with paclitaxel, including aggressive and metastatic breast cancer, lung cancer, and pancreatic cancer [51]. Unfortunately, paclitaxel therapy can increase the acquired cancer resistance, resulting in chemotherapeutic failure [52]. Paclitaxel may lead to numerous adverse effects on different organs, including the liver, kidney, and heart [53–56]. It promotes oxidative stress, decreases antioxidants, increases liver enzymes, and impairs renal function, which may be due to its mechanism of action and the oxidative stress that it caused [57]. Concurrent use of potent plant antioxidants with chemotherapeutic drugs protects cells and tissues from the harmful effects of free radicals [58].

The nephrotoxicity caused by the intraperitoneal injection of paclitaxel as Taxol was biochemically demonstrated by a significant amelioration in the level of serum creatinine, urea, and uric acid. Paclitaxel inhibits the kidney function and lowers the kidney's ability to remove hazardous metabolic chemicals based on these altered blood levels. These findings are comparable to those of Adikwu et al. [16], who found that paclitaxel deteriorated renal function and caused significant alleviation in blood levels of urea, creatinine, and uric acid, as well as a distortion in normal renal histology. Paclitaxel caused significantly elevated levels of serum creatinine and urea [59, 60]. These alterations in biochemical parameters strongly correlate with several deleterious renal histological changes and lesions, including degenerative changes and nuclear pyknosis of the lining epithelium of the renal tubules, associated with glomerulonephritis, focal interstitial nephritis, and congestion. Other studies have shown similar histological alterations [55, 61–63]. Paclitaxel-induced nephrotoxicity may reflect the alteration and degeneration of glomerular composition and decreased glomerular filtration rate in rats [60]. In our opinion, the kidney histological pathology in renal tissues is due to excessive free radical and ROS production and a reduction of antioxidant defenses. This explanation makes sense given that paclitaxel administration significantly increased renal LPO and significantly decreased renal GSH content of the kidney along with GPx and SOD activity.

In our article, delivering rutin, hesperidin, and their combination of paclitaxel-administered rats successfully reversed kidney pathology as shown by a decrease in serum levels of creatinine, urea, and uric acid as well as ameliorating the kidney histology. These results are consistent with Abou Seif [64] who reported that pretreatment with rutin and hesperidin protects the kidney against nephrotoxicity induced by doxorubicin by improving urea, creatinine, and uric acid serum levels. Rutin provides protection against nephrotoxicity after administration of carfilzomib and has also demonstrated improved histological profiles and ameliorating direct bilirubin, creatinine, and blood urea nitrogen levels [65]. Also, Emam and Madboly [66] showed hesperidin as a potent antioxidant agent that protects the kidney against acetaminophen-induced nephrotoxicity by reversing histopathological changes and reducing blood urea and serum creatinine levels. Likewise, flavonoids such as naringin and naringenin are potent anticancer agents and play a role in the management of various tumors [67].

By increasing serum LDH and CK-MB activity as well as releasing these enzymes from cardiomyocytes into the plasma, the current study discovered that paclitaxel treatment caused cardiotoxicity. These results agree with those of Saad et al. [68], who observed a significant rise in serum CK-

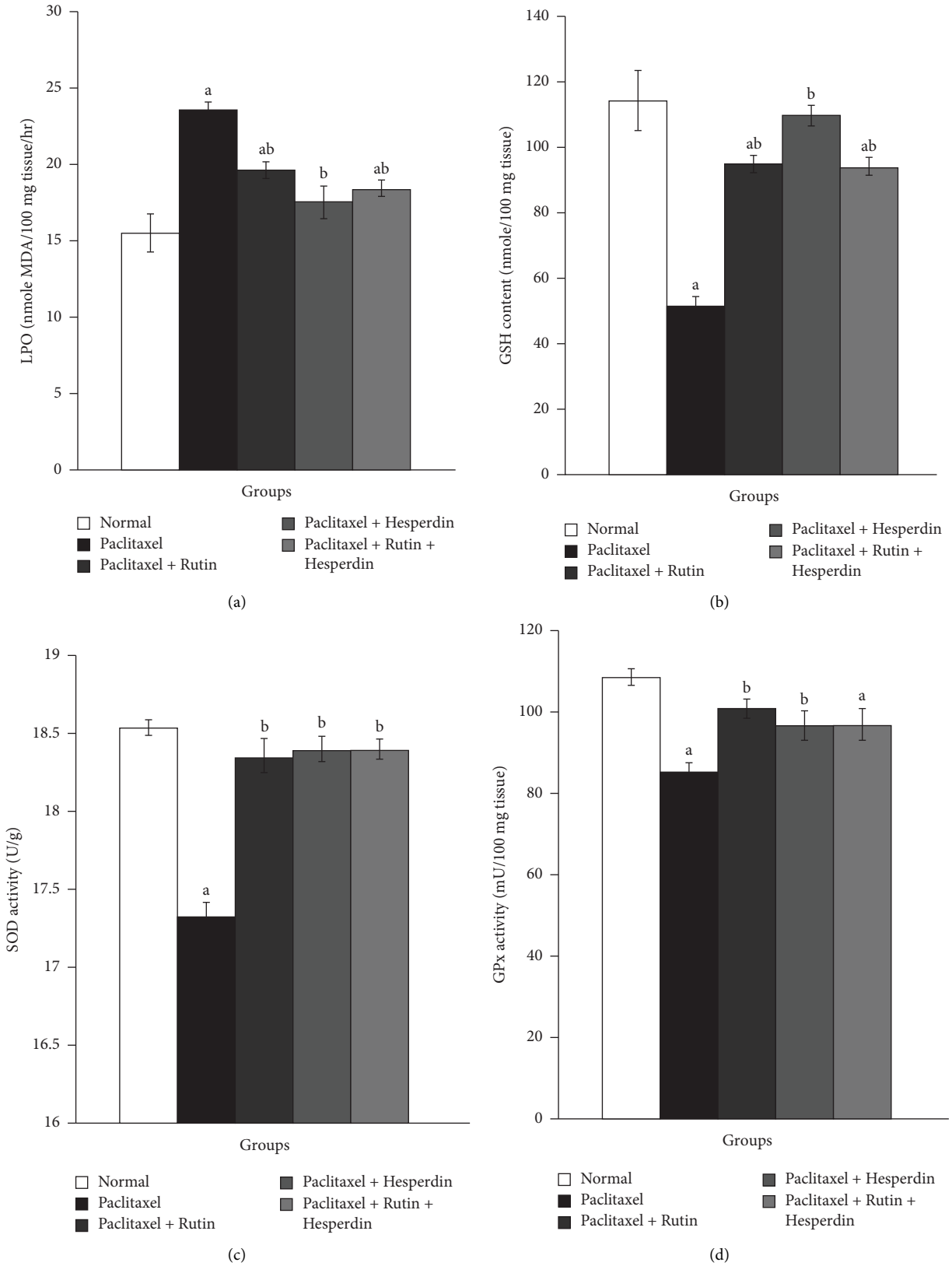

Figure 4: Graphs show the effects of rutin and hesperidin on the kidney LPO (a), GSH (b), SOD (c), and GPx (d) in paclitaxel-administered group. [a] $p < 0.05$: significant compared with normal group. [b] $p < 0.05$: significant compared with paclitaxel-administered group.

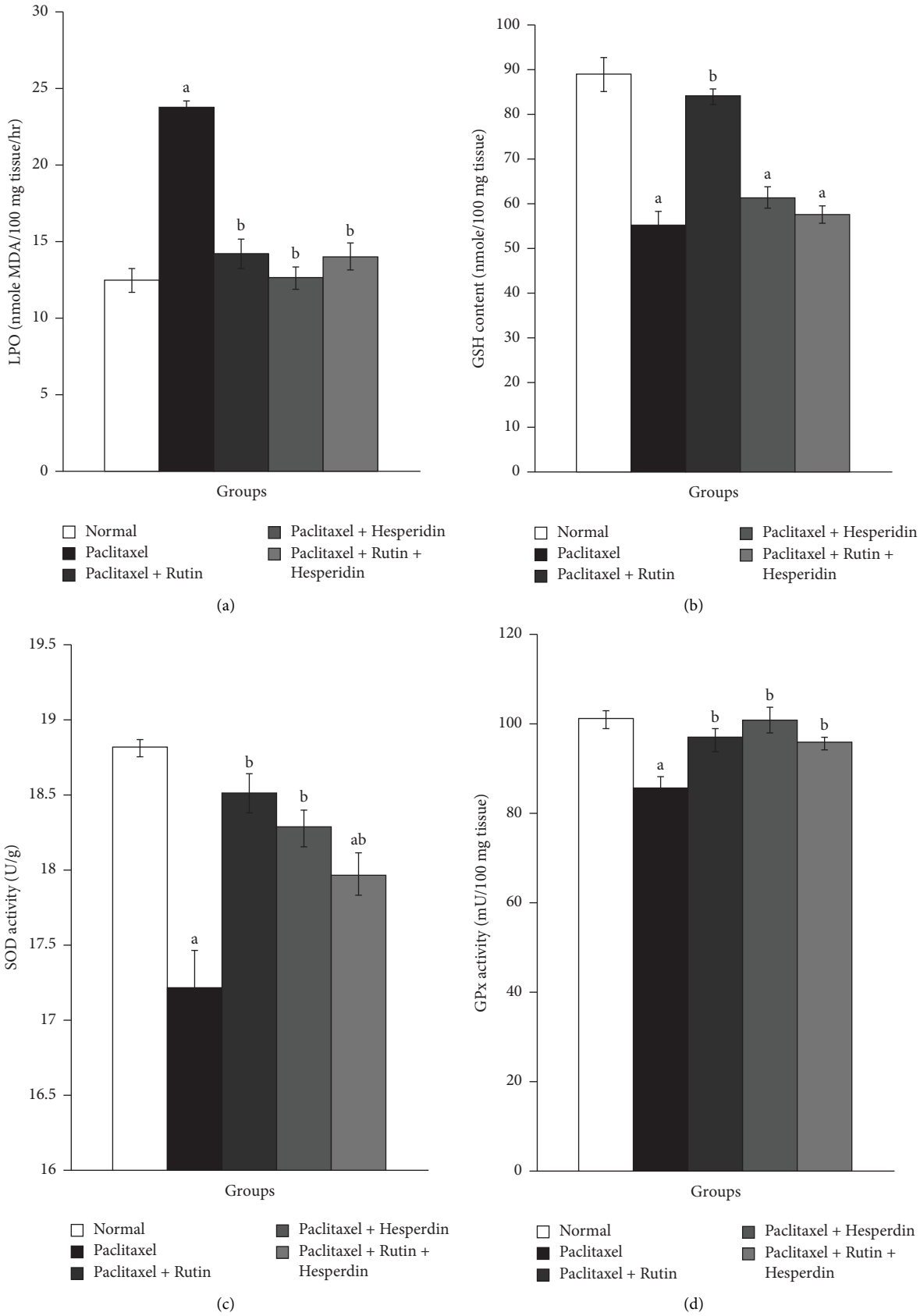

Figure 5: Graphs show the effects of rutin and hesperidin on heart LPO (a), GSH (b), SOD (c), and GPx (d) in paclitaxel-administered group. [a] $p < 0.05$: significant compared with normal group. [b] $p < 0.05$: significant compared with paclitaxel-administered group.

Table 1: Correlation between the kidney function biomarkers and oxidative stress bioindicators.

	Creatinine		Urea		Uric acid	
	r	p value	r	p value	r	p value
LPO	0.633	$p < 0.001$	0.457	$p < 0.05$	0.721	$p < 0.001$
GSH	−0.588	$p < 0.01$	−0.489	$p < 0.01$	−0.780	$p < 0.001$
SOD	−0.601	$p < 0.001$	−0.542	$p < 0.01$	−0.686	$p < 0.001$
GPx	−0.570	$p < 0.01$	−0.536	$p < 0.01$	−0.623	$p < 0.001$

r: correlation value. $p > 0.05$, nonsignificant; significance was calculated at these levels: $p < 0.05$, $p < 0.01$, and $p < 0.001$.

Table 2: Correlation between the heart function biomarkers and oxidative stress bioindicators.

	CK-MB		LDH	
	r	p value	r	p value
LPO	0.664	$p < 0.001$	0.705	$p < 0.001$
GSH	−0.589	$p < 0.01$	−0.421	$p < 0.05$
SOD	−0.645	$p < 0.001$	−0.600	$p < 0.001$
GPx	−0.607	$p < 0.001$	−0.504	$p < 0.01$

r: correlation value. $p > 0.05$, nonsignificant; significance was calculated at these levels: $p < 0.05$, $p < 0.01$, and $p < 0.001$.

Table 3: Pathological renal lesion scores in different groups.

Groups	Parameters				
	Degenerative renal tubules	Necrosis of renal tubules	Congestion	Leucocytic infiltration	Glomerulonephrosis
Normal	−	−	−	−	−
Paclitaxel	++	++	+++	+++	+++
Paclitaxel + rutin	++	−	++	++	++
Paclitaxel + hesperidin	++	+	++	++	+++
Paclitaxel + rutin + hesperidin	++	+	+++	+	++

Lesion types are (−) absence, (+) minimal, (++) mild, (+++) moderate, and (++++) severe.

MB, LDH, and AST activity, indicating paclitaxel-induced cardiac damage. Notably, Zhang et al. [69] revealed that paclitaxel-induced heart toxicity in normal rats caused significant increases in serum CK-MB levels [70]. These alterations in biochemical parameters correlate with cardiac histopathological findings and lesions that include severe hyalinosis associated with focal lymphocytic infiltration. These results match those of Malekinejad et al. [71], Razzaq et al. [72], and Saad et al. [68], who also found that animals treated with paclitaxel showed severe congestion and necrosis in the heart. Moreover, previous articles have reported that paclitaxel is cardiotoxic [17, 18, 73]. Paclitaxel also was reported to induce apoptosis in cardiac tissue [74]. The heart function and histological integrity may deteriorate from increased oxidative stress, along with a decline in the heart GSH levels, GPx, and SOD activity.

This present article illustrates the ability of rutin and hesperidin to ameliorate elevated CK-MB and LDH activities and normalize cardiac histology in paclitaxel-administered rats. Siti et al. [75] and Xianchu et al. [76] showed that rutin is cardioprotective, and Wang et al. [77] reported that pretreatment with rutin attenuated pirarubicin-induced histopathological alterations and lowered serum LDH and CK-MB activities. An article by Abdel-Raheem and Abdel-Ghany [78] showed that pretreatment with hesperidin protected rats' cardiac tissues from cardiotoxicity caused by doxorubicin *via* reversing histological alteration and reducing serum LDH and CK activities. Pretreatment with hesperidin conserved morphological and ultrastructural architecture of myocardium and reduced LDH and CK-MB activities, supporting a cardioprotective property for hesperidin [79].

Significant increases in the kidney and cardiac LPO, a significant decline in nonenzymatic antioxidant (GSH) concentration, and enzymatic antioxidant (GPx and SOD) activities are all related to detrimental biochemical and histological alterations in the current investigation. Similarly, Ren et al. [80] reported that paclitaxel exposure induced increased ROS and MDA concentrations, while the whole SOD activity declined. These results indicated that paclitaxel administration led to changes in protein expression associated with apoptosis and ROS generation. Also, according to an article, paclitaxel-triggered apoptosis in the renal tubular was linked to decreased mitochondrial membrane potential and a large rise in ROS production. In [81, 82], it was found that a reduction in SOD activity may cause a reduction in superoxide radical ion removal, which may be detrimental to the kidney [64]. An article of Malekinejad et al. [71] showed that paclitaxel administration produced a remarkable increase in the heart LPO and identified the critical role of oxidative and nitrosative stress. Paclitaxel has been recognized to produce reactive oxygen species (ROS) that trigger mitochondrial dysfunction to release cytochrome C into the cytoplasm and activate the

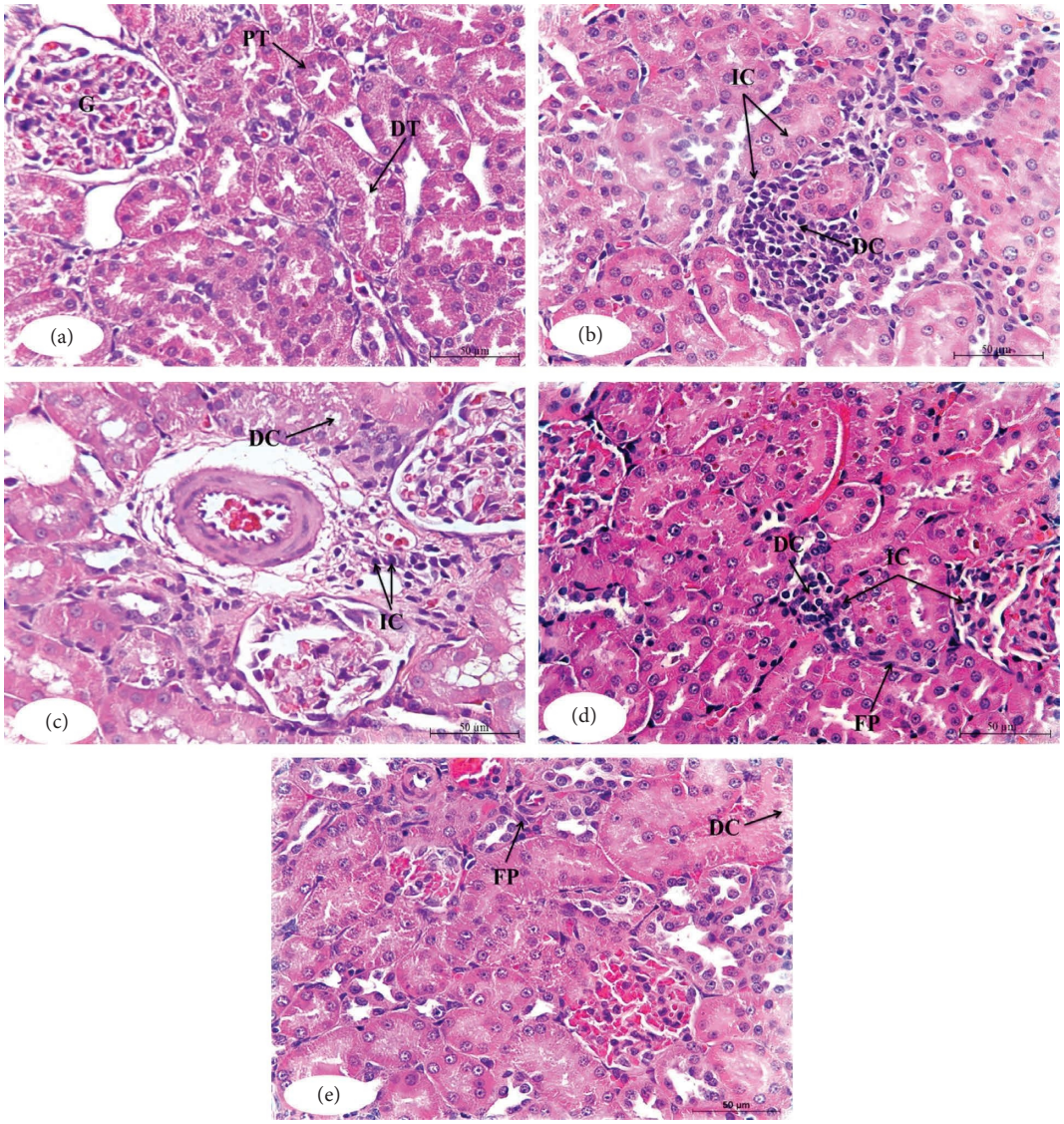

Figure 6: Photomicrographs of the kidney sections of the normal (a), paclitaxel-administered control group (b), and paclitaxel-administered groups treated with rutin (c), hesperidin (d), and their combination (e). G: glomeruli; PT: proximal tubules; DT: distal tubules; DC: degenerative changes; IC: inflammatory cells infiltration; FP: fibroblastic proliferation (H&E; ×400).

Table 4: Pathological cardiac lesion scores in different groups.

Groups	Parameters	
	Coagulative necrosis (hyalinosis)	Leucocytic infiltration
Normal	−	−
Paclitaxel	++	+++
Paclitaxel + rutin	+	+
Paclitaxel + hesperidin	++	−
Paclitaxel + rutin + hesperidin	+	−

Lesion types are (−) absence, (+) minimal, (++) mild, (+++) moderate, and (++++) severe.

caspase cascade and apoptosis stimulation [83, 84]. As a result of this investigation and previous articles, we believe that paclitaxel-induced renal and cardiac dysfunction and histopathology are caused by increased oxidative stress and attenuation of antioxidant defenses.

Paclitaxel-induced oxidative stress in the kidney or heart was remarkably suppressed by rutin and hesperidin treatment with reduced LPO and elevated GSH content and activities of antioxidant enzymes. Both compounds enhance endogenous antioxidant activity beyond their ability to

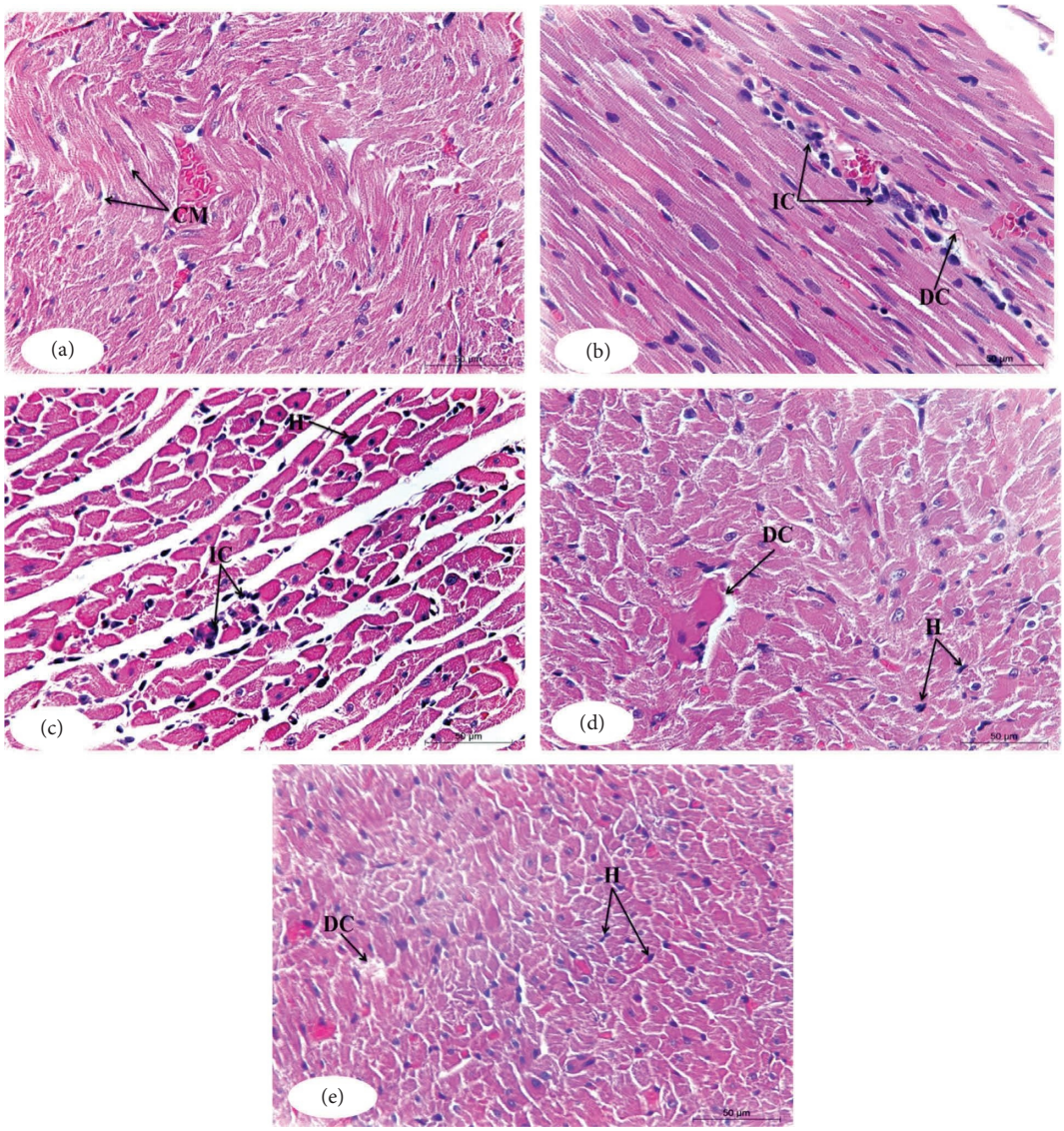

Figure 7: Photomicrographs of the heart sections of the normal (a), paclitaxel-administered control group (b), and paclitaxel-administered groups treated with rutin (c), hesperidin (d), and their combination (e). CM: cardiac muscles; DC: degenerative changes; IC: inflammatory cells infiltration; H: hyalinosis (H&E; ×400).

scavenge free radicals and reduce the formation of lipid peroxide radicals. Remarkably similar results were mentioned by Geetha et al. [85], Huang et al. [86], and Xianchu et al. [76], who found that rutin suppressed oxidative stress *via* lowering production of ROS and MDA and by augmenting antioxidant status through increasing SOD, GSH, and GPx in several models of cardiovascular disease. An article of Qu et al. [27] showed that rutin suppressed oxidative/nitrosative stress, inflammation, and apoptosis in rats' kidneys. Rutin exhibited a significant level of protection against acrylamide-induced oxidative DNA damage, likely due to its antioxidant property [87].

By alleviating the oxidative stress, endoplasmic reticulum stress, inflammation, apoptosis, and autophagy-induced by valproic acid, rutin administration ameliorated liver and kidney damage [88]. It was found that the protective effects of hesperidin were associated with countering oxidative/nitrosative stress, inflammation, and apoptosis, thus, preserving renal structure and function in mice intoxicated with cyclophosphamide [89]. Moreover, hesperidin reduced the heart LPO and increased antioxidant enzyme activities in ischemic myocardial rats [90]. Hesperidin's anticancer potential is controlled by ROS-dependent apoptotic pathways in certain cancer cells, despite the fact that it can be an excellent ROS scavenger and could operate as a powerful antioxidant defense mechanism [91, 92].

5. Conclusion

Coadministration of rutin, hesperidin, or their combination with paclitaxel in male Wistar rats might diminish the incidence and severity of detrimental effects of paclitaxel (Taxol)-induced toxicity in the kidney and heart. These

protective effects are likely mediated by suppressing oxidative stress and enhancing antioxidant defenses. Moreover, a combination of rutin and hesperidin treatment of paclitaxel-administered rats was most efficacious in preventing renal and cardiac dysfunction and adverse histological impacts. Before using rutin and hesperidin in patients and receiving FDA approval, more clinical trials are required to evaluate their effectiveness and safety.

Abbreviations

ANOVA: One-way analysis of variance
AST: Aspartate aminotransferase
CK: Creatine kinase
CK-MB: Creatine kinase-MB
CMC: Carboxymethylcellulose
CrEL: Cremophor/ethanol
DNA: Deoxyribonucleic acid
FDA: Food and Drug Administration
GPx: Glutathione peroxidase
GSH: Reduced glutathione
GSSG: Oxidized glutathione
H&E: Hematoxylin and eosin stain
H_2O_2: Hydrogen peroxide
b. wt: Body weight
LDH: Lactate dehydrogenase
LPO: Lipid peroxidation
MDA: Malondialdehyde or 1,1,3,3-tetramethoxypropane
rpm: Round per minute
ROS: Reactive oxygen species
SEM: Standard error of the mean
SPSS: Statistical package for social sciences
SOD: Superoxide dismutase
TBA: Thiobarbituric acid
TCA: Trichloroacetic acid.

Data Availability

All data are available from the corresponding author upon reasonable request.

Conflicts of Interest

The authors declare that there are no conflict of interest.

Acknowledgments

The authors extend their appreciation to the Deanship of Scientific Research at King Khalid University for funding this work through large Groups Project under grant number RGP. 2/38/43.

References

[1] T. M. Abu Samaan, M. Samec, A. Liskova, P. Kubatka, and D. Büsselberg, "Paclitaxel's mechanistic and clinical effects on breast cancer," *Biomolecules*, vol. 9, no. 12, p. 789, 2019.

[2] S. Ezrahi, A. Aserin, and N. Garti, "Basic principles of drug delivery systems–the case of paclitaxel," *Advances in Colloid and Interface Science*, vol. 263, pp. 95–130, 2019.

[3] B. Gorain, H. Choudhury, M. Pandey, and P. Kesharwani, "Paclitaxel loaded vitamin E-TPGS nanoparticles for cancer therapy," *Materials Science and Engineering: C*, vol. 91, pp. 868–880, 2018.

[4] N. P. Staff, J. C. Fehrenbacher, M. Caillaud, M. I. Damaj, R. A. Segal, and S. Rieger, "Pathogenesis of paclitaxel-induced peripheral neuropathy: a current review of *in vitro* and *in vivo* findings using rodent and human model systems," *Experimental Neurology*, vol. 324, Article ID 113121, 2020.

[5] L. Zhu and L. Chen, "Progress in research on paclitaxel and tumor immunotherapy," *Cellular and Molecular Biology Letters*, vol. 24, no. 1, pp. 40–11, 2019.

[6] S. M. Swain, S. F. Honig, M. C. Tefft, and L. Walton, "A phase II trial of paclitaxel (Taxol®) as first line treatment in advanced breast cancer," *Investigational New Drugs*, vol. 13, no. 3, pp. 217–222, 1995.

[7] F. Gelsomino, M. Tiseo, F. Barbieri et al., "Phase 2 study of NAB-paclitaxel in SensiTivE and refractory relapsed small cell lung cancer (SCLC) (NABSTER TRIAL)," *British Journal of Cancer*, vol. 123, no. 1, pp. 26–32, 2020.

[8] A. Hernández-Prat, A. Rodriguez-Vida, N. Juanpere-Rodero et al., "Novel oral mTORC1/2 inhibitor TAK-228 has synergistic antitumor effects when combined with paclitaxel or PI3Kα inhibitor TAK-117 in preclinical bladder cancer models," *Molecular Cancer Research*, vol. 17, no. 9, pp. 1931–1944, 2019.

[9] A. Y. Kilcar, O. Yildiz, T. Dogan, E. Sulu, G. Takan, and F. Z. B. Muftuler, "Bitter melon (*Momordica charantia*) extract effect against 99mTc labeled paclitaxel: *in vitro* monitoring on breast cancer cells," *Anti-Cancer Agents in Medicinal Chemistry*, vol. 20, no. 12, pp. 1497–1503, 2020.

[10] D. Qu, M. Jiao, H. Lin et al., "Anisamide-functionalizedpH-responsive amphiphilic chitosan-based paclitaxel micelles for sigma-1 receptor targeted prostate cancer treatment," *Carbohydrate Polymers*, vol. 229, Article ID 115498, 2020.

[11] L. Della Corte, F. Barra, V. Foreste et al., "Advances in paclitaxel combinations for treating cervical cancer," *Expert Opinion on Pharmacotherapy*, vol. 21, no. 6, pp. 663–677, 2020.

[12] A. M. Cirrincione, A. D. Pellegrini, J. R. Dominy et al., "Paclitaxel-induced peripheral neuropathy is caused by epidermal ROS and mitochondrial damage through conserved MMP-13 activation," *Scientific Reports*, vol. 10, no. 1, pp. 1–12, 2020.

[13] M. L. Costa, J. A. Rodrigues, J. Azevedo, V. Vasconcelos, E. Eiras, and M. G. Campos, "Hepatotoxicity induced by paclitaxel interaction with turmeric in association with a microcystin from a contaminated dietary supplement," *Toxicon*, vol. 150, pp. 207–211, 2018.

[14] M. J. Gil-Gil, M. Bellet, S. Morales et al., "Pegylated liposomal doxorubicin plus cyclophosphamide followed by paclitaxel as primary chemotherapy in elderly or cardiotoxicity-prone patients with high-risk breast cancer: results of the phase II CAPRICE study," *Breast Cancer Research and Treatment*, vol. 151, no. 3, pp. 597–606, 2015.

[15] G. I. Harisa, "Blood viscosity as a sensitive indicator for paclitaxel induced oxidative stress in human whole blood," *Saudi Pharmaceutical Journal*, vol. 23, no. 1, pp. 48–54, 2015.

[16] E. Adikwu, N. Ebinyo, and D. O. Orakpor, "Coenzyme Q10 and resveratrol protect against paclitaxel-induced

nephrotoxicity in rats," *Trends in Pharmaceutical Sciences*, vol. 7, no. 1, pp. 49–58, 2021.

[17] M. Ashrafizadeh, A. Zarrabi, F. Hashemi et al., "Curcumin in cancer therapy: a novel adjunct for combination chemotherapy with paclitaxel and alleviation of its adverse effects," *Life Sciences*, vol. 256, Article ID 117984, 2020.

[18] M. Osman and M. Elkady, "A prospective study to evaluate the effect of paclitaxel on cardiac ejection fraction," *Breast Care*, vol. 12, no. 4, pp. 255–259, 2017.

[19] S. Ince, D. Arslan Acaroz, O. Neuwirth et al., "Protective effect of polydatin, a natural precursor of resveratrol, against cisplatin-induced toxicity in rats," *Food and Chemical Toxicology*, vol. 72, pp. 147–153, 2014.

[20] E. Sengul, V. Gelen, and S. Gedikli, "Cardioprotective activities of quercetin and rutin in Sprague Dawley rats treated with 5-flourouracil," *JAPS: Journal of Animal and Plant Sciences*, vol. 31, no. 2, pp. 423–443, 2021.

[21] E. Sengul, V. Gelen, S. Yildirim, S. Tekin, and Y. Dag, "The effects of selenium in acrylamide-induced nephrotoxicity in rats: roles of oxidative stress, inflammation, apoptosis, and DNA damage," *Biological Trace Element Research*, vol. 199, no. 1, pp. 173–184, 2021.

[22] M. Addi, A. Elbouzidi, M. Abid, D. Tungmunnithum, A. Elamrani, and C. Hano, "An overview of bioactive flavonoids from citrus fruits," *Applied Sciences*, vol. 12, no. 1, p. 29, 2021.

[23] K. Borowiec and A. Michalak, "Flavonoids from edible fruits as therapeutic agents in neuroinflammation: a comprehensive review and update," *Critical Reviews in Food Science and Nutrition*, vol. 62, no. 24, pp. 6742–6760, 2021.

[24] C. Del Bo, S. Bernardi, and M. Marino, "Systematic review on polyphenol intake and health outcomes: is there sufficient evidence to define a health-promotingpolyphenol-rich dietary pattern?" *Nutrients*, vol. 11, no. 6, p. 1355, 2019.

[25] R. K. Sharma, N. Sharma, U. Kumar, and S. S. Samant, "Antioxidant properties, phenolics and flavonoids content of some economically important plants from North-west Indian Himalaya," *Natural Product Research*, vol. 36, no. 6, pp. 1565–1569, 2021.

[26] A. Satari, S. Ghasemi, S. Habtemariam, S. Asgharian, and Z. Lorigooini, "Rutin: a flavonoid as an effective sensitizer for anticancer therapy; insights into multifaceted mechanisms and applicability for combination therapy," *Evidence-based Complementary and Alternative Medicine*, vol. 2021, Article ID 9913179, 10 pages, 2021.

[27] S. Qu, C. Dai, F. Lang et al., "Rutin attenuates vancomycin-induced nephrotoxicity by ameliorating oxidative stress, apoptosis, and inflammation in rats," *Antimicrobial Agents and Chemotherapy*, vol. 63, no. 1, Article ID e01545-18, 2019.

[28] R. Cannataro, A. Fazio, C. La Torre, M. C. Caroleo, and E. Cione, "Polyphenols in the mediterranean diet: from dietary sources to microRNA modulation," *Antioxidants*, vol. 10, no. 2, p. 328, 2021.

[29] Q. Li, D. Xu, Z. Gu, T. Li, P. Huang, and L. Ren, "Rutin restrains the growth and metastasis of mouse breast cancer cells by regulating the microRNA-129-1-3p-mediated calcium signaling pathway," *Journal of Biochemical and Molecular Toxicology*, vol. 35, no. 7, Article ID e22794, 2021.

[30] M. Qin, Q. Li, Y. Wang et al., "Rutin treats myocardial damage caused by pirarubicin *via* regulating miR-22-5p-regulated RAP1/ERK signaling pathway," *Journal of Biochemical and Molecular Toxicology*, vol. 35, no. 1, Article ID e22615, 2021.

[31] M. Zhou, G. Zhang, J. Hu et al., "Rutin attenuates sorafenib-induced chemoresistance and autophagy in hepatocellular carcinoma by regulating BANCR/miRNA-590-5P/OLR1 Axis," *International Journal of Biological Sciences*, vol. 17, no. 13, pp. 3595–3607, 2021.

[32] A. M. Ali, M. A. Gabbar, S. M. Abdel-Twab et al., "Antidiabetic potency, antioxidant effects, and mode of actions of *Citrus reticulata* fruit peel hydroethanolic extract, hesperidin, and quercetin in nicotinamide/streptozotocin-induced Wistar diabetic rats," *Oxidative Medicine and Cellular Longevity*, vol. 2020, Article ID 1730492, 21 pages, 2020.

[33] S. Moustafa, R. Hashish, and R. Abdel-Karim, "The possible ameliorative effect of hesperidin administration in aluminum phosphide induced acute nephrotoxicity in adult albino rats," *Ain Shams Journal of Forensic Medicine and Clinical Toxicology*, vol. 38, no. 1, pp. 46–56, 2022.

[34] P. Pandey and F. Khan, "A mechanistic review of the anticancer potential of hesperidin, a natural flavonoid from citrus fruits," *Nutrition Research*, vol. 92, pp. 21–31, 2021.

[35] A. Mangaiarkkarasi, S. Rameshkannan, and R. M. Ali, "Effect of gabapentin and pregabalin in rat model of taxol induced neuropathic pain," *Journal of Clinical and Diagnostic Research: Journal of Clinical and Diagnostic Research*, vol. 9, no. 5, pp. FF11–FF14, 2015.

[36] S. L. Patil, H. Somashekarappa, and K. Rajashekhar, "Radiomodulatory role of rutin and quercetin in Swiss albino mice exposed to the whole body gamma radiation," *Indian Journal of Nuclear Medicine*, vol. 27, no. 4, pp. 237–242, 2012.

[37] L. Xu, Z. L. Yang, P. Li, and Y. Q. Zhou, "Modulating effect of Hesperidin on experimental murine colitis induced by dextran sulfate sodium," *Phytomedicine*, vol. 16, no. 10, pp. 989–995, 2009.

[38] O. M Ahmed, S. R Galaly, M. Raslan, and M. A. M A Mostafa, "Thyme oil and thymol abrogate doxorubicin-induced nephrotoxicity and cardiotoxicity in Wistar rats *via* repression of oxidative stress and enhancement of antioxidant defense mechanisms," *Biocell*, vol. 44, no. 1, pp. 41–53, 2020.

[39] D. L. Fabiny and G. Ertingshausen, "Automated reaction-rate method for determination of serum creatinine with the CentrifiChem," *Clinical Chemistry*, vol. 17, no. 8, pp. 696–700, 1971.

[40] A. Tabacco, F. Meiattini, E. Moda, and P. Tarli, "Simplified enzymic/colorimetric serum urea nitrogen determination," *Clinical Chemistry*, vol. 25, no. 2, pp. 336-337, 1979.

[41] P. Fossati, L. Prencipe, and G. Berti, "Use of 3,5-dichloro-2-hydroxybenzenesulfonic acid/4-aminophenazone chromogenic system in direct enzymic assay of uric acid in serum and urine," *Clinical Chemistry*, vol. 26, no. 2, pp. 227–231, 1980.

[42] D. S. Young, *Effects of Drugs on Clinical Laboratory Tests*, The American Association for Clinical Chemistry, Washington, DC, USA, 4th edition, 1995.

[43] A. Pesce, "Lactate dehydrogenase," in *Clinical Chemistry*p. 1124, The CV Mosby Co, Toronto, Canada, 1984.

[44] H. G. Preuss, S. T. Jarrell, R. Scheckenbach, S. Lieberman, and R. A. Anderson, "Comparative effects of chromium, vanadium and *Gymnema sylvestre* on sugar-induced blood pressure elevations in Spontaneously hypertensive rats (SHR)," *Journal of the American College of Nutrition*, vol. 17, no. 2, pp. 116–123, 1998.

[45] E. Beutler, O. Duren, and B. M. Kelly, "Improved method for the determination of blood glutathione," *The Journal of Laboratory and Clinical Medicine*, vol. 61, pp. 882–888, 1963.

[46] B. Matkovics, M. Kotorman, I. S. Varga, D. Q. Hai, and C. S. Varga, "Oxidative stress in experimental diabetes induced by streptozotocin," *Acta Physiologica Hungarica*, vol. 85, no. 1, pp. 29–38, 1997.

[47] S. Marklund and G. Marklund, "Involvement of the superoxide anion radical in the autoxidation of pyrogallol and a convenient assay for superoxide dismutase," *European Journal of Biochemistry*, vol. 47, no. 3, pp. 469–474, 1974.

[48] J. D. Banchroft, A. Stevens, and D. R. Turner, *Theory and Practice of Histological Techniques*, Churchil Living Stone, London, UK, 4th edition, 1996.

[49] A. H. El-Far, M. A. Lebda, A. E. Noreldin et al., "Quercetin attenuates pancreatic and renal D-galactose-inducedaging-related oxidative alterations in rats," *International Journal of Molecular Sciences*, vol. 21, no. 12, pp. 4348–48, 2020.

[50] A. M. Zaazaa, "Studying the anticancer properties of bone MarrowDerived mesenchymal stem cells against hepatocellular carcinoma induced by N-nitrosodiethylamine in male rats," *Biointerface Research in Applied Chemistry*, vol. 13, no. 1, pp. 1–13, 2022.

[51] I. Klein and H. C. Lehmann, "Pathomechanisms of paclitaxel-induced peripheral neuropathy," *Toxics*, vol. 9, no. 10, p. 229, 2021.

[52] Y. Wang, Y. Zhou, Z. Zheng, J. Li, Y. Yan, and W. Wu, "Sulforaphane metabolites reduce resistance to paclitaxel *via* microtubule disruption," *Cell Death & Disease*, vol. 9, no. 11, pp. 1134–1149, 2018.

[53] A. Grigorian and C. B. O'Brien, "Hepatotoxicity secondary to chemotherapy," *Journal of Clinical and Translational Hepatology*, vol. 2, no. 2, pp. 95–102, 2014.

[54] P. D. King and M. C. Perry, "Hepatotoxicity of chemotherapy," *The Oncologist*, vol. 6, no. 2, pp. 162–176, 2001.

[55] N. Lameire, "Nephrotoxicity of recent anti-cancer agents," *Clinical Kidney Journal*, vol. 7, no. 1, pp. 11–22, 2014.

[56] G. Miolo, N. La Mura, P. Nigri et al., "The cardiotoxicity of chemotherapy: new prospects for an old problem," *Radiology and Oncology*, vol. 40, no. 3, pp. 149–161, 2006.

[57] D. T. Al-Gabri, A. J. Al-Naely, and H. A. Alghanmi, "Using of nanocomposite loading klisinema persicum for reducing the damage of the liver and kidneys in female rats caused by taxol (paclitaxel)," *Turkish Journal of Physiotherapy and Rehabilitation*, vol. 32, no. 3, 2021.

[58] Y. Zhang, Z. Wu, H. Yu et al., "Chinese herbal medicine *Wenxia Changfu* Formula reverses cell adhesion-mediated drug resistance *via* the integrin β1-PI3K-AKT pathway in lung cancer," *Journal of Cancer*, vol. 10, no. 2, pp. 293–304, 2019.

[59] O. M. Ahmed, T. M. Ali, M. A. Abdel Gaid, and A. A. Elberry, "Effects of enalapril and paricalcitol treatment on diabetic nephropathy and renal expressions of TNF-α, p53, caspase-3 and Bcl-2 in STZ-induced diabetic rats," *PLoS One*, vol. 14, no. 9, Article ID e0214349, 2019.

[60] B. Ali, "A study of the physiological effects of the anticancer paclitaxel in men," *Al-Qadisiyah Journal of Pure Science*, vol. 21, no. 4, pp. 33–38, 2016.

[61] H. Choudhury, B. Gorain, R. K. Tekade, M. Pandey, S. Karmakar, and T. K. Pal, "Safety against nephrotoxicity in paclitaxel treatment: oral nanocarrier as an effective tool in preclinical evaluation with marked *in vivo* antitumor activity," *Regulatory Toxicology and Pharmacology*, vol. 91, pp. 179–189, 2017.

[62] X. Guo, W. Li, J. Hu, E. C. Zhu, and Q. Su, "Hepatotoxicity in patients with solid tumors treated with PD-1/PD-L1 inhibitors alone, PD-1/PD-L1 inhibitors plus chemotherapy, or chemotherapy alone: systematic review and meta-analysis," *European Journal of Clinical Pharmacology*, vol. 76, no. 10, pp. 1345–1354, 2020.

[63] S. O. Rabah, "Acute taxol nephrotoxicity: histological and ultrastructural studies of mice kidney parenchyma," *Saudi Journal of Biological Sciences*, vol. 17, no. 2, pp. 105–114, 2010.

[64] H. S. Abou Seif, "Protective effect of rutin and hespridin against doxorubicin induced nephrotoxicity," *Journal of Applied Sciences*, vol. 1, no. 2, pp. 1–18, 2012.

[65] N. O. Al-Harbi, F. Imam, M. M. Al-Harbi et al., "Rutin inhibits carfilzomib-induced oxidative stress and inflammation *via* the NOS-mediated NF-κB signaling pathway," *Inflammopharmacology*, vol. 27, no. 4, pp. 817–827, 2019.

[66] H. T. Emam and A. G. Madboly, "Ameliorative effects of hesperidin and melatonin against acetaminophen-induced nephrotoxicity in adult albino rats," *The Egyptian Journal of Forensic Sciences and Applied Toxicology*, vol. 21, no. 1, pp. 31–46, 2021.

[67] A. Rauf, M. A. Shariati, M. Imran et al., "Comprehensive review on naringenin and naringin polyphenols as a potent anticancer agent," *Environmental Science and Pollution Research*, vol. 29, no. 21, pp. 31025–31041, 2022.

[68] S. Y. Saad, T. A. O. Najjar, and M. Alashari, "Cardiotoxicity of doxorubicin/paclitaxel combination in rats: effect of sequence and timing of administration," *Journal of Biochemical and Molecular Toxicology*, vol. 18, no. 2, pp. 78–86, 2004.

[69] K. Zhang, F. M. Heidrich, B. DeGray, W. Boehmerle, and B. E. Ehrlich, "Paclitaxel accelerates spontaneous calcium oscillations in cardiomyocytes by interacting with NCS-1 and the InsP3R," *Journal of Molecular and Cellular Cardiology*, vol. 49, no. 5, pp. 829–835, 2010.

[70] C. Panis, R. Binato, S. Correa et al., "Short infusion of paclitaxel imbalances plasmatic lipid metabolism and correlates with cardiac markers of acute damage in patients with breast cancer," *Cancer Chemotherapy and Pharmacology*, vol. 80, no. 3, pp. 469–478, 2017.

[71] H. Malekinejad, S. Ahsan, F. Delkhosh-Kasmaie, H. Cheraghi, A. Rezaei-Golmisheh, and H. Janbaz-Acyabar, "Cardioprotective effect of royal jelly on paclitaxel-inducedcardiotoxicity in rats," *Iranian Journal of Basic Medical Sciences*, vol. 19, no. 2, pp. 221–227, 2016.

[72] S. Razzaq, A. Rauf, A. Raza et al., "A multifunctional polymeric micelle for targeted delivery of paclitaxel by the inhibition of the P-glycoprotein transporters," *Nanomaterials*, vol. 11, no. 11, p. 2858, 2021.

[73] H. M. Babiker, A. McBride, M. Newton et al., "Cardiotoxic effects of chemotherapy: a review of both cytotoxic and molecular targeted oncology therapies and their effect on the cardiovascular system," *Critical Reviews in Oncology*, vol. 126, pp. 186–200, 2018.

[74] J. Li, T. Yin, L. Wang, L. Yin, J. Zhou, and M. Huo, "Biological evaluation of redox-sensitive micelles based on hyaluronic acid-deoxycholic acid conjugates for tumor-specific delivery of paclitaxel," *International Journal of Pharmaceutics*, vol. 483, no. 1-2, pp. 38–48, 2015.

[75] H. N. Siti, J. Jalil, A. Y. Asmadi, and Y. Kamisah, "Roles of rutin in cardiac remodeling," *Journal of Functional Foods*, vol. 64, Article ID 103606, 2020.

[76] L. Xianchu, Z. Lan, L. Ming, and M. Yanzhi, "Protective effects of rutin on lipopolysaccharide-induced heart injury in mice," *Journal of Toxicological Sciences*, vol. 43, no. 5, pp. 329–337, 2018.

[77] Y. D. Wang, Y. Zhang, B. Sun, X. W. Leng, Y. J. Li, and L. Q. Ren, "Cardioprotective effects of rutin in rats exposed to pirarubicin toxicity," *Journal of Asian Natural Products Research*, vol. 20, no. 4, pp. 361–373, 2018.

[78] I. T. Abdel-Raheem and A. A. Abdel-Ghany, "Hesperidin alleviates doxorubicin-induced cardiotoxicity in rats," *Journal of the Egyptian National Cancer Institute*, vol. 21, no. 2, pp. 175–184, 2009.

[79] P. Bhargava, D. Arya, and J. Bhatia, "Cardioprotective effect of hesperidin in an experimental model of cardiac hypertrophy," *Journal of Hypertension*, vol. 37, pp. e183–e184, 2019.

[80] X. Ren, B. Zhao, H. Chang, M. Xiao, Y. Wu, and Y. Liu, "Paclitaxel suppresses proliferation and induces apoptosis through regulation of ROS and the AKT/MAPK signaling pathway in canine mammary gland tumor cells," *Molecular Medicine Reports*, vol. 17, no. 6, pp. 8289–8299, 2018.

[81] D. Selimovic, M. Hassan, Y. Haikel, and U. R. Hengge, "Taxol-induced mitochondrial stress in melanoma cells is mediated by activation of c-JunN-terminal kinase (JNK) and p38 pathways *via* uncoupling protein 2," *Cellular Signalling*, vol. 20, no. 2, pp. 311–322, 2008.

[82] G. Varbiro, B. Veres, F. Gallyas, and B. Sumegi, "Direct effect of taxol on free radical formation and mitochondrial permeability transition," *Free Radical Biology and Medicine*, vol. 31, no. 4, pp. 548–558, 2001.

[83] V. Annamalai, M. Kotakonda, and V. Periyannan, "JAK1/STAT3 regulatory effect of β-caryophyllene on MG-63 osteosarcoma cells *via* ROS-induced apoptotic mitochondrial pathway by DNA fragmentation," *Journal of Biochemical and Molecular Toxicology*, vol. 34, no. 8, Article ID e22514, 2020.

[84] A. W. Kwak, J. S. Choi, K. Liu et al., "Licochalcone C induces cell cycle G1 arrest and apoptosis in human esophageal squamous carcinoma cells by activation of the ROS/MAPK signaling pathway," *Journal of Chemotherapy*, vol. 32, no. 3, pp. 132–143, 2020.

[85] R. Geetha, C. Sathiya Priya, and C. V. Anuradha, "Troxerutin abrogates mitochondrial oxidative stress and myocardial apoptosis in mice fed calorie-rich diet," *Chemico-Biological Interactions*, vol. 278, pp. 74–83, 2017.

[86] R. Huang, Z. Shi, L. Chen, Y. Zhang, J. Li, and Y. An, "Rutin alleviates diabetic cardiomyopathy and improves cardiac function in diabetic ApoEknockout mice," *European Journal of Pharmacology*, vol. 814, pp. 151–160, 2017.

[87] C. Uthra, M. S. Reshi, A. Jaswal et al., "Protective efficacy of rutin against acrylamide-induced oxidative stress, biochemical alterations and histopathological lesions in rats," *Toxicology Research*, vol. 11, no. 1, Article ID tfab125, pp. 215; 225, 2022.

[88] F. M. Kandemir, M. Ileriturk, and C. Gur, "Rutin protects rat liver and kidney from sodium valproate-induce damage by attenuating oxidative stress, ER stress, inflammation, apoptosis and autophagy," *Molecular Biology Reports*, vol. 49, no. 7, pp. 6063–6074, 2022.

[89] A. A. Fouad, S. A. Abdel-Gaber, and M. I. Abdelghany, "Hesperidin opposes the negative impact of cyclophosphamide on mice kidneys," *Drug and Chemical Toxicology*, vol. 44, no. 3, pp. 223–228, 2019.

[90] P. Selvaraj and K. V. Pugalendi, "Hesperidin, a flavanone glycoside, on lipid peroxidation and antioxidant status in experimental myocardial ischemic rats," *Redox Report*, vol. 15, no. 5, pp. 217–223, 2010.

[91] M. S. Antunes, F. V. L. Ladd, A. A. Ladd, A. L. Moreira, S. P. Boeira, and L. Cattelan Souza, "Hesperidin protects against behavioral alterations and loss of dopaminergic neurons in 6-OHDA-lesioned mice: the role of mitochondrial dysfunction and apoptosis," *Metabolic Brain Disease*, vol. 36, no. 1, pp. 153–167, 2021.

[92] S. S. Khaled, H. A. Soliman, M. Abdel-Gabbar et al., "The preventive effects of naringin and naringenin against paclitaxel-induced nephrotoxicity and cardiotoxicity in male wistar rats," *Evidence-based Complementary and Alternative Medicine*, vol. 2022, Article ID 8739815, 11 pages, 2022.

Hindawi
Evidence-Based Complementary and Alternative Medicine
Volume 2023, Article ID 9766002, 12 pages
https://doi.org/10.1155/2023/9766002

Research Article

Antibacterial, Antioxidant, and *in silico* NADPH Oxidase Inhibition Studies of Essential Oils of *Lavandula dentata* against Foodborne Pathogens

Youness El Abdali,[1] Ghada Beniaich,[2] Adil M. Mahraz,[2] Abdelfattah El Moussaoui,[1] Yousef A. Bin Jardan,[3] Mohamed Akhazzane,[2] Mohamed Chebaibi,[4] Hiba-Allah Nafidi,[5] Noureddine Eloutassi,[6] Mohammed Bourhia,[7] and Abdelhak Bouia[1]

[1]*Laboratory of Biotechnology, Environment, Agri-Food and Health, Faculty of Sciences Dhar El Mahraz, Sidi Mohamed Ben Abdellah University, P.O. Box 1796, Atlas, Fez 30000, Morocco*
[2]*Engineering Laboratory of Organometallic, Molecular Materials and Environment, Faculty of Sciences Dhar El Mahraz, Sidi Mohamed Ben Abdellah University, P.O. Box 1796, Atlas, Fez 30000, Morocco*
[3]*Department of Pharmaceutics, College of Pharmacy, King Saud University, Riyadh, Saudi Arabia*
[4]*Biomedical and Translational Research Laboratory, Faculty of Medicine and Pharmacy, University of Sidi Mohamed Ben Abdellah, BP 1893, Km 22, Road of Sidi Harazem, Fez, Morocco*
[5]*Department of Food Science, Faculty of Agricultural and Food Sciences, Laval University, Quebec City 2325, QC G1V0A6, Canada*
[6]*Laboratory of Pedagogy and Technological Innovation, Regional Centre of Education and Formation Professions, Fez 30000, Morocco*
[7]*Laboratory of Chemistry and Biochemistry, Faculty of Medicine and Pharmacy, Ibn Zohr University, Laayoune 70000, Morocco*

Correspondence should be addressed to Youness El Abdali; youness.elabdali@usmba.ac.ma and Mohammed Bourhia; bourhiamohammed@gmail.com

Received 13 August 2022; Revised 11 September 2022; Accepted 19 September 2022; Published 11 February 2023

Academic Editor: Salah M. El Sayed

Food is always subjected to microbial infection and lipid peroxidation, which frequently leads to serious food intoxications. In the present study, essential oils (EOs) extracted from *Lavandula dentata* Moroccan species and its major component (linalool) were chemically characterized and their antioxidant potential and antibacterial properties against foodborne pathogenic bacteria were examined. EOs phytochemical profile was carried out using gas chromatography-mass spectrometry analysis (GC-MS). The antioxidant potential was evaluated, *in vitro*, by use of the β-carotene discoloration assay and *in silico* vs. NADPH oxidase enzymatic complex as an antioxidant marker. The antibacterial proprieties were assessed by use of minimal inhibitory concentration (MIC) and disc diffusion methods, against Gram (−) bacteria (*Pseudomonas aeruginosa*, *Salmonella enterica*, and *Escherichia coli*) and Gram (+) bacteria (*Bacillus subtilis* and *Staphylococcus aureus*). Linalool (49.71%) was the major component among the eighteen components identified in *Lavandula dentate* EO, followed by camphor (14.36%) and borneol (8.21%). The studied EO and linalool compounds showed important antioxidant activity through the β-carotene discoloration test with IC_{50} values of 35.72 ± 1.21 mg/mL and 30.32 ± 1.23 mg/mL, respectively. Among all the analyzed compounds of lavender EOs, thymol, carvacrol, and α-terpineol were the most active compounds against NADPH oxidase with a glide score of −6.483, −6.17, and −4.728 kcal/mol, respectively. 2D and 3D views showed the formation of hydrogen bonds between the most active compounds and the active site of NADPH oxidase. The antibacterial data showed a significant activity of *Lavandula dentata* essences against tested foodborne pathogenic bacteria, especially against *S. aureus* and *B. subtilis*. Linalool proved active toward the same bacteria and had closer activity to that of lavender essential oil. In light of the obtained findings, the essential oil of *Lavandula dentata* Moroccan species can be used in the packaging sector as a promising natural food conservative to limit lipid oxidation and treat foodborne infections.

1. Introduction

Antibiotic resistance is the leading cause of food poisoning outbreaks. Infections caused by resistant microbes can occur after eating contaminated food. *Campylobacter*, *Salmonella*, methicillin-resistant*Staphylococcus aureus* (MRSA), and some *Escherichia coli* strains are among antibiotic-resistant zoonotic bacteria that may infect humans through food and lead to treatment failure. Furthermore, the commensal bacterial flora may serve as a source of resistance genes that can be transmitted to resistant species and involve in illness in people and animals [1].

In fact, the emergence of antibiotic-resistant bacteria, both zoonotic and food-borne, is mainly due to the overuse of animal antibiotics in livestock and animal husbandry, as treatment or growth promoters. Animal foodstuffs contaminated with these microorganisms are potential vectors for human infections [2, 3]. One of the greatest threats to human health today is antibiotic resistance, which presents a significant obstacle to alternative drug research initiatives throughout the world [4]. Since bacteria cannotresist EOs, they represent potential alternatives to control antibiotic resistance in this regard [5].

Free radicals can harm the body's cells, causing damage to various oxygen substrates, DNA, proteins, fatty acids, and lipids [6, 7]. Today, the presence of antioxidants in food has become essential for quality and food safety. As synthetic antioxidants have negative effects on human health, aromatic plants can be used as a source of antioxidants and natural antibacterial agents for the agri-food industry, especially in food packaging systems [8, 9]. During the last few years, natural products have aroused great interest as medications, pharmaceutical products, cosmetics, and food additives [10].

Widely used in prophetic medicine, as well as in traditional medicine in Morocco, *Lavandula dentata* (lavender) possesses a large spectrum of biological activities, including sedative, antidepressant, anti-inflammatory, antioxidant, antibacterial, and antifungal properties [11]. However, there is a lack of research and information on the activities of Moroccan varieties, especially against food-borne pathogens resistant to antibiotics, which deserve to be examined in order to expand the spectrum of biological activities and applications of Moroccan *Lavandula dentata*. It is thus fitting that we were interested in investigating this emblematic plant of the Moroccan pharmacopoeia, through phytochemical characterization of its essential oils and their antioxidant (*in vitro* and *in silico*) and antibacterial activities against antibiotic-resistant pathogens.

2. Materials and Methods

2.1. Chemicals. Butylated hydroxytoluene (BHT), dimethylsulfoxide (DMSO), resazurin, and β-carotene were obtained from Sigma-Aldrich (Germany). Antibiotics and bacterial culture media were obtained from Biokar Diagnostics (France).

2.2. Plant Materials. The flowering tops of *Lavandula dentata* were used in the present study for testing (Figure 1). The plant specimens were collected from around Imouzzer Kandar city (33°44′ N, 5°01′ W at 1300 m altitude) of Morocco at the end of May, 2020. The samples were vouchered under the number DL78/24811, after being identified by a botanist. The collected samples were cleaned and dried for 15 days in a shaded and ventilated area before being subjected to extraction.

2.3. Extraction of Essential Oil. A total of 100 g of dried aerial parts were hydrodistillated with 1 L of distilled water using a clevenger-type apparatus for 3 h as documented elsewhere [12]. By use of anhydrous sodium sulfate, EOs were stored in darkness at 4 F02D 5°C in the dark until use. The yield of EOs was calculated and given in percentage (v/w).

2.4. Chemical Characterization of Essential Oil. The chemical composition of *L. dentata* EO was investigated using gas chromatography TQ8040 NX (Shimadzu, Tokyo, Japan) coupled with a triple quadrupole, tandem mass spectrometer (GC-MSMS). The EO chemical compounds were identified using an apolar, capillary RTxi-5 Sil MS column (30.00 m long, 00.25 mm inside diameter, and a film thickness of 0.25). 200°C and 280°C were the source and interface temperatures, respectively. Helium was employed as the carrier gas (with an injection volume of 1 μL). The oven temperature was programmed to start at 50°C for 2 minutes and it increased following two rises, rise 1 was set to 5°C/min to 160°C for 2 min and rise 2 was set to 5°C/min to 280°C for 2 min. The injection was in mode split (split opening at 4 min, with an injection temperature of 250°C and a pressure of 37.10 kPa). The composition of EO was presented as a proportion of the overall peak area. EO phytochemicals in EOs were identified by comparing the resulted retention indices referring to those of the literature database [13].

2.5. In Vitro Antioxidant Activity of Essential Oil. The antioxidant propriety of the extracted EO and its major compound (linalool) was evaluated using the β-carotene/linoleic acid assay [14]. In this assay, 1 mL of a chloroformic solution of β-carotene (1 mg/10 mL) was mixed with 20 mg of linoleic acid and 200 mg of Tween 40. Using a rotary evaporator, the chloroform was evaporated at 40°C for 5 minutes. Afterward, 50 mL of hydrogen peroxide was slowly added to the residue obtained with continuous stirring until an emulsion was formed. A volume of 5 mL of the obtained emulsion was added to all tubes containing 0.20 mL of ethanolic solution of EO and linalool (at various concentrations), and then, the absorbance at 470 nm was immediately measured relative to a blank not containing β-carotene. After incubation at 50°C for 5 minutes in a water bath, the absorbance of the tubes was measured again. BHT and ethanol were utilized as standard and negative control, respectively.

Figure 1: Flowering tops of *Lavandula dentate* L.

The antioxidant activity of the EO and linalool was evaluated as the percentage (%) of β-carotene discoloration inhibition using the following formula:

$$\beta - \text{carotene antiradical activity}\,(\%) = \left[\frac{(A_t - C_t)}{C_0 - C_t}\right] \times 100, \quad (1)$$

where A_t and C_t are the absorbance of the lavender EO and the control after 5 min of incubation, respectively. C_0 is the control absorbance measured at zero minute.

The kinetics of this activity were allowed to determine the sample's concentration corresponding to a 50% inhibition of β-carotene discoloration (IC_{50}).

2.6. In Silico Molecular Docking of Antioxidant Activity of Essential Oil. In this test, the antioxidant activity was conducted to examine the, *in silico*, inhibitory potency of *Lavandula dentata* EO against nicotinamide-adenine dinucleotide phosphate (NADPH) oxidase as an important antioxidant marker. All compounds identified in the studied EO were downloaded from the PubChem database in SDF format. Afterward, the Maestro 11.5 of the Schrödinger Software was used to prepare chemicals using the OPLS3 force field and the LigPrep tool. At a pH of 7.0 ± 2.0, ionization states generated 32 stereoisomers per ligand. The NADPH oxidase crystal structure in the Protein Data Bank was accessible through the following PDB ID : 2CDU. The structure was prepared and refined using the Protein Preparation Wizard of Schrödinger-Maestro v11.5. The minimization of the structure was conducted using the OPLS3 force field. The receptor grid was set at the following coordinates: $X = 0.395$, $Y = 10.379$, and $Z = 53.876$, where the volumetric spacing performed was $20 \times 20 \times 20$. SP flexible ligand docking was carried out in glide of Schrödinger-Maestro v 11.5 [15].

2.7. Antibacterial Activity of Essential Oil

2.7.1. Growth Medium and Chemicals. Tryptic soy agar (TSA) was the growth medium used for the bacterial strains in this study. It was prepared and autoclaved at 120°C for 20 min. Dimethylsulfoxide (DMSO) was used as a negative control. Disc antibiograms of vancomycin, streptomycin, and chloramphenicol were used as standard drugs.

2.7.2. Bacterial Strains. The antibacterial activity of *Lavandula dentata* EO and its major compound (linalool) was tested against five bacterial strains: Gram (−) bacteria including *Pseudomonas aeruginosa* (CIP 82118), *Salmonella entérica* (CIP 8039), and *Escherichia coli* (CIP 53126) and Gram (+) bacteria including *Bacillus subtilis* (CIP 5262) and *Staphylococcus aureus* (CIP 483), which were obtained from the collection of the Pasteur Institute (Rabat, Morocco). The selected bacteria are pathogenic and frequently involved in the contamination and spoilage of foodstuffs, which may constitute a major public health problem. The purity of the studied strains was verified by macroscopic characterization (colony characteristics) and microscopic observation of smears stained with the Gram stain.

The microbial suspension was made by collecting 2 to 3 colonies from a fresh culture (aged 24 hours) and suspending them in a 0.9% NaCl solution. The optical density of the suspensions was then determined using a UV-visible spectrophotometer at a wavelength of $\lambda = 625$ nm (Selecta, E. U). The final bacterial suspension was approximately of 5×10^5 CFU/mL [16].

2.7.3. Agar Disk Diffusion Assay. First, the bacterial sensitivity was assessed using the agar disk diffusion technique, which is extensively used to assess antimicrobial activity [17]. Initially, the Petri dishes (9 cm) containing TSA medium were inoculated with 0.1 mL of fresh bacterial culture and left to solidify. Next, sterile discs (6 mm) soaked with 15 μL of the test material (EO and linalool) and standard drugs were deposited on the agar surface. Finally, the zones around the disks were measured in mm after incubation at 37°C for 24 h. The test was repeated three times [18].

2.7.4. Determination of the Minimal Inhibitory Concentration (MIC). Microdilution in a 96-well microplate assay was used to investigate the MICs of the test material [17]. First, 100 μL of the TSA broth was deposited in every well of the microplate. Afterward, 100 μL of the EOs solution (25 mg/mL, w/v in DMSO 90%), linalool (25 mg/mL), and chloramphenicol (50 mg/mL) were deposited in the first wells. Then, excluding the last well (positive growth control), a microdilution was conducted by transferring 100 μL from the first well to the second and so on (diluting the material by a factor of 1/2 in each well). Next, inoculation was performed by depositing 10 μL of the microbial suspension, prepared previously, into each well except the negative control. Finally, the microplate was incubated for 24 h at 37°C. After incubation, 10 μL of resazurin (6.75 mg/mL in sterile distilled water) was added to each well to read the results [19]. The microplate was placed for the second time for 2 h in an incubator at 37°C. Indeed, wells containing bacterial growth changed their color from purple to pink, while wells without bacterial growth remained purple. Consequently, the MIC value with the lowest concentration did not produce a color change [20].

2.8. Statistical Analysis. GraphPad Prism 8, a Microsoft Software (California, USA), was employed to calculate mean values and standard deviations. Data of all tests were compared statistically by one-way ANOVA and Tukey's test, using the same software. At $p < 0.05$, the difference was considered significant.

3. Results

3.1. Chemical Composition and Yield of Lavandula dentata Essential Oil. The EO obtained from *Lavandula dentata* was pale yellow-green in color with a fresh and characteristic odor and yielded 3.47% of EO. The GC/MS profile and the phytochemicals identified in EO are summarized in Table 1. The findings of the chemical analysis revealed eighteen compounds in *Lavandula dentata* EO representing 99.97% of the total oil mass. Linalool (49.71%) was the major component followed by camphor (14.36%) and borneol (8.21%). Monoterpene chemical classes constituted the major chemical groups in *L. dentata* EO (92.51%). The β-farnesene (0.67%) was the only sesquiterpene hydrocarbon, while other compounds were listed with a rate not exceeding 6.79% of the studied EO.

3.2. In Vitro Antioxidant Activity of Lavandula dentata Essential Oil. The capacity of lavender EO in limitation of lipid oxidation was assessed in this study by evaluating the inhibitory effect of linoleic acid oxidation in the presence of β-carotene as a marker. β-carotene usually discolors rapidly in absence of antioxidants due to free radicals released from linoleic acid [21]. The results (Figure 2) showed that *Lavandula dentata* EO exhibited an important antioxidant effect in a concentration-dependent manner, limiting a maximum of 77.2% oxidation of linoleic acid when compared to the antioxidant effect obtained with BHT (84%). Linalool showed a potent antioxidant capacity of 82.1%. The concentrations of samples required to inhibit 50% of β-carotene discoloration (IC_{50}) are presented in Figure 3. IC_{50} values of both lavender EO and linalool were 35.72 ± 1.21 mg/mL and 30.32 ± 1.23 mg/mL, respectively. Notably, the IC_{50} value for the BHT standard was 16.46 ± 1.13 mg/mL.

3.3. In Silico Molecular Docking of Antioxidant Activity of Lavandula dentata Essential Oil. The antioxidant effect of lavender EO was also tested, *in silico*, against NADPH oxidase enzyme complex as an antioxidant marker. As shown in Table 2, the EO compounds exhibited an inhibitory effect against NADPH oxidase expressed in free binding energy. Thymol, carvacrol, α-terpineol, and camphor were the most active compounds against the active site of NADPH oxidase with a glide score of −6.483, −6.17, −4.728, and −4.541 kcal/mol, respectively.

2D and 3D views of *Lavandula dentata* EO, docked in the active site of NADPH oxidase, showed the formation of hydrogen bonds between the VAL 214 residue and the OH group of thymol and carvacrol; between the OH group of α-terpineol and GLY 180 and between the carbonyl group of camphor and TYR 188 residue (Figures 4 and 5). These results agreed with antioxidant potency tested by the use of β-carotene discoloration assay (Figures 2 and 3).

3.4. Antibacterial Activity of Lavandula dentata Essential Oil. The antibacterial activity of *Lavandula dentata* EO and linalool compound was studied, *in vitro,* using agar disc diffusion and minimal inhibitory concentration (MIC) methods against five food-bornepathogenic-bacterial strains (*S. enterica, S. aureus*, *P. aeruginosa, B. subtilis,* and *E. coli*), involved in food illness for both humans and animals [1]. Data obtained are summarized in Table 3 and Figure 6.

In fact, the obtained results of the growth inhibition zone scored in Tryptic soy agar demonstrated a wide antibacterial spectrum of studied EO and its major compound linalool (49.71%) against all tested strains, with different inhibition zone diameters. Both Gram (+) and Gram (−) bacteria were sensitive to lavender EO, which was particularly effective against *Escherichia coli* with a 17.08 ± 0.79 mm growth inhibition diameter, except for *Pseudomonas aeruginosa* (9.06 ± 0.63 mm), which was the least sensitive strain to the same EO. Compared to the EO, the linalool compound was more active against all tested bacterial strains marking larger diameters of growth inhibition. When subjected to treatment with the linalool compound, the Gram (+) *Bacillus subtilis* was the most sensitive of the strains tested followed by *Staphylococcus aureus* marked by a clear growth inhibition diameter of 29.00 ± 1.15 mm and 25.00 ± 1.73 mm, respectively. However, linalool showed a low activity against the Gram (−) *P. aeruginosa* (15.08 ± 0.50 mm). These results were sometimes better than those of some standard antibiotics tested such as streptomycin and vancomycin (Table 3).

The results of the bacteriostatic effectiveness of the tested samples estimated by minimum inhibitory concentration (MIC) are shown in Figure 6. According to the findings, the lowest inhibitory concentrations of lavender EO were observed for Gram (+) bacterial strains with concentrations of 0.332 mg/mL and 0.511 mg/mL in the case of *S. aureus* and *B. subtilis,* respectively. On the other hand, linalool exhibited a bacteriostatic effect close to that of lavender EO, with MIC values that ranged from 0.412 mg/mL for Gram (+) *S. aureus* to 1.443 mg/mL for Gram (−) *P. aeruginosa*, which was the least sensitive. Notably, the chloramphenicol antibiotic exhibited lower MICs against the tested strains.

4. Discussion

Hydrodistillation of *Lavandula dentata* resulted in 3.47% of characteristic EO. This yield is higher in comparison with that obtained from Tunisian lavender (0.89%) [22], and also exceeded that of the same plant collected from other regions of Morocco (2.9%) [23]. The impact of various environmental conditions can be responsible for the variation in extraction yield across plants [24]. Linalool (49.71%), followed by camphor (14.36%) and borneol (8.21%), were the major components identified in *Lavandula dentata* EO by GC-MS analysis. Other chemotypes of lavender in Morocco were reported to be rich in 1.8 cineol (41.28%) in eastern

Table 1: Chemicals identified in *L. dentata* EO.

RT (min)	RI	Compounds	Formula	Content (%)	Chemical structure
7.922	948	α-Pinene	$C_{10}H_{16}$	0.91	
10.828	1059	1,8-Cineole	$C_{10}H_{18}O$	5.47	
11.971	1164	cis-Linalool oxide	$C_{10}H_{18}O$	0.98	
12.450	1164	trans-Linalool oxide	$C_{10}H_{18}O$	0.67	
12.824	1082	Linalool	$C_{10}H_{18}O$	49.71	
14.278	1121	Camphor	$C_{10}H_{16}O$	14.36	
14.735	1146	Lavandulol	$C_{10}H_{18}O$	1.13	
15.019	1138	Borneol	$C_{10}H_{18}O$	8.21	
15.269	1137	Terpinen-4-ol	$C_{10}H_{18}O$	7.05	
15.421	1112	cis-Ocimenone	$C_{10}H_{14}O$	0.42	
15.530	1183	*n*-Hexyl butanoate	$C_{10}H_{20}O_2$	0.52	
15.678	1143	α-Terpineol	$C_{10}H_{18}O$	1.11	
17.197	1272	Linalyl acetate	$C_{12}H_{20}O_2$	4.81	

Table 1: Continued.

RT (min)	RI	Compounds	Formula	Content (%)	Chemical structure
18.133	1270	Lavandulyl acetate	$C_{12}H_{20}O_2$	1.00	
18.319	1262	Thymol	$C_{10}H_{14}O$	1.71	
18.557	1262	Carvacrol	$C_{10}H_{14}O$	0.78	
22.642	1440	β-Farnesene	$C_{15}H_{24}$	0.67	
23.846	1504	(R)-Lavandulyl (R)-2-methylbutanoate	$C_{15}H_{26}O_2$	0.46	
		Chemical classes (%)			
		Monoterpene hydrocarbons			92.51
		Sesquiterpene hydrocarbons			0.67
		Other compounds			6.79
		Total (%)			99.97

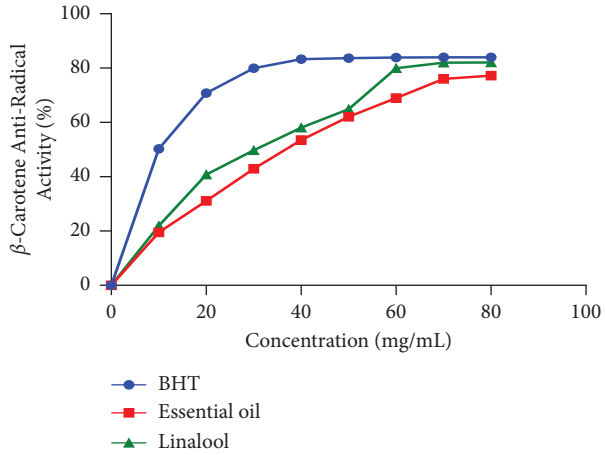

Figure 2: β-carotene antiradical activity of linalool and EO extracted from *L. dentata*.

Morocco [25], while those collected in the Moroccan Middle Atlas were marked by high camphor content (49.75%) [26]. The EO extracted from the leaves of Tunisian *L. dentata* was characterized by the dominance of camphor (26.52%) and 1.8 cineole (22.90%) [22], followed by β-eudesmol (21.17%), myrtenol (13.02%), and sabinol (11.02%) [27]. Similarly, the 1,8 cineole (63.25%) was also found to be the major component of the EO of lavender growing in Brazil [28]. Carvacrol (14.82%), terpinen-4-ol (5.98%), α-pinene (2.57%), and linalool (0.54%) compounds were also found in *N. sativa* (black Caraway) EOs [29]. Camphor, α-pinene, and terpinen-4-ol were also reported among the compounds figured in the EO of Tunisian and French fennel (*F. vulgare* Mill.) [30]. In addition to the method of extraction, the difference in the composition of EOs can be related to different factors, including circadian rhythms, seasonal conditions, and environmental impacts [28]. Many compounds in the characterized EO such as linalool, borneol, camphor, carvacrol,

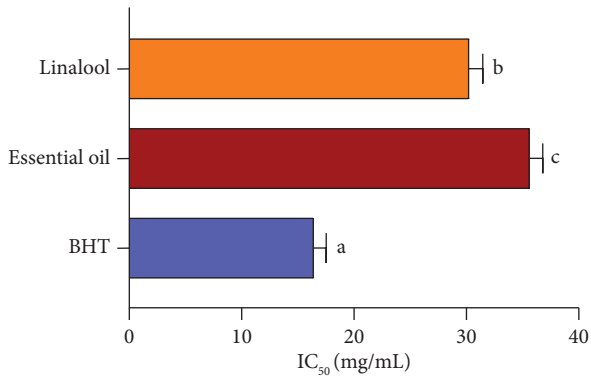

Figure 3: IC_{50} values (means ± SD) of antiradical activity of linalool and EO extracted from *L. dentata*. bars with different letters are significantly different ($p < 0.05$).

Table 2: Docking results of *L. dentata* EO in the active site of NADPH (PDB: 2CDU).

EO compounds	Glide score (kcal/mol)	Glide Emodel (kcal/mol)	Glide energy (kcal/mol)
Thymol	−6.483	−33.124	−23.764
Carvacrol	−6.17	−32.53	−23.46
α-Terpineol	−4.728	−25.282	−19.396
Camphor	−4.541	−28.001	−21.354
Terpinen-4-ol	−4.483	−23.15	−18.4
Borneol	−4.362	−27.569	−21.336
Lavandulyl acetate	−3.841	−33.464	−30.354
α-pinene	−3.763	−18.56	−15.108
cis-Linalool oxide	−3.689	−29.897	−25.14
trans-Linalool oxide	−3.634	−35.376	−29.279
Cineole	−3.56	−23.689	−19.321
Linalool	−2.951	−23.6	−20.027
cis-Ocimenone	−2.87	−22.441	−19.37
Linalyl acetate	−2.653	−24.182	−21.123
Lavandulol	−2.25	−21.265	−19.572
(R)-Lavandulyl (R)-2-methylbutanoate	−0.919	−24.344	−25.495
n-Hexyl butanoate	0.395	−22.499	−24.571
β-Farnesene	0.422	−20.402	−21.975

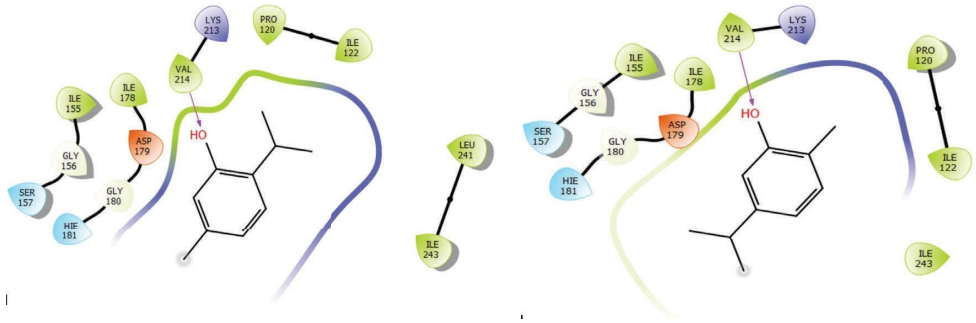

(a) (b)

Figure 4: Continued.

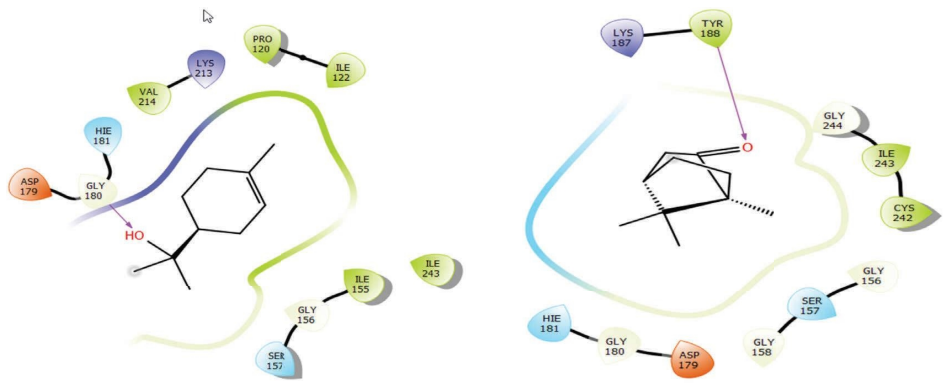

(c) (d)

Figure 4: 2D diagrams of ligand interactions with the active site of NADPH. (a) Thymol; (b) carvacrol; (c) α-terpineol; (d) camphor.

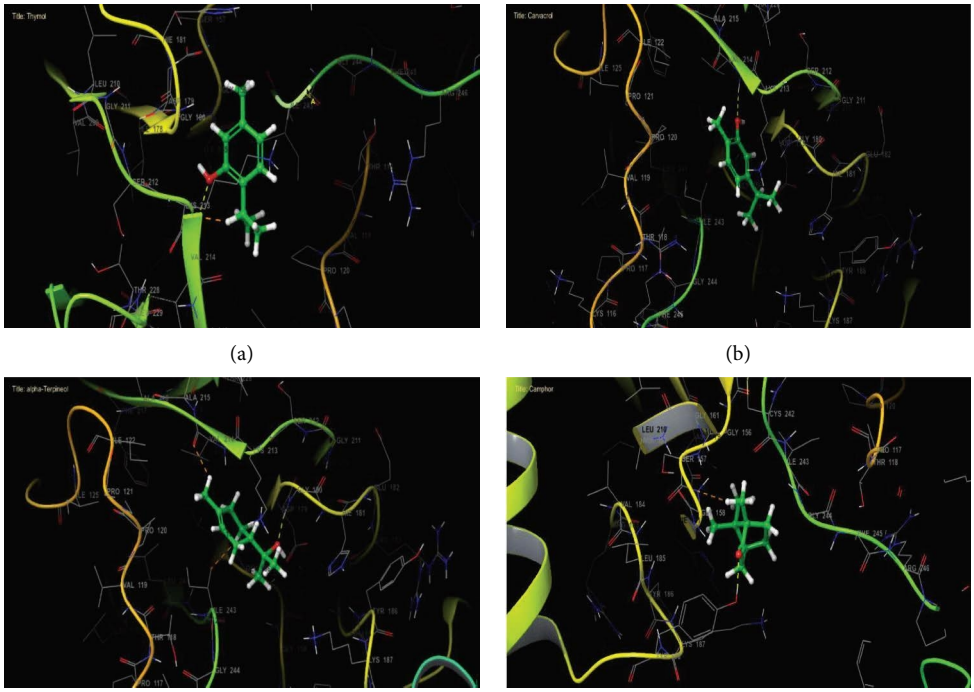

(a) (b)

(c) (d)

Figure 5: 3D diagrams of ligand interactions with the active site of NADPH. (a) Thymol; (b) carvacrol; (c) α-terpineol; (d) camphor.

Table 3: Inhibition zone diameter (mm) of linalool and EO extracted from *L. dentata* against bacterial strains (means ± SEM).

	Inhibition diameter (mm)				
	Gram-negative bacteria			*Gram-positive bacteria*	
	E. coli (CIP 53126)	*P. aeruginosa* (CIP 82118)	*S. enterica* (CIP 8039)	*B. subtilis* (CIP 5262)	*S. aureus* (CIP 483)
Lavender EO	17.08 ± 0.79^{b}	9.06 ± 0.63^{c}	15.16 ± 0.72^{c}	15.08 ± 0.65^{c}	15.08 ± 1.22^{c}
Linalool	20.08 ± 0.65^{b}	15.08 ± 0.50^{b}	23.08 ± 1.22^{b}	29.00 ± 1.15^{b}	25.00 ± 1.73^{b}
Streptomycin	NI	9.00 ± 0.57^{c}	—	10.08 ± 1.22^{c}	NI
Vancomycin	NI	12.91 ± 0.50^{bc}	—	—	14.08 ± 0.65^{c}
Chloramphenicol	35.08 ± 1.80^{a}	34.00 ± 1.44^{a}	36.91 ± 1.80^{a}	35.00 ± 2.30^{a}	36.83 ± 1.87^{a}

NI: no inhibition. In every column, values with different letters are significantly different ($p < 0.05$).

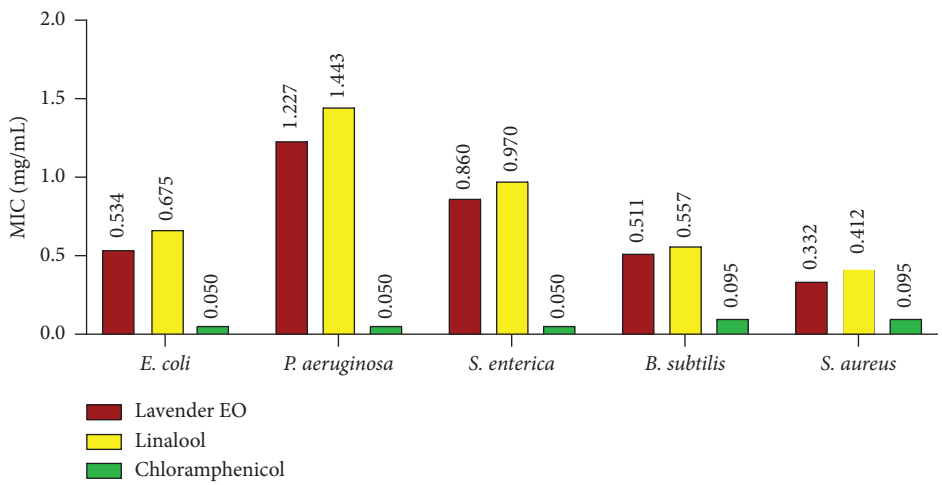

Figure 6: Minimal inhibitory concentration values (mg/mL) of linalool and EO extracted from *L. dentata* against bacterial strains.

and thymol were reported to be potentially implicated in several biological activities [31].

Then, *in vitro*, the antioxidant capacities of *Lavandula dentata* EO and linalool compound to limit lipid oxidation were assessed, in this study, using the β-carotene assay. As multiple studies showed that fatty acid oxidation represents one of the principal causes of food deterioration. Natural food preservatives are frequently used to reduce lipid oxidation [32]. The obtained results demonstrated that lavender EO possessed the ability to limit lipid oxidation. This inhibitory ability increased with increasing concentrations (Figures 2 and 3). Several studies reported a moderate antioxidant effect of *Lavandula dentata* EO using various tests [28, 33, 34]. The antioxidant potential of Tunisian *Lavandula dentata* was also proved, by recording IC_{50} values of 53.029 mg/mL, 113.29 mg/mL, and 43.20 mg/mL, respectively, for the ABTS test, the DPPH test, and the reducing power test [27]. Our results are more promising than those of other spices of the lavender plant such as *L. officinalis, L. stoechas,* and *L. pedunculata* which displayed lesser lipid peroxidation inhibition activity that did not exceed $52.52 \pm 2.01\%$, $14.8 \pm 3.1\%$, and $17.2 \pm 1.3\%$, respectively [35, 36]. The capacity of lavender EO to inhibit lipid peroxidation is probably due to the combination of molecules it contains and the high proportion of unsaturated compounds and oxygenated compounds (91.07%), which have distinct polarity and functional groups, resulting in diverse chemical behavior [32]. On the other hand, linalool as a major component of the lavender EO, showed better antioxidant capacity, which was very close to that of BHT at high concentrations. These findings suggest that this compound may be the most implicated in antioxidant activity. According to some research studies on the antioxidant capacity of many chemicals found in our investigated plant, linalool has a higher antioxidant potential than camphor, 1.8 cineole, borneol, and terpinene-4-ol in several tests. Whereas, thymol and carvacrol displayed a higher antioxidant activity [31]. Consequently, this wide variety of molecules in the examined EO, as well as their probable action modes and interactions, makes it difficult to assign the antioxidant activity to just one or only a few active components. Nowadays, common antioxidant tests, such as inhibition of linoleic acid oxidation, could provide important information about the activities of molecules of interest and how food products oxidize. In modern biotechnology, EOs and isolated phenolic compounds as potential additives (as effective antioxidants with low toxicity) have been employed in various forms, both free and encapsulated, in nondegradable and biodegradable materials [8]. Moreover, and through several tests, numerous studies have evaluated the antioxidant capacity using different food matrices by combining various films and EOs. The results were promising [8]. Therefore, the remarkable antioxidant potential of EOs extracted from aromatic plants such as *L. dentata* makes them promising alternatives to synthetic food preservatives.

Then, *in silico*, molecular docking of the antioxidant activity of *Lavandula dentata* EO against NADPH oxidase was also examined in this work. Thymol, carvacrol, α-terpineol, and camphor were the most active lavender compounds exhibiting an inhibitory effect against NADPH oxidase. In fact, NADPH oxidase is a major enzymatic source of oxygen-free radicals in stimulated endothelial cells [37]. The inhibition of this protein represents a major key in the protection of cells against free radicals. Several *in vitro* studies have reported the antioxidant activity of lavender EO [7, 27]. Our results are in agreement with a study where derivatives of thymol and carvacrol exhibited remarkable antioxidant activity according to 1,1-diphenyl-2-picrylhydrazyl assay and Rancimat assay [38]. Another study noted high antioxidant activity *in vitro* of camphor extract using the DPPH test [39]. The obtained results demonstrate that EOs from *Lavandula dentata* may constitute natural NADPH inhibitors.

The antibacterial activities of *Lavandula dentata* EO and linalool were evaluated, qualitatively and quantitatively, against food-borne pathogenic bacteria. Results showed that lavender EO was generally active against a broad spectrum of food intoxication isolated strains including both Gram (−) bacteria (*S. enterica, E. coli,* and *P. aeruginosa*) and Gram (+) (*S. aureus* and *B. subtilis*) bacteria. Our data confirm

previous conclusions and attest, in some cases, to the superiority of our results [25, 28, 34]. These investigations reported the antibacterial activity of *Lavandula dentata* against a wide spectrum of bacteria including *E. coli, S. aureus, S. pneumoniae, L. monocytogenes, K. pneumoniae, P. aeruginosa, S. pyogenes, N. meningitidis,* and *Salmonella* sp. Similarly, EOs extracted from *Lavandula dentata* of southern Morocco were likewise found to be effective against *E. coli* and *S. aureus* by marking characteristic inhibition zones of 12 ± 0.29 mm and 30 ± 0.00 mm and MIC values of 0.14 mg/mL and 0.08 mg/mL, respectively [23]. Tunisian *Lavandula dentata* essences were also significantly active against six bacterial strains, including *P. aeruginosa*, *S. aureus,* and *E. coli*, where MIC values ranged between 0.1 and 0.6 μg/mL [27]. The antibacterial activity of lavender EO was confirmed in another study against *E. coli* and *S. aureus* with low MIC values ranging between 2000 ppm and 1000–1200 ppm, respectively [40]. Likewise, recent works showed that the application of *Lavandula stoechas* EO at a concentration of 60 μL of EO/disc totally inhibited the growth of *Staphylococcus aureus* strains and exhibited a marked action on the growth of the majority of Gram (+) bacteria tested [41]. The probable mechanisms of the antimicrobial power of lavender EOs especially against Gram (+) bacteria may be related to the direct interaction of their hydrophobic components with the cell membrane, and their power to partition bacterial phospholipids by making them more permeable, which may result in structural damage or total rupture of cell membranes and loss of nutrients [23]. Gram (−) bacteria possess an outside lipopolysaccharides membrane, which can limit the diffusion of hydrophobic components [18]. Moreover, research studies on terpenes' effects on the isolated bacterial membrane suggested that the high potential of EOs is due to the lipophilic properties of terpenes, the strength of their functional groups, and their aqueous solubility. Several processes including protein translocation, phosphorylation, inhibition of electron transport, and other enzymatic reactions may also be involved [23]. Several reports have shown the significant antimicrobial potential of some EO's major compounds such as thymol, carvacrol, camphor, linalyl acetate, 1.8-cineole, and terpinen-4-ol against many foodborne pathogen bacterial strains (*E. faecalis*, *P. aeruginosa*, *B. cereus*, *E. coli*, and *S. aureus*) and against lactic acid bacteria, especially against *L. acidophilus* [31, 42]. Linalool was the major compound of our investigated EO. This unsaturated monoterpene with a phenolic ring demonstrated in the current study that it possessed antimicrobial potential that is comparable to and close to that of the EO against five food-borne pathogenic bacterial strains, attesting to its significant contribution to the antibacterial activity of lavender EO. In general, phytochemicals in the EO may act synergistically rather than individually, as numerous studies showed that the antimicrobial effect of EOs exceeded sometimes that of its single compounds tested separately [31, 43]. Since 2000, the number of antibiotics recommended for clinical usage has decreased and the majority of them are only effective against gram (+) bacteria, while their effectiveness against Gram (−) strains decreases with time, which may constitute a real threat to human health [32]. Therefore, the restricted treatment strategies for drug-resistant pathogens require the development of new and more effective alternatives. Moreover, in the field of food preservation and packaging, the current tendency is to use natural substances instead of chemically synthesized ones. Lavender EO has already been tested as a food preservative. In this context, a previous study showed that the incorporation of chitosan beads containing lavender EO at 2 concentrations (0.125 and 0.25 g/sachet) into strawberry packed in clamshell can effectively inhibit *B. cinerea* growth. Experiments showed also a maintenance of appearance, color, and firmness [44]. Consequently, the authors recommended the application of lavender EOs inside the packaging system to promote an antifungal activity against grey mold rot on strawberry fruit [45, 46]. Therefore, *L. dentata* EO can be a promising agent to combat food-borne pathogens and it can also constitute as a good food preservative.

5. Conclusions

In conclusion, the findings of the present study confirm that the essential oils extracted from Moroccan *L. dentata*, through their bioactive chemical compounds such as linalool, exhibit interesting antimicrobial activity against a spectrum of food-borne pathogens, in addition to their high capacity to limit lipid peroxidation, and to inhibit NADPH oxidase enzymatic complex in stimulated endothelial cells. These results suggest promising usage of these essential oils in the treatment of food-borne microbial infections, as well as in the food industry and packaging systems as alternatives to synthetic food preservatives. However, further research studies dealing with toxicities on humans and nontarget organisms is needed before any application.

Data Availability

The data used to support the findings of the study are included within the article.

Conflicts of Interest

The authors declare that they have no conflicts of interest.

Acknowledgments

The authors would like to extend their sincere appreciation to the Researchers Supporting Project, King Saud University, Riyadh, Saudi Arabia, for funding this work through the project number (RSP2023R457).

References

[1] Efsa and Ecdpc, "The European Union Summary Report on Antimicrobial Resistance in zoonotic and indicator bacteria from humans,animals and food in 2017/2018," 2020, https://www.efsa.europa.eu/en/efsajournal/pub/6007.

[2] F. Safarpoor Dehkordi, H. Gandomi, A. A. Basti, A. Misaghi, and E. Rahimi, "Phenotypic and genotypic characterization of antibiotic resistance of methicillin-resistant Staphylococcus

aureus isolated from hospital food," *Antimicrobial Resistance and Infection Control*, vol. 6, no. 1, pp. 104–111, Oct. 2017.

[3] D. Sergelidis and A. S. Angelidis, "Methicillin-resistant Staphylococcus aureus: a controversial foodborne pathogen," *Letters in Applied Microbiology*, vol. 64, no. 6, pp. 409–418, 2017.

[4] V. Shriram, T. Khare, R. Bhagwat, R. Shukla, and V. Kumar, "Inhibiting bacterial drug efflux pumps via phyto-therapeutics to combat threatening antimicrobial resistance," *Frontiers in Microbiology*, vol. 9, 2018.

[5] F. Moussaoui and T. Alaoui, "Evaluation of antibacterial activity and synergistic effect between antibiotic and the essential oils of some medicinal plants," *Asian Pacific Journal of Tropical Biomedicine*, vol. 6, no. 1, pp. 32–37, 2016.

[6] I. Sifaoui, A. López-Arencibia, C. M. Martín-Navarro et al., "Activity of olive leaf extracts against the promastigote stage of Leishmania species and their correlation with the antioxidant activity," *Experimental Parasitology*, vol. 141, no. 1, pp. 106–111, 2014.

[7] Y. El Abdali, A. Agour, A. Allali et al., "Lavandula dentata L.: phytochemical analysis, antioxidant, antifungal and insecticidal activities of its essential oil," *Plants*, vol. 11, no. 3, 2022.

[8] M. Carpena, B. Nuñez-Estevez, A. Soria-Lopez, P. Garcia-Oliveira, and M. A. Prieto, "Essential oils and their application on active packaging systems: a review," *Resources*, vol. 10, no. 1, pp. 7–20, 2021.

[9] S. Bhavaniramya, S. Vishnupriya, M. S. Al-Aboody, R. Vijayakumar, and D. Baskaran, "Role of essential oils in food safety: antimicrobial and antioxidant applications," *Grain & Oil Science and Technology*, vol. 2, no. 2, pp. 49–55, 2019.

[10] Y. El AbdaliA. Allali et al., "Phytochemical screening, and in vitro antiradical and immunostimulant potential of linum usitatissimum L," *Pharmacologyonline*, vol. 3, pp. 602–614, 2021.

[11] M. Zuzarte, L. Vale-Silva, M. J. Gonçalves et al., "Antifungal activity of phenolic-rich Lavandula multifida L. Essential oil," *European Journal of Clinical Microbiology & Infectious Diseases*, vol. 31, no. 7, pp. 1359–1366, 2012.

[12] Edqm, *European Pharmacopoeia*, Council of Europe, Strasbourg, France, 5th ed edition, 2004.

[13] R. P. Adams, "Identification of essential oil components by gas chromatograpy/mass spectrometry," *Carol Stream*, Allured Pub. Corp, Illinois, IL, USA, 4th ed edition, 2007.

[14] M. S. Taga, E. E. Miller, and D. E. Pratt, "Chia seeds as a source of natural lipid antioxidants," *Journal of the American Oil Chemists' Society*, vol. 61, no. 5, pp. 928–931, 1984.

[15] M. A. M. Aboul-Soud, H. Ennaji, A. Kumar et al., "Antioxidant, anti-proliferative activity and chemical fingerprinting of centaurea calcitrapa against breast cancer cells and molecular docking of caspase-3," *Antioxidants*, vol. 11, no. 8, 2022.

[16] F. E. Z. Amrati, M. Bourhia, H. Saghrouchni et al., "Caralluma europaea (guss.) N.E.Br.: anti-inflammatory, antifungal, and antibacterial activities against nosocomial antibiotic-resistant microbes of chemically characterized fractions," *Molecules*, vol. 26, no. 3, 2021.

[17] M. Balouiri, M. Sadiki, and S. K. Ibnsouda, "Methods for in vitro evaluating antimicrobial activity: a review," *Journal of Pharmaceutical Analysis*, vol. 6, no. 2, pp. 71–79, Apr. 2016.

[18] Y. El Atki, I. Aouam, F. El Kamari et al., "Phytochemistry, antioxidant and antibacterial activities of two Moroccan Teucrium polium L. subspecies: preventive approach against nosocomial infections," *Arabian Journal of Chemistry*, vol. 13, no. 2, pp. 3866–3874, 2020.

[19] B. P. McNicholl, J. W. McGrath, and J. P. Quinn, "Development and application of a resazurin-based biomass activity test for activated sludge plant management," *Water Research*, vol. 41, no. 1, pp. 127–133, Jan. 2007.

[20] A. I. Hussain, F. Anwar, S. A. S. Chatha, A. Jabbar, S. Mahboob, and P. S. Nigam, "Rosmarinus officinalis essential oil: antiproliferative, antioxidant and antibacterial activities," *Brazilian Journal of Microbiology*, vol. 41, no. 4, pp. 1070–1078, 2010.

[21] G. K. Jayaprakasha, R. P. Singh, and K. K. Sakariah, "Antioxidant activity of grape seed (Vitis vinifera) extracts on peroxidation models in vitro," *Food Chemistry*, vol. 73, no. 3, pp. 285–290, 2001.

[22] I. Bettaieb Rebey, S. Bourgou, M. Saidani Tounsi, M.-L. Fauconnier, and R. Ksouri, "Etude de la composition chimique et de l'activité antioxydante des différents extraits de la Lavande dentée (Lavandula dentata)," *Journal of New Sciences Agricultural biotechnology*, vol. 39, no. 2, pp. 2096–2105, 2017.

[23] L. Bachiri, G. Echchegadda, J. Ibijbijen, and L. Nassiri, "Etude Phytochimique Et Activité Antibactérienne De Deux Espèces De Lavande Autochtones Au Maroc: «Lavandula stoechas L. et Lavandula dentata L," *European Scientific Journal, ESJ*, vol. 12, no. 30, 2016.

[24] A. El Moussaoui, M. Bourhia, and F. Z. Jawhari, "Responses of withania frutescens (L .) pauquy (solanaceae) growing in the mediterranean area to changes in the environmental conditions: an approach of adaptation description of study areas," *Frontiers in Ecology and Evolution*, vol. 9, Article ID 666005, 2021.

[25] B. Imelouane, A. Elbachiri, M. Ankit, H. Benzeid, and K. Khedid, "Physico-chemical compositions and antimicrobial activity of essential oil of eastern moroccan Lavandula dentata," *International Journal of Agriculture and Biology*, vol. 11, no. 2, pp. 113–118, 2009.

[26] k. D. Soro, K. Majdouli, Y. Khabbal, and T. Zaïr, "Chemical composition and antibacterial activity of Lavandula species L.dentata L. , L. pedunculata Mill and Lavandula abrialis essential oils from Morocco against foodborne and nosocomial pathogens," *International Journal of Innovation and Applied Studies*, vol. 7, no. 2, pp. 774–781, 2014.

[27] D. Imen, H. H. Soumaya, C. Imed, M. B. J. Jouda, L. Ahmed, and C. Rym, "Essential oil from flowering tops of lavandula dentata (L): chemical composition, aantimicrobial, antioxidant and insecticidal activities," *Journal of Essential Oil Bearing Plants*, vol. 24, no. 3, pp. 632–647, 2021.

[28] B. Justus, V. P. d. Almeida, M. M. Gonçalves et al., "Chemical composition and biological activities of the essential oil and anatomical markers of lavandula dentata L. Cultivated in Brazil," *Brazilian Archives of Biology and Technology*, vol. 61, Article ID e18180111, 2018.

[29] O. Zouirech, A. A. Alyousef, A. El Barnossi et al., "Phytochemical analysis and antioxidant, antibacterial, and antifungal effects of essential oil of black Caraway (*Nigella sativa* L.) seeds against drug-resistant clinically pathogenic microorganisms," *BioMed Research International*, vol. 2022, Article ID 5218950, 11 pages, 2022.

[30] F. Kalleli, I. Bettaieb Rebey, W. A. Wannes et al., "Chemical composition and antioxidant potential of essential oil and methanol extract from Tunisian and French fennel (Foeniculum vulgare Mill.) seeds," *Journal of Food Biochemistry*, vol. 43, no. 8, Article ID e12935, 2019.

[31] A. B. Cutillas, A. Carrasco, R. Martinez-Gutierrez, V. Tomas, and J. Tudela, "Thyme essential oils from Spain: aromatic profile ascertained by GC–MS, and their antioxidant, anti-lipoxygenase and antimicrobial activities," *Journal of Food and Drug Analysis*, vol. 26, no. 2, pp. 529–544, Apr. 2018.

[32] A. El Moussaoui, M. Bourhia, F. Z. Jawhari et al., "Chemical profiling, antioxidant, and antimicrobial activity against drug-resistant microbes of essential oil from withania frutescens L," *Applied Sciences*, vol. 11, no. 11, 2021.

[33] I. Dammak, Z. Hamdi, S. Kammoun El Euch et al., "Evaluation of antifungal and anti-ochratoxigenic activities of Salvia officinalis, Lavandula dentata and Laurus nobilis essential oils and a major monoterpene constituent 1,8-cineole against Aspergillus carbonarius," *Industrial Crops and Products*, vol. 128, pp. 85–93, 2019.

[34] R. A. Mothana, M. S. Alsaid, and S. S. Hasoon, "Antimicrobial and antioxidant activities and gas chromatography mass spectrometry (GC/MS) analysis of the essential oils of Ajuga bracteosa Wall. ex Benth. and Lavandula dentata L. growing wild in Yemen," *Journal of Medicinal Plants Research*, vol. 6, no. 15, pp. 3066–3071, 2012.

[35] R. Baptista, A. M. Madureira, R. Jorge et al., "Antioxidant and antimycotic activities of two native Lavandula species from Portugal," *Evidence-based Complementary and Alternative Medicine*, vol. 2015, Article ID 570521, 10 pages, 2015.

[36] M. Viuda-Martos, M. A. Mohamady, J. Fernández-López et al., "In vitro antioxidant and antibacterial activities of essentials oils obtained from Egyptian aromatic plants," *Food Control*, vol. 22, no. 11, pp. 1715–1722, 2011.

[37] D. K. Johnson, K. J. Schillinger, D. M. Kwait et al., "Inhibition of NADPH oxidase activation in endothelial cells by ortho -Methoxy-Substituted catechols," *Endothelium*, vol. 9, no. 3, pp. 191–203, 2009.

[38] J. Mastelić, I. Jerković, I. Blažević et al., "Comparative study on the antioxidant and biological activities of carvacrol, thymol, and eugenol derivatives," *Journal of Agricultural and Food Chemistry*, vol. 56, no. 11, pp. 3989–3996, 2008.

[39] S. H. A. Muhamad, S. On, S. N. A. Sanusi, A. A. Hashim, and M. H. Addinna Zai, "Antioxidant activity of Camphor leaves extract based on variation solvent," *Journal of Physics: Conference Series*, vol. 1349, no. 1, Article ID 012102, 2019.

[40] J. F. Martucci, L. B. Gende, L. M. Neira, and R. A. Ruseckaite, "Oregano and lavender essential oils as antioxidant and antimicrobial additives of biogenic gelatin films," *Industrial Crops and Products*, vol. 71, pp. 205–213, Sep. 2015.

[41] N. Amara, M. N. Boukhatem, M. A. Ferhat, N. Kaibouche, O. Laissaoui, and A. Boufridi, "Applications potentielles de l'huile essentielle de lavande papillon (Lavandula stoechas L.) comme conservateur alimentaire naturel," *Phytothérapie*, vol. 16, no. S1, pp. S164–S172, 2018.

[42] L. De Martino, V. De Feo, F. Fratianni, and F. Nazzaro, "Chemistry, antioxidant, antibacterial and antifungal activities of volatile oils and their components," *Natural Product Communications*, vol. 4, no. 12, 2009.

[43] Z. Yu, J. Tang, T. Khare, and V. Kumar, "The alarming antimicrobial resistance in ESKAPEE pathogens: can essential oils come to the rescue?" *Fitoterapia*, vol. 140, Article ID 104433, 2020.

[44] J. Sangsuwan, T. Pongsapakworawat, P. Bangmo, and S. Sutthasupa, "Effect of chitosan beads incorporated with lavender or red thyme essential oils in inhibiting Botrytis cinerea and their application in strawberry packaging system," *Lebensmittel-Wissenschaft und -Technologie*, vol. 74, pp. 14–20, 2016.

[45] R. Ribeiro-Santos, M. Andrade, N. R. d. Melo, and A. Sanches-Silva, "Use of essential oils in active food packaging: recent advances and future trends," *Trends in Food Science & Technology*, vol. 61, pp. 132–140, 2017.

[46] M. Carocho, M. F. Barreiro, P. Morales, and I. C. F. R. Ferreira, "Adding molecules to food, pros and cons: a review on synthetic and natural food additives," *Comprehensive Reviews in Food Science and Food Safety*, vol. 13, no. 4, pp. 377–399, J2014.

Hindawi
Evidence-Based Complementary and Alternative Medicine
Volume 2022, Article ID 3143733, 18 pages
https://doi.org/10.1155/2022/3143733

Research Article

Treatment of Gout with TCM Using Turmeric and Corn Silk: A Concise Review Article and Pharmacology Network Analysis

Haoyu Zhang,[1,2] **Huizhong Jiang**,[3] **Mengya Zhao**,[3] **Yan Xu**,[4] **Jiabin Liang**,[1] **Yufeng Ye**,[2] **and Hanwei Chen**[2,5]

[1]*Guangzhou University of Chinese Medicine, Guangzhou 510405, China*
[2]*Guangzhou Panyu Central Hospital, Guangzhou 511400, China*
[3]*Guizhou University of Traditional Chinese Medicine, Guiyang 550000, China*
[4]*School of Pediatrics, Henan University of Chinese Medicine, Zhengzhou 450000, China*
[5]*Panyu Health Management Center (Panyu Rehabilitation Hospital), Guangzhou 511495, China*

Correspondence should be addressed to Yufeng Ye; 838554325@qq.com and Hanwei Chen; docterwei@sina.com

Received 4 July 2022; Revised 17 September 2022; Accepted 21 September 2022; Published 14 October 2022

Academic Editor: Salah M. El Sayed

Objective. This work aimed to study the compounds, targets, and pathways of turmeric and corn silk for gout and to explore the mechanism of "the same disease with different treatments" based on network pharmacology and molecular docking. *Methods*. We used the TCMSP, PubChem, and SEA databases to screen the compounds and targets of turmeric and corn silk, gout-related proteins through TTD, Drugbank, DisGeNET, GeneCards, OMIM, and PharmGkb, and used Cytoscape to construct a "compound-target-disease" network. Then, we constructed a protein-protein interaction network (PPI) and used Metascape to perform GO and KEGG analysis. Finally, molecular docking (SYBYL) was used to verify the degree of binding between key targets and compounds. *Results*. We found bisacumol, campesterol, and stigmasterol to be the main turmeric compounds that exerted a marked effect on gout treatment by targeting protein processing in the endoplasmic reticulum through the HSPA1B, HSP90AB1, and STUB1 proteins. The main corn silk compound, Mandenol, treated gout by targeting the Hippo signaling pathway through the CTNNB1, YWHAG, and YWHAZ proteins. *Conclusion*. Turmeric and corn silk can treat the same disease, gout, through different pathways and targets. The scientific connotation of "same disease with different treatments" can be preliminarily clarified by analyzing targets and pathways.

1. Introduction

With the global outbreak of COVID-19 in 2020, lifestyles changed significantly. Success in the treatment of the disease achieved by the combined use of traditional Chinese medicine (TCM) and modern medicine garnered the attention of society for TCM. As one of the four ancient civilizations, China has a lengthy history, with a traditional health-preserving and TCM culture. TCM is a treasure house of natural herbs. In recent years, its application worldwide has increased dramatically due to its excellent therapeutic effects and a paucity of side effects. The equilibrium state is one of TCM's main theories and includes the balance of the human body, the balance between man and nature, and the balance between man and the social environment [1]. Once the balance is disturbed, the human body will produce various pathological substances, such as static blood, phlegm, and dampness, and further produce different symptoms. Therefore, various treatments are adopted according to different symptoms (syndrome differentiation), which is the basis of TCM [2]. During treatment, different methods are adopted according to various conditions, i.e., different treatments for the same disease [3]. The application of

"same disease with different treatments" reflects the characteristics of TCM in the diagnosis and treatment, emphasizing syndrome differentiation.

Gout, the most common inflammatory arthritis, is caused by hyperuricemia, which causes sodium urate crystals to deposit in joints, tendons, and other tissues [4]. Several recent reports have shown that the worldwide prevalence of gout is between 1 and 6.8%, and these percentages are rising [5]. In addition, many studies have shown that gout is a risk factor for diseases such as hypertension, diabetes, cardiovascular and cerebrovascular diseases, and chronic kidney disease, and it is also a predictor of premature death [6]. Gout treatment primarily involves antiinflammatory and analgesic treatment in acute arthritis, uric acid control in the chronic phase, and daily personal life management [7]. Medications for acute gout attacks include colchicine, nonsteroidal antiinflammatory drugs (NSAIDS), steroids, and biological agents [7]. Although these are recommended as first-line drugs for the clinical treatment of gout, they are restricted due to their respective liver and kidney toxicities and gastrointestinal adverse reactions [8]. Biological agents, such as interleukin-1 blockers, can achieve better therapeutic results with minimal side effects, but are expensive [9]. Lowering uric acid requires persistence, but most of the above drugs are challenging to use for a long time due to toxic side effects. Therefore, more natural products need to be found for gout treatment.

Gout (*tong-feng*) (also known as *damp bi*) is a common disease name used in TCM and modern medicine; in TCM, both gout and hyperuricemia are in the category of gout [10]. Furthermore, in TCM, the development of gout is related to congenital liver and kidney deficiency and the accumulation of dampness, phlegm, and static blood, resulting in the formation of dampness syndrome, phlegm syndrome, and blood stasis syndrome, respectively, as well as kidney deficiency syndrome. Based on the syndrome, different methods, such as the promotion of blood circulation, diuresis, and invigorating the kidney, are adopted [11]. Through syndrome differentiation, effective Chinese medicines for gout treatment have been discovered, such as turmeric [12], corn silk [13], and tuckahoe [14]. Both clinical applications and modern pharmacological research have confirmed the uric acid-lowering effect of these herbs. Through literature research, it has been found that turmeric and corn silk are effective medicines for gout and are also part of the concept of "medicine and food homology" [15, 16]. The coexistence of nutrients and active ingredients is strong evidence for the dual use of medicine and food. They avoid the drug's toxicity and side effects and simultaneously restore or maintain human health through daily intake of the prescribed dose [16].

This study adopted the network pharmacology method, taking turmeric and corn silk as examples. Constructing a drug-component-target-disease network reveals the mechanism of "the same disease with different treatments" to explain the scientific connotation of TCM and the pharmacological mechanism of Chinese medicine (Figure S1, Supporting Information).

2. Materials and Methods

2.1. Prediction of Turmeric and Corn Silk Compounds and Their Targets. The turmeric and corn silk components were collected through the herbal platform TCMSP and screened according to absorption, distribution, metabolism, and excretion (ADME) parameters. The screening criterion was oral bioavailability (OB) ≥ 30% and drug-likeness (DL) ≥ 0.18, and this was combined with relevant literature to supplement the compounds. In addition, the PubChem database was used to confirm the molecular structure of the compounds, and TCMSP targets and the SEA database prediction model were used to predict the possible targets of the compounds (Table 1).

2.2. Collection of Disease Targets. The keywords "hyperuricemia" and "gout" were used, and "Homo sapiens" was selected for the species. Next, the keyword search was conducted in the Drugbank, DisGeNET, GeneCards, OMIM, and PharmGkb databases. Lastly, duplicate genes were deleted.

2.3. Network Construction. Cytoscape [17] was used to construct the "medicine-compound-target-disease" network of turmeric and corn silk, where "node" was used to represent the compounds or target, and "edge" was used to represent the relationship. The NetworkAnalyzer (Cytoscape plug-in) was used to analyze the network characteristics, including the degree, betweenness, and closeness, to study the relationship between the compounds and targets.

2.4. Protein-Protein Interaction (PPI) and Candidate Target Screening. The Cytoscape plug-in BisoGenet was used to construct a protein-protein interaction (PPI) network for compound potential and disease targets. Merge was used in the software to fuse the two network diagrams and extract the intersection. The direct and indirect intervention target regulation network graphs for turmeric and corn silk were obtained for gout. The plug-in CytoNCA [18] in Cytoscape was used to screen the degree, betweenness, closeness, LAC, and network, with the degree ≥2 times the median as the condition, and the PPI node was selected. With the degree, betweenness, closeness, LAC, and network greater than or equal to the median as the condition, the turmeric, and corn silk candidate targets for gout were selected.

2.5. Module Analysis Using GO and KEGG. Metascape [18] is a tool that integrates multiple databases such as Gene Ontology (GO), Kyoto Encyclopedia of Genes and Genomes (KEGG), and Drugbank, which can be used for biological process annotation and pathway analysis and can mainly

Table 1: Database and software used in this study.

No.	Database and software	Function	Website
1	Traditional Chinese medicine systems pharmacology (TCMSP)	Screening herbal compounds	https://tcmspw.com/tcmspsearch.php
2	SEA database	Screening herbal compounds	https://sea.Bkslab.org/
3	Drugbank	Collection of disease targets	https://www.drugbank.ca/
4	DisGeNET	Collection of disease targets	http://www.disgenet.org/home/
5	GeneCards	Collection of disease targets	https://www.genecards.org/
6	OMIM	Collection of disease targets	https://www.omim.org/
7	PharmGkb	Collection of disease targets	https://www.pharmgkb.org/
8	R Packages	Visualized analysis	https://www.r-project.org/
9	Metascape	GO and KEGG analysis	https://metascape.org/
10	Cytoscape	Network construction	https://www.cytoscape.org

guarantee the timeliness of the data. The above-mentioned candidate targets were imported into Metascape, and the species was set to *H. sapiens* for analysis. The results of protein interaction and module analysis, GO enrichment analysis, and KEGG pathway analysis were retained, and the results were sorted according to the number of targets. Finally, the top results were retained and analyzed, and *R* package [19] visualization was performed.

2.6. Molecular Docking. SYBYL-X [20] was used to optimize proteins and small molecules according to the related molecular docking literature [21], for protein processing, while the Surflex-Dock module was used for molecular docking. The compound and target protein interaction was scored according to the Total-Score scoring function. The larger the Total-Score value, the better the matching and binding effect of the compound and the protein. With a Total-Score >5 as the threshold, Pymol was used to select the best results of the two medicines' protein binding for graphing.

3. Results

3.1. Turmeric and Corn Silk Compounds and Targets. The three turmeric and twelve corn silk compounds were screened through the TCMSP database and supplemented by turmeronol A, turmeronol B, and bisacumol in turmeric [22]. Their OB and DL values were less than the screening conditions and were deleted by the system, but they were included in the search literature, given their potential significance. A total of six turmeric compounds were included in the follow-up study. The potential targets of the compounds were queried through the TCMSP and SEA databases, and after deleting duplicates, 31 turmeric targets and 92 corn silk targets were obtained. As shown in Table 2, the potential turmeric compounds were stigmasterol, campesterol, and bisacumol, among others. Table 3 shows that the potential compounds of corn silk include mandenol, schottenols, and luteolin.

3.2. Disease Targets of Gout. The keywords "hyperuricemia" and "gout" were entered into the TTD, Drugbank, DisGeNET, Genecards, OMIM, and PharmGkb databases to obtain gout-related targets. The numbers of disease-related targets were 20, 66, 258, 2319, 13, and 4, respectively, and after deduplication were 20, 38, 234, 1971, 13, and 4, respectively. A total of 2081 targets were obtained. After using *R* studio 4.0.5 to cross the compound targets of turmeric and corn silk with the disease targets of gout, we get 6 and 36 intersection targets, respectively. The above targets are presented as a Venn diagram (Figure S2, Supporting Information) with the *R* packages [19].

3.3. "Medicine-Compounds-Target-Disease" Network. We import the turmeric and corn silk compounds and target gene symbols into Cytoscape 3.8.2 to obtain the network diagrams of turmeric and corn silk for gout, involving 15 nodes and 34 edges (turmeric), 49 nodes, and 62 edges (corn silk), respectively. In the nodes, purple represents disease, yellow represents turmeric (JH), corn silk (YMX), green represents compounds, and red represents the targets of turmeric and corn silk for gout (Figure S3, Supporting Information).

3.4. Construction of PPI Networks. BisoGenet constructed the PPI network of turmeric and corn silk for gout. The results showed that: turmeric candidate targets can interact directly or indirectly with 1,101 targets, and their correlations can reach 17095; corn silk candidate targets can interact with 5145 targets, have direct or indirect effects, and their correlations can reach 109,046; there were 13010 targets directly or indirectly related to gout, and there were 241,154 interconnected targets. The intersection of the disease and targets was shown in Figures S4 and S5 (Supporting Information). After calculating the attribute value for the network topology characteristic of the intersection PPI, turmeric and corn silk targets were screened twice, and 32 and 10 candidate targets were obtained, respectively. As shown in Table 4, candidate targets of turmeric for gout were HSPA8, VCP, HSP90AB1, HSPA5, HSPA1B, NFKB1, and STUB1. As shown in Table 5, it could be seen that the candidate targets of corn silk for gout were YWHAZ, CTNNB1, YWHAG, and NPM1.

3.5. Module Description of Turmeric and Corn Silk for Gout. The candidate targets obtained mentioned above were imported into the Metascape database, the interaction

Table 2: Corresponding table of turmeric compounds and targets.

No.	Mol ID	MOl name	OB (%)	DL	Targets
1	MOL000449	Stigmasterol*	43.83	0.76	IGHG1, RXRA, ADRA2A, SLC6A2, ADRB2, CHRM3, CHRM1, ADRB1, SCN5A, COLQ, CDC25A, GLRA1
2	MOL000493	Campesterol*	37.58	0.71	CYP17A1, NPC1L1, RORC, CYP19A1, RORA
3	MOL000953	CLR	37.87	0.68	NA
4	MOL000955	Turmeronol A	59.42	0.08	CHRM3, CHRM1, COLQ, CHRM2, ADRA1B, CHRNA2, DRD5, APH1B, MAPK8, MAPK10, NR1D1
5	MOL000966	Turmeronol B	35.84	0.08	DRD1, APH1B, DRD4, EPHX1, DRD5
6	MOL000963	Bisacumol*	31.41	0.07	AR, RXRA, COLQ, APH1B, CYP17A1

Note. "*" indicates important compounds.

relationship was analyzed through the molecular complex detection algorithm, and the module was obtained. In the module analysis results, turmeric involves 4 modules, 32 nodes, and 240 edges; corn silk involves 1 module, 10 nodes, and 18 edges. A functional description of the biological process in the module suggests that these targets may play an essential role in the treatment of gout through turmeric and corn silk. The results are shown in Figure 1.

3.6. GO Enrichment Results and KEGG Pathway Enrichment Results. R packages ("ggplot2" and "clusterProfiler") [19] were used to perform gene enrichment analysis on the above 32 (turmeric) and 10 (corn silk) candidate targets, including GO's biological process (BP) and cellular component (CC), molecular function (MF), and KEGG pathways. Bar and bubble graphs were compiled for the BP, CC, and MF results, and *R* package was used to draw column charts and bubble plots for the KEGG pathway results. The bubble color from red to blue reflected the p value from small to large. The size of the bubble indicated the number of genes in this pathway, and the numbers on the bottom were the proportions of genes. Simultaneously, visual analysis of candidate targets and the primary GO function and KEGG pathway enrichment were performed, and the principal enrichment pathway diagrams were presented.

As shown in Figure 2, the biological processes involved in turmeric's 32 targets are enriched in the cellular response to heat and the regulation of protein stability. The genes are located in the inclusion body, ficolin-1-rich granule, and their molecular functions include ubiquitin protein ligase binding, heat shock protein binding, and unfolded protein binding. Figure 3 shows the KEGG pathway enrichment analysis of turmeric. Twenty results were selected based on their p values, and these were primarily involved in protein processing in the endoplasmic reticulum, the HIF-1 signaling pathway, and the MAPK signaling pathway.

As shown in Figure 4, the biological processes involved in the ten corn silk targets are enriched in protein targeting, mRNA, and RNA biological processes, with genes coding for focal adhesion, cell-substrate junction, and their molecular functions, including ubiquitin protein ligase binding and protein kinase inhibitor activity. Figure 5 shows the KEGG pathway enrichment analysis for corn silk. Five results were selected based on their p values. These compounds are primarily involved in the Hippo signaling pathway, antigen processing and presentation, and the cell cycle.

3.7. Molecular Docking. The results of the KEGG analysis showed that potential turmeric compounds might play a role in the treatment of gout by targeting protein processing in the endoplasmic reticulum signaling pathway, and potential corn silk compounds may play a therapeutic role by targeting the Hippo signaling pathway. We used SYBYL-X2.0 software [20] to verify these results and dock all targets enriched in protein processing in the endoplasmic reticulum pathway with the turmeric compounds. In addition, all targets enriched in the Hippo signaling pathway and potential corn silk compounds were docked. The results are shown in Table 6. A T_score >7 indicates that the ligand molecule binds to the receptor protein with high activity, and a T_score ≥5 indicates that it has good binding activity.

The scoring results showed that the turmeric, bisacumol, campesterol, and stigmasterol compounds had high activity when docking with the target HSPA1B and good activity when docking with the STUB1 and HSP90AB1 targets, suggesting that bisacumol, campesterol, and stigmasterol may be the key compounds of turmeric for gout. Mandenol, the corn silk compound, had high activity when docking with the target YWHAG and good activity when docking with the CTNNB1 and YWHAZ targets, suggesting that Mandenol may be an essential corn silk compound for gout (Table 6). For example, as shown in Figure 6(a) is the docking diagram of the turmeric target HSPA1B and the compound campesterol, and B is the docking diagram of the corn silk target YWHAG and the compound Mandenol.

4. Discussion

In this study, the potential mechanism of gout treatment using turmeric and corn silk was investigated using the network pharmacology method, including compound target network construction, PPI network analysis, GO enrichment analysis, and KEGG pathway analysis.

Network analysis of compound targets and molecular docking showed that bisacumol, campesterol, and stigmasterol might be the key turmeric compounds, and Mandenol might be the key corn silk compound. Bisacumol is a sesquiterpenoid [23]. The sesquiterpene compounds of turmeric have strong antimicrobial, antiinflammatory, neuroprotective, anticancer, antiviral, and antithrombotic activities [24]. Campesterol can be antiinflammatory, antiangiogenic, anticancer, antioxidant, and cholesterol-lowering [25, 26]. In addition, campesterol reduces the accumulation of proinflammatory phospholipids in the

Table 3: Corresponding table of corn silk compounds and targets.

No.	Mol ID	MOl name	OB (%)	DL	Targets
1	MOL010862	α-Tocopherylquinone	35.91	0.50	INSRR, DAGLA, CALCA, MTTP, IL6R, GPBAR1, CYP19A1, ATP6AP2, NPC1L1, MAPK8, MAPK9, BCL2, DRD2, DRD3, PGA4, KCNA5, SEMA4D
2	MOL013356	Stigmasta-4,22-diene-3beta,6beta-diol	39.32	0.79	NPC1L1, RORC, CYP19A1, RORA, CHRM2, CYP17A1, COLQ, KCNA3, DRD2, KCNA5, MDM4, CYP24A1, MAPK8, CHRM4, CHRM1, CHRM3, CDK8, EPHX1
3	MOL013357	(3S,6R,8S,9S,10R,13R,14S,17R)-17-[(1R,4R)-4-ethyl-1,5-dimethylhexyl] -10,13-dimethyl-2,3,6,7,8,9,11,12,14,15,16,17 -dodecahydro-1H-cyclopenta[a]phenanthrene-3,6-diol	34.37	0.78	NA
4	MOL013359	Stigmasta-7-en-3-ol	37.42	0.75	NA
5	MOL001494	Mandenol*	42.00	0.19	CYP17A1, CYP19A1, APH1B, FFAR1, FABP1, GRIN2B, SCD, PTGIR, KIF11, SLC6A15, CETP, BRD4, BRD2, BRD3, PICK1, TRAF5
6	MOL001749	ZINC03860434	43.59	0.35	SCN5A, CHRM3, ADRB2, CHRM1
7	MOL003044	Chrysoeriol	35.85	0.27	AR, CDK2, CAMTA2, SERPINB2, ABCB1, ABCG2, TTR, COLQ, CYP19A1, MCL1, DRD4, GPR35, CNOT1, CABLES1, EID3
8	MOL003059	Kryptoxanthin	47.25	0.57	CDC25A, GLRA1, CYP19A1, RORC, NPC1L1, CYP17A1
9	MOL000359	Sitosterol	36.91	0.75	NPC1L1, CYP17A1, RORC, CYP19A1, RORA, CHRM2, COLQ, CDC25A, GLRA1, CDC25B, DRD2
10	MOL000449	Stigmasterol	43.83	0.76	IGHG1, RXRA, ADRA2A, SLC6A2, ADRB2, CHRM3, CHRM1, ADRB1, SCN5A, ADRA1A, CHRM2, ADRA1B, CHRNA7, NPC1L1, CYP17A1, CYP19A1, RORC, RORA, COLQ, CDC25A, GLRA1
11	MOL000006	Luteolin	36.16	0.25	Ar, RELA, CCND1, CDKN1A, IL10RB, RB1, CDK4, TNF, JUN, IL6R, TP53, NFKBIA, APP, MCL1, BIRC5, IL2RA, CCNB1, IL4R, XIAP, SLC2A4, INSRR, TTR, ABCG2, COLQ, ABCB1, CYP19A1, GPR35, DRD4, SERPINB2, KDM4E, CNOT1, GSKIP
12	MOL006756	Schottenol	37.42	0.75	NPC1L1, RORC, CYP19A1, CYP17A1, COLQ, CHRM2, RORA, NR1I3, GLRA1, CDC25A, PREPL, CDC25B, ATP12A, FABP1

Note. "*" indicates important compounds.

Table 4: Targets of turmeric for gout.

Number	Hub name	Degree
1	HSPA8*	102
2	VCP	94
3	HSP90AB1*	92
4	HSPA5*	82
5	CUL1	74
6	SP1	71
7	PRKDC	71
8	ACTB	70
9	HNRNPK	68
10	ABL1	68
11	HNRNPU	67
12	HSPA1B*	65
13	HSPA1A	65
14	NFKB1	64
15	DDX5	62
16	GAPDH	62
17	CDKN1A	61
18	HSPA9	61
19	PPP1CA	61
20	PARP1	60
21	VHL	59
22	STUB1*	58
23	RPS27A	57
24	HSPD1	56
25	CUL2	56
26	ARRB1	55
27	XRCC6	52
28	CDK1	52
29	SIRT1	51
30	HIF1A	51
31	RAF1	51
32	FLNA	49

Note. "*" indicates important targets.

Table 5: Targets of corn silk for gout.

Number	Hub name	Degree
1	YWHAZ*	430
2	NPM1	409
3	HNRNPA1	334
4	HSPA8	278
5	CTNNB1*	271
6	YWHAG*	268
7	RPS27A	238
8	HSPA4	225
9	TUBB	200
10	GAPDH	173

Note. "*" indicates important targets.

intestine and prevents the influx of mucosal myeloperoxidase-positive (MPO) cells, thereby inhibiting inflammation [26]. Stigmasterol can significantly suppress the expression of proinflammatory mediators (TNFα, IL-6, IL-1β, iNOS, and COX-2) and increase the expression of antiinflammatory cytokines (IL-10) in the joints of arthritic rats by down-regulating the expression of NF-kBp65 (inhibiting p-IKB-α activation) and p38MAPK [27]. Mandenol (ethyl linoleate), the active ingredient in corn silk, is an essential fatty acid with antibacterial and antiinflammatory properties [28]. The above compounds have antiinflammatory effects, suggesting that they may be key compounds in the treatment of gouty arthritis.

Our PPI analysis showed that turmeric and corn silk influence gout through their impact on a complex biological network, including HSPA1B, HSP90AB1, STUB1, CTNNB1, YWHAG, and YWHAZ. Furthermore, the results of molecular docking indicate that the above compounds can also be combined with turmeric and corn silk. The essential turmeric targets HSPA1B and HSP90AB1 belong to the heat shock proteins (HSP) family, which is thought to play an essential role in the immune response. Studies have shown that HSPA1B inhibits viral proliferation in a viral infection's middle and late stages [29]. HSP90AB1 is a subtype of HSP90, an intracellular chaperone and is known to regulate inflammatory processes, including the NLRP3 inflammasome and secretion of the proinflammatory cytokine interleukin (IL)-1β [30]. STUB1 belongs to the ligase class, has ligase activity, and participates in regulating energy metabolism pathways and metabolism. A study showed that silencing STUB1 increased apoptosis of HK-2 cells and the proinflammatory cytokine production of IL6, TNFα, and IL1β induced by cisplatin [31]. The critical target of corn silk, CTNNB1 (β-catenin), is a member of the cyclic catenin family, whose primary role is to regulate adhesion between cells and intercellular substances. In addition, some studies have indicated that activation of the canonical Wnt-1/β-catenin pathway regulates the immune response and induces appropriate T cell responses [32]. YWHAG and YWHAZ belong to the YWHA protein family. Studies have shown that long-chain noncoding RNA NORAD has a protective effect on brain injury and inflammation induced by cerebral ischemia/reperfusion injury by regulating miR-30a-5p/YWHAG [33]. When cells are in an unfavorable living environment (e.g., hypoxia), it can regulate cell autophagy, promote DNA damage repair, inhibit cell apoptosis, and protect cells from stress damage [34]. Studies have shown that the down-regulation of YWHAZ can reduce the inflammatory response [35]. All of the above targets can regulate the immune or inflammatory response, suggesting a role for turmeric and corn silk in gout treatment.

By referring to GO and KEGG pathway enrichment analyses for turmeric and corn silk targets for gout, module and overall analyses' results were found to be the same, indicating that protein processing in the endoplasmic reticulum, HIF-1 signaling pathway, and Hippo signaling pathway is important. The endoplasmic reticulum (ER) is a subcellular organelle in which proteins are folded with the help of luminal chaperones. Accumulating misfolded proteins in the ER causes ER stress and activates a signaling pathway called the unfolded protein response (UPR). Studies have shown that tophi can promote osteoclast differentiation and proliferation by a mechanism closely related to ER stress [36]. This process shows that the protein processing in the ER is closely related to gout. In addition, research has suggested that hypoxia can cause an increase in purine metabolites (uric acid, xanthine, and hypoxic purine). Hypoxia is closely related to the hypoxia-

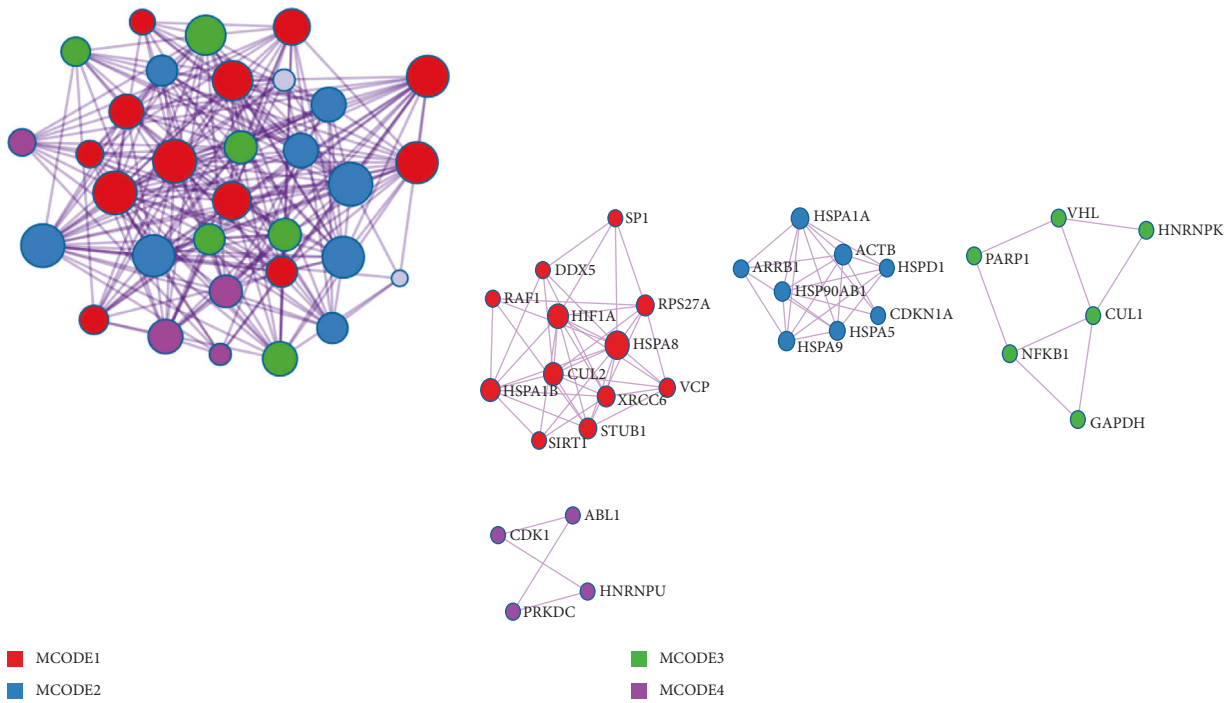

(a)

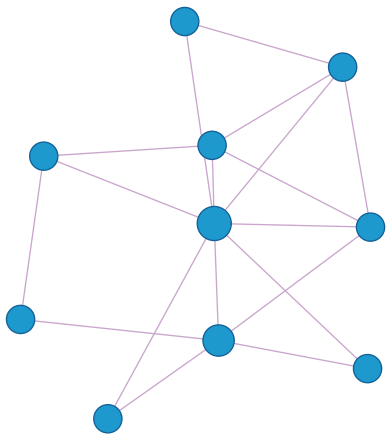

(b)

Figure 1: Continued.

Color	MCODE	GO	Description	Log10 (P)
	MCODE_1	R-HSA-2262752	Cellular responses to stress	-9.9
	MCODE_1	R-HSA-8953897	Cellular responses to stimuli	-9.9
	MCODE_1	GO:0034605	cellular responses to heat	-7.8
	MCODE_2	GO:0042026	protein refolding	-10.5
	MCODE_2	GO:0006986	response to unfolded protein	-9.9
	MCODE_2	GO:0035966	response to topologically incorrect protein	-9.5
	MCODE_3	hsa04066	HIF-1 signaling pathway	-5.8
	MCODE_3	R-HSA-3108232	SUMO E3 ligases SUMOylate target proteins	-5.3
	MCODE_3	ko05168	Herpes simplex infection	-5.3
	MCODE_4	GO:2000736	regulation of stem cell differentiation	-7.5
	MCODE_4	WP707	DNA damage response	-7.3
	MCODE_4	GO:0007346	regulation of mitotic cell cycle	-7.2

(c)

GO	Description	Log10 (P)
CORUM:5199	Kinase maturation complex 1	-7.7
WP706	Sudden infant death syndrome (SIDS) susceptibility pathways	-6.7
R-HSA-109581	Apoptosis	-6.5

(d)

Figure 1: Module analysis results. (a) Interaction network and module analysis of target proteins of turmeric for gout. (b) Interaction network and module analysis of target proteins of corn silk for gout. (c) Module network function description of turmeric for gout. (d) Module network function description of corn silk for gout.

inducible factor 1 (HIF-1) signaling pathway [37]. HIF-1 plays an essential role in executing an optimal inflammatory response by immune cells [38]. The Hippo signaling pathway is an evolutionarily conserved signaling pathway that participates in critical biological processes such as the size control and development of different organs in mammals, tissue regeneration, and stem cell regulation [39]. The Hippo pathway plays a crucial role in maintaining homeostasis, inflammation-induced regeneration, and innate immunity [40]. In summary, turmeric may have a therapeutic effect on gout through protein processing in the endoplasmic reticulum and HIF-1 signaling pathway, and corn silk may act through the Hippo signaling pathway.

Turmeric is the dried rhizome of *Curcuma longa* L., a member of the ginger family [41] recorded in the "Compendium of Materia Medica" and has the effects of promoting qi, breaking stasis, and unblocking meridians to relieve pain [42]. In addition, turmeric is widely used as a food. Its powder can be used as a spice in curries, soups, noodles, and steamed buns to enhance the fragrance, and it can also be used to make turmeric latte, turmeric milkshakes, and other beverages [43]. Shen et al. found that the curcumin group could significantly reduce the levels of uric acid (UA), xanthine oxidase (XOD), creatinine (CRE), and blood urea nitrogen (BUN) in hyperuricemic mice compared with the model group ($p < 0.01$), significantly down-regulating glutamic oxaloacetic transaminase (AST) and glutamic pyruvic

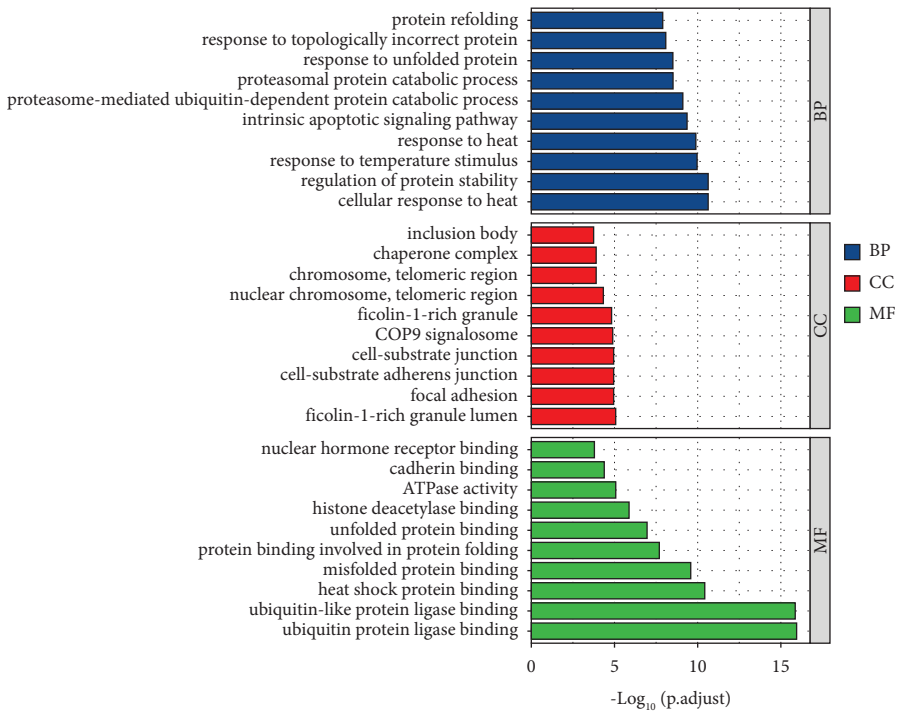

(a)

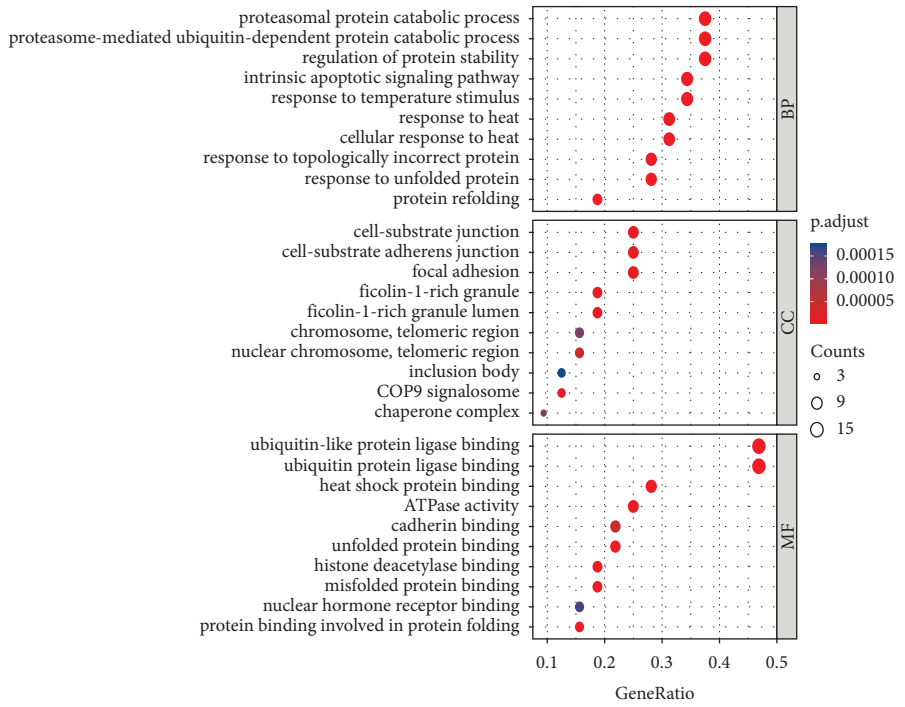

(b)

Figure 2: GO functional enrichment analysis of turmeric targets. (a) Column chart. (b) Bubble plot.

transaminase (ALT) levels ($p < 0.05$), and improving liver and kidney tissue morphology ($p < 0.05$) [44]. Chen et al. found that curcumin treatment markedly inhibited the activation of the NF-κB signaling pathway and expression levels of the NF-κB downstream inflammatory genes such as IL-1β, IL-6, TNFα, COX-2, and PGE2 ($p < 0.05$) in MSU-stimulated THP-1-derived macrophages [45]. Furthermore, intraperitoneal administration of curcumin alleviated MSU crystal-induced paw and ankle joint swelling and inflammatory cell infiltration ($p < 0.05$) in mouse models of acute gout [45]. Corn silk (*Stigma madis*) is a style of maize (*Zea mays* L.) in the grass family [13] and causes

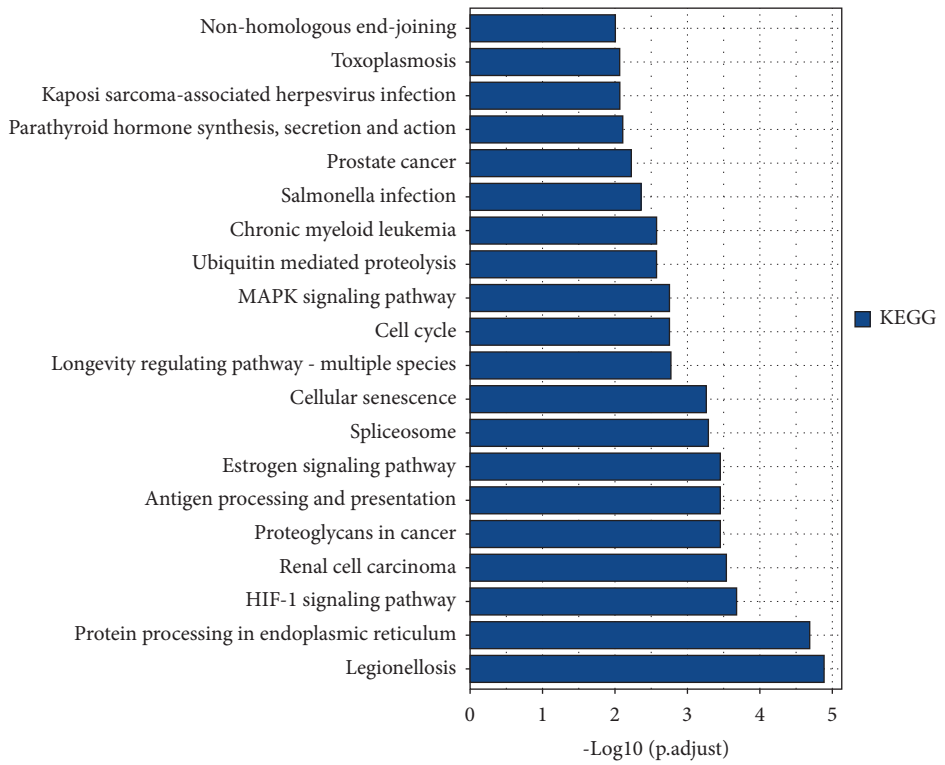

(a)

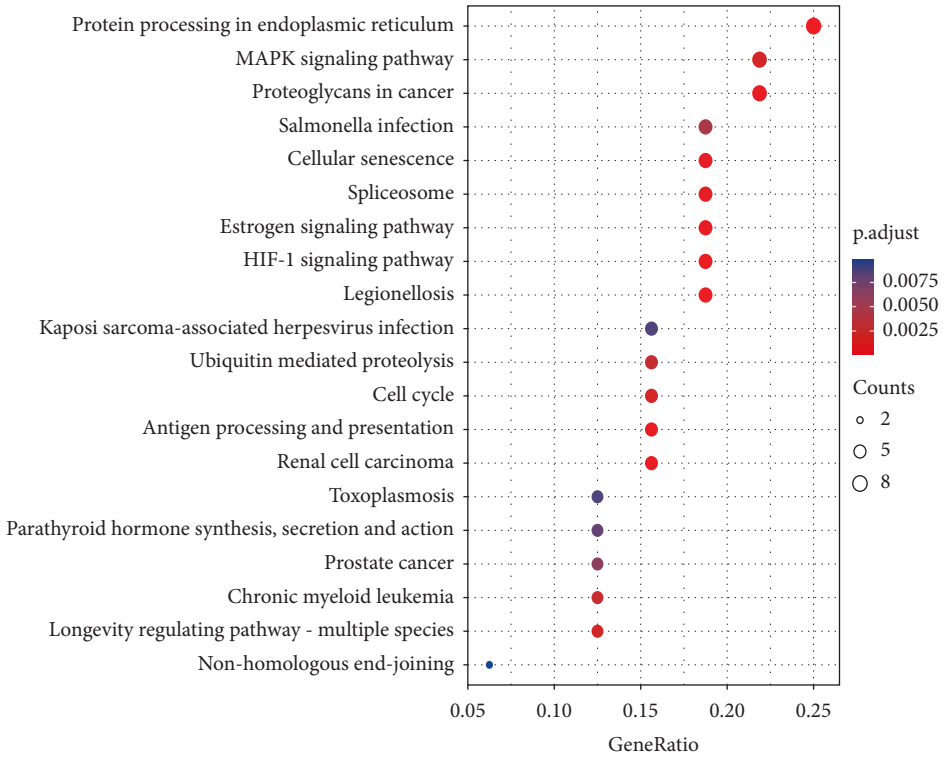

(b)

Figure 3: Continued.

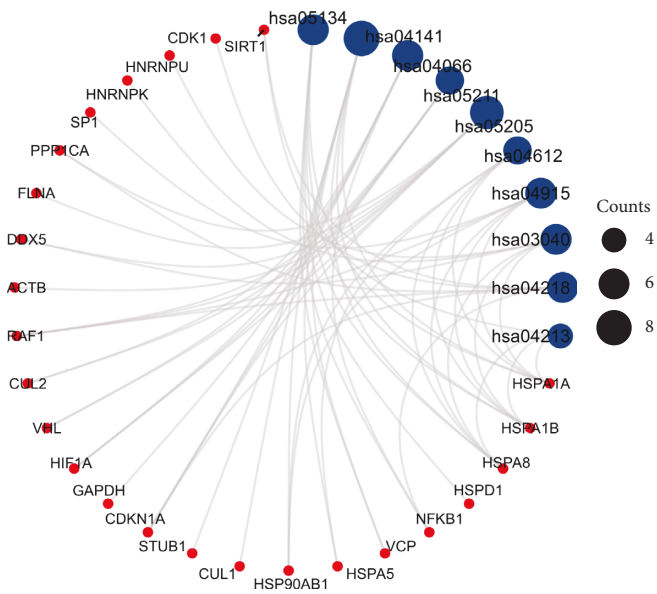

Ontology	ID	Description
KEGG	hsa05134	Legionellosis
KEGG	hsa04141	Protein processing in endoplasmic reticulum
KEGG	hsa04066	HIF-1 signaling pathway
KEGG	hsa05211	Renal cell carcinoma
KEGG	hsa05205	Proteoglycans in cancer
KEGG	hsa04612	Antigen processing and presentation
KEGG	hsa04915	Estrogen signaling pathway
KEGG	hsa03040	Splicesome
KEGG	hsa04218	Cellular senescene
KEGG	hsa04213	Longevity regulating pathway - multiple species

(c)

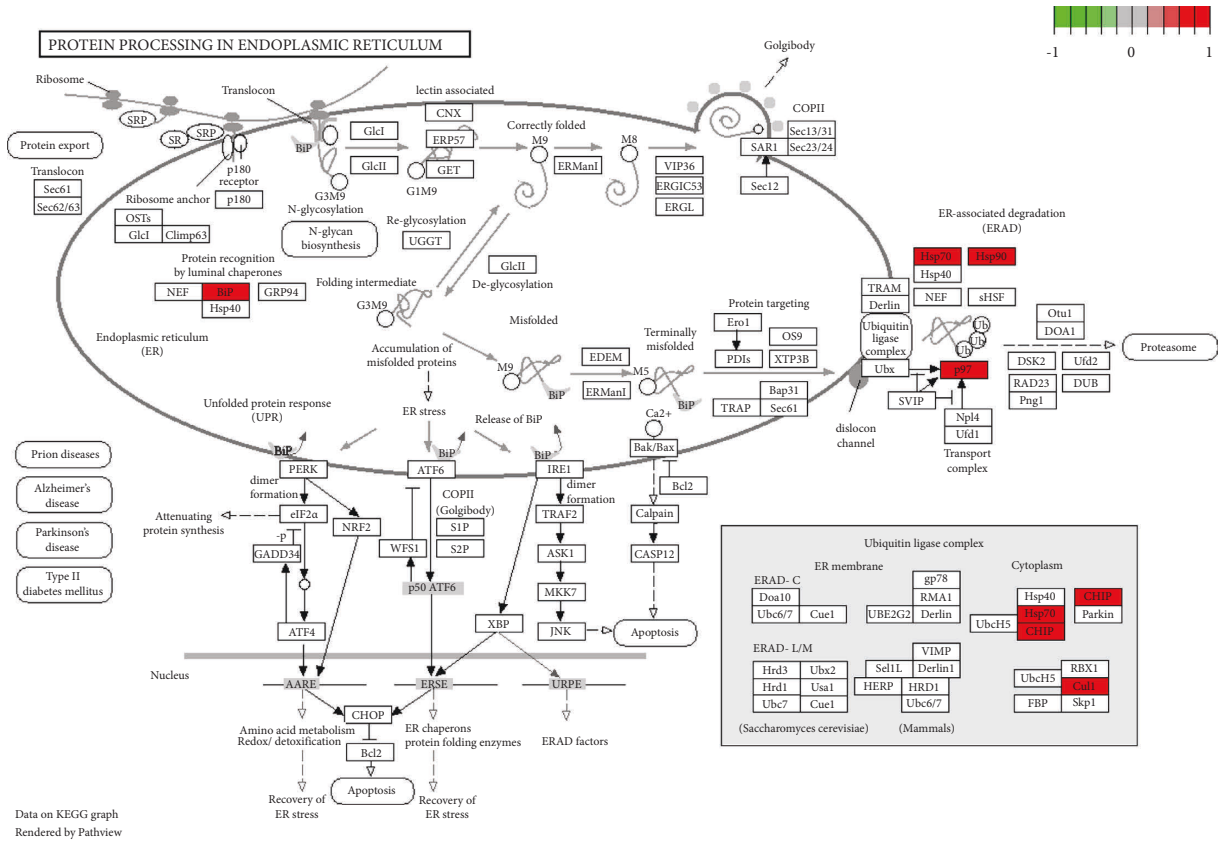

(d)

Figure 3: KEGG pathway enrichment analysis of turmeric targets. (a) Column chart. (b) Bubble plot. (c) KEGG pathway enrichment analysis results. (d) KEGG pathway diagram.

diuresis, dispelling dampness and alleviating swelling. "Southern Yunnan Materia Medica" records its treatment of swelling and pain [46]. Modern research shows that corn silk contains sugars, flavonoids, mineral elements, volatile oils, alkaloids, amino acids, and other chemical components that have anti-oxidant [47], antibacterial [48], antitumor [49], blood sugar-lowering [50], and other pharmacological effects. A recent study found that corn silk can reduce serum uric acid levels by 26.69% ($p < 0.05$) and serum xanthine oxidase (XO) activity by 11.29% ($p < 0.05$) [51]. In addition,

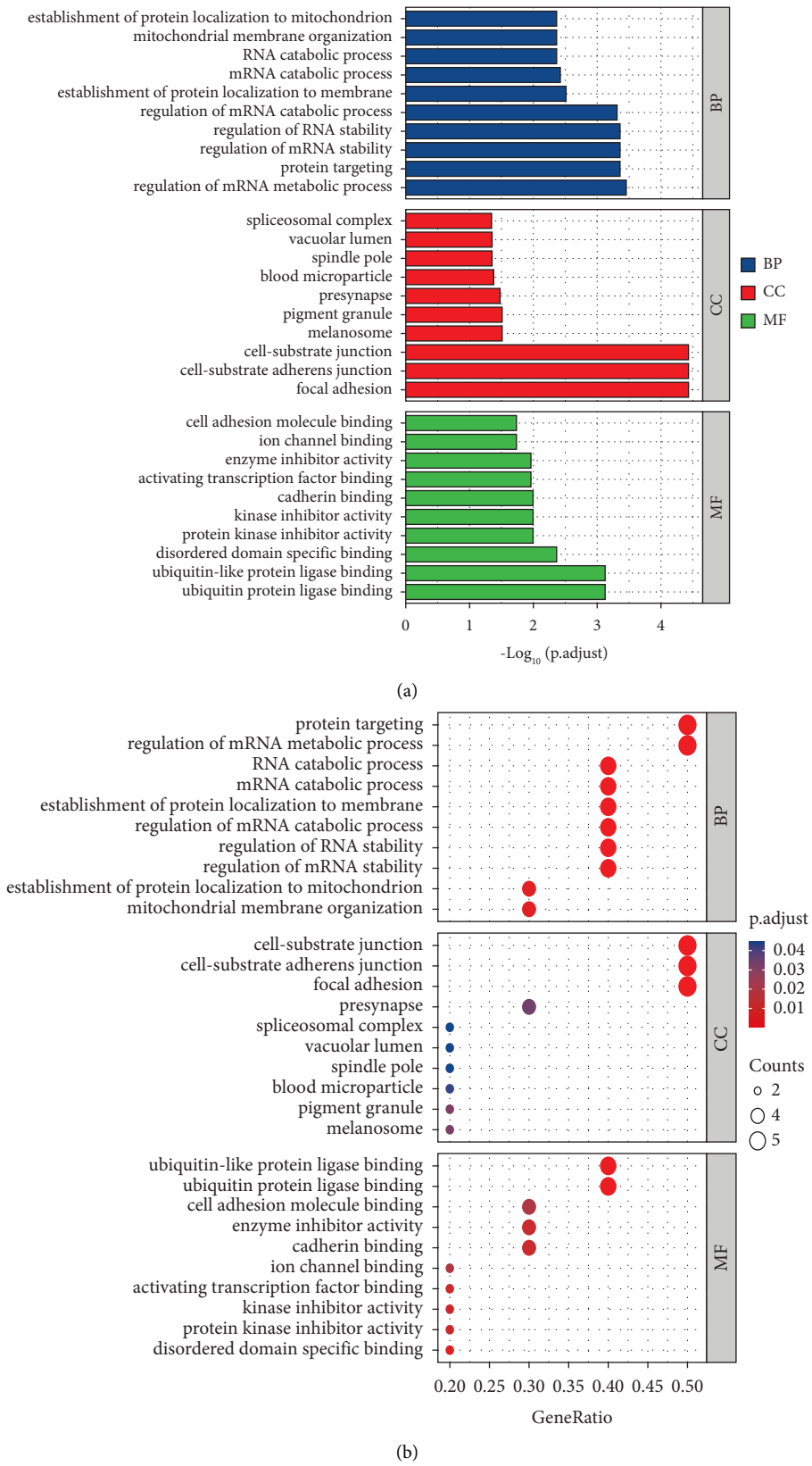

Figure 4: GO functional enrichment analysis of corn silk targets. (a) Column chart. (b) Bubble plot.

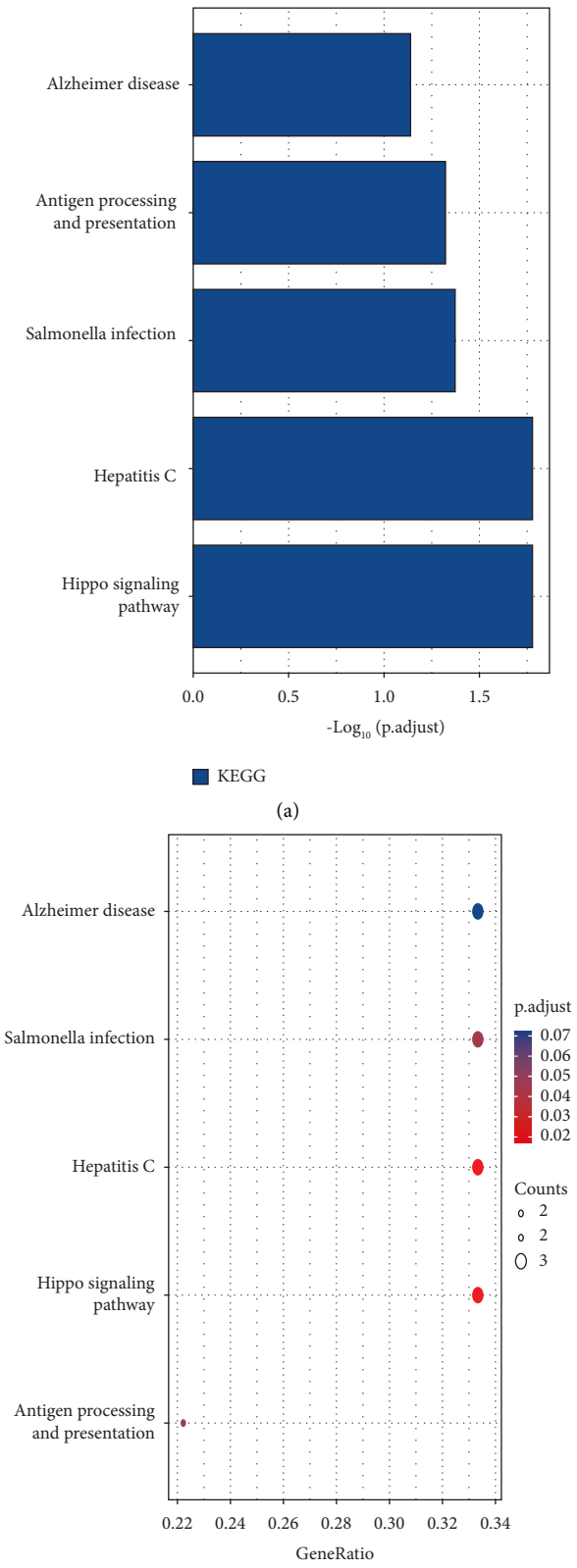

Figure 5: Continued.

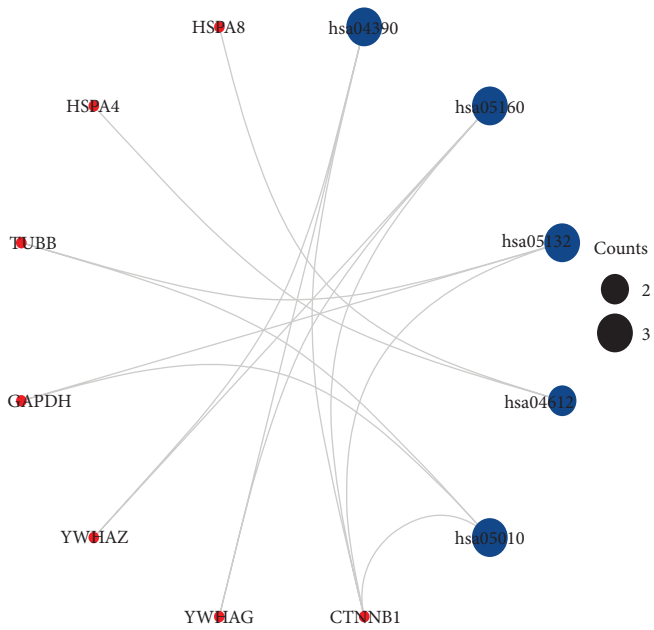

Ontology	ID	Description
KEGG	hsa04390	Hippo signaling pathway
KEGG	hsa05160	Hepatitis C
KEGG	hsa05132	Salmonella infection
KEGG	hsa04612	Antigen processing and presentation
KEGG	hsa05010	Alzheimer disease

(c)

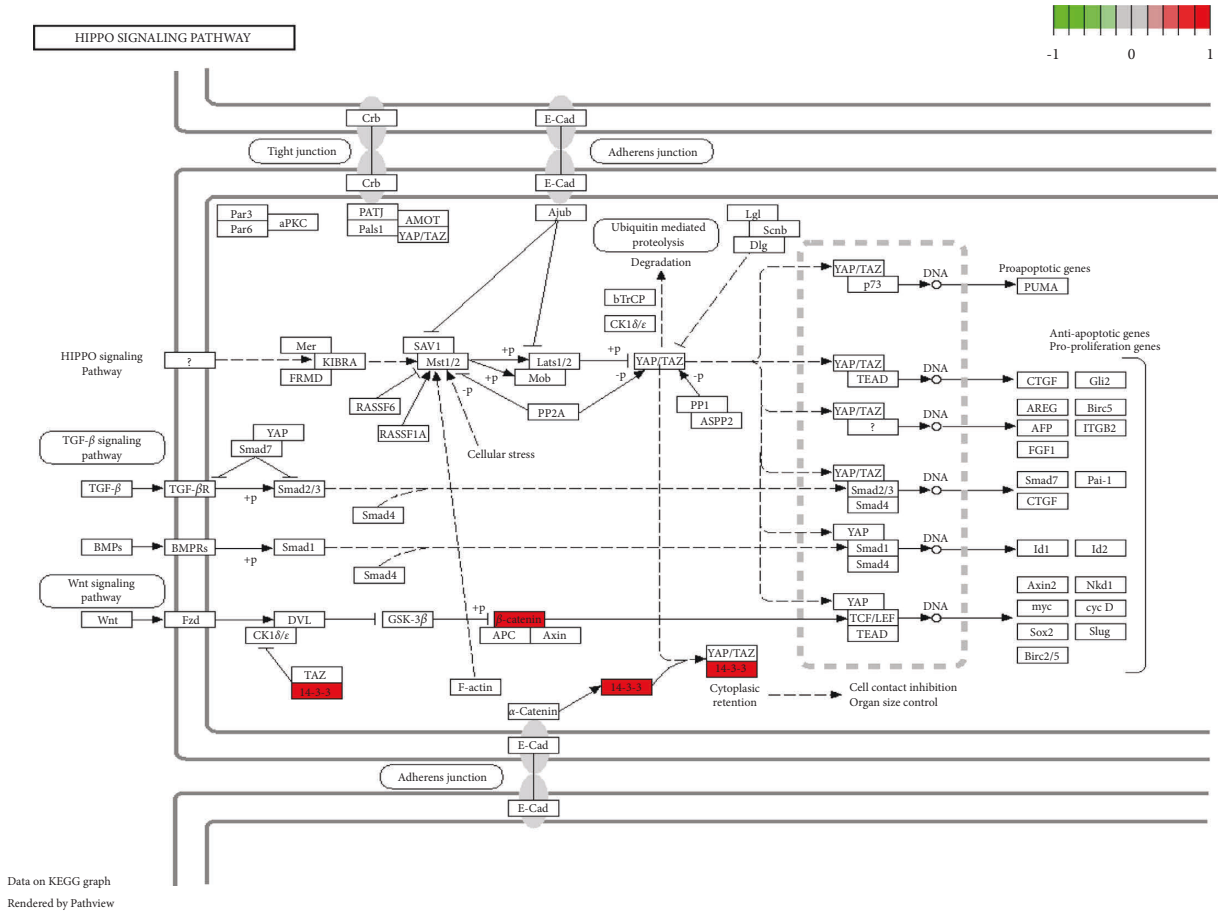

(d)

Figure 5: KEGG pathway enrichment analysis of corn silk targets. (a) Column chart. (b) Bubble plot. (c) KEGG pathway enrichment analysis results. (d) KEGG pathway diagram.

Table 6: Molecular docking scoring.

Target protein	Compound			
	Bisacumol*	Campesterol*	Stigmasterol*	Mandenol#
HSPA1B*	8.60	8.97	7.61	——
HSP90AB1*	6.75	5.18	5.35	——
STUB1*	6.93	6.83	5.64	——
YWHAG#	——	——	——	7.56
CTNNB1#	——	——	——	6.14
YWHAZ#	——	——	——	6.04

Note. "*" represents turmeric. "#" represents corn silk.

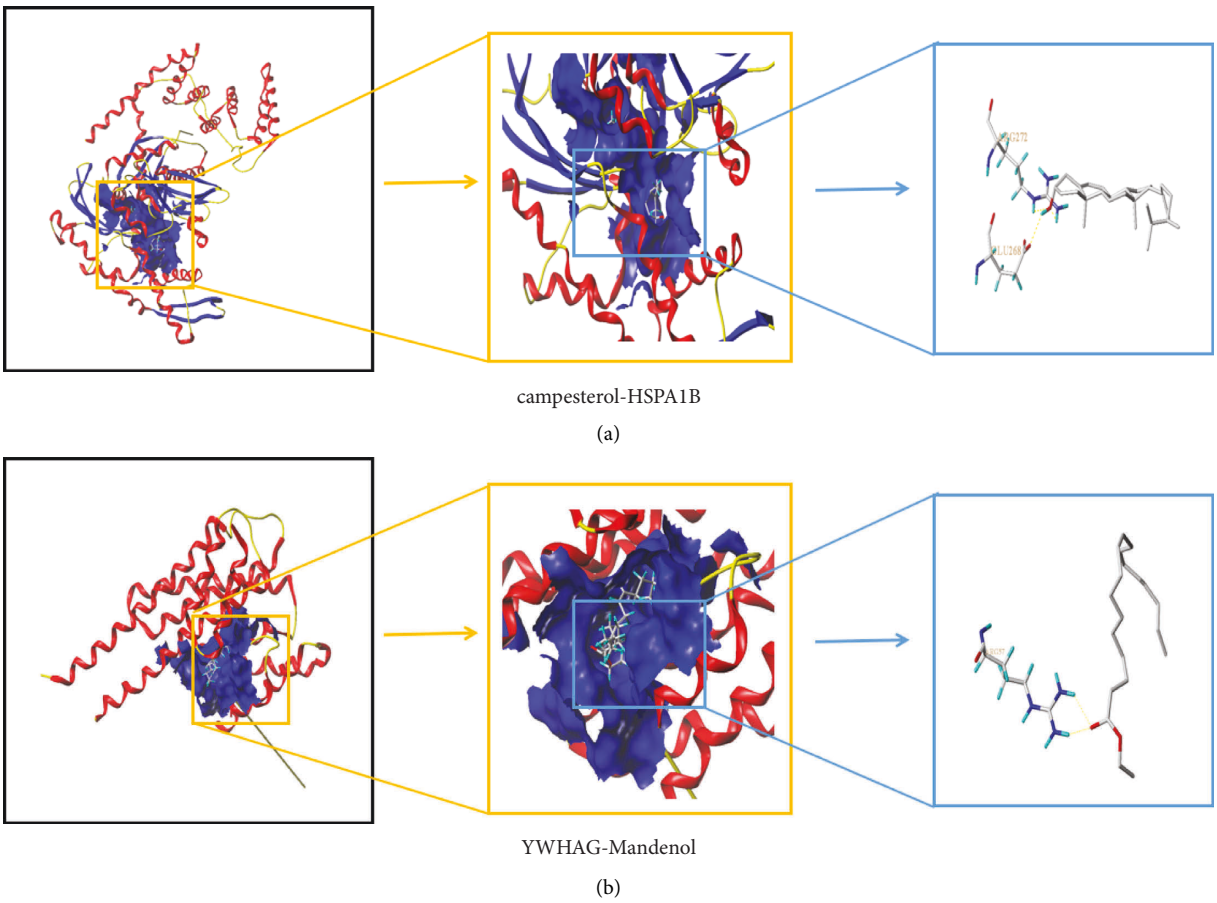

Figure 6: Docking diagram. (a) Turmeric. (b) Corn silk.

a study found that corn silk extract suppressed plasma uric acid in high salt-fed rats ($p < 0.05$) [13]. In China, corn production is abundant. Corn is a medicinal crop with a wide range of sources, is low-cost, and is easy to harvest. In daily life, corn silk is processed and used in beverages, oral liquids, and tea to relieve gout and other diseases, and is often used in combination with other medicines. For gout patients, the long-term use of traditional western medicine can be costly and have significant side effects. Turmeric and corn silk can make up for this deficiency as they are economical and easy to obtain, have few side effects, and can be taken for a long time. In addition, these compounds prevent gouty arthritis by delaying the onset and progression of the disease course. Therefore, in some circumstances, TCM has broad development prospects in supplementing and replacing western medicine.

Traditional culture has endured in China for thousands of years, and TCM has been integral to the country's traditions. Theories and thousands of years of practice, be it the same disease with different treatments, the theory of medicine and food homology, or other traditional Chinese medicine theories, have significantly protected the health of the country's people. Although modern medicine is mainstream in today's society, health problems persist. TCM has the potential to lead to breakthroughs in the health field, as evidenced by Youyou Tu, who invented artemisinin as a cure for malaria. We hope that TCM can better benefit people across the world.

5. Conclusion

Through network pharmacology and molecular docking, bisacumol, campesterol, and stigmasterol have been found to be essential turmeric compounds for gout treatment. These active ingredients may target protein processing in the endoplasmic reticulum through HSPA1B, HSP90AB1, and STUB1 proteins and play a significant role in treating gout. The essential compound of corn silk is mandenol, which may target the hippo signaling pathway to treat gout through CTNNB1, YWHAG, and YWHAZ proteins. Turmeric is a blood-activating medicine, and corn silk is a diuretic medicine. These compounds have different effects and applications but can treat the same disease through different pathways and targets. Hence, the scientific definition of the TCM theory is "same disease with different treatments."

Data Availability

The data used to support the findings of this study are included within the article and in the supplementary information.

Conflicts of Interest

The authors declare no conflicts of interest.

Authors' Contributions

Haoyu Zhang, Hanwei Chen, and Yufeng Ye designed this study, Huizhong Jiang and Haoyu Zhang conducted the network pharmacology, Haoyu Zhang and Mengya Zhao performed the data analysis, and Haoyu Zhang wrote the manuscript. Yufeng Ye, Yan Xu, Mengya Zhao, and Jiabin Liang revised the manuscript. All the authors have read and approved the final version of the manuscript. Haoyu Zhang, Huizhong Jiang, Mengya Zhao, Yufeng Ye, and Hanwei Chen contributed equally to this work.

Acknowledgments

This work was supported by the Science and Technology Project of the Guangzhou Health Commission (No. 20211A011114) and National Natural Science Foundation of China (Nos. 82205190 and 81729003).

Supplementary Materials

Fig.S1: research schematic. Fig.S2: Venn diagram of disease targets and compound targets. (A) Venn diagram of intersection targets of 6 6 gout disease databases. (B) Venn diagram of the intersection targets of the turmeric compound targets and the gout targets. (C) Venn diagram of the intersection targets of the corn silk compound targets and the gout targets. Fig.S3: "medicine-compounds -target-disease" network. (A) Turmeric network diagram. (B) corn silk network diagram. Fig.S4: the PPI network of turmeric -gout targets. Note: degree centrality (DC), closeness centrality (CC), betweenness centrality (BC), network centrality (NC), and local average connectivity (LAC). Fig.S5: the PPI network of corn silk -gout targets. Note: degree centrality (DC), closeness centrality (CC), betweenness centrality (BC), network centrality (NC), and local average connectivity (LAC). (*Supplementary Materials*)

References

[1] L. Sun, D. Wang, Y. Xu, W. Qi, and Y. Wang, "Evidence of TCM theory in treating the same disease with different methods: treatment of pneumonia with ephedra sinica and scutellariae radix as an example," *Evidence-Based Complementary and Alternative Medicine*, vol. 2020,23 pages, Article ID 8873371, 2020.

[2] J. Yang, S. Tian, J. Zhao, and W. Zhang, "Exploring the mechanism of TCM formulae in the treatment of different types of coronary heart disease by network pharmacology and machining learning," *Pharmacological Research*, vol. 159, Article ID 105034, 2020.

[3] M. Chen, "Application of the same disease with different treatments in synopsis of golden chamber," *Guangming Journal of Chinese Medicine*, vol. 36, no. 18, pp. 3070–3072, 2021.

[4] N. Dalbeth, T. R. Merriman, and L. K. Stamp, "Gout," *The Lancet*, vol. 388, pp. 2039–2052, 2016.

[5] M. Dehlin, L. Jacobsson, and E. Roddy, "Global epidemiology of gout: prevalence, incidence, treatment patterns and risk factors," *Nature Reviews Rheumatology*, vol. 16, no. 7, pp. 380–390, 2020.

[6] T. Bardin and P. Richette, "Impact of comorbidities on gout and hyperuricaemia: an update on prevalence and treatment options," *BMC Medicine*, vol. 15, no. 1, p. 123, 2017.

[7] H. Xu, J. Wu, S. Wang et al., "Network pharmacology and in vivo experiments reveal the pharmacological effects and molecular mechanisms of Simiao Powder in prevention and treatment for gout," *BMC complementary medicine and therapies*, vol. 22, no. 1, 2022.

[8] G. Ragab, M. Elshahaly, and T. Bardin, "Gout: an old disease in new perspective - a review," *Journal of Advanced Research*, vol. 8, no. 5, pp. 495–511, 2017.

[9] P. Richette, M. Doherty, E. Pascual et al., "2016 updated EULAR evidence-based recommendations for the management of gout," *Annals of the Rheumatic Diseases*, vol. 76, no. 1, pp. 29–42, 2017.

[10] T. Qin and Q. Meng, "Study on the name of gout in Chinese medicine," *Traditional Chinese Medicinal Research*, vol. 34, no. 6, pp. 49–53, 2021.

[11] S. Huo, *Blood Metabonomics Analysis of Patients with Hyperuricemic Nephropathy and Experimental Study on Treating Hyperuricemic Nephropathy by Clerodendranthus Spicatus*, 2020.

[12] M. M. Mustafa Kiyani, M. F. Sohail, G. Shahnaz et al., "Evaluation of turmeric nanoparticles as anti-gout agent: modernization of a traditional drug," *Medicina*, vol. 55, no. 1, p. 10, 2019.

[13] A. O. Oyabambi, E. D. Areola, L. A. Olatunji, and A. O. Soladoye, "Uric acid is a key player in salt-induced endothelial dysfunction: the therapeutic role of Stigma maydis (corn silk) extract," *Applied Physiology Nutrition and Metabolism*, vol. 45, no. 1, pp. 67–71, 2020.

[14] X. Du, L. Zhao, Y. Yang et al., "Investigation of the mechanism of action of Porana sinensis Hemsl. against gout arthritis using network pharmacology and experimental validation," *Journal of Ethnopharmacology*, vol. 252, Article ID 112606, 2020.

[15] W. Gu and X. Niu, "Research progress in the treatment of gouty arthritis by anti-inflammatory Chinese herbs and their extracts," *Research of Integrated Traditional Chinese and Western Medicine*, vol. 13, no. 1, pp. 47–50, 2021.

[16] H. Guo and B. Xin, "Research progress on prevention and treatment of hyperuricemia with edible and medicinal herb," *World Latest Medicine Information*, vol. 18, no. 86, pp. 50–53, 2018.

[17] D. Otasek, J. H. Morris, J. Bouças, A. R. Pico, and B. Demchak, "Cytoscape Automation: empowering workflow-based network analysis," *Genome Biology*, vol. 20, no. 1, p. 185, 2019.

[18] Y. Zhou, B. Zhou, L. Pache et al., "Metascape provides a biologist-oriented resource for the analysis of systems-level datasets," *Nature Communications*, vol. 10, no. 1, p. 1523, 2019.

[19] G. Yu, L. G. Wang, Y. Han, and Q. Y. He, "clusterProfiler: an R package for comparing biological themes among gene clusters," *OMICS: A Journal of Integrative Biology*, vol. 16, no. 5, pp. 284–287, 2012.

[20] *Tripos International:Sybyl-X 2.0,Molecular Modeling Software Package*, Tripos International, St. Louis, MO, USA, 2012.

[21] J. Zhu, Y. Wu, L. Xu, and J. Jin, "Theoretical studies on the selectivity mechanisms of glycogen synthase kinase 3Î² (GSK3Î²) with pyrazine ATP-competitive inhibitors by 3DQSAR, molecular docking, molecular dynamics simulation and free energy calculations," *Current Computer-Aided Drug Design*, vol. 16, no. 1, pp. 17–30, 2020.

[22] L. Sun, L. Qiao, and Z. Tian, "Research progress on chemical constituents and pharmacological effects of turmeric," *Journal of Shandong University of Traditional Chinese Medicine*, vol. 43, no. 2, pp. 207–212, 2019.

[23] R. Endang, L. Jun, and K. Youngmin, "Javanese turmeric (Curcuma xanthorrhiza Roxb.): ethnobotany, phytochemistry, biotechnology, and pharmacological activities," *Evidence-Based complementary and alternative medicine*, vol. 202115 pages, 2021.

[24] C. Lu, *Composition Analysis of Volatile Oil From Turmeric*, 2018.

[25] M. Le Goff, E. Le Ferrec, C. Mayer et al., "Microalgal carotenoids and phytosterols regulate biochemical mechanisms involved in human health and disease prevention," *Biochimie*, vol. 167, pp. 106–118, 2019.

[26] C. van Gorp, I. H. de Lange, O. B. Spiller et al., "Protection of the ovine fetal gut against ureaplasma-induced chorioamnionitis: a potential role for plant sterols," *Nutrients*, vol. 11, no. 5, p. 968, 2019.

[27] M. Ahmad Khan, A. H. M. G. Sarwar, R. Rahat, R. S. Ahmed, and S. Umar, "Stigmasterol protects rats from collagen induced arthritis by inhibiting proinflammatory cytokines," *International Immunopharmacology*, vol. 85, Article ID 106642, 2020.

[28] G. A. Ko and S. Kim Cho, "Ethyl linoleate inhibits α-MSH-induced melanogenesis through Akt/GSK3β/β-catenin signal pathway," *Korean Journal of Physiology and Pharmacology*, vol. 22, no. 1, pp. 53–61, 2018.

[29] J. H. Hao, H. J. Kong, M. H. Yan et al., "Inhibition of orf virus replication in goat skin fibroblast cells by the HSPA1B protein, as demonstrated by iTRAQ-based quantitative proteome analysis," *Archives of Virology*, vol. 165, no. 11, pp. 2561–2587, 2020.

[30] S. Nizami, K. Arunasalam, J. Green et al., "Inhibition of the NLRP3 inflammasome by HSP90 inhibitors," *Immunology*, vol. 162, no. 1, pp. 84–91, 2021.

[31] Y. Shi, G. Chen, and J. Teng, "Network-based expression analyses and experimental verifications reveal the involvement of STUB1 in acute kidney injury," *Frontiers in Molecular Biosciences*, vol. 8, Article ID 655361, 2021.

[32] R. Huo, X. Tian, Q. Chang et al., "Targeted inhibition of β-catenin alleviates airway inflammation and remodeling in asthma via modulating the profibrotic and anti-inflammatory actions of transforming growth factor-β1," *Therapeutic Advances in Respiratory Disease*, vol. 15, Article ID 1753466620981858, 2021.

[33] X. Zhou, Z. Wang, B. Xu et al., "Long non-coding RNA NORAD protects against cerebral ischemia/reperfusion injury induced brain damage, cell apoptosis, oxidative stress and inflammation by regulating miR-30a-5p/YWHAG," *Bioengineered*, vol. 12, 2021.

[34] J. Wang, H. Jia, B. Zhang et al., "HucMSC exosome-transported 14-3-3ζ prevents the injury of cisplatin to HK-2 cells by inducing autophagy in vitro," *Cytotherapy*, vol. 20, no. 1, pp. 29–44, 2018.

[35] Y. Wang, J. Li, Y. zhang, and D. Xu, "Effect of RNAi ywhaz gene on apoptosis and inflammatory factors in glomerular mesangial cells induced by high glucose," *Chinese Journal of Immunology*, vol. 35, no. 13, pp. 1631–1635, 2019.

[36] S. Nakamura, H. Miki, S. Kido et al., "Activating transcription factor 4, an ER stress mediator, is required for, but excessive ER stress suppresses osteoblastogenesis by bortezomib," *International Journal of Hematology*, vol. 98, no. 1, pp. 66–73, 2013.

[37] F. Cimmino, M. Avitabile, V. A. Lasorsa et al., "HIF-1 transcription activity: HIF1A driven response in normoxia and in hypoxia," *BMC Medical Genetics*, vol. 20, no. 1, 2019.

[38] L. Robrahn, L. Jiao, and T. Cramer, "Barrier integrity and chronic inflammation mediated by HIF-1 impact on intestinal tumorigenesis," *Cancer Letters*, vol. 490, pp. 186–192, 2020.

[39] Y. Zheng and D. Pan, "The Hippo signaling pathway in development and disease," *Developmental Cell*, vol. 50, no. 3, pp. 264–282, 2019.

[40] Q. Zhang, R. Zhou, and P. Xu, "The Hippo pathway in innate anti-microbial immunity and anti-tumor immunity," *Frontiers in Immunology*, vol. 11, p. 1473, 2020.

[41] B. Kocaadam and N. Şanlier, "Curcumin, an active component of turmeric (Curcuma longa), and its effects on health," *Critical Reviews in Food Science and Nutrition*, vol. 57, no. 13, pp. 2889–2895, 2017.

[42] Y. Qin, C. Fei, W. Zhang, and Y. Li, "Research progress on efficacy-related substances of curcuma genera commonly used TCM of blood-activating and stasis-removing," *China Journal of Chinese Materia Medica*, pp. 1–15.

[43] K. Patrick and M. B. Stanbrook, "Take turmeric with a grain of salt," *Canadian Medical Association Journal*, vol. 190, no. 43, Article ID E1270, 2018.

[44] Q. Shen, X. Du, and C. Pei, "Effect of curcumin on lowering uric acid and protecting liver and kidney in hyperuricemic mice," *Science and Technology of Food Industry*, vol. 41, no. 4, pp. 307–321, 2020.

[45] B. Chen, H. Li, G. Ou, L. Ren, X. Yang, and M. Zeng, "Curcumin attenuates MSU crystal-induced inflammation by inhibiting the degradation of IκBα and blocking mitochondrial damage," *Arthritis Research and Therapy*, vol. 21, no. 1, p. 193, 2019.

[46] P. Li, J. Song, and Q. Li, "Curative effect analysis of flavone extract from stigma maydis on rats of modified acute gouty arthritis model," *China Modern Medicine*, vol. 25, no. 34, pp. 8–11, 2018.

[47] D. Zhang, Y. Wang, and H. Liu, "Corn silk extract inhibit the formation of Nε-carboxymethyllysine by scavenging glyoxal/methyl glyoxal in a casein glucose-fatty acid model system," *Food Chemistry*, vol. 309, Article ID 125708, 2020.

[48] A. Gavriil, E. Zilelidou, A. E. Papadopoulos et al., "Evaluation of antimicrobial activities of plant aqueous extracts against Salmonella Typhimurium and their application to improve safety of pork meat," *Scientific Reports*, vol. 11, no. 1, Article ID 21971, 2021.

[49] H. Tao, X. Chen, Z. Du, and K. Ding, "Corn silk crude polysaccharide exerts anti-pancreatic cancer activity by blocking the EGFR/PI3K/AKT/CREB signaling pathway," *Food & Function*, vol. 11, no. 8, pp. 6961–6970, 2020.

[50] K. J. Wang and J. L. Zhao, "Corn silk (Zea mays L.), a source of natural antioxidants with α-amylase, α-glucosidase, advanced glycation and diabetic nephropathy inhibitory activities," *Biomedicine & Pharmacotherapy*, vol. 110, pp. 510–517, 2019.

[51] L. Yuan, Z. Bao, T. Ma, and S. Lin, "Hypouricemia effects of corn silk flavonoids in a mouse model of potassium oxonated-induced hyperuricemia," *Journal of Food Biochemistry*, vol. 45, no. 8, Article ID e13856, 2021.

Hindawi
Evidence-Based Complementary and Alternative Medicine
Volume 2022, Article ID 9707278, 14 pages
https://doi.org/10.1155/2022/9707278

Research Article

Antitoxic Effects of Curcumin against Obesity-Induced Multi-Organs' Biochemical and Histopathological Abnormalities in an Animal Model

Mohammed H. Hassan,[1] **Eatemad A. Awadalla**,[2] **Abd El-Kader M. Abd El-Kader**,[2] **Esraa A. Seifeldin**,[2] **Marwa Ahmed Mahmoud**,[3] **Abdel Rahim Mahmoud Muddathir**,[4] **and Ahmed Abdelsadik**[2]

[1]*Department of Medical Biochemistry, Faculty of Medicine, South Valley University, Qena 83523, Egypt*
[2]*Department of Zoology, Faculty of Science, Aswan University, Aswan 81528, Egypt*
[3]*Department of Medical Physiology, Faculty of Medicine, Sohag University, Sohag, Egypt*
[4]*Department of Hematology and Blood Transfusion, Faculty of Medical Laboratory Science, Alzaeim Alazhari University, Khartoum, Sudan*

Correspondence should be addressed to Abdel Rahim Mahmoud Muddathir; abdelrahimm@gmail.com

Received 23 August 2022; Revised 17 September 2022; Accepted 19 September 2022; Published 6 October 2022

Academic Editor: Salah M. El Sayed

Background. Obesity is a significant public health problem that is characterized by an increase in oxidative stress and enhanced inflammatory responses associated with immune cell invasion of adipose tissues. This study assessed several biochemical abnormalities, apoptosis, oxidative stress status, and associated histological changes in the liver, duodenum, and heart brought on by high-fat diet-induced obesity in rats. It also assessed the mechanistic benefits of curcumin in reversing these inflammatory, metabolic, and histological impairments. *Methods*. Rats were assigned into three groups each including ten rats: the control group (CD), the high-fat diet group (HFD), and the high-fat diet + curcumin (HFDC) group. Serum glucose, insulin, and triglycerides (TAGs) were observed. In addition, apoptosis (indicated by hepatic DNA fragmentation) and oxidative stress status (indicated by hepatic MPO, GSH, and SOD) were assessed. Histopathological examinations included the GIT (liver and duodenum) and heart in addition to quantitative real-time polymerase chain reaction (qRT-PCR) assays of the adipose tissue genetic expressions for inflammatory signaling pathways (TLR4, IL-6, and TNF-α). *Results*. The overall findings showed that the HFD group exhibited significantly higher levels of glucose, TAGs, and insulin than the control group ($P < 0.01$). The histological abnormalities of the studied organs in the HFD group were paralleled by these biochemical abnormalities, which were strongly associated with increased apoptosis, increased oxidative stress, and increased expression of the inflammatory signaling markers. There were significant improvements in the HFDC group in terms of biochemical, inflammatory, and histological investigations. *Conclusions*. This study's findings concluded that obesity is significantly associated with biochemical and microscopic alterations in many organs. Curcumin exerted potent antitoxic, antioxidant, tissue-protective, and antiobesity effects. Curcumin is recommended to be added to various dietary regimens to prevent or delay the organs' dysfunction among obese people.

1. Introduction

Obesity is a metabolic condition that is chronic and associated with a low-grade inflammatory response. Not only in the West but also in many developing countries, obesity is a major public health issue. Obesity is a significant risk factor for cardiovascular diseases, such as hypertension, metabolic disease, and diabetes mellitus [1, 2].

Because of its low satiety properties and high caloric density, a high-fat diet (HFD) has been linked in epidemiological studies to the development of obesity by encouraging food overconsumption and weight gain.

Furthermore, HFD alters the composition of gut microbes in a way that increases the energy extraction of indigestible dietary components, increasing the efficiency of food utilization [3].

Free fatty acids (FFAs) and hormones called adipokines are secreted by adipose tissues, which may be a crucial factor in the emergence of non-alcoholic fatty liver diseases (NAFLD). It is reported that toxic FFAs can cause c-Jun N-terminal kinase (JNK) to activate the intrinsic apoptotic pathway in hepatocytes. The proapoptotic protein Bim is activated by JNK, which also activates Bax and causes lipoapoptosis. Reduced adiponectin levels could create a proinflammatory environment, making people more susceptible to lipotoxicity, which encourages the development of non-alcoholic steatohepatitis (NASH) and even advanced hepatic fibrosis from simple steatosis [4].

According to previous publications, macrophages invade adipose tissues more as the level of obesity rises. An essential cell type in mediating the inflammation brought on by obesity in the adipose tissue is the macrophage. These macrophages may be the main source of cytokines that promote inflammation, e.g., interleukin-1 (IL-1), interleukin-6 (IL-6), and tumor necrosis factor-α (TNF-α). According to recent research, obesity is characterized by an increase in oxidative stress and amplified inflammatory reactions that occur along with immune cells infiltrating adipocytes [5, 6]. The antioxidant system of the living system possesses its own antioxidant defense that includes major antioxidant enzymes such as superoxide dismutase (SOD), catalase (CAT), glutathione peroxidase (GPx), and reduced glutathione (GSH) [7, 8]. Myeloperoxidase (MPO) is currently thought of as a novel inflammatory biomarker in acute coronary syndrome and ischemic heart diseases [9]. To kill pathogens, MPO produces a variety of oxidants, but it also damages the host's tissues [10].

A class of conserved intracellular and cell surface proteins called toll-like receptors (TLR) identify different pathogen-associated molecular patterns (PAMPs) and trigger innate immune reactions. The synchronization of immune response and nutrient-sensing pathways is made possible by these molecular sites. Several TLR proteins exist, but TLR2 and TLR4 are thought to be crucial metabolic inflammatory regulators throughout the emergence of obesity and associated co-morbidities [11]. It has been documented and proposed that obesity-related DNA damage has a role in the development of obesity-related diseases [12]. Obesity-related DNA damage appears to be repairable, and changes in diet and exercise routines can have an impact on genomic stability [13].

Turmeric (*Curcuma longa*) has more than 100 components that have been identified. Turmeric contains additional coloring compounds known as curcuminoids in addition to its volatile oil, which is the root's major component and contains turmerone. Turmeric contains natural antioxidants known as curcuminoids, including curcumin dimethoxy curcumin, 5′-methoxycurcumin, and dihydro curcumin [14, 15]. The most significant phenolic ingredient in turmeric is called curcumin, and it is yellow in color and is a natural phenolic antioxidant [16]. Due to its biological and pharmacological characteristics, which include antioxidant and anti-inflammatory features, curcumin has received a lot of interest in various research studies, including human or experimental animal models in various diseases, including obesity [17].

In light of the previous research efforts, it is crucial to assess the different biochemical abnormalities caused by high-fatdiet-induced obesity in rats, including glucose homeostasis, lipid profile, apoptosis (via assessment of hepatic DNA fragmentation), and oxidative stress status (via assessment of hepatic MPO, GSH, and SOD), as well as any possible associated histopathological changes in the GIT (liver and duodenum) and heart. Additionally, genetic analyses of the related inflammatory signaling pathways (via assessments of adipose tissue expressions of TLR4, IL-6, and TNF-α) were performed to explore the potential mechanistic benefits of curcumin in reversing these metabolic abnormalities.

2. Materials and Methods

2.1. Experimental Design. Thirty male albino rats were 50–60 grams when the experiment started. Before the study began, rats were procured from the Qena Breeding Center and given a week of acclimatization. Rats were divided into three groups at random. At a temperature of 25°C and a 12-hour cycle of dark and light, all groups were maintained in the same habitat. All experimental groups received the same feeding schedules and water supplements. Animals were kept in normal air-conditioned conditions in well-ventilated cages with sawdust bedding. According to the manual for the care and use of laboratory animals, the Aswan University Animal Ethical Committee in Egypt approved the treatment of the animals and the experimental techniques. The ethical approval code for the present study is ASW-Sci-ZOO-15-6-015 and the date of approval was January, 2020. Curcumin powder with the CAS number 458-37-7 was bought from Merck for use in this experiment (Figures 1(a) and 1(b)). The nutrition of the experimental animals include 50.17 grams of crude carbohydrate, 30.2 grams of crude protein, 6.4 grams of crude fat, 4.3 grams of crude fiber, 5.8 grams of mineral mixture, and 1.6 g of vitamin mixture/100 g diet, which made up the mash. To harmonize the dietary amounts utilized in various types of groups, we used 20 grams of beef grease in the high-fat diet. The rats were randomly divided into three groups, 10 rats each. The groups were assigned to a food type as follow:

(A) Control diet group (CD): This group fed 40 grams of mash.

(B) High-fat diet group (HFD): This group fed on 20 grams mash + 20 g beef grease (50% fat, wt./wt.) as was previously reported [18].

(C) High fat diet + curcumin (HFDC): This group fed on a high fat diet + 100 mg/kg body weight curcumin as was previously reported [19]. Each rat received 5-6 mg of curcumin on average.

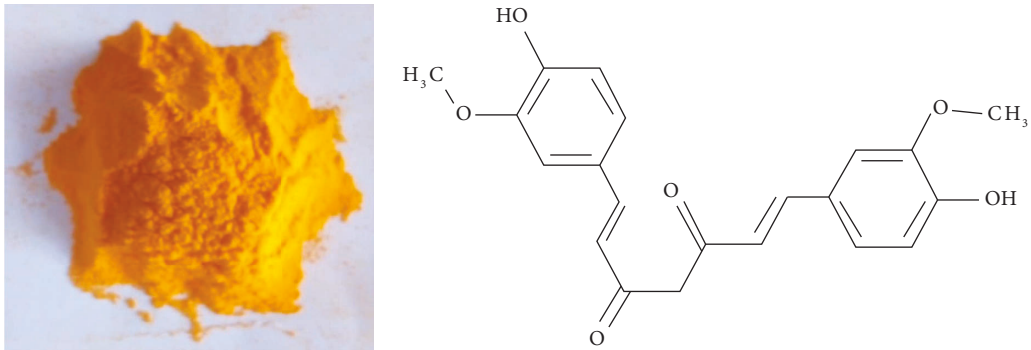

(a) (b)

Figure 1: Curcumin. (a): Curcumin powder; (b): chemical structure of curcumin.

As stated in a previously published work [20], the rats were treated daily for 8 weeks.

2.2. Body Weight Measurement. Rats having an equal initial body weight were assigned to the experimental diet for 56 days. Two times a week during the trial, body weight was recorded (56 days). All groups were then given unrestricted access to their respective diets [21, 22].

2.3. Collection and Preparation of Blood and Tissue Samples. Rats from various groups were decapitated and then scarified twenty-four hours after receiving the final dose of treatment. Blood samples were taken from the retro-orbital veins during scarification and placed in plain tubes. These tubes were then centrifuged at 4000 rpm for 10 minutes to separate the serum. The separated sera were then divided into aliquots using 1 ml cryotubes and stored at −80°C until used in subsequent serum biochemical analyses (serum glucose, triglycerides, and insulin assays).

From each group, samples of adipose tissues, liver, duodenum, and heart were taken and cleaned in sterile saline. Three portions of each liver sample were separated. For histological analysis, the first portion of the liver, the duodenum, and the heart were preserved in 10% neutral phosphate-buffered formalin (pH 7.0).

The supernatant was used to measure the activities of GSH, SOD, and MPO after homogenizing the second portion of liver tissues using phosphate buffer (pH 7.4), a tissue homogenizer (Glas-Col USA), and centrifugation at 4000 rpm for 30 min at 4°C.

Additionally, the final third portion of the hepatic tissue samples was used to measure DNA fragmentation as a potential marker for apoptosis using spectrophotometry.

For molecular investigations of TLR4, IL-6, and TNF-α tests by quantitative real-time PCR (qRT-PCR), pieces of adipose tissues were preserved in liquid nitrogen and kept at −80°C.

2.4. Biochemical Assays

(A) Serum insulin assays were performed by a microplate ELISA reader (EMR-500, USA), using commercially available ELISA assay kits (supplied by Chongqing Biospes Co., Ltd, China with catalog number: BEK1243). Serum glucose assays were performed by the o-toluidine method as was previously reported [23] and were supplied by (Sigma-Aldrich, Germany) with CAS number 119-93-7. Serum triglyceride concentrations were estimated by the GPO-PAP- enzymatic colorimetric method as was previously reported [24], supplied by (Spectrum Diagnostics, Egypt, catalog number 314-001).

(B) determination of total protein concentration in liver tissue homogenates: Total protein content in liver tissue was estimated by the Lowery technique and results were expressed as mg/total weight hepatic tissues [25] and were used for biochemical assessment of hepatic MPO, GSH, and SOD using colorimetric kinetic methods as follows

(1) Assays of hepatic MPO activity in the liver was measured by a modified procedure from earlier described methods [26, 27]. 400 mg of liver tissue samples were homogenized in 0.5 ml of 50 mM potassium phosphate buffer with a pH of 6.0 and centrifuged at $12,000 \times g$ for 20 min. at 4°C. The pellets were then suspended in 2 ml of 50 mMPB containing 0.5% hexadecyltrimethylammonium bromide (HETAB) from Sigma-Aldrich (PRD.NO. H5882). After three freeze and thaw cycles, with a vortex between cycles, the samples were centrifuged at $12,000g$ for 20 min. Aliquots (0.3 ml) were added to 2.3 ml of reaction mixture containing 50 mM O-dianisidine (Sigma, D9143) and 20 mMH_2O_2 solutions. A yellow compound was produced which has a maximum absorption peak of 460 nm. One unit of enzyme activity was defined as the amount of MPO present that caused a change in absorbance and measured at 460 nm for 3 min. MPO activity was expressed as U/mg tissue.

(2) Hepatic GSH concentration assays were based on the reduction of 5.5′ Dithiobis (2-Nitrobenzoic acid DTNB) with glutathione (GSH) to produce a yellow compound [28].

(3) Hepatic SOD activity was measured in tissues homogenate based on its inhibitory action on the phenazine methosulphate (PMS) that mediated reduction of the Nitroblue tetrazolium (NBT) dye [29].

2.5. Molecular Assays

2.5.1. Quantitative Real-Time PCR (qRT-PCR). As was previously reported, tissue total RNA was extracted from the adipose tissue (AT) using phenol/chloroform [30]. RNA was dissolved in water treated with dimethyl pyrocarbonate (DEPC-H_2O). Using a nanodrop/spectrophotometer, the RNA content and sample quality were assessed. A ratio of roughly 1.8 and 2.0 for RNA and DNA, respectively, was taken into consideration. RNA that met the requirements for quantity and quality was kept at −80°C for future assays.

First-strand DNA was created using oligo-dT primers and Superscript RT-II reverse transcriptase (Invitrogen). Utilizing the Power SYBR Green PCR Master Mix, PCR was carried out (Applied Biosystems). On the Applied Biosystems StepOnePlus real-time PCR system, TLR4, IL-6, and TNF-α were examined. Primer information was provided (Table 1), and results were standardized to the housekeeping gene GAPDH as a reference [31, 32]. Calculations for the relative gene expression profile analysis were made using the ΔΔCT method equation [33], according to the following formula: ΔCT (gene) = CT (gene, sample)−CT (gene, control). ΔCT (reference) = CT (reference, sample)−CT (reference, control). ΔΔ CT = ΔCT (gene)−ΔCT (reference). Due to exponential nature of PCR, "fold change" was calculated as $2^{-\Delta\Delta CT}$ [31].

Table 1: Primer sequences of target genes used for qRT-PCR in this experiment.

GAPDH	Forward	5′-AGACAGCCGCATCTTCTTGT-3′
	Reverse	5′-CTTGCCGTGGGTAGAGTCAT-3′
TLR4	Forward	5-GGGGCAACCGCTGGGAGAGA-3′
	Reverse	5′-AACCAGCGGAGGCCGTGAGA-3′
IL-6	Forward	5′-TCTCTCCGCAAGAGACTTCCA-3′
	Reverse	5′-ATACTGGTCTGTTGTGGGTGG-3
TNF-α	Forward	5-ACCACGCTCTTCTGTCTACTG-3′
	Reverse	5′-CTTGGTGGTTTGCTACGAC-3′

2.5.2. DNA Fragmentation Assays. DNA fragmentation (as a defiant marker for apoptosis in the hepatocytes) was assayed as was previously reported [34, 35], with minor modifications. 100 mg of tissue samples were dissected and minced finely with a razor blade/scalpel. The minced tissue was transferred to a microfuge containing 0.5 ml of hypotonic lysing buffer (10 mM Tris-HCl, 1 mM EDTA, pH 7.4, 0.2% Triton X-100) followed by mixing well for 5 minutes via vortex at low power. The lysates were immediately centrifuged at 12000g for 15 minutes to separate intact from fragmented chromatin. Supernatants and pellets were precipitated in separate microfuge tubes for 16 to 48 hours at −20°C in 50% isopropanol and 0.5 M/L NaCl. The precipitates were pelleted by centrifugation at 12000g for 10 minutes, air dried, suspended in TE buffer (10 mM Tris-HCl, 1 mM EDTA, pH 7.4) and heated at 55°C for 10 minutes. In this DNA fragmentation assay, intact chromatin and oligonucleosomal fragments were separated by centrifugation. DNA fragmentation was expressed spectrophotometrically at 260 nm using Thermo-Nanodrop using formula (1):

$$\%\text{DNA fragmentation} = \frac{\text{Optical density (O.D) of the supernatant}}{\text{O.D.Supernatant} + \text{O.D.Pellet}} \times 100. \quad (1)$$

2.6. Histological Examination of the Liver, Duodenum, and Heart Tissues. Liver, duodenum, and heart specimens were dehydrated gradually in ethyl alcohol (50–99%), cleaned in methyl benzoate, and embedded in molten paraffin wax at 58–62°C for microscopic preparations. For microscopic examination, tissue slices with a 5 μm thickness were produced and stained with hematoxylin and eosin as reported previously [36]. Under a high-power light microscope, the sections were examined to detect histological and histopathological changes (Olympus BX43F, Tokyo, 163-0914, Japan). Image analysis was carried out using a personal computer, a camera, software (Olympus DP74 Tokyo 163-0914, Japan) and an optical microscope.

2.7. Statistical Analysis. The obtained data were expressed as means ± SEM. Differences between means were tested by one-way analysis of variance (ANOVA) followed by the Student–Newman–Keuls T-test using Minitab 12 software so that the data obtained can be compared and statistically evaluated. Statistical significance was considered when $P < 0.05$.

3. Results

The data regarding body weight were recorded as previously published [36]. Briefly, the mean ± SEM of body weights of the HFD group (227.22 gm ± 25.88) was significantly increased compared with the CD group (190.88 gm ± 22.88), while it significantly decreased in the HFDC group (199.25 ± 14.33) compared with the HFD group, $p < 0.05$ for all (Figure 2(a)).

3.1. Serum Glucose, Insulin, and Triglycerides in Various Study Groups. There were significantly ($P < 0.01$) increased serum glucose, insulin, and triglycerides in the HFD group as compared with the CD group. Coadministration of curcumin in the HFDC group exhibited significantly ($P < 0.05$) decreased serum glucose, insulin, and

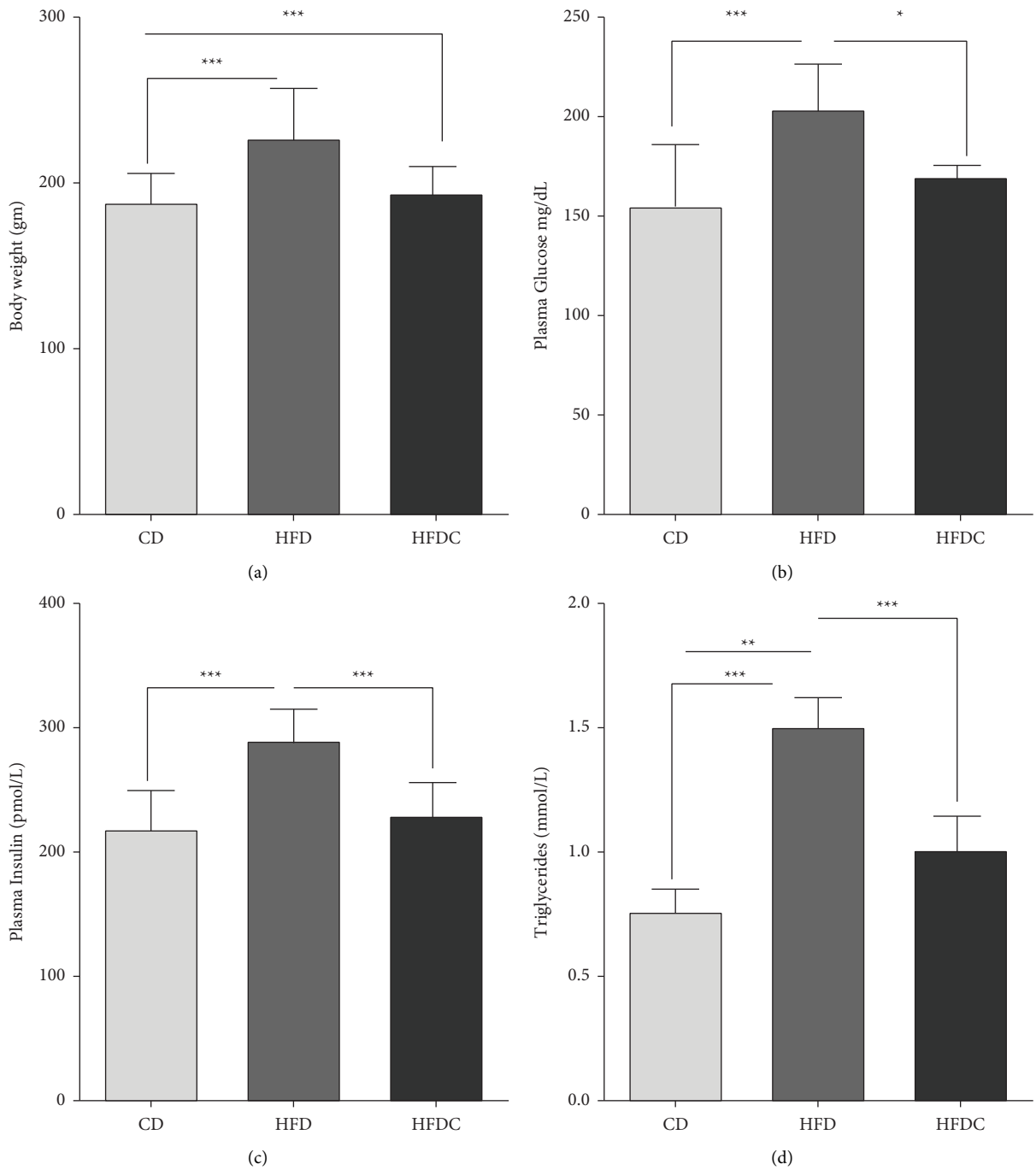

Figure 2: Mean values of (a) body weight (gm), (b) serum glucose (mg/dL), (c) insulin (pmol/L), and (d) triglycerides levels (mmol/L). Values are expressed as mean ± SEM. The sample size was $n = 10$ animal per group. CD, control diet; HFD, high-fat diet; HFDC, high-fat diet + curcumin. *indicates $P < 0.05$, **indicates $P < 0.01$ and ***indicates $P < 0.001$.

triglycerides when compared with the HFD group (Figures 2(b)–2(d)).

3.2. Hepatic DNA Fragmentations, MPO, GSH, and SOD Activities among the Included Study Groups. Fragmentation of DNA was significantly increased ($P < 0.01$) and MPO activity with significantly decreased GSH and SOD levels in the liver homogenates of the HFD group compared to the CD group. However, curcumin had caused a significant decrease in DNA fragmentation and MPO activity that was associated with significantly higher levels of GSH and SOD in the HFDC group when compared with the HFD group (Figures 3(a)–3(d)).

3.3. Adipose Tissue Genetic Expressions of TLR4, IL-6, and TNF-α of the Control and Different Treated Groups. Levels of

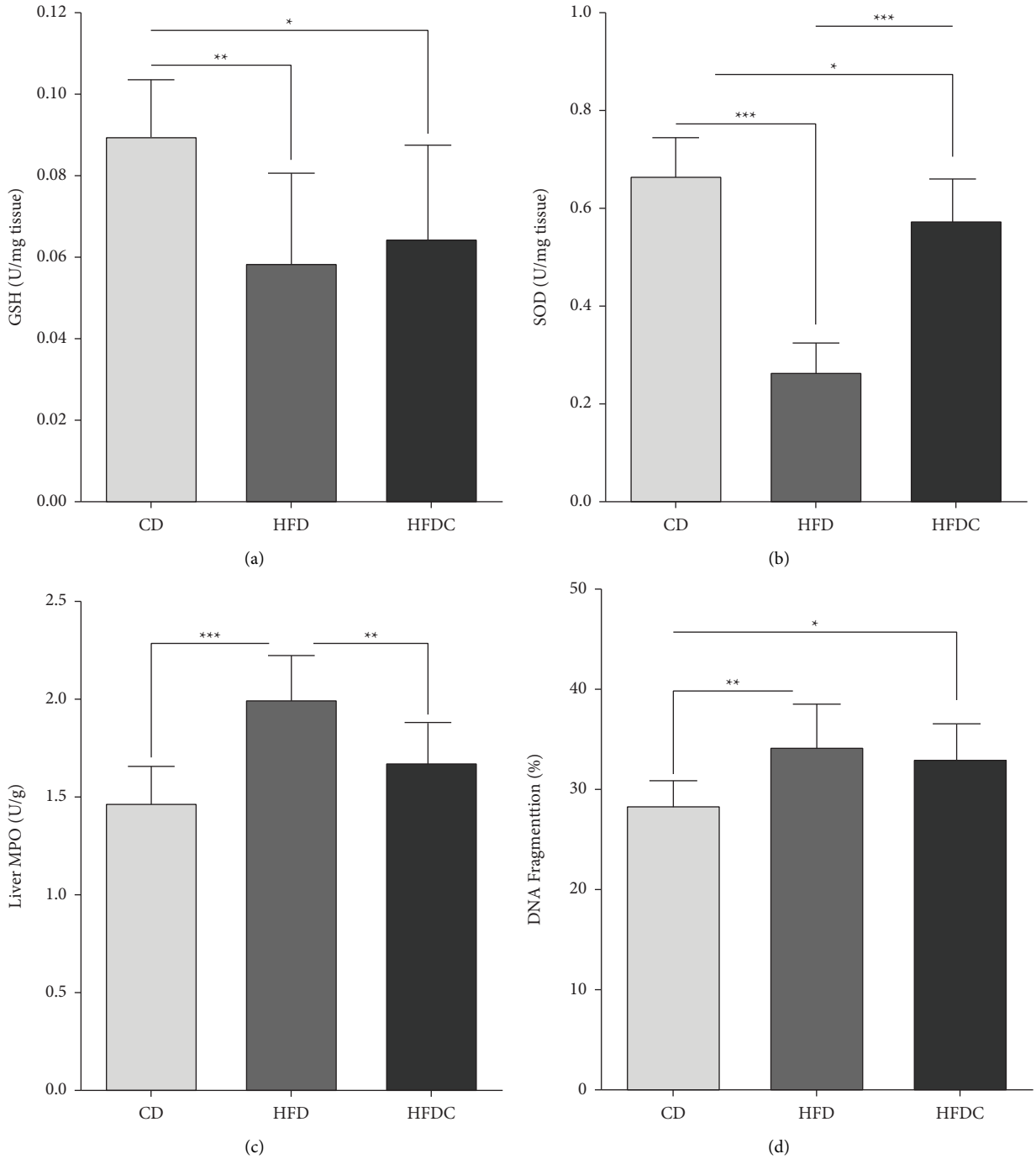

Figure 3: Hepatic profile of (a) glutathione reduced (GSH), (b) superoxide dismutase (SOD), (c) myeloperoxidase activity (MPO), and (d) DNA fragmentation percentage of control and treated rats. Each group consists of 10 rats. Values are represented as mean ± SEM. Bars without a common letter is not differ while *indicates $P < 0.05$, **indicates $P < 0.01$ and ***indicates $P < 0.001$.

TLR-4, IL-6, and TNF-α gene expressions of adipose tissues were significantly ($P < 0.01$) higher in the HFD group than in the CD group. In comparison with the HFD-fed rats, the HFDC group showed significantly ($P < 0.01$) lower levels of the previously mentioned three genes' expressions in adipose tissues (Figures 4(a)–4(c)).

3.4. Histopathological Findings of Liver, Duodenum, and Heart Tissues from Various Study Groups

3.4.1. Histopathological Findings of the Liver. Microscopic examinations of the CD group liver showed normal hepatic architecture including the normal arrangement of the cords

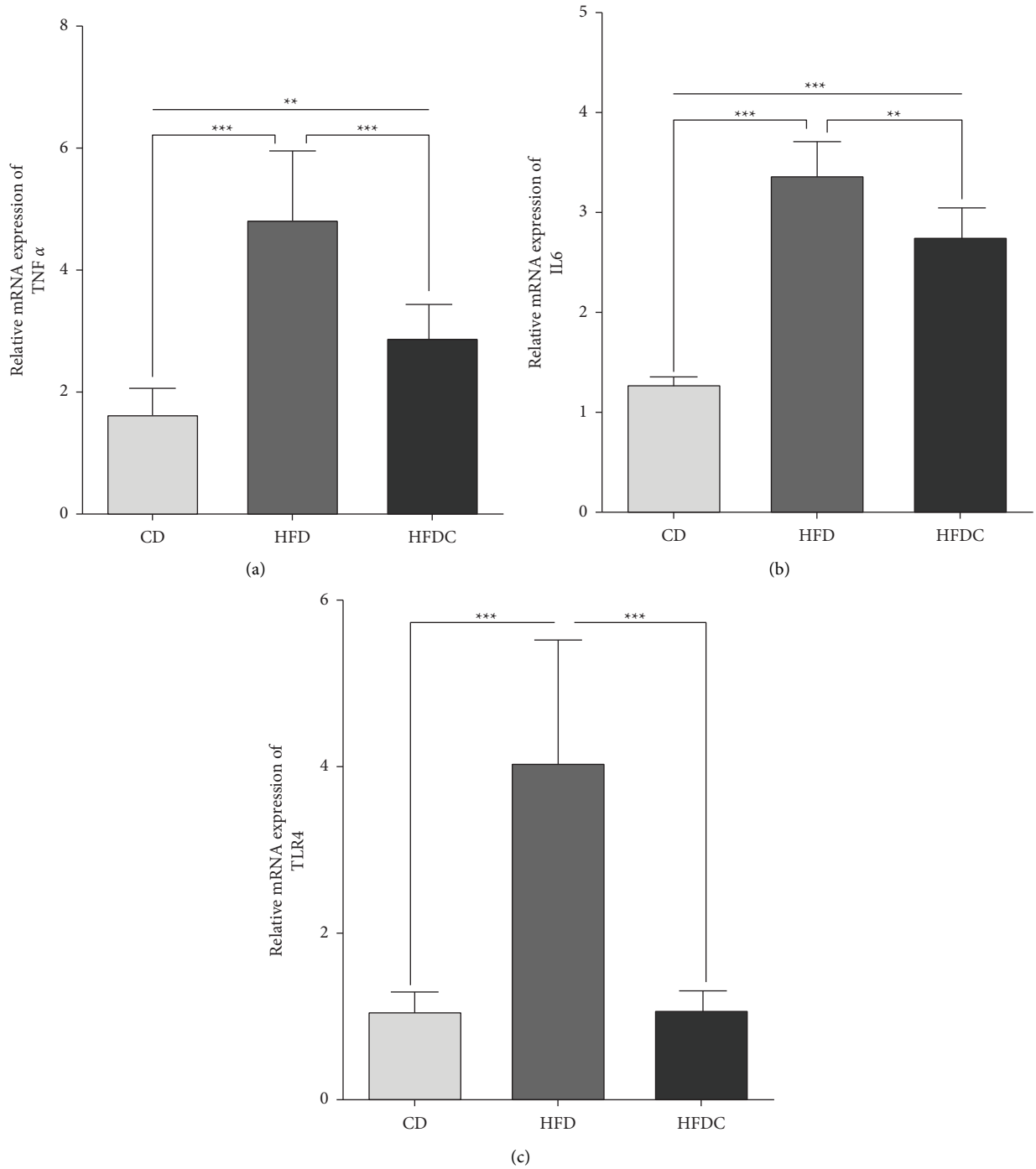

Figure 4: Alterations of adipose tissue inflammatory markers between control fed with control diet (CD) and those fed with high-fat diet without curcumin (HFD) or with curcumin (HFDC). The relative mRNA expression was demonstrated by reverse transcription-quantitative polymerase chain reaction. (a) tumor necrosis factor-alpha (TNF-α), (b) interleukin-6 (IL-6), and (c) toll like receptor-4 (TLR4). Each experiment was repeated three times. Values are given as the mean ± the standard error. $^{*}P < 0.05$, $^{**}P < 0.01$ and $^{***}P < 0.001$.

or plates of hepatocytes, central veins with the endothelial lining, and hepatic sinusoids which were extending in between the hepatic cords (Figure 5(a)). Liver sections of the HFD group rats showed disarrangement in the architecture of hepatic cords with widespread intracellular vacuolization of hepatocytes and congested central veins with irregular outlines. Macrovesicular steatosis and microvesicular steatosis were also detected (Figure 5(b)). Cotreatment with curcumin showed moderately congested central vein and a few hepatocytes with microvesicular steatosis (Figure 5(c)).

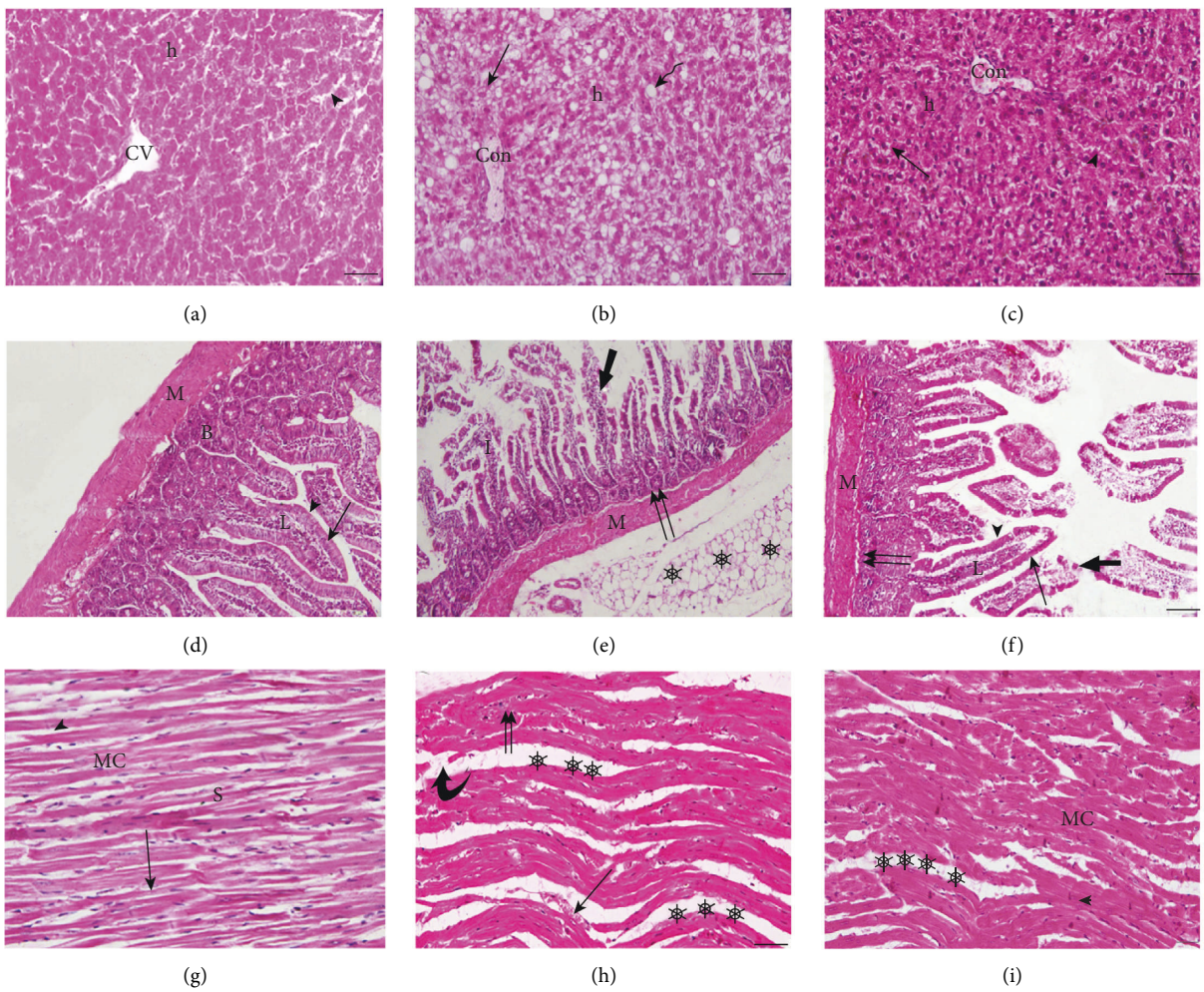

Figure 5: Histopathological findings of liver, duodenum and heart of various study groups. (a–c): Photomicrographs of male albino rat's liver stained with haematoxylin and eosin (HE). (×200 = 100 μm). (a): Liver photomicrograph of the CD group. (b): Liver photomicrograph of the HFD group. (c): Liver photomicrograph of the HFDC group. Central vein (CV), hepatocytes (h), blood sinusoids (arrowhead), congested central vein (Con), macrovesicular steatosis ( ), and microvesicular steatosis (thin arrow). (d–f): Photomicrographs of male albino rat's duodenum stained with haematoxylin and eosin (HE). (×200 = 100 μm). (d): Duodenal photomicrograph of the CD group. (e): Duodenal photomicrograph of the HFD group. (f): Duodenal photomicrograph of the HFDC group. Musculosa (M), Brunner's glands (B), Lamina propria (L), simple columnar epithelium of villus (thin arrow), Goblet cells (arrow head), epithelial erosion (thick arrow), inflammatory infiltration (I), Necrosis (double arrow) of the inner circular muscle fibers of musculosa, Massive amounts of adipose tissues (stars). (g–i): Photomicrographs of male albino rat's heart stained with haematoxylin and eosin (HE). (×400 = 50 μm). (a): Heart photomicrograph of the CD group. (b): Heart photomicrograph of the HFD group. (c): Heart photomicrograph of the HFDC group. Muscle fibers (MC), the intercellular spaces (S), vesicular nuclei (arrow), intercalated discs (I) (arrow head), damage of cardiac muscle fibers ( ), inflammatory cells (double arrows), separation of cardiac muscle fibers (stars), and extravasated red blood cells (thin arrow).

3.4.2. Histopathological Findings of the Duodenum. Microscopic examination of the duodenal sections of CD group (Figure 5(d)) revealed that the duodenum has the normal structure and is similar to all the other hollow organs of the gastrointestinal tract: mucosa, submucosa, muscularis, and serosa. Duodenal sections of the HF group (Figure 5(e)) revealed severe distortion of duodenal histoarchitecture; villi appeared with epithelial erosion and lamina propria infiltrated with inflammatory cells as well as degeneration of Brunner's glands and necrosis in the inner circular muscle fibers of musculosa. Massive amounts of adipose tissue around the duodenum were also observed. Co-treatment with curcumin showed significant improvements in the duodenal tissues of HFDC group (Figure 5(f)). The duodenal histoarchitecture of the HFDC group showed a good appearance versus to that of the duodenal HFD group, and the four layers of the duodenum displayed normal appearance to a large extent. However, degeneration and desquamation at the tips of some villi and necrosis in the inner circular muscle fibers of musculosa were discerned.

3.4.3. Histopathological Findings of the Heart. Microscopic investigations of the heart of the CD group (Figure 5(g)) revealed a normal myocardial structure; branching and anastomosing muscle fibers with centrally

located oval vesicular nuclei. Cardiac muscle cells appeared adherent to each other by intercalated discs that appeared as thin, typically dark-staining lines dividing adjacent cardiac muscle cells. Inspection of the (Figure 5(h)) revealed that histological examination of the HFD rat's myocardial tissue showed abnormality compared to the CD group. Rats fed on HFD showed a widespread myocardial structure and necrosis of cardiac muscle fibers. Also, extravasated red blood cells in between the muscle fibers and little inflammatory cellular infiltration were detected. Microscopical examination of the myocardial tissue sections of the HFDC group showed a cardioprotective effect of curcumin supplementation (Figure 5(i)). The same figure revealed near the normal architecture of myocardial muscle fibers with centrally located oval vesicular nuclei and intercalated discs. However, a few necrosis and separations in muscle fibers without inflammatory cells were detected.

4. Discussion

According to the World Health Organization, more than 1.6 billion people (aged 15 and over) are overweight. By 2030, 51% of the world's population is expected to be obese [37, 38]. To highlight the antioxidant and anti-inflammatory effects of curcumin against HFD-induced obesity and obesity-related multiorgan dysfunction using a rat model, some biochemical and immunological parameters along with some histological examinations of the liver, duodenum, and heart were assessed.

The results of the present study showed significantly higher serum levels of TAGs in the HFD group in comparison to the CD group. The increasing serum levels of TAGs observed in the present study could be attributed to the fact that in obesity, adipose tissue dysfunction will eventually lead to abnormalities in lipid metabolism, such as hypertriglyceridemia. Also, the primary dyslipidemia related to obesity is characterized by increased triglycerides, as previously reported by Abdelsadek [39]. The serum triglyceride levels in the HFDC group showed significantly decreased levels versus those of the HFD group. Our results were in agreement with previous studies [40–42] whose studies confirmed a significant effect of curcumin in reducing serum TG concentrations, suggesting the hypotriglyceridemic activity of curcumin. Also, Seo et al. [43] emphasized that curcumin significantly lowered the hepatic activities of fatty acid synthase, beta-oxidation, plasma FFA, cholesterol, and triglyceride concentrations. Similar conclusions were reported by Zhou et al. [44], who confirmed that the hypolipidemic effect of curcumin may depend on a balance between increased lipid mobilization from adipose tissue and increased lipid uptake and excretion by other tissues.

The present study showed significantly higher serum insulin and glucose levels in the HFD group compared to the control group. The present results coincide with several researchers who confirmed that oxidative stress and inflammation are the major components responsible for the pathogenesis of insulin resistance (IR) [45–47].

The present hyperinsulinemia could be attributed to the fact that insulin primarily increases the cellular uptake of glucose. During the development of IR, hepatocytes, adipocytes, and myocytes do not respond well to insulin. The β-cells of pancreatic islets increase insulin release sufficiently to overcome the reduced efficiency of insulin action to maintain normal glucose tolerance. Thus, people with IR also have hyperinsulinemia. As a result of IR, cellular uptake of glucose does not occur and the blood glucose level is elevated. The hyperglycemia displayed in the present study was in agreement with previous research studies [48].

Interestingly, coadministration of curcumin with a high-fat diet group exhibited significantly decreased serum insulin and glucose levels when compared with the HFD group. In parallel with our results, Hartogh et al. [49] reported that by lowering the harmful effects of liver fat and increasing cell sensitivity to insulin, curcuminoid can lower blood glucose levels in obese rats. The present results could be attributed to the ability of curcumin to reduce oxidative stress and inflammatory response which contributed to insulin resistance. Similarly, curcumin treatment attenuated glucose intolerance and boost insulin sensitizing response [50, 51].

In the present study, the HFD group showed significantly decreased hepatic GSH concentrations and SOD activities in the HFD group when compared with the CD group. These findings were supported by a previous research study that suggested that tissue antioxidant defenses in the HFD group may be reduced [39]. Also, our results were in accordance with Shen et al. [52] who concluded that obesity induced by high-a fat diet involved increased oxidative stress and decreased antioxidant capacity. Likewise, the lipid peroxidation induced by obesity displays a substantial decrease in the level of the main antioxidant enzymes like SOD, GPx, CAT, and GSH [53, 54].

The present study revealed a significant increase in the hepatic GSH and SOD activities in the HFDC group when compared with the HFD group. These results are in accordance with previous studies carried out by Panahi et al. [55] and Farzaei et al. [14], who observed an increase in GSH level and SOD, GPx, and CAT activities and a decrease in MDA level with curcumin treatment. Furthermore, curcumin administration caused strong induction of the antioxidant defenses, since SOD, CAT, and GSH-Px activities were significantly increased, reaching values similar to those of the control group [56, 57]. Curcumin's effects may act by either directly scavenging the reactive oxygen metabolites or due to the presence of various antioxidant principles such as flavonoids, steroids, tannins, glycosides, triterpenoids, and polyphenolic compounds [58–60].

In the present study, hepatic MPO of the HFD group showed significantly higher levels in comparison with the CD group. Parallel with these results, several studies reported that MPO was considered an early biomarker of inflammation and an obesity risk factor in obese individuals [61, 62].

In addition, our results were reinforced by Elgazar-Carmon et al. [63] and Wang et al. [64], who explained that neutrophils infiltrate adipose tissues in the early stage of HFD-induced obesity, promote macrophage infiltration,

and release various substances, including reactive oxygen species, TNF-α, and MPO, all of which have the capacity to induce inflammation.

In the current study, hepatic MPO of the HFDC group showed significantly lower levels as compared with the HFD group. These results were in agreement with those achieved by Fu et al. [50], who found that curcumin attenuated the infiltration of inflammatory cells and the activity of MPO. Also, our results are in line with Franck et al. [65], who demonstrated that curcumin is a reversible inhibitor of MPO by acting as an excellent electron donor in the peroxidase cycle of the enzyme.

During obesity, TLRs are essential as stimulants for metabolic inflammation and insulin resistance. TLRs, which are known to play a role in innate immunity, are also involved in the inflammatory reactions brought on by HFD. At the molecular level, activation of numerous signaling pathways caused by TLR stimulation leads to the release of proinflammatory cytokines, including IL-1β, IL-6, and TNF-α [66, 67].

In the current study, the HFD group exhibited significantly higher levels of TLR-4, IL-6 and TNF-α gene's expressions in adipose tissues (AT) when compared with the CD group. In the same context, the observations of Tramullas et al. [68] who reported that exposure to long-term high-fat diet induces both peripheral and central alterations in TLR-4 expression resulting in an increased level of proinflammatory cytokines. Also, others like Codoñer-Franch et al. and Heijden et al. reported that AT contains various cell types that all contribute to the inflammatory response results in local and systemic production of numerous soluble products as TNF-α, and IL-6 during obesity [69, 70].

The anti-inflammatory effects of curcumin form the basis of its potential clinical applications. In the present study, curcumin significantly reduces the inflammation state in HFDC group indicated by lower levels of TLR-4, IL-6, and TNF-α genes' expressions in AT in comparison with HFD group. These observations were confirmed by prior research studies [41, 71, 72]. Additionally, the present results were in accordance with Panahi et al. [55], who revealed that curcumin has been shown to block NF-κB translocation to the nucleus and decrease its DNA binding activity, thereby inhibiting the secretion of proinflammatory cytokines like IL-6 and TNF-α.

Curcumin may exert its anti-inflammatory effects through several signaling pathways that are associated with inflammation including the TLR-4 pathway via TLR-4 acting directly on receptor stimulation, by its downstream pathway, or by regulating target proteins in the inflammatory signaling TLR-4 pathway [73, 74].

Our data showed significantly increased DNA fragmentation in the liver homogenates of the HFD group compared to the CD group. Thus, our data agreed with the findings of Yuzefovych et al. [75] and Mu et al. [76], who found a positive association between HFD and DNA fragmentation that was reported in epidemiological studies. Also, this finding was in line with Mendes et al.'s findings [77] that HFD feeding dramatically increased cytoplasmic DNA fragmentation in the heart and liver tissues of HFD fed rats. The possible interpretation provided by Setayesh et al. [78] who emphasize that excess body fat causes DNA damage in multiple organs, including brain, liver, colon, and testes. Different molecular mechanisms may cause genetic instability in overweight/obese individuals.

Interestingly, the current investigation showed significantly decreased DNA fragmentation in liver homogenates of the HFDC group compared to the HFD group. This result was in agreement with many different studies that reported that curcumin compounds have been reported to induce antiproliferative and apoptotic effects. Curcumin is an excellent antioxidant agent and has an effective role in the regression of DNA damage [79, 80].

In the present study, the histopathological observations were done in the liver, duodenum, and heart of the HFD group. These findings were in parallel with van der Heijden et al. [70], Mahmoud et al. [74], and Avtanski et al. [81], who confirmed that the rats fed on a high-fat diet showed marked steatosis in a diffused manner all over the hepatocytes associated with focal necrosis and hepatocellular ballooning.

Additionally, the findings supported those of several researchers who found that HFD consumption resulted in decreased intestinal integrity, intestinal permeability, and histological abnormalities [82–84]. By producing much more ROS and proinflammatory cytokines, oxidative stress and inflammation can both affect the structure and function of the intestinal system, as suggested by Lan et al. [83].

Additionally, our results are in agreement with Chung et al. [85] who assessed the histopathology of the heart and showed significant structural alterations including disordered cardiac muscle fibers and deranged cellular structures in the HFD group.

Interestingly, the current study demonstrated that administration of curcumin to the HFD group provided protection against hepatic disorders, duodenal and myocardial histopathological changes as confirmed by these results are in line with those of many researchers who found a marked reduction in steatosis of hepatocytes and an improvement in liver histopathology [84, 86]. It is likely to postulate that the antioxidative property of curcumin is the key to its therapeutic effect on gastrointestinal injury as documented by many researchers [87–89]. Moreover, Gorabi et al. [90] revealed that high-fat diet plus curcumin showed no histopathological changes in the myocardial structure, indicating a preventive effect of curcumin against histological cardiac changes induced by a high-fat diet.

In general, the current work demonstrated the capacity of our experimental rat model to cause obesity's associated metabolic derangements as shown by biochemical, immunological, and histological alterations brought on by consuming a high-fat diet, which were associated with several microscopic changes in the liver, kidneys, and heart. There is no doubt that the use of curcumin improved the histological findings as well as modulated metabolic and oxidative stress markers, as well as downregulated inflammatory biomarkers and apoptosis. Therefore, it is advised that curcumin be evaluated as a possible supplemental therapy for metabolic diseases linked to obesity brought on by HFD.

Data Availability

The data used to support the findings of this study are available from the corresponding author upon request.

Ethical Approval

According to the manual for the care and use of laboratory animals, the Aswan University Animal Ethical Committee in Egypt approved the treatment of the animals and the experimental techniques used in this study were in accordance with the guidelines of the institutional animal care and use committee. The ethical approval code for the present study is ASW-Sci-ZOO-15-6-015 and the date of approval was January 2020.

Conflicts of Interest

The authors declare that they have no conflicts of interest.

References

[1] D. Albuquerque, C. Nobrega, L. Manco, and C. Padez, "The contribution of genetics and environment to obesity," *British Medical Bulletin*, vol. 123, no. 1, pp. 159–173, 2017.

[2] K. Amann and K. Benz, "Structural renal changes in obesity and diabetes," *Seminars in Nephrology*, vol. 33, no. 1, pp. 23–33, 2013.

[3] J. Liu, Z. He, N. Ma, and Z. Y. Chen, "Beneficial effects of dietary polyphenols on high-fatdiet-induced obesity linking with modulation of gut microbiota," *Journal of Agricultural and Food Chemistry*, vol. 68, no. 1, pp. 33–47, 2020.

[4] A. Wree, A. Kahraman, G. Gerken, and A. Canbay, "Obesity affects the liver-the link between adipocytes and hepatocytes," *Digestion*, vol. 83, no. 1-2, pp. 124–133, 2011.

[5] A. Vehapoglu, S. Turkmen, N. Goknar, and O. F. Ozer, "Reduced antioxidant capacity and increased subclinical inflammation markers in prepubescent obese children and their relationship with nutritional markers and metabolic parameters," *Redox Report*, vol. 21, no. 6, pp. 271–280, 2016.

[6] F. Zatterale, M. Longo, J. Naderi et al., "Chronic adipose tissue inflammation linking obesity to insulin resistance and type 2 diabetes," *Frontiers in Physiology*, vol. 10, p. 1607, 2019.

[7] G. Borgstahl and R. Oberley-Deegan, "Superoxide dismutases (SODs) and SOD mimetics," *Antioxidants*, vol. 7, no. 11, p. 156, 2018.

[8] I. Mirończuk-Chodakowska, A. M. Witkowska, and M. E. Zujko, "Endogenous non-enzymatic antioxidants in the human body," *Advances in Medical Sciences*, vol. 63, no. 1, pp. 68–78, 2018.

[9] G. S. Selders, A. E. Fetz, M. Z. Radic, and G. L. Bowlin, "An overview of the role of neutrophils in innate immunity, inflammation and host-biomaterial integration," *Regenerative Biomaterials*, vol. 4, no. 1, pp. 55–68, 2017.

[10] C. L. Hawkins and M. J. Davies, "Role of myeloperoxidase and oxidant formation in the extracellular environment in inflammation-induced tissue damage," *Free Radical Biology and Medicine*, vol. 172, pp. 633–651, 2021.

[11] M. A. Martínez-García, M. Ojeda-Ojeda, E. Rodriguez-Martin et al., "TLR2 and TLR4 surface and gene expression in white blood cells after fasting and oral glucose, lipid and protein challenges: influence of obesity and sex hormones," *Biomolecules*, vol. 10, no. 1, p. 111, 2020.

[12] M. Włodarczyk and G. Nowicka, "Obesity, DNA damage, and development of obesity-related diseases," *International Journal of Molecular Sciences*, vol. 20, no. 5, p. 1146, 2019.

[13] M. Zaki, W. Basha, H. T. El-Bassyouni, S. El-Toukhy, and T. Hussein, "Evaluation of DNA damage profile in obese women and its association to risk of metabolic syndrome, polycystic ovary syndrome and recurrent preeclampsia," *Genes & diseases*, vol. 5, no. 4, pp. 367–373, 2018.

[14] M. H. Farzaei, M. Zobeiri, F. Parvizi et al., "Curcumin in liver diseases: a systematic review of the cellular mechanisms of oxidative stress and clinical perspective," *Nutrients*, vol. 10, no. 7, p. 855, 2018.

[15] A. J. Ruby, G. Kuttan, K. Dinesh Babu, K. Rajasekharan, and R. Kuttan, "Anti-tumour and antioxidant activity of natural curcuminoids," *Cancer Letters*, vol. 94, no. 1, pp. 79–83, 1995.

[16] S. Sohaei, R. Amani, M. J. Tarrahi, and H. Ghasemi-Tehrani, "The effects of curcumin supplementation on glycemic status, lipid profile and hs-CRP levels in overweight/obese women with polycystic ovary syndrome: a randomized, double-blind, placebo-controlled clinical trial," *Complementary Therapies in Medicine*, vol. 47, Article ID 102201, 2019.

[17] S. C. Woods, R. J. Seeley, P. A. Rushing, D. D'Alessio, and P. Tso, "A controlled high-fat diet induces an obese syndrome in rats," *Journal of Nutrition*, vol. 133, no. 4, pp. 1081–1087, 2003.

[18] L. Ding, J. Li, B. Song et al., "Curcumin rescues high fat diet-induced obesity and insulin sensitivity in mice through regulating SREBP pathway," *Toxicology and Applied Pharmacology*, vol. 304, pp. 99–109, 2016.

[19] A. E.-K. M. Abd El-Kader, E. Awadalla, A. abdelsadik, and E. Seifeldin, "Therapeutic effects of curcumin against obesity and obesity induced renal pathology in experimental animal models," *Aswan University Journal of Environmental Studies*, vol. 2, pp. 270–279, 2021.

[20] R. Bravo, J. Cubero, L. Franco et al., "Body weight gain in rats by a high-fat diet produces chronodisruption in activity/inactivity circadian rhythm," *Chronobiology International*, vol. 31, no. 3, pp. 363–370, 2014.

[21] C. Marques, M. Meireles, S. Norberto et al., "High-fatdiet-induced obesity rat model: a comparison between wistar and sprague-dawley rat," *Adipocyte*, vol. 5, no. 1, pp. 11–21, 2016.

[22] T. Sasaki, "Effect of acetic acid concentration on the colour reaction in the O-toluidine boric acid method for blood glucose determination," *Rinsho Kagaku*, vol. 1, pp. 346–350, 1972.

[23] P. Fossati and L. Prencipe, "Serum triglycerides determined colorimetrically with an enzyme that produces hydrogen peroxide," *Clinical Chemistry*, vol. 28, no. 10, pp. 2077–2080, 1982.

[24] O. H. Lowry, N. Rosebrough, A. L. Farr, and R. Randall, "Protein measurement with the Folin phenol reagent," *Journal of Biological Chemistry*, vol. 193, no. 1, pp. 265–275, 1951.

[25] L. M. Hillegass, D. Griswold, B. Brickson, and C. Albrightson-Winslow, "Assessment of myeloperoxidase activity in whole rat kidney," *Journal of Pharmacological Methods*, vol. 24, no. 4, pp. 285–295, 1990.

[26] E. Beutler, O. Duron, and B. M. Kelly, "Improved method for the determination of blood glutathione," *The Journal of Laboratory and Clinical Medicine*, vol. 61, pp. 882–888, 1963.

[27] Z. Xie, L. Huang, B. Enkhjargal et al., "Recombinant netrin-1 binding UNC5B receptor attenuates neuroinflammation and brain injury via PPARγ/NFκB signaling pathway after subarachnoid hemorrhage in rats," *Brain, Behavior, and Immunity*, vol. 69, pp. 190–202, 2018.

[28] M. Nishikimi, N. Appaji Rao, and K. Yagi, "The occurrence of superoxide anion in the reaction of reduced phenazine methosulfate and molecular oxygen," *Biochemical and Biophysical Research Communications*, vol. 46, no. 2, pp. 849–854, 1972.

[29] L. S. Toni, A. M. Garcia, D. A. Jeffrey et al., "Optimization of phenol-chloroform RNA extraction," *MethodsX*, vol. 5, pp. 599–608, 2018.

[30] W. Rodenburg, J. Keijer, E. Kramer et al., "Salmonella induces prominent gene expression in the rat colon," *BMC Microbiology*, vol. 7, no. 1, pp. 84–16, 2007.

[31] M. W. Pfaffl, "Relative quantification," in *Real-time PCR*, pp. 89–108, Taylor & Francis, Abingdon, England, 2007.

[32] C. L. Roth, C. T. Elfers, D. P. Figlewicz et al., "Vitamin D deficiency in obese rats exacerbates nonalcoholic fatty liver disease and increases hepatic resistin and toll-like receptor activation," *Hepatology*, vol. 55, no. 4, pp. 1103–1111, 2012.

[33] N. A. Mohamed, M. H. Hassan, T. H. Saleem et al., "KIM-1 and GADDI-153 gene expression in paracetamol-induced acute kidney injury: effects of N-acetylcysteine, N-acetylmethionine, and N-acetylglucosamine," *Turkish Journal of Biochemistry*, vol. 47, 2021.

[34] K. S. Sellins and J. J. Cohen, "Gene induction by gamma-irradiation leads to DNA fragmentation in lymphocytes," *The Journal of Immunology*, vol. 139, no. 10, pp. 3199–3206, 1987.

[35] P. Jawaid, M. U. Rehman, Q. L. Zhao et al., "Helium-based cold atmospheric plasma-induced reactive oxygen species-mediated apoptotic pathway attenuated by platinum nanoparticles," *Journal of Cellular and Molecular Medicine*, vol. 20, no. 9, pp. 1737–1748, 2016.

[36] M. Gabe and M. Gabe, *Histological Techniques*, Springer, Berlin, Germany, 1976.

[37] P. Manna and S. K. Jain, "Obesity, oxidative stress, adipose tissue dysfunction, and the associated health risks: causes and therapeutic strategies," *Metabolic Syndrome and Related Disorders*, vol. 13, no. 10, pp. 423–444, 2015.

[38] T. Kelly, W. Yang, C. S. Chen, K. Reynolds, and J. He, "Global burden of obesity in 2005 and projections to 2030," *International Journal of Obesity*, vol. 32, no. 9, pp. 1431–1437, 2008.

[39] A. Abdelsadik, "High-fat diet modifies cytokine gene expression and exacerbates the effects of acute pancreatitis in the liver of rats," *Journal of Basic and Clinical Physiology and Pharmacology*, vol. 29, no. 6, pp. 651–658, 2018.

[40] A. F. G. Cicero, A. Sahebkar, F. Fogacci, M. Bove, M. Giovannini, and C. Borghi, "Effects of phytosomal curcumin on anthropometric parameters, insulin resistance, cortisolemia and non-alcoholic fatty liver disease indices: a double-blind, placebo-controlled clinical trial," *European Journal of Nutrition*, vol. 59, no. 2, pp. 477–483, 2020.

[41] D. Feng, J. Zou, D. Su et al., "Curcumin prevents high-fatdiet-induced hepatic steatosis in ApoE−/− mice by improving intestinal barrier function and reducing endotoxin and liver TLR4/NF-κB inflammation," *Nutrition and Metabolism*, vol. 16, no. 1, pp. 79–11, 2019.

[42] L. Zeng, T. Yang, K. Yang et al., "Efficacy and safety of curcumin and curcuma longa extract in the treatment of arthritis: a systematic review and meta-analysis of randomized controlled trial," *Frontiers in Immunology*, vol. 13, Article ID 891822, 2022.

[43] K. I. Seo, M. S. Choi, U. J. Jung et al., "Effect of curcumin supplementation on blood glucose, plasma insulin, and glucose homeostasis related enzyme activities in diabetic db/db mice," *Molecular Nutrition & Food Research*, vol. 52, no. 9, pp. 995–1004, 2008.

[44] H. Zhou, C. S Beevers, and S. Huang, "The targets of curcumin," *Current Drug Targets*, vol. 12, no. 3, pp. 332–347, 2011.

[45] M. I. Eissa, M. A. El-Sherbiny, A. M. Ibrahim, A. Abdelsadik, M. M. Mohamed, and M. S. El-Halawany, "Biochemical and histopathological studies on female and male wistar rats fed on genetically modified soybean meals (roundup ready)," *The Journal of Basic and Applied Zoology*, vol. 80, no. 1, pp. 54–12, 2019.

[46] A. Abdelsadik and M. M. Amin, "Low-dose aspirin improves glucose uptake and attenuates inflammation in rats fed high-fat diet," *Egyptian Pharmaceutical Journal*, vol. 17, no. 3, p. 171, 2018.

[47] V. Jayakumar, S. S. S. J. Ahmed, and K. K. Ebenezar, "Multivariate analysis and molecular interaction of curcumin with PPARγ in high fructose diet induced insulin resistance in rats," *Springer Plus*, vol. 5, no. 1, pp. 1732–1815, 2016.

[48] A. M. Freeman and N. Pennings, *Insulin Resistance*, StatPearls Publishing, Treasure Island, FL, USA, 2022.

[49] D. J. D. Hartogh, A. Gabriel, and E. Tsiani, "Antidiabetic properties of curcumin I: evidence from in vitro studies," *Nutrients*, vol. 12, no. 1, p. 118, 2020.

[50] Y. Fu, R. Gao, Y. Cao et al., "Curcumin attenuates inflammatory responses by suppressing TLR4-mediated NF-κB signaling pathway in lipopolysaccharide-induced mastitis in mice," *International Immunopharmacology*, vol. 20, no. 1, pp. 54–58, 2014.

[51] L. X. Na, Y. L. Zhang, Y. Li et al., "Curcumin improves insulin resistance in skeletal muscle of rats," *Nutrition, Metabolism, and Cardiovascular Diseases*, vol. 21, no. 7, pp. 526–533, 2011.

[52] X. Shen, W. Cai, Q. Tang, and Y. Feng, "Oxidative stress in a rat model of dietary-induced obesity," *Wei Sheng Yan Jiu = Journal of Hygiene Research*, vol. 36, no. 4, pp. 440–442, 2007.

[53] S. Sfar, R. Boussoffara, M. T. Sfar, and A. Kerkeni, "Antioxidant enzymes activities in obese Tunisian children," *Nutrition Journal*, vol. 12, no. 1, pp. 18–27, 2013.

[54] K. Ulrich and U. Jakob, "The role of thiols in antioxidant systems," *Free Radical Biology and Medicine*, vol. 140, pp. 14–27, 2019.

[55] Y. Panahi, N. Khalili, M. S. Hosseini, M. Abbasinazari, and A. Sahebkar, "Lipid-modifying effects of adjunctive therapy with curcuminoids-piperine combination in patients with metabolic syndrome: results of a randomized controlled trial," *Complementary Therapies in Medicine*, vol. 22, no. 5, pp. 851–857, 2014.

[56] M. C. Costa, T. F. O. Lima, C. A. Arcaro et al., "Trigonelline and curcumin alone, but not in combination, counteract oxidative stress and inflammation and increase glycation product detoxification in the liver and kidney of mice with high-fatdiet-induced obesity," *The Journal of Nutritional Biochemistry*, vol. 76, Article ID 108303, 2020.

[57] P. S. Rao, M. Farheen, and P. V. Diwan, "Alloxan induced diabetes and impairment of oxidative defense system in rat pancreas: protective effect of actinopteris dichotoma," *International Journal of Ayurvedic and Herbal Medicine*, vol. 12, 2018.

[58] S. J. Hewlings and D. S. Kalman, "Curcumin: a review of its effects on human health," *Foods*, vol. 6, no. 10, p. 92, 2017.

[59] B. M. Moukette, C. A. Pieme, J. R. Njimou, C. P. N. Biapa, B. Marco, and J. Y. Ngogang, "In vitro antioxidant properties, free radicals scavenging activities of extracts and polyphenol

composition of a non-timber forest product used as spice: *Monodora myristica*," *Biological Research*, vol. 48, no. 1, pp. 15–17, 2015.

[60] R. Tabrizi, S. Vakili, M. Akbari et al., "The effects of curcumin-containing supplements on biomarkers of inflammation and oxidative stress: a systematic review and meta-analysis of randomized controlled trials," *Phytotherapy Research*, vol. 33, no. 2, pp. 253–262, 2019.

[61] R. Parsanathan and S. K. Jain, "Glutathione deficiency induces epigenetic alterations of vitamin D metabolism genes in the livers of high-fatdiet-fed obese mice," *Scientific Reports*, vol. 9, no. 1, Article ID 14811, pages 14784, 2019.

[62] R. Xu, H. Huang, Z. Zhang, and F. S. Wang, "The role of neutrophils in the development of liver diseases," *Cellular and Molecular Immunology*, vol. 11, no. 3, pp. 224–231, 2014.

[63] V. Elgazar-Carmon, A. Rudich, N. Hadad, and R. Levy, "Neutrophils transiently infiltrate intra-abdominal fat early in the course of high-fat feeding," *The Journal of Lipid Research*, vol. 49, no. 9, pp. 1894–1903, 2008.

[64] Q. Wang, Z. Xie, W. Zhang et al., "Myeloperoxidase deletion prevents high-fatdiet-induced obesity and insulin resistance," *Diabetes*, vol. 63, no. 12, pp. 4172–4185, 2014.

[65] T. Franck, I. Aldib, K. Zouaoui Boudjeltia et al., "The soluble curcumin derivative NDS27 inhibits superoxide anion production by neutrophils and acts as substrate and reversible inhibitor of myeloperoxidase," *Chemico-Biological Interactions*, vol. 297, pp. 34–43, 2019.

[66] A. Abdelsadik and A. Trad, "Toll-like receptors on the fork roads between innate and adaptive immunity," *Human Immunology*, vol. 72, no. 12, pp. 1188–1193, 2011.

[67] Y. Benomar and M. Taouis, "Molecular mechanisms underlying obesity-induced hypothalamic inflammation and insulin resistance: pivotal role of resistin/TLR4 pathways," *Frontiers in Endocrinology*, vol. 10, p. 140, 2019.

[68] M. Tramullas, B. C. Finger, T. G. Dinan, and J. F. Cryan, "Obesity takes its toll on visceral pain: high-fat diet induces toll-like receptor 4-dependent visceral hypersensitivity," *PLoS One*, vol. 11, no. 5, Article ID e0155367, 2016.

[69] P. Codoñer-Franch, V. Valls-Belles, A. Arilla-Codoner, and E. Alonso-Iglesias, "Oxidant mechanisms in childhood obesity: the link between inflammation and oxidative stress," *Translational Research*, vol. 158, no. 6, pp. 369–384, 2011.

[70] R. A. Heijden, F. Sheedfar, M. C. Morrison et al., "High-fat diet induced obesity primes inflammation in adipose tissue prior to liver in C57BL/6j mice," *Aging*, vol. 7, no. 4, pp. 256–268, 2015.

[71] M. Boozari, A. E. Butler, and A. Sahebkar, "Impact of curcumin on toll-like receptors," *Journal of Cellular Physiology*, vol. 234, no. 8, pp. 12471–12482, 2019.

[72] T. Islam, I. Koboziev, S. Scoggin, L. Ramalingam, and N. Moustaid-Moussa, "Protective effects of curcumin in high fat diet (HFD)-induced obesity include anti-inflammatory effects in adipose tissue and changes in gut microbiome (P06-075-19)," *Current Developments in Nutrition*, vol. 3, no. 1, pp. nzz031–P06, 2019.

[73] H. D. Nguyen, "Two new triterpenoid saponins from the underground parts of Weigela x "Bristol Ruby"/NLRP3/Caspase-1/IL1B, TLR4/NF-κB pathways, and tau hyperphosphorylation Induced by 1, 2-diacetyl benzene: an in vitro and in silico study," *Journal of Asian Natural Products Research*, vol. 1–7, 2022.

[74] A. M. Mahmouda, N. R. A. El-Hagag, H. El-Bitar, and A. H. Afifi, "Potential protective effect of curcumin in high-fatdiet-induced nonalcoholic fatty liver disease in rats," *Journal of Current Medical Research and Practice*, vol. 6, no. 1, p. 92, 2021.

[75] L. V. Yuzefovych, S. I. Musiyenko, G. L. Wilson, and L. I. Rachek, "Mitochondrial DNA damage and dysfunction, and oxidative stress are associated with endoplasmic reticulum stress, protein degradation and apoptosis in high fat diet-induced insulin resistance mice," *PLoS One*, vol. 8, no. 1, Article ID e54059, 2013.

[76] Y. Mu, T. Yin, Y. Zhang, J. Yang, and Y. Wu, "Diet-induced obesity impairs spermatogenesis: the critical role of NLRP3 in sertoli cells," *Inflammation and Regeneration*, vol. 42, no. 1, pp. 24–18, 2022.

[77] N. P. Mendes, P. V. M. Ribeiro, and R. C. G. Alfenas, "Does dietary fat affect advanced glycation end products and their receptors? a systematic review of clinical trials," *Nutrition Reviews*, vol. 80, no. 3, pp. 598–612, 2022.

[78] T. Setayesh, A. Nersesyan, M. Misik et al., "Impact of obesity and overweight on DNA stability: few facts and many hypotheses," *Mutation Research/Reviews in Mutation Research*, vol. 777, pp. 64–91, 2018.

[79] A. J. Abadi, S. Mirzaei, M. K. Mahabady et al., "Curcumin and its derivatives in cancer therapy: potentiating antitumor activity of cisplatin and reducing side effects," *Phytotherapy Research*, vol. 36, no. 1, pp. 189–213, 2022.

[80] A. Acar, D. Singh, and A. K. Srivastava, "Assessment of the ameliorative effect of curcumin on pendimethalin-induced genetic and biochemical toxicity," *Scientific Reports*, vol. 12, no. 1, pp. 2195–2216, 2022.

[81] D. Avtanski, V. A. Pavlov, K. J. Tracey, and L. Poretsky, "Characterization of inflammation and insulin resistance in high-fat diet-induced male C57BL/6J mouse model of obesity," *Animal models and experimental medicine*, vol. 2, no. 4, pp. 252–258, 2019.

[82] N. Arias-Jayo, L. Abecia, L. Alonso-Saez, A. Ramirez-Garcia, A. Rodriguez, and M. A. Pardo, "High-fat diet consumption induces microbiota dysbiosis and intestinal inflammation in zebrafish," *Microbial Ecology*, vol. 76, no. 4, pp. 1089–1101, 2018.

[83] R. Lan, Q. Chang, L. Wei, and Z. Zhao, "The protect effects of chitosan oligosaccharides on intestinal integrity by regulating oxidative status and inflammation under oxidative stress," *Marine Drugs*, vol. 19, no. 2, p. 57, 2021.

[84] N. J. Zhao, M. J. Liao, J. J. Wu, and K. X. Chu, "Curcumin suppresses Notch-1 signaling: improvements in fatty liver and insulin resistance in rats," *Molecular Medicine Reports*, vol. 17, no. 1, pp. 819–826, 2018.

[85] A. P. Y. S. Chung, S. Gurtu, S. Chakravarthi, M. Moorthy, and U. D. Palanisamy, "Geraniin protects high-fatdiet-induced oxidative stress in sprague dawley rats," *Frontiers in Nutrition*, vol. 5, p. 17, 2018.

[86] Y. Panahi, Y. Ahmadi, M. Teymouri, T. P. Johnston, and A. Sahebkar, "Curcumin as a potential candidate for treating hyperlipidemia: a review of cellular and metabolic mechanisms," *Journal of Cellular Physiology*, vol. 233, no. 1, pp. 141–152, 2018.

[87] K. Burge, A. Gunasekaran, J. Eckert, and H. Chaaban, "Curcumin and intestinal inflammatory diseases: molecular mechanisms of protection," *International Journal of Molecular Sciences*, vol. 20, no. 8, p. 1912, 2019.

[88] A. Limaye, R. C. Yu, C. C. Chou, J. R. Liu, and K. C. Cheng, "Protective and detoxifying effects conferred by dietary selenium and curcumin against AFB1-mediated toxicity in livestock: a review," *Toxins*, vol. 10, no. 1, p. 25, 2018.

[89] S. Prasad, D. DuBourdieu, A. Srivastava, P. Kumar, and R. Lall, "Metal-curcumin complexes in therapeutics: an approach to enhance pharmacological effects of curcumin," *International Journal of Molecular Sciences*, vol. 22, no. 13, p. 7094, 2021.

[90] A. M. Gorabi, S. Hajighasemi, N. Kiaie et al., "Anti-fibrotic effects of curcumin and some of its analogues in the heart," *Heart Failure Reviews*, vol. 25, no. 5, pp. 731–743, 2020.

[91] M. N. Bari, U. Saleem, M. N. Faisal et al., "Anti-hyperglycemic efficacy of Derris ovalifolia in alloxan-induced diabetic wister rats," *Pakistan Veterinary Journal*, vol. 40, no. 1, 2020.

Hindawi
Evidence-Based Complementary and Alternative Medicine
Volume 2022, Article ID 7127037, 13 pages
https://doi.org/10.1155/2022/7127037

Research Article

Crocus sativus L. Stigmas, Tepals, and Leaves Ameliorate Gentamicin-Induced Renal Toxicity: A Biochemical and Histopathological Study

Sabir Ouahhoud,[1] Noureddine Bencheikh,[1] Amine Khoulati,[1] Salma Kadda,[2] Samira Mamri,[1] Anas Ziani,[1] Sanae Baddaoui,[1] Fatima-Ezzahra Eddabbeh,[1] Soufiane Elassri,[3] Iliass Lahmass,[4] Redouane Benabbes,[1] Mohamed Addi,[2] Christophe Hano,[5] Mohammed Choukri,[3] Amal Bennani,[3] Abdeslam Asehraou,[1] and Ennouamane Saalaoui[1]

[1]*Laboratory of Bioresources, Biotechnology, Ethnopharmacology and Health, Faculty of Sciences, Université Mohamed Premier, Oujda 60000, Morocco*
[2]*Laboratory of Improvement of Agricultural Production, Biotechnology, and Environment, Department of Biology, Faculty of Sciences, Université Mohamed Premier, Oujda 60000, Morocco*
[3]*Central Laboratory Service - CHU, Mohammed VI, Faculty of Medicine and Pharmacy, University Mohamed Premier, Oujda 60000, Morocco*
[4]*Laboratory of Biotechnology, Environment, Agri-food and Health, Faculty of Science Dhar Mahraz, Sidi Mohamed Ben Abdallah University, Fez 1796, Morocco*
[5]*Laboratoire de Biologie des Ligneux et des Grandes Cultures, INRA USC1328, Orleans University, CEDEX 2, Orléans 45067, France*

Correspondence should be addressed to Christophe Hano; hano@univ-orleans.fr

Received 2 June 2022; Revised 10 August 2022; Accepted 28 August 2022; Published 1 October 2022

Academic Editor: Salah M. El Sayed

The most costly spice in the world, *Crocus sativus* L. (*C. sativus*), has been used for more than 3,000 years. It has various beneficial applications in a range of fields, including aromas, colorants, and medications, but its usefulness as a food flavoring and coloring ingredient is the highest. Large quantities of by-products from the processing of saffron are typically thrown as unwanted bio-residues. This study's goal was to assess and compare the nephroprotective effects of hydroethanolic extracts of *C. sativus* stigmas, tepals, and leaves on gentamicin (GM)-induced nephrotoxicity in rats. For that, we used a biochemical and histological investigation to propose new pharmaceutical valorizations. Based on the biochemical and histological analyses, it is concluded that all the studied parts of *C sativus* showed a renoprotective effect. Markedly, tepals revealed the most significant reduction of relative liver weight ($p < 0.05$), water intake ($p < 0.05$), plasma creatinine ($p < 0.01$), plasma urea ($p < 0.01$), plasma uric acid ($p < 0.05$), urinary protein ($p < 0.01$) and albumin ($p < 0.001$), and renal malondialdehyde (MDA) ($p < 0.001$). In addition, *C. sativus* tepals caused a significant increase in body weight ($p < 0.05$), urinary creatinine ($p < 0.01$), creatinine clearance ($p < 0.05$), and urinary urea ($p < 0.05$) compared with the gentamicin untreated (GM) group. This is confirmed by the histopathological study which shows that treatment with stigmas, tepals, and leaves preserved kidney morphology at the glomerular and tubular cell level. The studied extracts exhibit good recovery potential for nephrotoxicity induced by gentamicin. In order to create potent dietary supplements or phytomedicines, it would also be very interesting to confirm these actions through clinical research.

1. Introduction

Since more than 3000 years ago, saffron has been used as a spice. It is a part of the Iridaceae family and the *Crocus* genus, which has roughly 80 species. Saffron, the priciest spice in the world is mainly found in the Mediterranean and Southwest Asia [1]. Since ancient times, saffron has been used in many fields, including cosmetics, colorants, and medicines, although it is most commonly employed as a food flavoring and coloring ingredient [2]. Recent research have revealed the antioxidant [3], antitumor [4], antigenotoxic [5], antidiabetic [6], hepatoprotective [7, 8], and nephroprotective [9] properties of saffron stigma. Large volumes of by-products from the manufacture of saffron are typically thrown as unwanted bio-residues [10]. In order to get just 1 kg of the dry stigmas, approximately 63 kg of flowers, 1500 kg of leaves, and hundreds of defective or undersized bulbs are destroyed [11]. The profitability and sustainability of saffron production would significantly boost with the usage of these bioactive substances discovered in this organic waste [11]. A common antibiotic known as an aminoglycoside called gentamicin is used to treat severe infections brought on by aerobic bacteria [12]. One of the most significant side effects of aminoglycoside antibiotics, which can occur in 10–20% of patients, is renal impairment [13, 14]. Researchers have reported that aminoglycosides are antibiotics capable of causing nephrotoxicity by producing oxidative stress [15, 16]. This study's goal was to assess and compare the nephroprotective effects of extracts of *C. sativus* from the Moroccan Taliouine region on rat which the nephrotoxicity caused by gentamicin (GM). We performed a biochemical and histological investigation to offer novel valorizations, particularly in the pharmaceutical industry.

2. Materials and Methods

2.1. Chemicals. All of the chemicals utilized in this study were analytical-grade materials that were provided by Sigma Chemicals (MA, USA).

2.2. Plant Material. The *C. sativus* plant's stigmas, tepals, and leaves were gathered at a farm near Taliouine (30°31′54″ north, 7° 55′ 25″ west, Southern Morocco). Saffron was grown naturally in this area without the use of chemicals. The plant's various components were gathered between October and November of 2016. Botanical professor Fennane Mohammed of the Scientific Institute of Rabat, Morocco, determined the plant's botanical classification. Under the voucher code HUMPOM210, three species of the plant have been identified in the herbarium of the University Mohammed First in Oujda, Morocco.

2.3. Plant Material Preparation. Preparation of the plant material was done using the technique outlined by Ouahhoud et al. [8]. First, the stigmas and various *C. sativus* components were manually separated. The stigmas were indeed dried in an oven for four hours at 37°C. Tepals and leaves were dried in an oven for 24 hours each at 37°C. An electric mill was then used to grind the dry plant material.

2.4. Making Hydroethanolic Saffron Extracts. According to our early research, 80% ethanol was the solvent with the best biological characteristics [6, 8]. The Ouahhoud et al. [6] procedure is the one that is in use for this study. For 24 hours, stirring was done at ambient temperature and in the darkness, while the vegetable material was macerated in an 80/20 (v/v) ethanol/water mixture. The extraction ratio was 2 g of plant powder to 50 ml of solvent. The solvent was then filtered (0.45 m) after the first extraction, and the marc was collected for the subsequent extraction. Following three further iterations of this procedure, a rotary evaporator (at 40°C) was used to dry the entire extract phase.

2.5. Animals. Male Wistar rats those were nine-week-old and weighed 200–250 g were kept in the animal house of the Biology Department at the Faculty of Sciences in Oujda, Morocco, where they were subjected to a 12-hour light/dark cycle. Water and food were freely available to the rats [8].

2.6. Ethical Approval. The Faculty of Sciences, University Mohammed Premier, Oujda (01/21-LBBEH-04 and 15 March, 2021) approved the study, which was carried out in accordance with the US National Institutes of Health's recommendations. All of the animal experiments that were conducted during this investigation complied with the globally recognized manual for the handling and use of laboratory animals.

2.7. Plant Extracts Administration. The dry extracts (hydroethanolic) of the by-products of *C. sativus* are dissolved in distilled water. The administration of the stigma (STG), tepal (TPL), and leaf (LV) extract is performed orally using an intragastric tube for rats. The concentrations that would be employed were selected based on our preliminary research carried out in our laboratory [6, 8].

2.8. Animal Distribution and Experimental Protocol. Thirty male rats (nine-week-old, weight 200–250 g) were randomly divided into 5 groups of 5 rats which are as follows: N Group: normal control rats received daily, by intraperitoneal injection, physiological water and 1 hour later, by gavage, distilled water for 14 days of the study; GM group: intoxicated control rats receiving daily, by intraperitoneal injection, 80 mg/kg of gentamicin and 1 hour later, by gavage, distilled water for 14 days; STG group: intoxicated control rats receiving daily, intraperitoneally 80 mg/kg of gentamicin, and 1 hour later, orally, 50 mg/kg of the hydroethanolic extract of the stigmas for 14 days; TPL group: intoxicated control rats receiving daily, intraperitoneally 80 mg/kg of gentamicin, and 1 hour later, orally, 250 mg/kg of the hydroethanolic extract of tepals for 14 days; and LV group: intoxicated control rats receiving daily, intraperitoneally 80 mg/kg of gentamicin, and 1 hour

later, orally, 250 mg/kg of the hydroethanolic extract of the leaves for 14 days. Urine was collected using metabolic cages for a full 24 hours after the treatment was finished. Both before and after the trial, the animals are weighed. The rats underwent pentobarbital anesthesia after receiving the therapy for 14 days. Blood is drawn from the abdominal aorta into heparin-filled tubes. The samples were then centrifuged for 10 min at 3000 rpm. The plasma was recovered and stored at −20°C for biochemical tests. The right kidney was then removed, rinsed with physiological water (NaCl 0.9%), and weighed. Finally, it was stored at −20°C for malondialdehyde (MDA) determination. The left kidney is rinsed with physiological water (0.9% NaCl), weighed, and stored in 10% formalin (fixation) for histological study.

2.9. Relative Kidney Weight. The following formula was used to determine the relative kidney weight:

$$\text{Relative weight of the kidneys}\,(\%) = \frac{\text{Absolute kidney weight}\,(g)X100}{\text{Body weight of the rat}\,(g)}. \quad (1).$$

2.10. Histological Analysis. The purpose of this histological analysis (stained with hematoxylin and eosin) is to explore the structure of the renal tissue, the constitutive and functional relationships between their functional elements, and the turnover of the tissue. It is performed in several steps according to the protocol described by Hewitson and Darby [17].

2.11. Biochemical Tests Performed. In this study, the authors determined creatinine, urea, uric acid, and electrolyte (Na+, K+, and Cl−) plasma levels. Also, the urinary levels of creatinine, total protein, albumin, and uric acid were measured, and the creatinine clearance was calculated. Biochemical analysis was realized on a COBAS INTEGRA autoanalyzer (Roche Diagnostics) at the Mohammed VI Hospital in Oujda.

2.12. Creatinine Clearance. Based on plasma and urine creatinine concentrations, the following formula was used to determine creatinine clearance in order to evaluate the glomerular filtration rate:

$$\text{Creatinine clearance}\left(\frac{ml}{\min Xkg}\right) = \frac{\text{Urine creatinine}\,(mg/ml)X\ \text{Urine flow rate}\,(ml/\min)X1000}{\text{Plasma creatinine}\,(mg/ml)X\ \text{rat weight}\,(kg)}. \quad (2)$$

The urine flow rate was calculated using the following formula:

$$\text{Urine flow rate}\left(\frac{ml}{\min}\right) = \frac{\text{urine volume value}\,(24h)}{1440\,(60\min X24h = 1440)}. \quad (3)$$

2.13. Malondialdehyde (MDA) Determination. A method developed by Ouahhoud et al. was used to measure lipid peroxidation [8]. For this, 0.5 g of the kidney was homogenized in a Potter tube with 5 ml of PBS (pH 7.4) at 0°C (ice). After that, the homogenate was centrifuged for 15 minutes at 14500 rpm. 2 ml of reagent (consisting of 0.375% TBA (thiobarbituric acid) and 15% TCA (trichloroacetic acid) that were dissolved in 0.25 N hydrochloric acid) were added with one milliliter of supernatant. The mixture was centrifuged at 4750 rpm for 5 minutes after being boiled in water for 30 minutes. The supernatant's absorbance was calculated at 535 nm. The amount of MDA is determined using the molar extinction coefficient of MDA ($\varepsilon = 1.56 \times 10^5 M^{-1} cm^{-1}$). Values were expressed as nmol of MDA per mg of the tissue.

2.14. The Qualitative Analysis of C. sativus Extract. The hydroethanolic extracts from *C sativus* was analyzed by high-performance liquid chromatography (Waters AllianceTM e2695 XC HPLC system outfitted with a 2998 Photodiode Array Detector. Samples (10 mg/ml) were injected onto a reversed-phase C18 column (5 μm, 250 mm × 4.6 mm) at a flow rate of 1 mL/min. The following gradient of binary solvents (2% of acetic acid in water (solvent A) and methanol (solvent B)) was used for elution: initial 80% A and 20% B; 20 min 100% B; 25 min 100% B; 30 min 50% A and 50% B; 35 min 80% A and 20% B. The UV detection was carried out in the 220–575 nm range with an injection volume of 20 L. By comparing the retention period and maximum wavelength with reference materials and standards, the active compounds were found.

2.15. Statistical Analysis. With $n = 5$ for each group, the data were presented as mean SEM. The results of the data's normality test showed that all of the data had a normal distribution. One-way ANOVA was used to statistically analyze using the GraphPad Prism 5.0 program. With significant levels of $p < 0.05$, $p < 0.01$ and $p < 0.001$, Tukey's multiple comparison posttest was used to examine differences between the treatment groups.

3. Results

3.1. The Effect of Gentamicin and Extracts of Different Parts of C. sativus on Renal Histology. Figure 1 shows the effect of extracts from different parts of *C. sativus* on the histological changes of the kidney (A, B, C, D, and E) in gentamicin-intoxicated rats.

3.2. The Effect of Gentamicin and C. sativus Extracts on Body Weight and Relative Kidney Weight. The effects of hydroethanolic extracts of the stigmas, tepals, and leaves of *C. sativus* on gaining weight and relative kidney weight in rats with gentamicin nephrotoxicity are shown in Figures 2(a) and 2(b). In comparison to normal rats, the daily injection of gentamicin (80 mg/kg) caused a considerable drop in body weight ($p < 0.001$). However, daily administration of stigma, tepal, and leaf extracts significantly ($p < 0.05$) protected gentamicin-intoxicated rats against weight loss compared to untreated rats (GM group). Rats given GM showed a significant increase in relative kidney weight ($p < 0.01$) as compared to control rats. Rats given tepal extract treatment had a significant lower in relative kidney weight ($p < 0.05$) than the GM group. However, there was no discernible decrease in relative kidney weight between the GM group, stigma, and leaf extracts.

3.3. The Effect of Gentamicin and C. sativus Extracts on Water Intake and Urine Volume. Figure 3 shows the effect of hydroethanolic extracts of some *C. sativus*by-products on water intake and urine volume in gentamicin-intoxicated rats. The gentamicin-treated group showed a significant increase in water intake ($p < 0.001$) and urine volume ($p < 0.01$) compared with the normal group. Administration of the stigma and tepal extracts significantly ($p < 0.05$) decreased water intake compared to gentamicin-intoxicated rats (GM group). However, compared to the GM group, administration of the leaf extract had no discernible impact on the group's water consumption. In comparison to the GM group, the administration of the stigma, tepal, and leaf extracts had no significant influence on the urine volume.

3.4. The Effect of Gentamicin and C. sativus on Plasma Creatinine, Urinary Creatinine, and Clearance. Figures 4(a), 4(b), and 4(c) show the variation in plasma and urine creatinine levels and creatinine clearance in gentamicin-intoxicated rats treated with the stigma, tepal, and leaf extracts. The findings show that daily gentamicin injection significantly increased plasma creatinine ($p < 0.001$) and significantly decreased urine creatinine clearance ($p < 0.001$) in comparison to normal rats. Daily administration of stigma, tepal, and leaf extracts significantly ($p < 0.05$, $p < 0.01$, and $p < 0.05$, respectively) protected gentamicin-intoxicated rats against the increase in the plasma creatinine level compared to untreated rats (GM group). In addition, the STG and TPL-treated groups showed a significant increase in the urinary creatinine level compared to the GM group. The TPL-treated group showed significant prevention against the decrease in creatinine clearance. But the rats treated with STG and LV revealed no significant effect on clearance compared to the GM group.

3.5. The Effect of Gentamicin and C. sativus Extracts on Plasma and Urinary Urea. Figures 5(a) and 5(b) represent the variation of plasma and urinary urea levels in gentamicin-intoxicated rats treated with stigma, tepal, and leaf extracts. Rats intoxicated by gentamicin showed a significant ($p < 0.001$) increase in the plasma urea level and a significant ($p < 0.001$) decrease in the urine urea level compared to the normal group. However, STG and TPL treatment significantly reduced the plasma urea level ($p < 0.05$ and $p < 0.01$, respectively) compared with the GM group. LV treatment showed no significant effect on plasma urea levels compared with the GM group. LV administration significantly ($p < 0.05$) increased the urinary urea level compared with the GM group. But administration of STG and LV showed no significant effect compared with the GM group.

3.6. The Effect of Gentamicin and C. sativus Extracts on Plasma and Urinary Uric Acid. Figures 6(a) and 6(b) examine the change in plasma and urinary uric acid levels in gentamicin-intoxicated rats treated with STG, TPL, and LV. Gentamicin treatment of rats caused a significant increase in the plasma uric acid level ($p < 0.01$) and a significant decrease in the urinary uric acid level ($p < 0.01$) compared with healthy rats. Administration of STG, TPL, and LV significantly reduced the plasma uric acid level ($p < 0.05$) compared with the GM group. In contrast, treatment with STG, TPL, and LV did not significantly reduce urinary uric acid levels compared with the GM group.

3.7. The Effect of Gentamicin and C. sativus Extracts on Urinary Protein and Albumin. The effect of STG, TPL, and LV on urinary protein and albumin levels in rats treated with gentamicin is shown in Figures 7(a) and 7(b). Gentamicin caused a significant increase in urinary protein and albumin levels ($p < 0.01$ and $p < 0.001$, respectively) compared with healthy rats. Administration of STG, TPL, and LV significantly protected against elevation in urinary protein ($p < 0.05$, $p < 0.01$, and $p < 0.05$, respectively) and albumin ($p < 0.001$) levels compared with the GM group.

3.8. The Effect of Gentamicin and C. sativus Extracts on Plasma Electrolytes (Na^+, K^+, and Cl^-). The effect of STG, TPL, and LV on plasma sodium, potassium, and chlorine levels in gentamicin-treated rats is shown in Figures 8(a), 8(b), and 8(c). Daily injection for 14 days of gentamicin caused a significant increase in plasma potassium levels ($p < 0.05$) compared with normal rats. Gentamicin treatment did not significantly influence plasma sodium and chlorine levels compared with the GM group. The administration of STG, TPL, and LV did not significantly influence plasma electrolyte levels compared with the GM group.

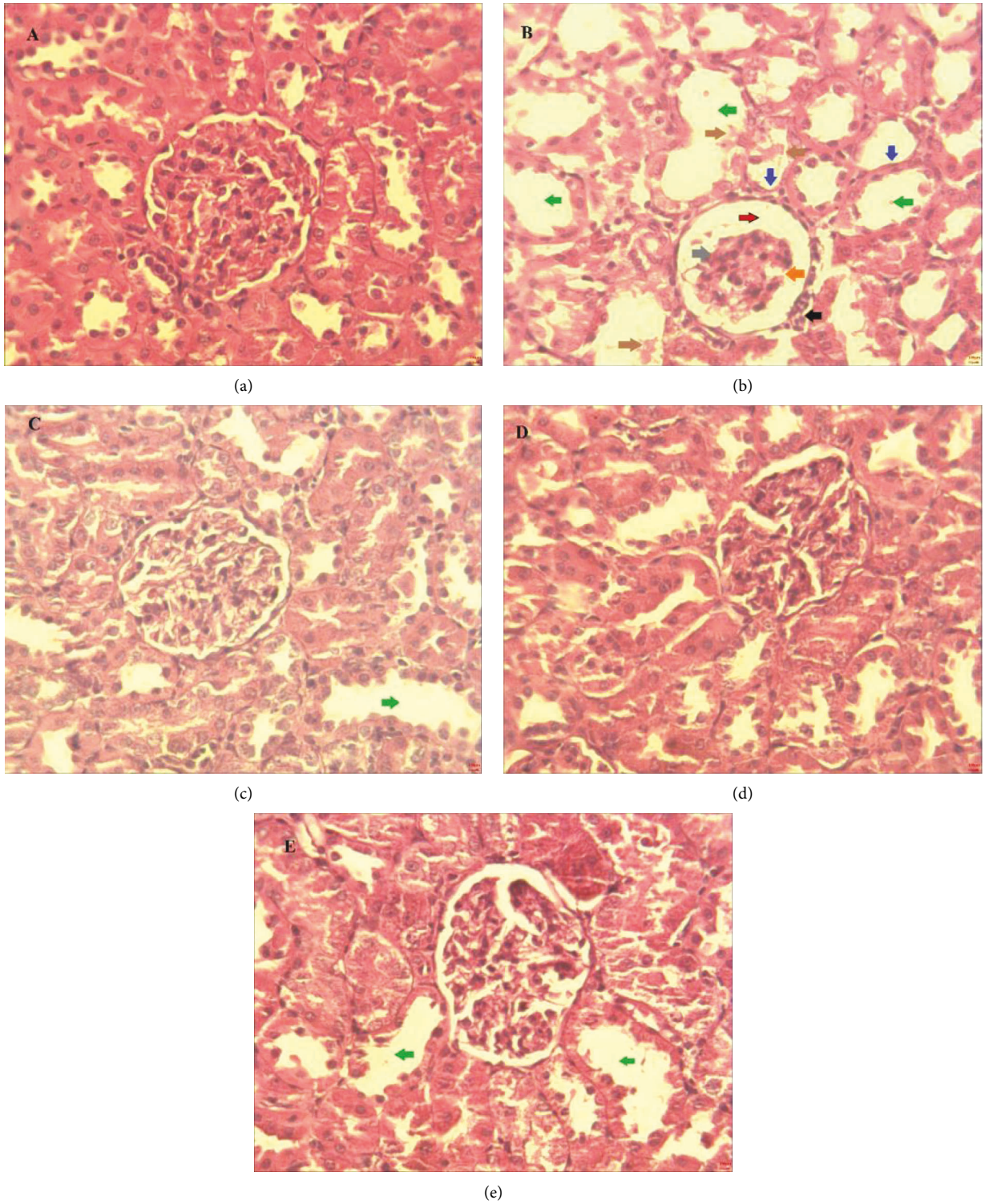

Figure 1: Effect of extracts from stigmas (50 mg/kg), tepals (250 mg/kg), and leaves (250 mg/kg) of *C. sativus* on histological changes of the kidney ((a), (b), (c), (d), and (e)) in gentamicin-intoxicated rats. Histological sections of the kidney tissue (stained with hematoxylin and eosin) were taken from the normal group (a), the gentamicin + distilled water group (b), the gentamicin + STG group (c), the gentamicin + TPL group (d), the and gentamicin + LV group (e). Glomerular degeneration (orange arrow), necrosis at Bowmen's capsule (gray arrow), distinction of Bowman's space (red arrow), mononuclear cell infiltration (black arrow), renal tubule desquamation (brown arrow), renal tubule atrophy (blue arrow), and renal tubule dilatation (green arrow).

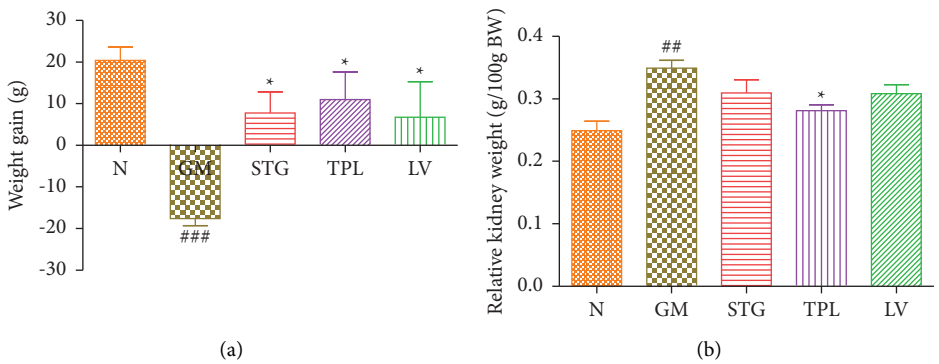

Figure 2: Effects of gentamicin and *C. sativus* extracts of stigmas (50 mg/kg), tepals (250 mg/kg), and leaves (250 mg/kg) on weight gain (a) and relative kidney weight (b) in rats. Values were expressed as mean ± SEM. ($n = 5$); $^{###}p < 0.001$ and $^{##}p < 0.01$ in comparison with the N group; $^{*}p < 0.05$ in comparison with the GM group.

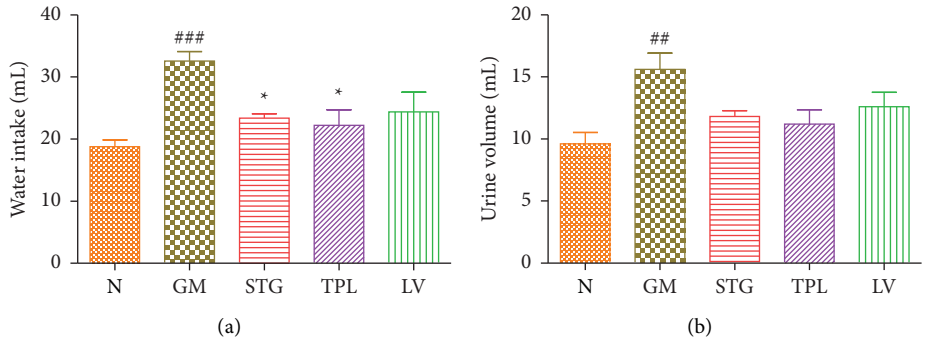

Figure 3: Effect of extracts from stigmas (50 mg/kg), tepals (250 mg/kg), and leaves (250 mg/kg) of *C. sativus* on water intake (a) and urine volume (b) in gentamicin-intoxicated rats. Values were expressed as mean ± SEM. ($n = 5$); $^{###}p < 0.001$ and $^{##}p < 0.01$ in comparison with the N group; $^{*}p < 0.05$ in comparison with the GM group.

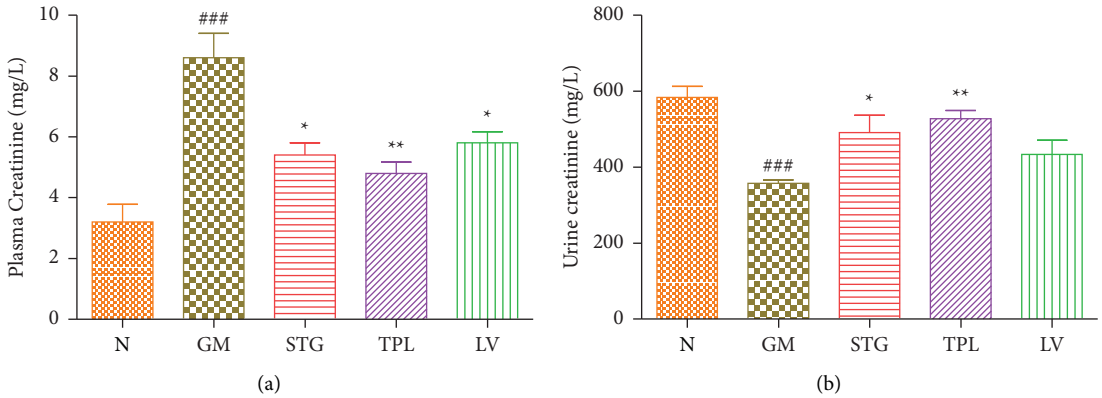

Figure 4: Continued.

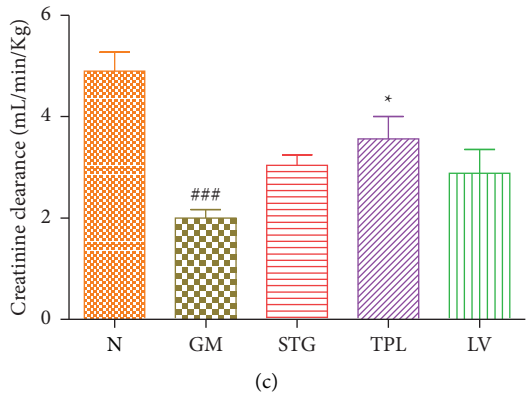

Figure 4: The effect of gentamicin and extracts of *C. sativus* stigmas (50 mg/kg), tepals (250 mg/kg), and leaves (250 mg/kg) on plasma creatinine (a), urine creatinine (b), and creatinine clearance (c) in rats. Values were expressed as mean ± SEM. ($n = 5$); $^{###}p < 0.001$ in comparison with the N group; $^{*}p < 0.05$ and $^{**}p < 0.01$ in comparison with the GM group.

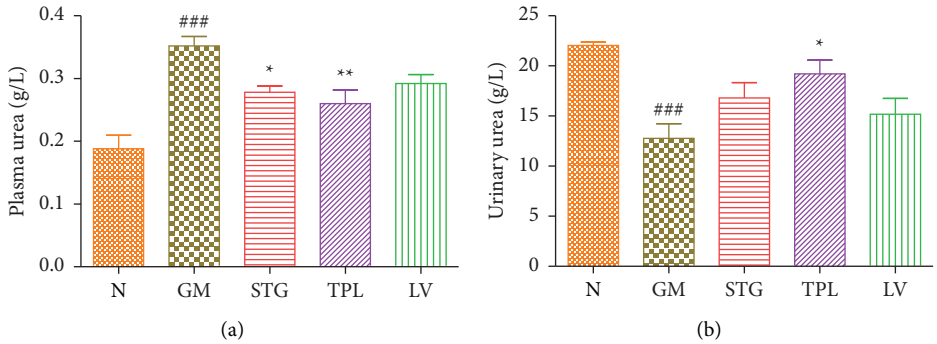

Figure 5: The effect of gentamicin and *C. sativus* extracts from stigmas (50 mg/kg), tepals (250 mg/kg), and leaves (250 mg/kg) on plasma (a) and urine (b) urea in rats. Values were expressed as mean ± SEM. ($n = 5$); $^{###}p < 0.001$ in comparison with the N group; $^{*}p < 0.05$ and $^{**}p < 0.01$ in comparison with the GM group.

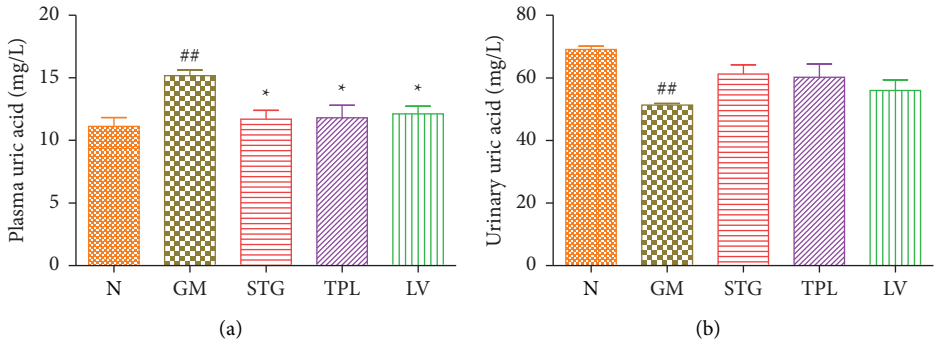

Figure 6: Effect of extracts from stigmas (50 mg/kg), tepals (250 mg/kg), and leaves (250 mg/kg) of *C. sativus* on plasma and urinary uric acid levels ((a) and (b)) in gentamicin-intoxicated rats. Values were expressed as mean ± SEM. ($n = 5$); $^{##}p < 0.01$ in comparison with the N group; $^{*}p < 0.05$ in comparison with the GM group.

3.9. The Effect of Gentamicin and C. sativus Extracts on Lipid Peroxidation (MDA). The impact of the effect of *C. sativus*by-product extracts on lipid peroxidation in treated experimental animals is presented in Figure 9. The intraperitoneal injection of GM caused a significant ($p < 0.001$) elevation of hepatic MDA compared to normal

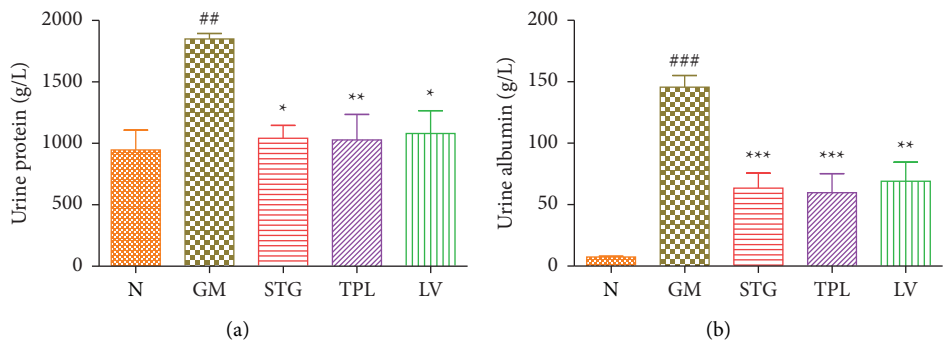

Figure 7: Effect of extracts from stigmas (50 mg/kg), tepals (250 mg/kg) and leaves (250 mg/kg) of *C. sativus* on urinary protein and albumin levels ((a) and (b)) in gentamicin-intoxicated rats. Values were expressed as mean ± SEM. ($n = 5$); $^{###}p < 0.001$ and $^{##}p < 0.01$ in comparison with the control group; $^{*}p < 0.05$ and $^{**}p < 0.01$ in comparison with gentamicin-intoxicated rats.

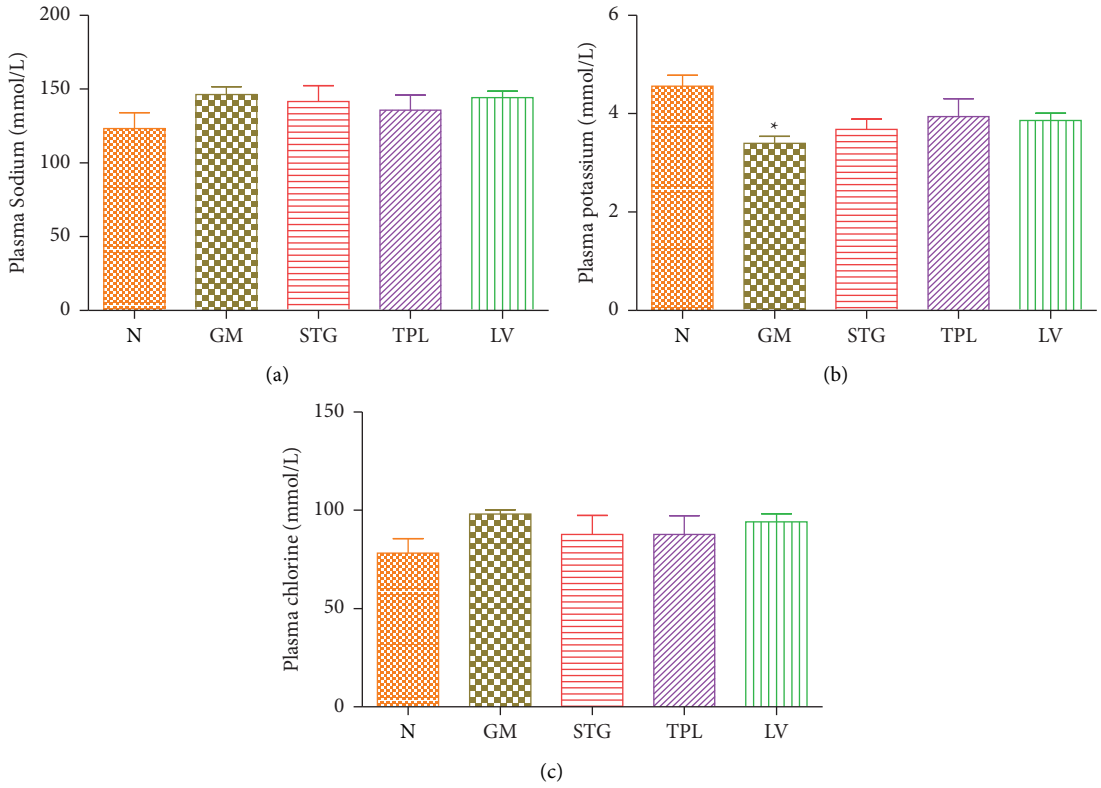

Figure 8: ((a), (b), and (c)): The effect of extracts from stigmas (50 mg/kg), tepals (250 mg/kg), and leaves (250 mg/kg) of *C. sativus* on plasma electrolytes (Na^+, K^+, and Cl^-) in gentamicin-intoxicated rats. Values were expressed as mean ± SEM. ($n = 5$); $^{\#}p < 0.05$ in comparison with the N group.

rats. Daily treatment of intoxicated and treated rats with the extracts of stigmas, tepals, and leaves gave a significant reduction ($p < 0.01$, $p < 0.001$, and $p < 0.05$ respectively)

3.10. Chemical Composition of C. sativus Stigmas, Tepals, and Leaves. The HPLC-DAD chromatograms and the chemical composition of *C. sativus* stigmas, tepals, and leaves are shown in Figures 10(a), 10(b), and 10(c) and in Table 1 (A, B, and C), respectively. The hydroethanolic extract of stigmas was found to be rich in crocin and picrocrocin (Figure 1(a); Table 1 A). The chemical analysis of the hydroethanolic extract of tepals revealed the presence of isorhamnetin, quercetin, and kaempferol (Figure 1(b); Table 1 (A)). The hydroethanolic extract of leaves is rich in hesperidin, mangiferin, and kaempferol (Figure 1(c); Table 1 (C)).

4. Discussion

The results showed that gentamicin-treated rats showed glomerular degeneration, necrosis in Bowmen's capsule, a distinction of Bowman's space, mononuclear cell

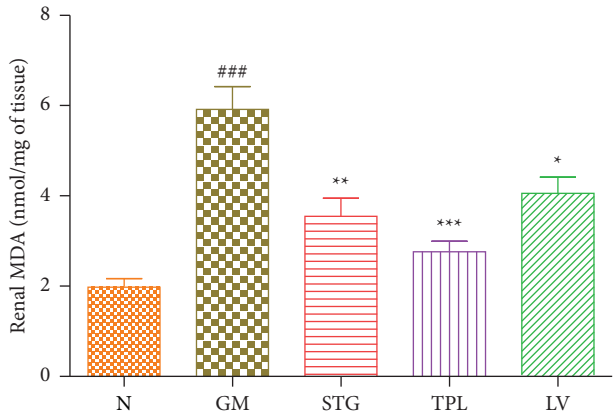

Figure 9: Effect of extracts from stigmas (50 mg/kg), tepals (250 mg/kg), and leaves (250 mg/kg) of *C. sativus* on MDA levels in GM-intoxicated rats. Values were expressed as mean ± SEM. ($n = 5$); $^{###}p < 0.001$ in comparison with the N group; $^{*}p < 0.05$, $^{*}p < 0.01$, and $^{***}p < 0.001$ in comparison with the GM group.

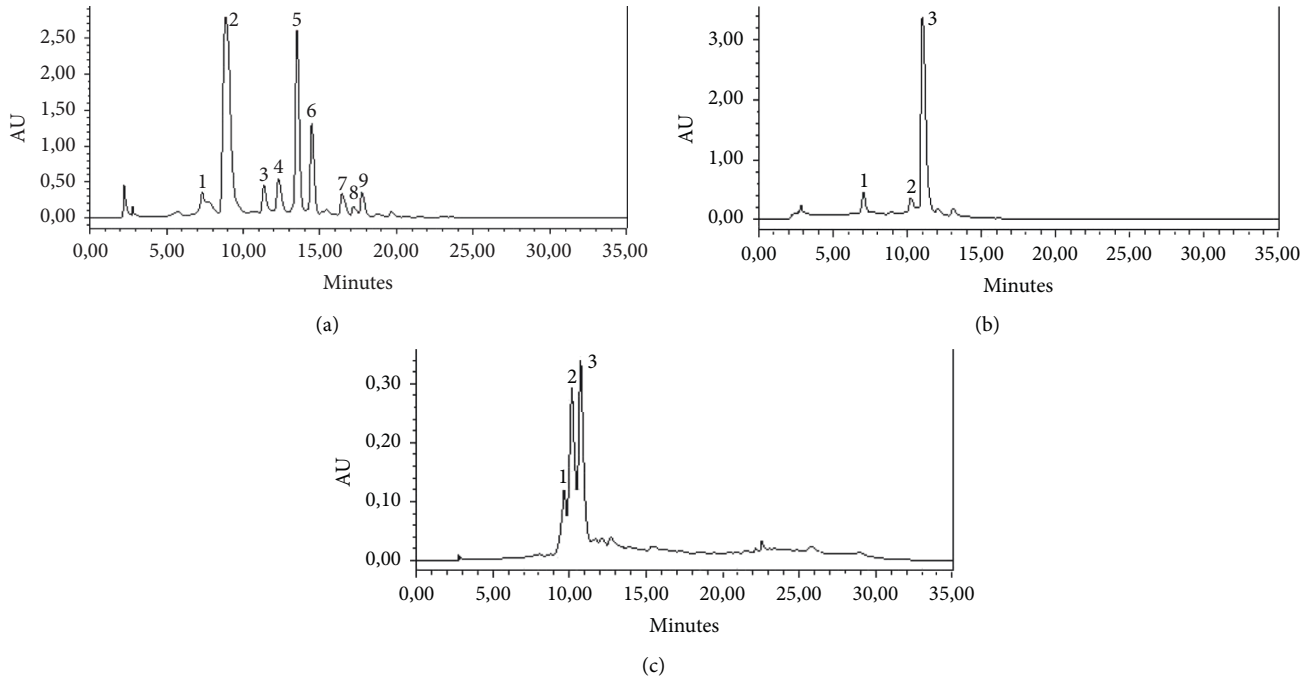

Figure 10: HPLC-DAD chromatograms of *C. sativus* stigmas (a), tepals (b), and leaves (c).

infiltration, tubular atrophy, tubular dilatation, and cellular desquamation. These histological changes are in agreement with several studies [18, 19]. However, treatment with stigmas, tepals, and leaves preserved kidney morphology at the glomerular and tubular cell level. Indeed, we have shown that intraperitoneal administration of gentamicin significantly reduces body weight, which are consistent with the results found by several authors [20]. According to Hashim and these collaborators, anorexia and increased catabolism are responsible for the decrease in food intake and resulted in weight loss [21]. In addition, damage to tubular cells, involved in renal water reabsorption, leads to dehydration and decreased body weight [22]. An inflammatory response and renal edema may be to blame for the considerable rise in the relative kidney weight seen in the group treated with gentamicin. [23]. This was confirmed by histological sections, which showed apparent renal tubular swelling (Figure 1).

Rats from the gentamicin-intoxicated group (GM group) drank a lot of water and peed a lot. Our results are therefore supported by those of Ogundipe et al. [24]. The polyuria seen during GM treatment is likely caused by the distal convoluted tubules and cortical collecting ducts' inability to reabsorb water from urine, which may be caused by gentamicin's direct effect on the tubules making the tubules less sensitive to ADH (antidiuretic hormone), resulting in

Table 1: Chemical composition of *C. sativus* stigmas (A), tepals (B), and leaves (C).

Peak numbers	Compounds	Retention time (min)	% of areas
(A)			
1	Safranal	7.328	3.44
2	Picrocrocin	8.872	41.39
3	Kaempferol	11.340	4.11
4	Trans-crocin-5	13.503	20.54
5	Trans-crocin-4	14.466	10.03
6	Trans-crocin-3	16.435	2.79
7	Trans-crocin-2	17.176	1.13
8	Cis-crocin-4	17.747	2.60
9	Cis-crocin-3	18.863	0.46
(B)			
1	Isorhamnetin	7.051	6.12
2	Quercetin	10.223	5.72
3	Kaempferol	11.035	76.97
(C)			
1	Hesperidin	9.668	13.54
2	Mangiferin	10.15	41.52
3	Kaempferol	10.721	44.94

Crocin-2: ester-di-(β-D-glucosyle)-crocétine; crocin-3: ester-(β-D-glucosyle)-(β-gentiobiosyle)-crocétine; crocin-4: ester-di-(β-D-gentiobiosyle)-crocétine; and crocin-5: ester-(β-D-triglucosyle)-(β-D-gentiobiosyle)-crocétine.

difficulty in reabsorbing water [25]. This is confirmed by histology which reveals the presence of damage to the nephrons.

Creatinine has been described as a potent biomarker for clinically evaluating the renal function [26]. The liver and proximal tubules of the kidney release creatinine, which the blood subsequently carries to the muscles. Glomerular filtration and, to a lesser extent, tubular secretion are processes that creatinine goes through. Depending on the source of measurement and the individual muscle mass, creatinine concentrations can change (serum or urine). Our results are confirmed by those of Erdem et al. [27], who reported that gentamicin induced an elevation of plasma creatinine and a decrease in urinary creatinine compared to the control. In addition, they showed that this imbalance is linked to significant kidney histological changes that point to a deterioration in the renal function. An indicator of the glomerular filtration rate is creatinine clearance. Reduced glomerular filtration rate and renal blood flow as a result of increased renal blood vessel constriction or injury to the glomerular capillary endothelium are indicated by decreased creatinine clearance. The considerable reduction in creatinine clearance seen in gentamicin-treated rats suggests both significant tissue damage and reduced glomerular function. Histopathology, which depicts the modification of the glomeruli and the loss of cellular components of the tubules, served as a representation of this. These findings concur with those of Nafiu et al. and Ogundipe et al. [24, 25].

Urea, a product of amino acid metabolism, represents an efficient means of eliminating NH3, which is toxic to the body. The urinary tract is permeable to urea except for the distal convoluted tubule and the initial part of the collecting tube. Reabsorption of urea is passive and takes place mainly in the proximal convoluted tubule: reaching about 50% of the urea filtered at the glomerulus. About 10% of urea molecules are reabsorbed in the collecting tubules near the papilla. In total, 40% of the urea molecules in the glomerular filtration are excreted. Urea is considered an important indicator for examining the renal status. Their elevated concentration in plasma indicates renal failure [28]. According to the findings of our investigation, gentamicin caused a large increase in plasma urea and a considerable fall in urine urea, results that are similar to those of Udapa and Prakash [29].

The breakdown of nucleic acids results in the production of uric acid, on the one hand, and dietary purine compounds on the other. Their excretion is low compared to urea. The distal tubule then secretes it after being completely reabsorbed and filtered in the glomerulus. According to reports, uric acid is a sign that chronic renal disease is developing [30]. We found that gentamicin injection caused a significant elevation in plasma uric acid, a result that is supported by the study of Aiswarya et al. [14].

Proteinuria above the norm indicates renal damage whether tubular or glomerular [31]. The glomerular filtration barrier (GFB) usually does not allow the passage of proteins that are retained by their size and charge. The proximal renal tubule participates in the reabsorption of small proteins that pass this barrier. Our results indicate that gentamicin caused a significant increase in the urinary protein content. These findings are confirmed by those of Govindappa et al. [22].

The amount of albumin filtered under physiological conditions is debated. It is then reabsorbed into the proximal tubule by endocytosis and does not appear in significant amounts in the urine. In the presence of filtration barrier abnormalities or tubular reabsorption abnormalities, increased amounts of albumin and protein may be found in the urine, indicating a pathological condition [32]. In this study, the significant increase in albuminuria following gentamicin injection confirms the nephrotoxic effect of this substance via alteration of the glomerular filtration barriers

or via tubular damage. Similar results were obtained by the study of Helmy et al. [33].

Aminoglycosides build up on the proximal tubule membranes, affecting electrolyte reabsorption and secretion, and ultimately leading to a homeostatic imbalance that results in renal failure [25]. The proximal tubules are where the majority of the filtered potassium is reabsorbed. Any morphological change in these tubules lowers potassium reabsorption and, as a result, increases urine output of this electrolyte. According to Govindappa et al. [22], GM causes cell necrosis in the proximal tubules [22]. In this study, a significant reduction in the plasma potassium concentration was observed in GM-treated rats, which may be due to the effect of GM on the proximal tubules. In addition, glomerular dysfunction and impaired tubular reabsorption led to a slight increase in sodium and decrease in potassium and magnesium levels in rat plasma [34]. Plasma potassium ion levels may have decreased as a result of gentamicin due to the drug's stimulation of aldosterone secretion [35].

The end product of polyunsaturated fatty acid peroxidation, malondialdehyde (MDA), is typically utilized as a biomarker of this process [35]. MDA levels in the kidneys of the rats used in this investigation significantly increased after receiving injections of GM; that is supported by several studies [22, 36].

Researchers have reported that aminoglycosides are antibiotics capable of causing nephrotoxicity by producing reactive oxygen species, specifically hydrogen peroxide and superoxide [15, 16]. The reaction between hydrogen peroxide and superoxide can produce the hydroxyl radical, a reactive and unstable radical. As a result of the reaction between H_2O_2 and Fe^{2+}, this radical is created [37]. Thus, gentamicin-induced nephrotoxicity appears to be largely mediated by this mechanism. Through a variety of mechanisms including DNA damage, protein denaturation, and membrane lipid peroxidation, reactive oxygen species can impair and necrotize cells [38]. Our results indicate that renal MDA levels were significantly attenuated by the administration of tepals, stigmas, and leaf extracts. GM-induced nephrotoxicity in rats may be prevented by using herbal extracts with antioxidant capabilities, according to the studies of Bazm et al. and Khazaei et al. [39, 40]. Also, hydroxyl scavengers such as iron chelators have been shown to prevent GM-induced chronic renal failure [41]. Moreover, we have demonstrated in our previous article that the stigmas, tepals, and leaves of *C sativus* are rich in antioxidant molecules, have a strong antioxidant activity, an important metal chelating ability (fe^{2+} and Cu^{2+}), and a significant DNA protective effect [42].

Crocetin esters, picrocrocin, and safranal are moreover the three essential components of saffron, they are primarily in charge of flavor, color, and aroma, respectively [43]. Flavonols in stigma are abundant, and specifically, kaempferol derivatives [44]. *C. sativus* leaves and tepals are abundant in bioactive substances including flavonols. Kaempferol, quercetin, and isorhamnetin have been found to be the primary flavonols in the hydroalcoholic extract of tepals [45]. Will, leaves are rich in hesperidin, mangiferin, and Kaempferol [46]. The nephroprotective effect of major components of stigmas, crocin, and safranal has been confirmed by several studies [47, 48]. Similarly, the nephroprotective effect of kaempferol, quercetin, isorhamnetin, hesperidin, and mangiferin, major components of tepals and leaves, had been noted by various investigations [49–53].

Therefore, the nephroprotective effect found in the present study may be related to these bioactive molecules and their characteristics. Compared to other synthetic antioxidants, which could have negative or undesirable side consequences, these natural antioxidants seem to offer safer substitutes.

5. Conclusions

The outcomes of the various experiments supported the necessity of utilizing these by-products. Tested extracts have great therapeutic potential for treating gentamicin-induced renotoxicity. The hydroethanolic tepal and stigma extracts appear to have the most significant nephroprotective effect. In order to create potent dietary supplements or phytomedicines, it would also be highly intriguing to confirm these actions through clinical research.

Data Availability

All the data used to support the findings of this study are included within the article.

Conflicts of Interest

The authors declare that they have no conflicts of interest.

Authors' Contributions

Conceptualization was done by Sabir Ouahhoud and Ennouamane Saalaoui; writing—original draft preparation by Sabir Ouahhoud and Salma Kadda; methodology by Noureddine Bencheikh and Amal Bennani; software by Amine Khoulati and Samira Mamri; validation and Mohammed Addi, Mohammed Choukri, and Ennouamane Saalaoui; formal analysis by Anas Ziani, Sanae Baddaoui, and Fatima-Ezzahra Eddabbeh; investigation by Soufiane Elassri and Redouane Benabbes; resources by Abdeslam Asehraou and Iliass Lahmass; writing—review and editing by Christophe Hano and Mohammed Addi; supervision by Ennouamane Saalaoui; and project administration by Ennouamane Saalaoui.

Acknowledgments

The authors gratefully acknowledge the assistance of Mostapha Badraoui, Karim Ramdaoui, and Abdelaziz Joudar in the areas of animal care and technical advice. The National Agency of Medicinal and Aromatic Plants and the National Center for Scientific and Technical Research provided funding for this study. The Conseil départemental d'Eure-et-Loir and Region Centre-Val de Loire provided funding for some of this work.

References

[1] B. T. Cenci-Goga, R. Torricelli, Y. Hosseinzadeh Gonabad et al., "In vitro bactericidal activities of various extracts of saffron (*Crocus sativus L.*) stigmas from torbat-e heydarieh, gonabad and Khorasan, Iran," *Microbiology Research*, vol. 9, no. 1, p. 7583, 2018.

[2] S. Sharma and D. Kumar, "Chemical composition and biological uses of L (Saffron)," in *Edible Plants in Health and Diseases*, pp. 249–277, Springer, Berlin, Germany, 2022.

[3] A. Zhang, Y. Shen, M. Cen et al., "Polysaccharide and crocin contents, and antioxidant activity of saffron from different origins," *Industrial Crops and Products*, vol. 133, pp. 111–117, 2019.

[4] A. Lambrianidou, F. Koutsougianni, I. Papapostolou, and K. Dimas, "Recent advances on the anticancer properties of saffron (*Crocus sativus L.*) and its major constituents," *Molecules*, vol. 26, no. 1, p. 86, 2020.

[5] S. Oz and S. C. Arica, "The genoprotective effect of *crocus sativus L.*(saffron) extract on doxorubicin-induced genotoxicity in drosophila melanogaster," *Fresenius Environmental Bulletin*, vol. 28, pp. 2545–2552, 2019.

[6] S. Ouahhoud, I. Lahmass, M. Bouhrim et al., "Antidiabetic effect of hydroethanolic extract of Crocus sativus stigmas, tepals and leaves in streptozotocin-induced diabetic rats," *Physiology and Pharmacology*, vol. 23, pp. 9–20, 2019.

[7] R. Hoshyar, A. Sebzari, M. Balforoush, M. Valavi, and M. Hosseini, "The impact of Crocus sativus stigma against methotrexate-induced liver toxicity in rats," *Journal of Complementary and Integrative Medicine*, vol. 17, no. 2, Article ID 20190201, 2019.

[8] S. Ouahhoud, I. Touiss, A. Khoulati et al., "Hepatoprotective effects of hydroethanolic extracts of Crocus sativus tepals, stigmas and leaves on carbon tetrachloride induced acute liver injury in rats," *Physiology & Pharmacology*, p. 25, 2021.

[9] B. Zarei and S. Elyasi, "Saffron nephroprotective effects against medications and toxins: a review of preclinical data," *Iranian Journal of Basic Medical Sciences*, vol. 25, no. 4, pp. 419–434, 2022.

[10] M. Abbasvali, A. Ranaei, S. S. Shekarforoush, and H. Moshtaghi, "The Effects of aqueous and alcoholic saffron (Crocus sativus) tepal extracts on quality and shelf life of pacific white shrimp (Litopeneous vannamei) during iced storage," *Journal of Food Quality*, vol. 39, no. 6, pp. 732–742, 2016.

[11] S. Zara, G. L. Petretto, A. Mannu et al., "Antimicrobial activity and chemical characterization of a non-polar extract of saffron stamens in food matrix," *Foods*, vol. 10, no. 4, p. 703, 2021.

[12] W. Meka Kedir, A. Dukassa Dubiwak, and E. Tofik Ahmed, "Nephroprotective effect of asparagus africanus lam. root extract against gentamicin-induced nephrotoxicity in swiss albino mice," *Journal of Toxicology*, pp. 1–8, 2022.

[13] M. Mahi-Birjand, S. Yaghoubi, M. Abdollahpour-Alitappeh et al., "Protective effects of pharmacological agents against aminoglycoside-induced nephrotoxicity: a systematic review," *Expert Opinion on Drug Safety*, vol. 19, no. 2, pp. 167–186, 2020.

[14] N. Aiswarya, R. Rashmi, S. Preethi et al., "Nephroprotective effect of aqueous extract of Pimpinella anisum in gentamicin induced nephrotoxicity in wistar rats," *Pharmacognosy Journal*, vol. 10, no. 3, pp. 403–407, 2018.

[15] P. Randjelovic, S. Veljkovic, N. Stojiljkovic, D. Sokolovic, and I. Ilic, "Gentamicin nephrotoxicity in animals: current knowledge and future perspectives," *EXCLI Journal*, vol. 16, pp. 388–399, 2017.

[16] M. A. Perazella, "Pharmacology behind common drug nephrotoxicities," *Clinical Journal of the American Society of Nephrology*, vol. 13, no. 12, pp. 1897–1908, 2018.

[17] T. D. Hewitson and I. A. Darby, *Histology Protocols: Methods in Molecular Biology*, 2010.

[18] K. Jaikumkao, A. Pongchaidecha, L. Thongnak et al., "Amelioration of renal inflammation, endoplasmic reticulum stress and apoptosis underlies the protective effect of low dosage of atorvastatin in gentamicin-induced nephrotoxicity," *PLoS One*, vol. 11, no. 10, Article ID e0164528, 2016.

[19] A. Fauzi, N. Titisari, and V. Mellisa, "Gentamicin nephrotoxicity in animal model: study of kidney histopathology and physiological functions," in *Proceedings of the IOP Conference Series: Earth and Environmental Science*, Article ID 012005, 2020.

[20] N. Fatima and A. Sultana, "Renoprotective and anti-oxidant effects of coleus forskohlii against gentamicin induced nephrotoxicity in albino wistar rats," *Acta Pharmaceutica Sciencia*, vol. 56, no. 2, p. 67, 2018.

[21] M. U. Hashim, S. H. A. Al-Cekal, and A. J. AL-Khamas, *Determination the Effect of Ciprofloxacin and Gentamicin Alone and in Combination to Induce Nephrotoxicity in Experimental Rats*, Annals of Tropical Medicine & Public Health, 2020.

[22] P. K. Govindappa, V. Gautam, S. M. Tripathi, Y. P. Sahni, and H. L. S. Raghavendra, "Effect of withania somnifera on gentamicin induced renal lesions in rats," *Revista Brasileira de Farmacognosia*, vol. 29, no. 2, pp. 234–240, 2019.

[23] A. D. Atsamo, A. Lontsie Songmene, M. F. Metchi Donfack, O. B. Ngouateu, T. B. Nguelefack, and T. Dimo, "Aqueous extract from cinnamomum zeylanicum (lauraceae) stem bark ameliorates gentamicin-induced nephrotoxicity in rats by modulating oxidative stress and inflammatory markers," *Evidence-based Complementary and Alternative Medicine*, pp. 2021–12, 2021.

[24] D. J. Ogundipe, R. O. Akomolafe, A. A. Sanusi, C. E. Imafidon, O. S. Olukiran, and A. A. Oladele, "Ocimum gratissimum ameliorates gentamicin-induced kidney injury but decreases creatinine clearance following sub-chronic administration in rats," *Journal of Evidence-Based Complementary & Alternative Medicine*, vol. 22, no. 4, pp. 592–602, 2017.

[25] A. O. Nafiu, R. O. Akomolafe, Q. K. Alabi, C. O. Idowu, and O. O. Odujoko, "Effect of fatty acids from ethanol extract of Moringa oleifera seeds on kidney function impairment and oxidative stress induced by gentamicin in rats," *Biomedicine & Pharmacotherapy*, vol. 117, Article ID 109154, 2019.

[26] K. Kashani, M. H. Rosner, and M. Ostermann, "Creatinine: from physiology to clinical application," *European Journal of Internal Medicine*, vol. 72, pp. 9–14, 2020.

[27] A. Erdem, N. Ü. Gündogan, A. Usubütün et al., "The protective effect of taurine against gentamicin-induced acute tubular necrosis in rats," *Nephrology Dialysis Transplantation*, vol. 15, no. 8, pp. 1175–1182, 2000.

[28] Y. Yang, T. Pan, and J. Zhang, "Global optimization of norris derivative filtering with application for near-infrared analysis of serum urea nitrogen," *American Journal of Analytical Chemistry*, vol. 10, no. 05, pp. 143–152, 2019.

[29] V. Udupa and V. Prakash, "Gentamicin induced acute renal damage and its evaluation using urinary biomarkers in rats," *Toxicology Reports*, vol. 6, pp. 91–99, 2019.

[30] K. Hahn, M. Kanbay, M. A. Lanaspa, R. J. Johnson, and A. A. Ejaz, "Serum uric acid and acute kidney injury: a mini

review," *Journal of Advanced Research*, vol. 8, no. 5, pp. 529–536, 2017.

[31] M. G. Helal, M. M. A. F. Zaki, and E. Said, "Nephroprotective effect of saxagliptin against gentamicin-induced nephrotoxicity, emphasis on anti-oxidant, anti-inflammatory and anti-apoptic effects," *Life Sciences*, vol. 208, pp. 64–71, 2018.

[32] B. R. Griffin, S. Faubel, and C. L. Edelstein, "Biomarkers of drug-induced kidney toxicity," *Therapeutic Drug Monitoring*, vol. 41, no. 2, pp. 213–226, 2019.

[33] M. M. Helmy and S. M. Mouneir, "Reno-protective effect of linagliptin against gentamycin nephrotoxicity in rats," *Pharmacological Reports*, vol. 71, no. 6, pp. 1133–1139, 2019.

[34] G. Ali Alshehry, "The role of gum arabic for a protective kidney dysfunction induced gentamicin on diabetes rats," *Advances in Materials Science and Engineering*, pp. 1–8, 2022.

[35] H. M. Al-Kuraishy, A. I. Al-Gareeb, and M. S. Al-Naimi, "Renoprotective effect of irbesartan in a rat model of gentamicin-induced nephrotoxicity: role of oxidative stress," *Journal of Laboratory Physicians*, vol. 11, no. 03, pp. 200–205, 2019.

[36] H. Laaroussi, M. Bakour, D. Ousaaid et al., "Protective effect of honey and propolis against gentamicin-induced oxidative stress and hepatorenal damages," *Oxidative Medicine and Cellular Longevity*, pp. 2021–2119, 2021.

[37] M. R. Arhoutane, M. S. Yahya, M. E. Karbane, and K. E. Kacemi, "Oxidative degradation of gentamicin present in water by an electro-Fenton process and biodegradability improvement," *Open Chemistry*, vol. 17, no. 1, pp. 1017–1025, 2019.

[38] H. Sies and D. P. Jones, "Reactive oxygen species (ROS) as pleiotropic physiological signalling agents," *Nature Reviews Molecular Cell Biology*, vol. 21, no. 7, pp. 363–383, 2020.

[39] M. A. Bazm, M. Khazaei, E. Ghanbari, and L. Naseri, "Protective effect of Vaccinium arctostaphylos L. fruit extract on gentamicin-induced nephrotoxicity in rats," *Comparative Clinical Pathology*, vol. 27, no. 5, pp. 1327–1334, 2018.

[40] M. Khazaei, M. Akbaribazm, N. Goodarzi, M. Rahimi, and L. Naseri, "Anti-inflammatory, anti-oxidative and anti-apoptotic effects of Heracleum persicum L. extract on rats with gentamicin-induced nephrotoxicity," *Asian Pacific Journal of Tropical Biomedicine*, vol. 11, no. 2, p. 47, 2021.

[41] R. A. Ungur, I. M. Borda, R. A. Codea et al., "A flavonoid-rich extract of Sambucus nigra L. reduced lipid peroxidation in a rat experimental model of gentamicin nephrotoxicity," *Materials*, vol. 15, no. 3, p. 772, 2022.

[42] S. Ouahhoud, A. Khoulati, S. Kadda et al., "Antioxidant activity, metal chelating ability and dna protective effect of the hydroethanolic extracts of crocus sativus stigmas, tepals and leaves," *Antioxidants*, vol. 11, no. 5, p. 932, 2022.

[43] L. Cardone, D. Castronuovo, M. Perniola, N. Cicco, and V. Candido, "Evaluation of corm origin and climatic conditions on saffron (Crocus sativus L.) yield and quality," *Journal of the Science of Food and Agriculture*, vol. 99, no. 13, pp. 5858–5869, 2019.

[44] S. Chaouqi, N. Moratalla-López, M. Lage, C. Lorenzo, G. L. Alonso, and T. Guedira, "Effect of drying and storage process on Moroccan saffron quality," *Food Bioscience*, vol. 22, pp. 146–153, 2018.

[45] C. I. Tuberoso, A. Rosa, P. Montoro, M. A. Fenu, and C. Pizza, "Antioxidant activity, cytotoxic activity and metabolic profiling of juices obtained from saffron (Crocus sativus L.) floral by-products," *Food Chemistry*, vol. 199, pp. 18–27, 2016.

[46] O. Mykhailenko, L. Ivanauskas, I. Bezruk, L. Sidorenko, R. Lesyk, and V. Georgiyants, "Characterization of phytochemical components of Crocus sativus leaves: a new attractive by-product," *Scientia Pharmaceutica*, vol. 89, no. 2, p. 28, 2021.

[47] A. Derakhshanfar, M. Hashempour Sadeghian, N. Abbasabadi, and M. H. Imanian, "Histopathologic and biochemical study of the effect of saffron extract on gentamicin-induced nephrotoxicity in rats," *Comparative Clinical Pathology*, vol. 24, no. 6, pp. 1347–1351, 2015.

[48] Z. M. Yarijani, H. Najafi, and S. Hamid Madani, "Protective effect of crocin on gentamicin-induced nephrotoxicity in rats," *Iranian Journal of Basic Medical Sciences*, vol. 19, no. 3, pp. 337–343, 2016.

[49] K. Langeswaran, J. Selvaraj, R. Ponnulakshmi, M. Mathaiyan, and S. Vijayaprakash, "Protective effect of Kaempferol on biochemical and histopathological changes in mercuric chloride induced nephrotoxicity in experimental rats," *Journal of Biologically Active Products from Nature*, vol. 8, no. 2, pp. 125–136, 2018.

[50] N. Pinar, Y. Karataş, Y. K. Dağlioğlu, and G. Gönlüşen, "Quercetin ve Koenzim Q10'un sıçanlarda gentamisin kaynaklı nefrotoksisite üzerine etkileri," *Cukurova Medical Journal*, vol. 45, no. 1, pp. 251–256, 2020.

[51] R. Ungur, R. Buzatu, R. Lacatus et al., "Evaluation of the nephroprotective effect of Sambucus nigra total extract in a rat experimental model of gentamicine nephrotoxicity," *Revue Chimique*, vol. 70, no. 6, pp. 1971–1974, 2019.

[52] S. Akter, A. Moni, G. M. Faisal et al., "Renoprotective effects of mangiferin: pharmacological advances and future perspectives," *International Journal of Environmental Research and Public Health*, vol. 19, no. 3, p. 1864, 2022.

[53] B. Hanedan, M. Ozkaraca, A. Kirbas et al., "Investigation of the effects of hesperidin and chrysin on renal injury induced by colistin in rats," *Biomedicine & Pharmacotherapy*, vol. 108, pp. 1607–1616, 2018.

Hindawi
Evidence-Based Complementary and Alternative Medicine
Volume 2022, Article ID 6305672, 13 pages
https://doi.org/10.1155/2022/6305672

Research Article

GC-MS Profiling, *In Vitro* Antioxidant, Antimicrobial, and *In Silico* NADPH Oxidase Inhibition Studies of Essential Oil of *Juniperus thurifera* Bark

Soufyane Lafraxo,[1] Abdelfattah El Moussaoui,[1] Yousef A Bin Jardan,[2] Azeddin El Barnossi,[1] Mohamed Chebaibi,[3] Soukayna Baammi,[4] Aziz Ait Akka,[5] Khalid Chebbac,[5] Mohamed Akhazzane,[6] Tarik Chelouati,[7] Hiba-Allah Nafidi,[8] Khallouki Farid,[9] Mohammed Bourhia,[10] and Amina Bari[1]

[1]*Laboratory of Biotechnology and Environment, Agri-Food and Health, Faculty of Sciences Dhar El Mahraz, Sidi Mohammed Ben Abdellah University, P.O. Box 1796 (Atlas), 30000 Fez, Morocco*
[2]*Department of Pharmaceutics, College of Pharmacy, King Saud University, Riyadh, Saudi Arabia*
[3]*Laboratory of Biomedical and Translational Research, Faculty of Medicine and Pharmacy of Fez, University of Sidi Mohamed Ben Abdellah, BP 1893, Km 22, Road of Sidi Harazem, Fez, Morocco*
[4]*African Genome Centre (AGC), Mohammed VI Polytechnic University, Benguerir, Morocco*
[5]*Laboratory of Biotechnology, Conservation and Valorisation of Natural Resources, Faculty of Sciences Dhar ElMahraz, Sidi Mohammed Ben Abdallah University, P.O. Box 1796 (Atlas), Fez 30000, Morocco*
[6]*Engineering Laboratory of Organometallic and Molecular Materials and Environment, Faculty of Sciences Dhar El Mahraz, Sidi Mohamed Ben Abdellah University, P.O. Box 1796 (Atlas), 30000 Fez, Morocco*
[7]*Substance Naturelle Pharmacologie Environnement Modelisation Sante et Qualite de Vie, Fez, Morocco*
[8]*Department of Food Science, Faculty of Agricultural and Food Sciences, Laval University, 2325 Quebec City, QC G1V 0A6, Canada*
[9]*Biology Department, FSTE, University Moulay Ismail, BP. 609, 52000 Errachidia, Morocco*
[10]*Higher Institute of Nursing Professions and Technical Health, Laayoune 70000, Morocco*

Correspondence should be addressed to Mohammed Bourhia; bourhiamohammed@gmail.com

Received 1 August 2022; Revised 24 August 2022; Accepted 6 September 2022; Published 27 September 2022

Academic Editor: Salah M. El Sayed

Juniperus thurifera is a native species to the mountains of the western Mediterranean region. It is used in traditional medicine as a natural treatment against infections. The present study aimed to carry out the chemical analysis and evaluate the antioxidant, antimicrobial, as well as *in silico* inhibition studies of the essential oils from *Juniperus thurifera* bark (EOEJT). Chemical characterization of EOEJT was done by gas chromatography (GC-MS). We have performed three antioxidant assays (Reducing power (FRAP), 2, 2-diphenylpicrylhydrazyl (DPPH), and total antioxidant capacity (TAC)) of the EOEJT. We next evaluated the antimicrobial activity against *in silico* study, which was carried out to help evaluate the inhibitory effect of EOEJT against NADPH oxidase. Results of the GC/MS analysis revealed seven major compounds in EOEJT wherein muurolol (36%) and elemol (26%) were the major components. Moreover, EOEJT possessed interesting antioxidant potential with an IC_{50} respectively of $21.25 \pm 1.02\,\mu g/mL$, $481.02 \pm 5.25\,\mu g/mL$, and $271\,\mu g$ EAA/mg in DPPH, FRAP, and total antioxidant capacity systems. Molecular docking of EOEJT in NADPH oxidase active site showed inhibitory activity of α-cadinol and muurolol with a glide score of -6.041 and -5.956 Kcal/mol, respectively. As regards the antibacterial and antifungal capacities, EOEJT was active against all tested bacteria and all fungi, notably, against *Escherichia coli* K12 with an inhibition diameter of 21 mm and a MIC value of 0.67 mg/mL, as well as against *Proteus mirabilis* ATCC 29906 with an inhibition diameter of 18.33 ± 1.15 mm and a MIC value of 1.34 mg/mL. A more pronounced effect was recorded for the fungal pathogens *Fusarium oxysporum* MTCC 9913 with inhibition of $37.44 \pm 0.28\%$ and MIC value of 6.45 mg/mL, as well as against *Candida albicans* ATCC 10231 with an inhibition diameter of 20.33 ± 1.15 mm

and a MIC value of 0.67 ± 0.00 mg/mL. Altogether, these results highlight the importance of EOEJT as a source of natural antibacterial and antioxidant drugs to fight clinically important pathogenic strains.

1. Introduction

Morocco is the most biodiverse country in the western Mediterranean region [1]. Within it, the eastern half of the forest formations of the Middle Atlas is a veritable mosaic, with a wide range of forest species including cedar, holm oak, Phoenician juniper as well as *Juniperus thurifera* [2]. The Bouiblane site made up of two distinct regions (Bouiblane I and Bouiblane II) is part of the Sites of Biological and Ecological Interest (SBEI) of the Moroccan Eastern Middle Atlas. This locality stands out by its different agro-climatic conditions, its floristic diversity, and its significant but unquantified rate of endemism, as well as its wide range of plant forms [3]. *Juniperus thurifera* is a variably sized tree that belongs to the family Cupressaceae. This species is native to mountainous areas of the Mediterranean basin's western region [4]. In Morocco, *Juniperus thurifera* grows more particularly in the High and Middle-Atlas Mountains [5, 6]. The two arboreal plants that can grow with it are *Quercus ilex* and *Cedrus atlantica*. Such hardy species may tolerate a wide range of weather conditions and may reach up to 19 meters tall and live for up to 800 years. The *thurifer* covers an estimated area of almost 20 000 hectares. It is the most regressed forest species in Morocco, with a 90 percent regression from its potential range [7].

Different phytoconstituents have been isolated from this species, and include mainly polyphenols, essential oils, and sterols [8, 9]. Such metabolites exhibited potential bioactivities such as anti-inflammatory, and antibacterial agents among other wide therapeutic applications [8–10].

Multidrug-resistant organisms have become a major concern and the situation is far from being mastered. Therefore, the research for antibacterial from natural origins has become a vivid area of exploration. Essential oils are combinations of volatile secondary metabolites that occur naturally in plants, which mostly represent the various smells and scents of a variety of plants [10]. A myriad of published reports has provided evidence of their potent bioactivities as antioxidants, antibacterials, antifungals, and insecticides [8–12].

This study aimed at characterizing the bark essential oils of *Juniperus thurifera* by GC/MS. Next, we conducted the antioxidant potential of essential oils *in vitro* and explore *in silico* as NADPH oxidase inhibitors. Finally, the antibacterial and antifungal effects against drug-resistant microbial strains were also described.

2. Materials and Methods

2.1. Plant Material. *Juniperus thurifera* (Figure 1) was collected from a mountainous area in the Middle Atlas, Morocco before being identified by a botanist and given the voucher number (FJT/02D20). Next, the bark was isolated from the plant branches, and then cleaned and dried by use of an oven at 35°C before grinding into powder by use of an electric grinder [13].

2.2. Chemicals. Ferric chloride ($FeCL_3$), sodium phosphate, ammonium molybdate, butylated hydroxytoluene (BHT), 2, 2-diphenylpicrylhydrazyl (DPPH), and 2, 3, 5-triphenyltetrazolium chloride (TTC). Malt extract (ME), sodium chloride (NaCl), trichloroacetic acid (TCA), potassium ferricyanide ($K_3Fe(CN)6$), agar, erythromycin, fluconazole, and dimethylsulfoxide (DMSO) were bought from Sigma-Aldrich (St. Louis, MO, USA).

2.3. Extraction of EOEJT. Using a Clevenger device, 200 g of the plant powder was immersed in 800 mL of water before being mixed and heated at boiling temperature for two hours. Next, the essential oils (EOEJT) were recovered and placed at 4°C until further use [13, 14].

2.4. Chromatographic Analysis of EOEJT by GC/MS. Analysis was done using a gas chromatograph (GCMS-TQ8040 NX Shimadzu brand) with an apolar capillary column (RTxi-5 Sil MS-30.00 m × 0.250 mm ID × 0.250 μm Film thickness). One microliter of EOEJT was used for chromatographic analysis after being diluted in hexane (10 : 100 dilution). The oven temperature program was initially set to 40°C for 2 minutes and followed by 260°C for 10 minutes, then increased by 5°C/min up to 280°C. Finally, the temperature was held at 280°C for 10 minutes. The carrier gas was nitrogen and the flow rate was 1 mL/min. The temperatures of the injector and detector were adjusted to 250 and 280°C. The ionization energy was set to 70 eV, the ion source temperature was set at 200°C, the interface line temperature was 280°C, and the scan mass range was m/z 40–650.00. Volatile compounds of essential oil were identified by the use of the Kovats index and NIST-MS Search Version 2.0 [13, 15].

2.5. Antioxidant Activity of EOEJT. The antioxidant capacity of EOEJTs was assayed by the use of three systems DPPH, TAC test, and FRAP, respectively. EOEJTs were prepared in a dilution series from 1 μg/mL to 1000 μg/mL in methanol; thus, positive controls of quercetin and BHT were used in this evaluation and were prepared under the same conditions as the EOEJTs.

2.5.1. DPPH Test. Free radical powder was prepared in methanol [16,17]. Briefly, 0.004 mg in 100 mL. 100 μL of the sample (EOEJT, BHT, and quercetin) were diluted in methanol before being added to 750 μL DPPH, while a solution consisting of 750 μL DPPH and 100 μL methanol was used as a negative control. The reaction media were

Figure 1: Photograph of *Juniperus thurifera*.

incubated for 25 minutes, and the optical density (DO) was measured at $\lambda = 517$ nm. The antioxidant efficiency was determined according to the following formula:

$$\mathrm{EA}\,(\%) = \left(\frac{1 - \mathrm{Ds}}{\mathrm{Ct}}\right) \times 100. \quad (1)$$

EA: antioxidant efficiency in percent (%); Ds: optical density of sample; Ct: optical density of negative control (White).

2.5.2. FRAP Test. This test was assayed by preparing a reaction medium using phosphate buffer with 200 mM-pH = 6.6 and $K_3Fe(CN)6$ (1%) [14,18]. Briefly, 200 µL of each solution was mixed with 50 μL EOEJT before being incubated at 50°C for 30 minutes. To prepare for analysis, the sample was remixed with 200 μL of trichloroacetic acid (10 mg/mL), 500 μL of distilled water (H_2O), and 100 μL of $FeCl_3$ (1 mg/mL). At 700 nm, absorbance was measured against a negative control (50 μL of methanol without EOEJT). The EC-50 effective concentration was used to present the results.

2.5.3. TAC Test by Use of Phosphomolybdenum Method. Briefly, EOEJT was combined with 1 mL of a reagent solution before being heated at 95°C for one hour and then cooled at room temperature for 20 minutes. The optical density was measured at $\lambda = 695$ nm against a negative control containing 25 μL of methanol without EOEJT, while ascorbic acid was used as a positive reference. Results of the TAC assay were expressed in micrograms equivalent to ascorbic acid per milligram of the sample (μg AAE/mg) [19].

2.6. Antimicrobial Capacity

2.6.1. Method for Assessing Antimicrobial Capacity. The disk diffusion assay was used to determine whether or not EOEJT has antimicrobial capabilities [20]. In a nutshell, the double-layer approach was used in order to inoculate bacterial and fungal strains onto Petri plates that contained Mueller–Hinton (MH) agar and malt extract (ME), respectively. The inoculum was prepared from fresh cultures grown in MH and ME media with (0.9% NaCl). Next, Wattman paper discs measuring sex millimeters in diameter were immersed in 20 μL of EOEJT before being placed on Petri dishes surfaces that were previously inoculated with bacteria (10^6 to 10^8 CFU/mL) and fungi. Erythromycin and fluconazole served as positive controls, respectively, for bacteria and fungi. Subsequently, Petri dishes inoculated with bacteria and fungi were meticulously incubated at 37°C and 30°C for bacterial and fungi strains, respectively [21]. After 24 hours and 48 hours postinoculation, respectively, inhibition diameters and inhibition percentages were computed for bacterial strains and *C. albicans*. However, after 7 days postinoculation, these calculations were performed for *A. flavus*, *F. oxysporum*, and *A. niger* [13].

2.6.2. Minimum Inhibitory Concentration (MIC). The MIC of EOEJT against microbial strains was determined using the microdilution method [22]. Briefly, the microplates were prepared in sterile conditions, each sterile 96-well microplate was labeled, and then a 100 μL of EOEJT with a 1 : 10 (*V*/*V*) dilution of DMSO (10 %) was pipetted into the first column of the plate to perform a series of dilution using sterile MH for bacteria and sterile ME for fungi, and lastly, 30 μL of microbial suspension of each strain (108 CFU/mL) was added to wells. After an incubation period ranging from 48 hours to 7 days for fungi and 24 hours for bacteria at 37°C [13, 22], the MIC was ascertained by using the colorimetric method (TTC 0.2%), [22, 23].

2.7. Molecular Docking

2.7.1. Ligand Preparations. For ligand preparations, we used the PubChem database to download all the molecules identified by GC/MS in EOEJT in SDF format. Next, the OPLS3 force field was applied, and the LigPrep tool in Schrödinger's Maestro 11.5 software was used to prepare the structures. Based on the ionization states at pH 7.0 2.0, a total of 32 stereoisomers were generated for each ligand.

2.7.2. Protein Preparation. For receptor preparation, the three-dimensional crystal structure of NADPH oxidase was downloaded from the PDB data bank in PDB format. Protein Preparation Wizard of Schrödinger-Maestro v11.5 was used to add hydrogen atoms to heavy atoms, transform selenomethionine into methionine, and remove water. Next, the OPLS3 force was used for minimization, and fixing the maximum heavy atoms RMSD (root mean square deviation) at 0.30 Å [24].

2.7.3. Receptor Grid Generation. The receptor grid was set at the following coordinates: $X = 17.584$, $Y = 9.05$, and $Z = 51.541$. When the volumetric spacing performed was

$20 \times 20 \times 20$, the glide of Schrödinger-Maestro v11.5 was used for SP flexible ligand docking [24].

2.7.4. Receptor Grid Generation. The receptor grid was set at the following coordinates: $X = 17.584$, $Y = 9.05$, and $Z = 51.541$. When the volumetric spacing performed was $20 \times 20 \times 20$, the glide of Schrödinger-Maestro v11.5 was used for SP flexible ligand docking. The ligand was coupled to the grid box produced from protein using "Standard precision" (SP), while SP GScore was used to evaluate the results [24].

2.7.5. Glide Standard Precision (SP) Ligand Docking. In ligand docking, the penalties were applied to noncis/trans amide bonds. The partial charge cutoff was set to 0.15 and the Van der Waals scaling factor and partial charge cutoff were set to 0.80 for each ligand atom, The energy-minimized poses presented by the glide score were used to calculate the final score. The best-docked pose with the lowest glide score value was recorded [25].

3. Statistical Analysis

Data were all provided as the mean value and standard deviation of tests performed in triplicate. GraphPad Prism was used to perform statistical analysis. Levine's test was used to verify homogeneity, while Shapiro–Wilks test was used to verify normality. Analysis of variance (ANOVA) flowed by Tukey's HSD test was used to arrange multiple comparisons. p values lower than 0.05 were regarded to indicate a statistically significant difference.

4. Results

4.1. Phytochemical Identification of EOEJTs by GC/MS. The yield of EOEJTs was about 0.89%, and it is somewhat comparable to what was previously found in the leaves (0.96%) *of Juniperus thurifera* [13]. Seven compounds were identified with a dominance of eudesmane-type cryptomeridiol (37.02%) followed by a cadinane-type muurolol (36.31%) and elemane-type sesquiterpenoid which is elemol (26.93%). The representative GC-MS total ion chromatography (TIC) of EOEJT from the bark of *Juniperus thurifera* is shown in Figure 2 and Table 1.

4.2. Antioxidant Activity of EOEJT. By use of the DPPH assay, EOEJT showed remarkable antioxidant potency in a dose-dependent manner. The concentration of 50 μg/mL scored an inhibition of about 75%, 85%, and 70%, respectively, for EOEJT, BHT, and quercetin. At a higher concentration, 250 μg/mL, the inhibition percentage was found to be 89.21% (EOEJT), 94% (BHT), and 92% (quercetin), Figure 3(a) Depicts the effectiveness of the tested products, which were determined by the MIC of 50% of free radicals (IC50). The calculated IC_{50} were 21.25 ± 1.02 μg/mL, 17.25 ± 1.20 μg/mL, and 20.15 ± 1.30 μg/mL, respectively, for EOEJT, BHT, and quercetin (Figure 3(b)).

Concerning the FRAP method, EOEJT showed also significant antioxidant effects in a doses-dependant manner compared to the positive controls BHT and quercetin. In this respect, 50 μg/mL of EOEJT or BHT, or quercetin revealed an optical density of 0.33, 0.39, and 0.36, respectively (Figure 3(c)). The EC50 of EOEJT, BHT, and quercetin were 481.02 ± 5.25 μg/mL, 214.08 ± 2.51 μg/mL, and 189.11 ± 2.20 μg/mL, respectively (Figure 3(d)). The antioxidant power of EOEJT was slightly lower than that recorded for *J. thurifera* leaves in previous work with an EC50 of 190 μg/mL [13].

Total antioxidant power was determined using the ammonium phosphomolybdate (TAC) method. Results showed that EOEJT had a good antioxidant capacity since it scored 271 μg AAE/mg, while PHT used as positive control scored 263 μg EAA/mg (Figure 3(e)). These results were comparable to EOs from *Dittrichia viscosa*, which revealed 192 μg AAE/mg as TAC [26]. In addition, the EOs of the leaves of *Lavandula dentata* scored 81.28 μg AAE/mg [27]. EOs from *Withania frutescens* also scored 91 μg AAE/mg [14].

4.3. Antibacterial Capacity. EOEJT showed promising antibacterial results when compared to erythromycin, particularly vs. *E. coli* wherein we noted an inhibition zone diameter of 21 ± 0.00 mm and MIC of 0.67 ± 0.00 mg/mL, and against *P. mirabilis* with an inhibition diameter of 18.33 ± 1.15 mm and a MIC of 1.34 ± 0.00 mg/mL (Figure 4, Figure 5 and Table 2). The antibacterial activity of EOEJT may be due to their physicochemical compositions, most importantly the presence of bioactive molecules such as muurolol, elemol, and pinene.

4.4. Antifungal Capacity. For antifungal susceptibility testing, *in vitro* evaluation of EOEJT against harmful fungal strains was conducted by the use of the diffusion assay. We found a potent antifungal potency with an inhibition percentage of 37.44 ± 0.28% and MIC value of 6.45 ± 0.00 mg/mL against *F. oxysporum* compared to fluconazole (Figure 6 and Table 3). Similarly, EOEJT exhibited significant activity against *C. albicans* with an inhibition zone diameter of 20.33 ± 1.15 mm and a MIC value of 0.67 ± 0.00 mg/mL (Table 3). Besides, EOEJT showed a fungistatic activity vs. *A. niger* and *F. oxusporum* and a fungicidal activity vs. *C. albicans*.

The antimicrobial effect of EOEJT was significant in comparison with one bacterial (erythromycin) and one fungal (fluconazole) specific antimicrobials. The results showed that the EOEJT test was more effective against Gram-negative or Gram-positive bacterial strains. Moreover, the principal component analysis (Figure 7) indicated that all bacterial and fungal strains used for testing showed almost similar sensitivities to EOEJT except for *A. flavus,* which was resistant to both EOEJT and fluconazole.

4.5. Molecular Docking. Molecular docking was accomplished to understand the interaction profile between EOEJT and NADPH oxidase. Among all molecules studied,

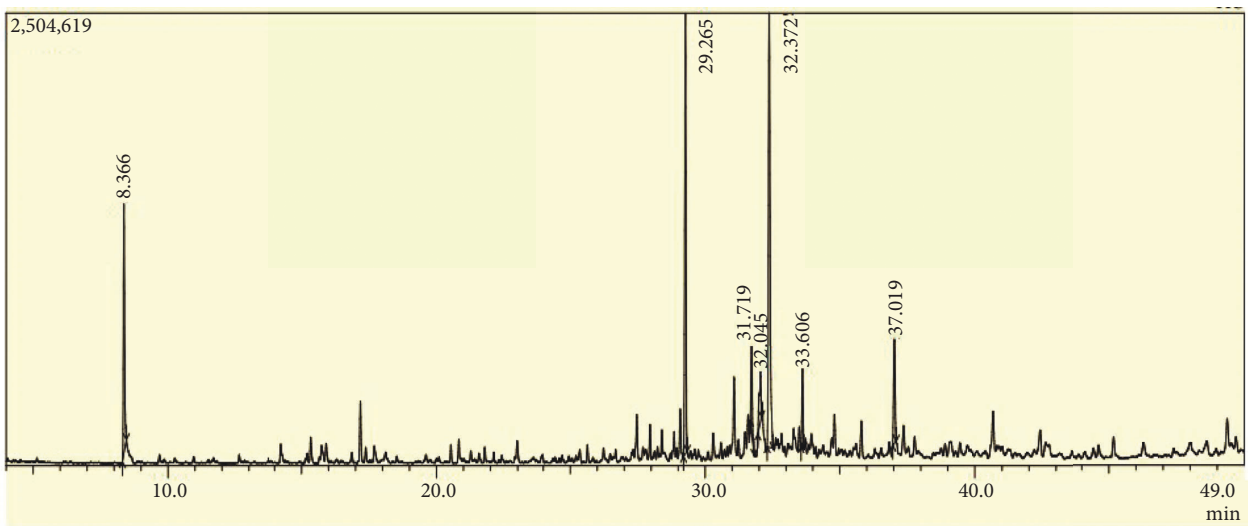

Figure 2: Gas chromatographic profile of EOEJT by GC/MS.

Table 1: Tabulation of the GC-MS analysis of EOEJT.

Peaks	RT	Name	Area (%)	Calculated RI	Literature RI	Molecular structure
1	8.36	α-Pinene	14.76	948	939	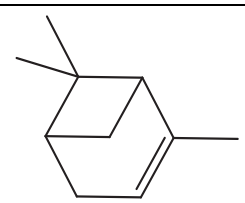
2	29.26	Elemol	26.93	1528	1529	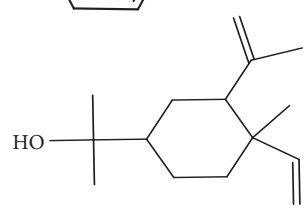
3	31.72	γ-Eudesmol	5.23	1664	1662	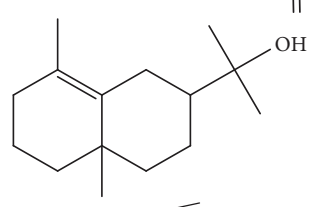
4	32.05	α-Cadinol	4.42	1650	1654	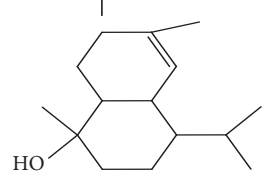
5	32.37	Muurolol	36.31	1640	1642	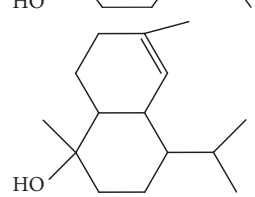
6	33.61	Eicosane	4.55	2007	2009	

Table 1: Continued.

Peaks	RT	Name	Area (%)	Calculated RI	Literature RI	Molecular structure
7	37.02	Cryptomeridiol	7.78	1811	1813	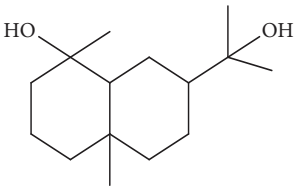
				Total 99.98%		

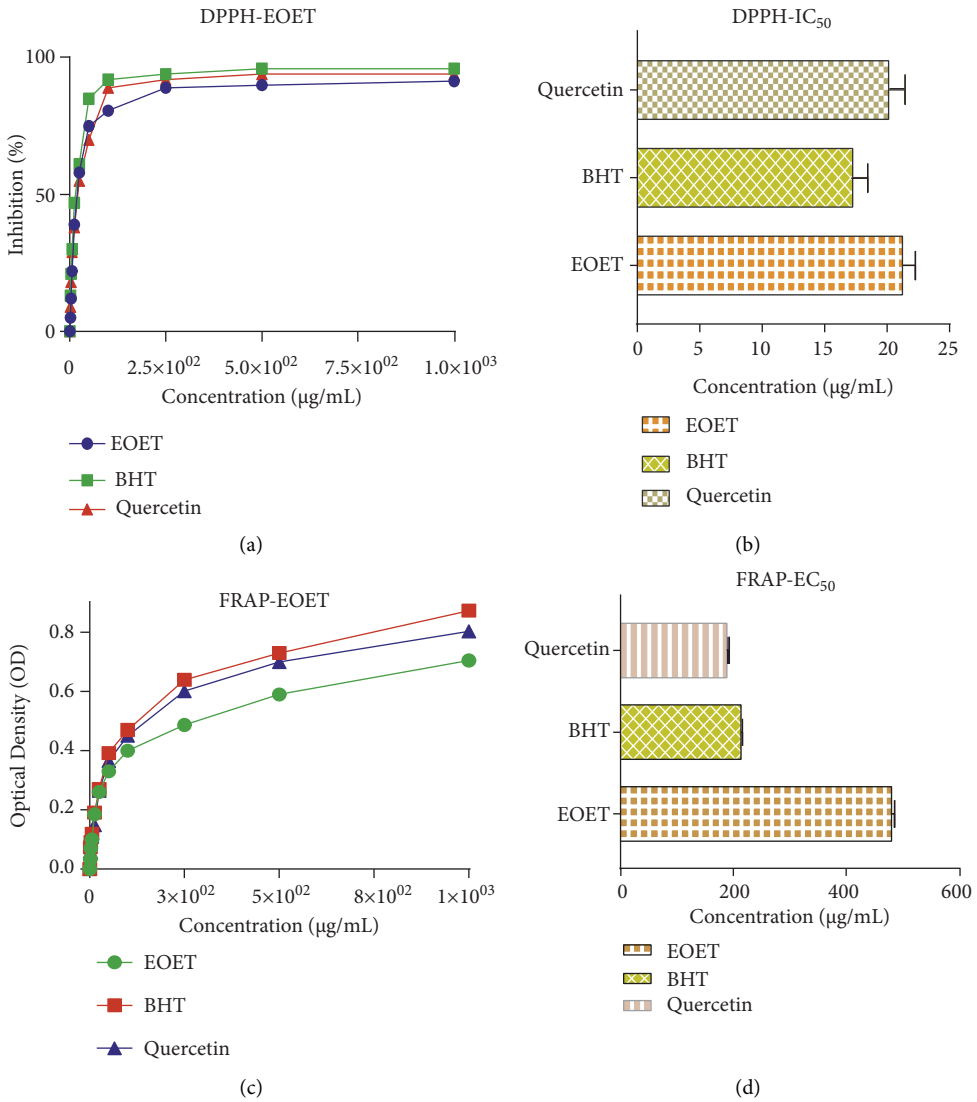

Figure 3: Continued.

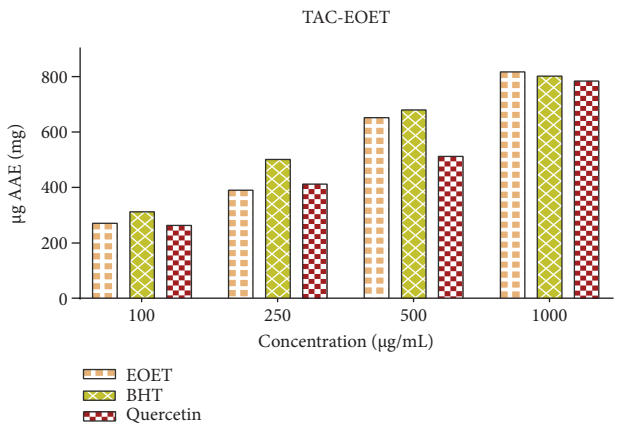

(e)

Figure 3: (a, b) Antioxidant capacity using DPPH, (c, d) FRAP method, (e) and total antioxidant capacity.

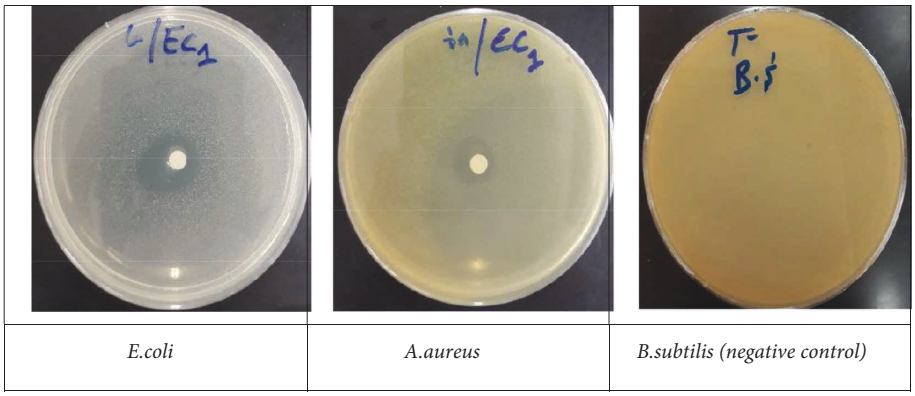

Figure 4: The antibacterial capacity for EOEJT on solid media (disc diffusion method).

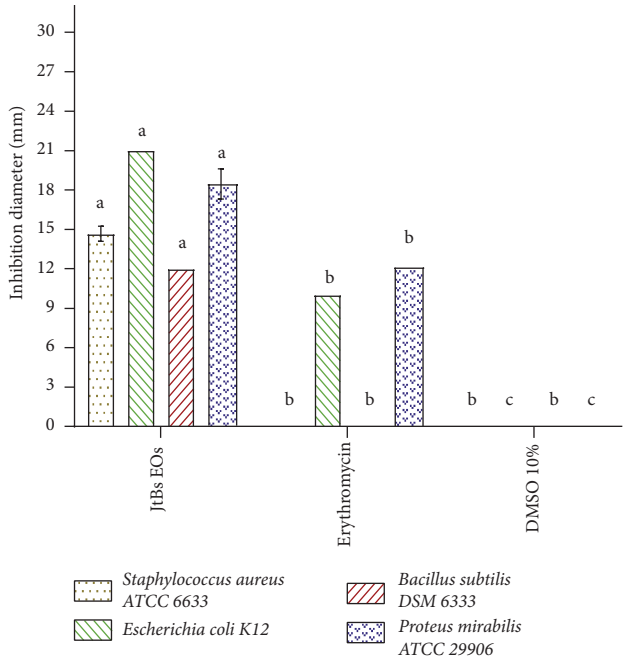

Figure 5: The antibacterial capacity of EOEJT in a solid medium (disc diffusion method), (means ± SD, $n = 3$) marked with the same letter for each strain indicated no significant difference at $p \leq 0.05$.

Table 2: antibacterial capacity of EOEJT in a liquid medium (microdilution method).

	Staphylococcus aureus ATCC 6633 (mg/mL)	*Escherichia coli* K12 (mg/mL)	*Bacillus subtilis* DSM 6333 (mg/mL)	*Proteus mirabilis* ATCC 29906 (mg/mL)
EOEJT	$1.34 \pm 0{,}00^{a}$	0.67 ± 0.00^{a}	2.69 ± 0.00^{a}	1.34 ± 0.00^{a}
Erythromycin	$-^{b}$	3.125 ± 0.00^{b}	$-^{b}$	3.125 ± 0.00^{b}
DMSO 10%	$-^{b}$	$-^{c}$	$-^{b}$	$-^{c}$

(Mean ± SD, $n = 3$) with different letters in the same column are significantly different (Tow-way ANOVA; Tukey's test, $p \leq 0.05$).

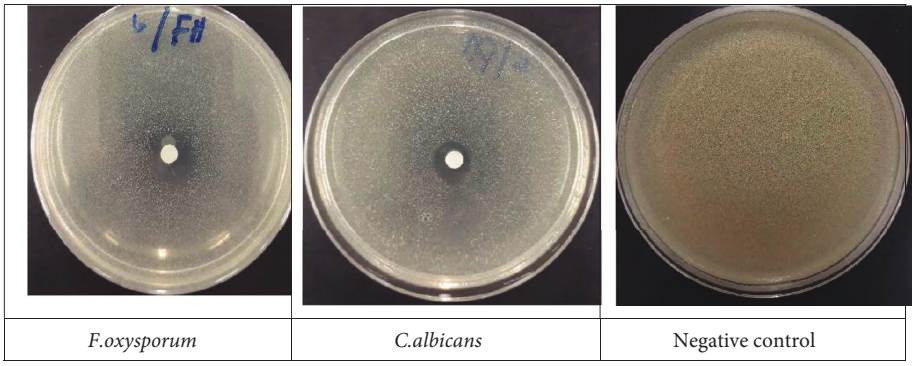

Figure 6: The antifungal capacity for EOEJT on solid media (disc method).

α-cadinol, muurolol, gamma-eudesmol, elemol, and α-pinene present the highest glide score value of −6.041, −5.956, −5.542, −4.538, and −4.358 kcal/mol, respectively (Table 4).

Regarding the nature of the bonds between EOEJT and the active site of NADPH oxidase, the molecules which present lower binding energy include α-cadinol, γ-eudesmol, and muurolol, each one, establishing two hydrogen bonds with the ASP 282 and LYS 134 residues and elemol which formed a single hydrogen bond with residue ASP 282 (Figures 8 and 9).

5. Discussion

In the present work, EOs extracted from *Juniperus thurifera* were evaluated for their chemical composition, antioxidant, and antimicrobial effects as no previous work dealing with these pharmacological activities of EOs extracted from *Juniperus thurifera* grows in Morocco to the best of our knowledge. Regarding EOEJT, *Juniperus thurifera* leaves were more qualitatively richer in terpenic compounds and identified 31 compounds with a dominance of α-thujene (25%), elemol (12%), and muurolol (12%) [13]. Previously, 24 compounds were reported to account for 99.46% of the mass of *Juniperus thurifera* EOs [28]. Such differences may be due to climatic factors variation (altitude latitude, substrate, etc.), harvest period, organs explored (leaves, stem, and bark), as well as the extraction method used [29]. The assessment of oxidative stress is becoming increasingly significant since this particular type of oxidation has been connected to a wide range of health issues, including rheumatoid arthritis, atherosclerosis, diabetes, cancer, and aging [30–32]. It has been reported that the hydroxyl function present in the phytochemical compositions of EOs is responsible for their antioxidant capacities. Terpenes and phenolic components in EOs are strong antioxidant agents [33–38], which is in agreement with our study. The phytochemical diversity in EOTJ (Table 1), may be responsible for the antioxidant efficiency, whether major or minor compounds may work in synergistic ways [16]. Recent studies have shown the richness of *Juniperus thurifera* of terpinene, which is considered among the compounds that have been shown to increase the antioxidant power [39].

Concerning the antibacterial power, taking a closer look at the published literature supported that muurolol exerted significant antibacterial activity against pathogenic bacteria [40]. Elemol compound, on the other side, has also shown some high biological activity [41]. The active ingredient pinene exhibited significant antibacterial capacity against *P. aeruginosa* and other multidrug-resistant bacteria [42,43]. More particularly, it also had strong antibacterial activity against *S. aureus* and *E. coli* strains [44]. The current results were in agreement with the results reported by Rahhal et al. [45], who showed that *Juniperus thurifera* essential oils exhibited substantial antibacterial capacity against bacteria strains, particularly against *S. aureus* (31.12 ± 3.11 mm of inhibition), *E. coli* (13.23 ± 2.59 mm of inhibition), and *P. aeruginosa* (18.27 ± 2.29 mm of inhibition). Our results are also in agreement with several other studies such as the study by Zeraib et al. [46], which reported that *S. aureus* was highly sensitive to the EO of Algerian *Juniperus thurifera*, and also the study by Bahri et al. [47] demonstrated that the essential oil of *Juniperus thurifera* had potent antibacterial activity against *S. aureus* ATCC 33862 (inhibition zone diameter: 27 mm; minimum inhibitory concentration: 450 μg/mL), *E. coli* ATCC 25922 (inhibition zone diameter: 25.6 mm; minimum inhibitory concentration: 530 μL/mL), and *P. mirabilis* ATCC 7002 (inhibition zone diameter: 18.8 mm).

Table 3: antifungal activity of EOEJT.

	Candida albicans ATCC 10231		Aspergillus niger MTCC 282		Aspergillus flavus MTCC 9606		Fusarium oxysporum MTCC 9913	
	Antifungal activity (mm)	MIC (mg/mL)	Antifungal activity (%)	MIC (mg/mL)	Antifungal activity (%)	MIC (mg/mL)	Antifungal activity (%)	MIC (mg/mL)
EOEJT	20.33 ± 1.15^{a}	0.67 ± 0.00^{a}	21.39 ± 0.57^{a}	10.75 ± 0.00^{a}	0.00 ± 0.00^{a}	$-^{a}$	37.44 ± 0.28^{a}	6.45 ± 0.00^{a}
Fluconazole	13.00 ± 1.00^{b}	7.50 ± 0.00^{b}	21.33 ± 1.53^{a}	7.5 ± 0.00^{b}	0.00 ± 0.00^{a}	$-^{a}$	30 ± 0.50^{b}	7.5 ± 0.00^{a}
DMSO 10%	0.00 ± 0.00^{c}	$-^{c}$	0.00 ± 0.00^{b}	$-^{c}$	0.00 ± 0.00^{a}	$-^{a}$	0.00 ± 0.00^{c}	$-^{b}$

(Mean ± SD, $n = 3$) with different letters in the same column are significantly different (Tow-way ANOVA; Tukey's test, $p \leq 0.05$).

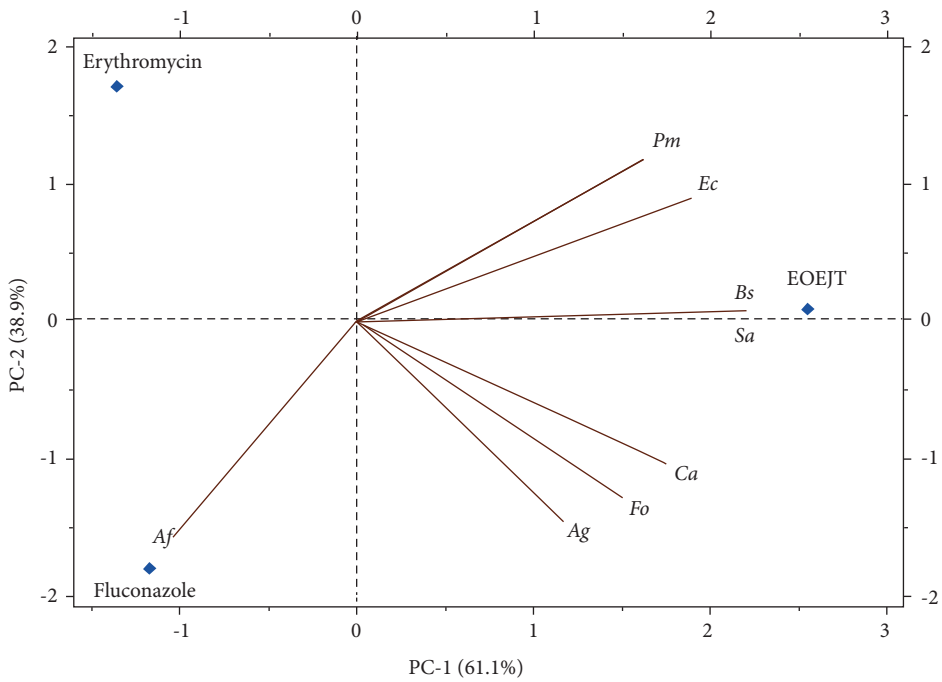

Figure 7: Principal component analysis (PCA) in the C1-C2 plane presents the correlations of antimicrobial activity of EOEJT compared to erythromycin and fluconazole. *Ag. A. niger; Af: A. flavus;* Fo: *F. oxysporum; Ca: C. albicans; Sa: S. aureus; Ec: E. coli; Bs: B. subtilis; Pm: P. mirabilis.*

Table 4: Docking results of EOEJT in the active site of NADPH.

	Glide Gscore	Glide emodel	Glide energy
α-Cadinol	−6.041	−39.399	−28.218
Muurolol	−5.956	−40.689	−28.987
γ-Eudesmol	−5.542	−34.926	−26.230
Elemol	−4.538	−34.725	−26.235
α-Pinene	−4.358	−20.490	−16.077

The interesting antifungal capacity of EOEJT against *A. niger, C. albicans,* and *F. oxysporum* may be due to their active ingredients, especially the high content of bioactive molecules in EOEJT such as muurolol, elemol, and pinene. Many studies have reported that these molecules have a strong antifungal activity, most notably, the study by Chang et al. [48], which showed that muurolol had strong antifungal activity against harmful fungi, whereas elemol was also shown to have strong antifungal activity [41]. For pinene compound, many studies have shown that this compound has significant antifungal activity. Nóbrega et al. [49], showed a significant antifungal action of α-pinene against *Candida* spp, and Shi et al. [50], reported also significant antifungal activity of pinene against five plant pathogens including *C. gloeosporioides*, *F. proliferatum*, *A. kikuchiana*, and *Phomopsis* sp.

Many strategies had been devoted to the control of *A. flavus, F. oxysporum, A. niger,* and *C. albicans* using different types of substances, either natural or chemically synthesized. Our results are in agreement with previous

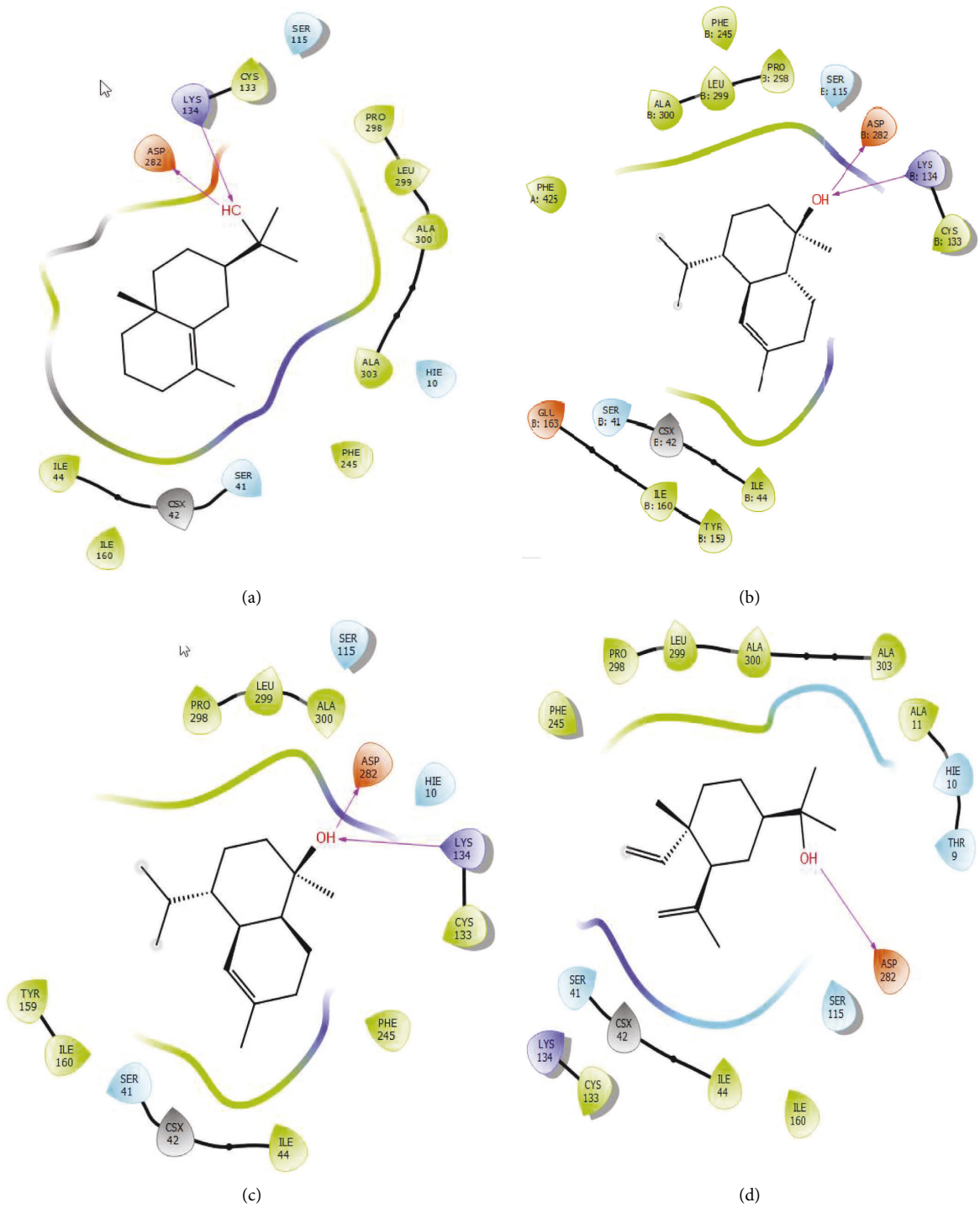

Figure 8: 2D diagrams of ligands interactions with the active site of NADPH. (a) α-Cadinol; (b) muurolol; (c) γ-eudesmol; (d) elemol.

reports e.g., the study of Jemli et al. [51], which showed a substantial antifungal activity against *A. alternata*, *F. solani*, *F. oxysporum*, *V. dahlia,* and *R. solani* with a percentage of inhibition ranging from 24% to 92.1%. Lafraxo et al. [13] showed that the essential oil of *Juniperus thurifera* leaves exhibited potent antifungal activity vs. *F. oxysporum* and *C. albicans* at a concentration of 0.095 g/mL.

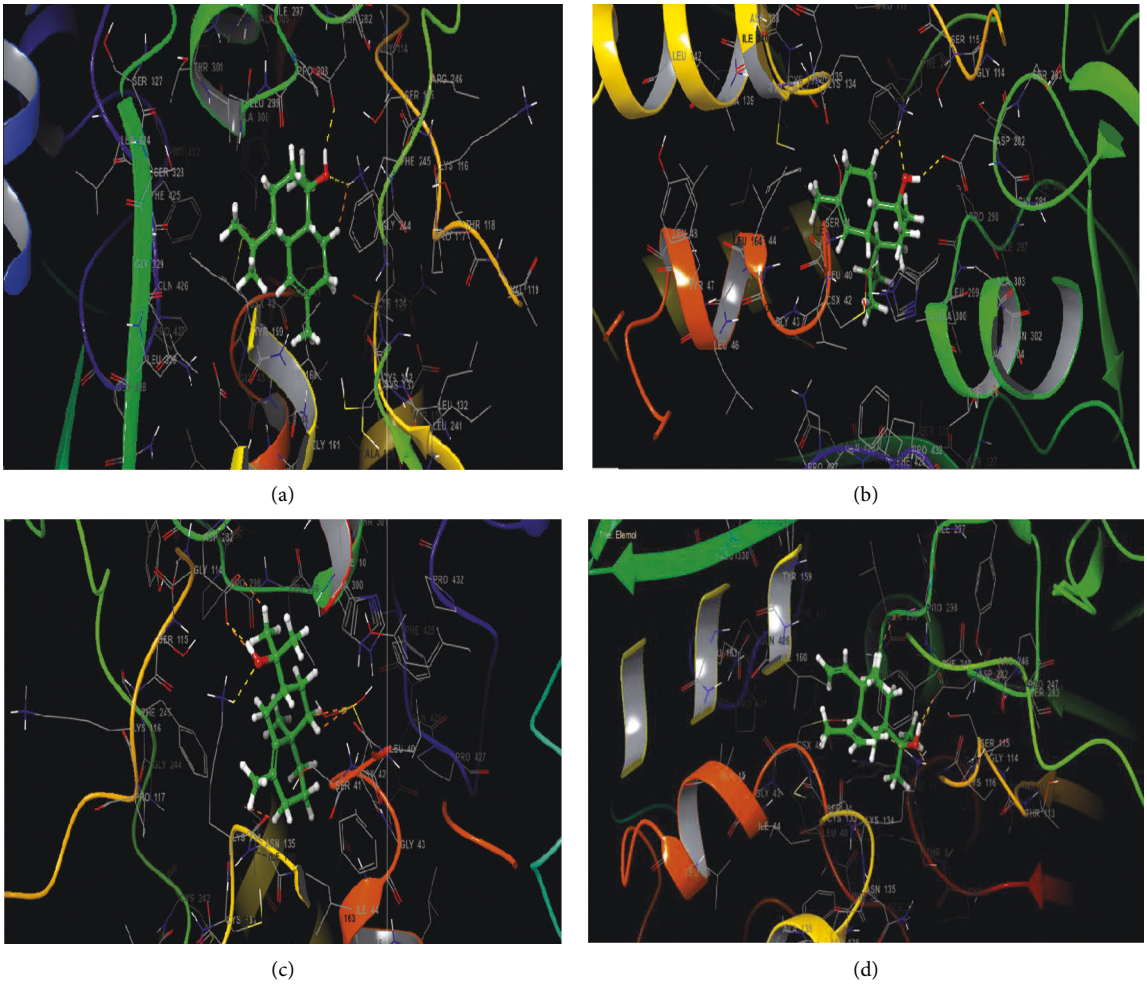

Figure 9: 3D diagrams of ligands' interactions with the active site of NADPH. (a) α-Cadinol; (b) muurolol; (c) γ-eudesmol; (d) Elemol.

6. Conclusion

This study showed that *Juniperus thurifera* bark essential is rich in terpene compounds, which were extracted and characterized by GC-MS. Additionally, the *Juniperus thurifera* essential oil also had proven antimicrobial, antifungal, and antioxidant capacity. This opens up the possibility of encapsulating this essential oil through complex biotechnology applications with antibiotics to enhance their effects against pathogen resistance. However, before any potential application, further studies dealing with toxicity are warranted.

Data Availability

Data used to support the findings are included within the article.

Conflicts of Interest

The authors declare that they have no conflicts of interest.

Acknowledgments

The authors would like to extend their sincere appreciation to the Researchers Supporting Project, King Saud University, Riyadh, Saudi Arabia, for funding this work through the project number RSP2022R457.

References

[1] B. Abdelmalek, *Flore et écosystèmes du Maroc: évaluation et préservation de la biodiversité*, Kalila Wa Dimna, 2002.

[2] P. Christian, *Contribution à l'etude de la vegetation du moyen atlas oriental: le versant sud-oriental du massif de bouiblane*, https://bibli.cbnbl.org/index.php?lvl=notice_display&id=116911, 1975.

[3] F. Mohamed, *Propositions de zones importantes pour les plantes au Maroc (ZIP Maroc)*, Institut Scientifique, Rabat, Morocco, 2004.

[4] R. P. Adams, *Junipers of the World: The Genus Juniperus*, Trafford Publishing Consultant, Bloomington, USA, 2011.

[5] M. Barbero and P. Quezel, *Biogéographie et écologie des conifères sur le pourtour méditerranéen In pesson: Actualités d'écologie forestière*, Borbas. Edition, Paris, London, 1980.

[6] M. Lecompte, "La végétation du Moyen Atlas central (Esquisse phytogéographique et carte des séries de végétation au 1/200 000)," *Trav.Inst. Sc. Cher. Sér. Bot. BV*, vol. 31, pp. 1–34, 1969.

[7] T. Gauquelin, M. Idrissi Hassani, and P. Lebreton, "Le *genévrier thurifère*, *Juniperus thurifera* L. (cupressacées): analyse biométrique et biochimique; propositions systématiques," *Ecologia Mediterranea*, vol. 14, no. 3, pp. 31–42, 1988.

[8] O. Y. Celiktas, E. H. Kocabas, E. Bedir, F. V. Sukan, T. Ozek, and K. Baser, "Antimicrobial activities of methanol extracts and essential oils of *Rosmarinus officinalis*, depending on location and seasonal variations," *Food Chemistry*, vol. 100, no. 2, pp. 553–559, Jan. 2007.

[9] R. A. Hammami I and M. A. Triki, "Chemical compositions, antibacterial and antioxidant activities of essential oil and various extracts of *Geranium sanguineum* L. flowers," *Archives of Applied Science Research*, vol. 3, no. 3, pp. 135–144, 2011.

[10] M. Simões, M. Lemos, and L. C. Simões, "Phytochemicals against drug-resistant microbes," *Diet. Phytochem. Microbes*, vol. 9789400739260, pp. 185–205, 2012.

[11] I. Gutiérrez-del-Río, J. Fernández, and F. Lombó, "Plant nutraceuticals as antimicrobial agents in food preservation: terpenoids, polyphenols and thiols," *International Journal of Antimicrobial Agents*, vol. 52, no. 3, pp. 309–315, 2018.

[12] M. Moghaddam and L. Mehdizadeh, "Chemistry of essential oils and factors influencing their constituents," *Soft Chem. Food Ferment.*, pp. 379–419, Jan. 2017.

[13] S. Lafraxo, A. El Barnossi, A. El Moussaoui et al., "Essential oils from leaves of *juniperus thurifera* L., exhibiting antioxidant, antifungal and antibacterial activities against antibiotic-resistant microbes," *Horticulturae*, vol. 8, no. 4, p. 321, 2022.

[14] A. El Moussaoui, M. Bourhia, F. Z. Jawhari et al., "Chemical profiling, antioxidant, and antimicrobial activity against drug-resistant microbes of essential oil from *withania frutescens* l," *Applied Sciences*, vol. 11, no. 11, p. 5168, Jun. 2021.

[15] R. P. Adams, "Identification of essential oil components by gas chromatography/mass spectrometry," 2007, https://pubs.acs.org/doi/10.1016/j.jasms.2005.07.008.

[16] Y. El Atki, I. Aouam, and F. El Kamari, "Phytochemistry, antioxidant and antibacterial activities of two Moroccan *Teucrium polium* L. subspecies: preventive approach against nosocomial infections," *Arabian Journal of Chemistry*, 2019.

[17] K. Chebbac, A. E. L. Moussaoui, M. Bourhia, A. M. Salamatullah, A. Alzahrani, and R. Guemmouh, "Chemical analysis and antioxidant and antimicrobial activity of essential oils from *artemisia negrei* L. Against drug-resistant microbes," *Evidence-based Complementary and Alternative Medicine*, vol. 2021, Article ID 5902851, 9 pages, 2021.

[18] M. Öztürk, "Anticholinesterase and antioxidant activities of Savoury (*Satureja thymbra* L.) with identified major terpenes of the essential oil," *Food Chemistry*, vol. 134, no. 1, pp. 48–54, Sep. 2012.

[19] P. Prieto, M. Pineda, and M. Aguilar, "Spectrophotometric quantitation of antioxidant capacity through the formation of a phosphomolybdenum complex: specific application to the determination of vitamin E," *Analytical Biochemistry*, vol. 269, no. 2, pp. 337–341, May 1999.

[20] A. El Barnossi, F. Moussaid, and A. Iraqi Housseini, "Antifungal activity of Bacillussp. Gn-A11-18isolated from decomposing solid green household waste in water and soil against *Candida albicans* and *Aspergillus Niger*," *E3S Web of Conferences*, vol. 150, Article ID 02003, 2020.

[21] A. Agour, I. Mssillou, and H. Mechchate, "*Brocchia cinerea* (delile) vis. essential oil antimicrobial activity and crop protection against cowpea weevil *callosobruchus maculatus* (fab.)," *Plants (Basel)*, vol. 11, pp. 1–13, 2022.

[22] S. D. Sarker, L. Nahar, and Y. Kumarasamy, "Microtitre plate-based antibacterial assay incorporating resazurin as an indicator of cell growth, and its application in the *in vitro* antibacterial screening of phytochemicals," *Methods*, vol. 42, no. 4, pp. 321–324, 2007.

[23] K. Chebbac, H. K. Ghneim, and A. El Moussaoui, "Antioxidant and antimicrobial activities of chemically-characterized essential oil from artemisia," 2022, https://www.tandfonline.com/doi/abs/10.1080/0972060X.2019.1602083?journalCode=teop20.

[24] O. Herrera-Calderon, L. J. Chacaltana-Ramos, and I. C. Huayanca-Gutiérrez, "Chemical constituents, *in vitro* antioxidant activity and *in silico* study on nadph oxidase of *allium sativum* l. (garlic) essential oil," *Antioxidants*, vol. 10, no. 11, 2021.

[25] S. Omaye, M. A. M. Aboul-Soud, and H. Ennaji, "Antioxidant, anti-proliferative activity and chemical fingerprinting of *centaurea calcitrapa* against breast cancer cells and molecular docking of caspase-3," *Antioxidants*, vol. 11, no. 8, 2022.

[26] I. Mssillou, A. Agour, A. Allali et al., "Antioxidant, antimicrobial, and insecticidal properties of a chemically characterized essential oil from the leaves of *Dittrichia viscosa* L," *Molecules*, vol. 27, no. 7, 2022.

[27] Y. El Abdali, A. Agour, A. Allali et al., "*Lavandula dentata L.*: phytochemical analysis, antioxidant, antifungal and insecticidal activities of its essential oil," *Plants*, vol. 11, no. 3, p. 311, 2022.

[28] N. Mansouri, B. Satrani, M. Ghanmi, L. El ghadraoui, A. Aafi, and A. Farah, "Valorization of the essential oils of Moroccan *Juniperus thurifera* and *Juniperus oxycedrus*," *Phytothérapie*, vol. 8, no. 3, pp. 166–170, 2010.

[29] A. E. Moussaoui, M. Bourhia, F. Z. Jawhari et al., "Responses of *withania frutescens* (L.) pauquy (solanaceae) growing in the mediterranean area to changes in the environmental conditions: an approach of adaptation," *Front. Ecol. Evol*, vol. 9, p. 470, Aug. 2021.

[30] B. M. Hybertson, B. Gao, S. K. Bose, and J. M. McCord, "Oxidative stress in health and disease: the therapeutic potential of NRF2 activation," *Molecular Aspects of Medicine*, vol. 32, no. 4–6, pp. 234–246, 2011.

[31] D. Liang, Q. Zhou, W. Gong et al., "Studies on the antioxidant and hepatoprotective activities of polysaccharides from *Talinum triangulare*," *Journal of Ethnopharmacology*, vol. 136, no. 2, pp. 316–321, Jun. 2011.

[32] J. L. Rains and S. K. Jain, "Oxidative stress, insulin signaling, and diabetes," *Free Radical Biology and Medicine*, vol. 50, no. 5, pp. 567–575, 2011.

[33] A. K. Tiqwari, "Imbalance in antioxidant defence and human diseases: multiple approach of natural antioxidants therapytle," *Current Science*, vol. 81, no. 9, pp. 1179–1181, 2001.

[34] S. Bouhdid, S. N. Skali, M. Idaomar, and A. Zhiri, "Antibacterial and antioxidant activities of origanum compactum essential oil," *African Journal of Biotechnology*, vol. 7, no. 10, pp. 1563–1570, May 2008.

[35] W. Gulcin, I. G. Şat, Ş. Beydemir, M. Elmastaş, and Ö. I. Küfrevioğlu, "Comparison of antioxidant activity of clove (*Eugenia caryophylata Thunb*) buds and lavender (*Lavandula stoechas* L.)," *Food Chemistry*, vol. 87, no. 3, pp. 393–400, 2004.

[36] S. S. Chun, D. A. Vattem, Y. T. Lin, and K. Shetty, "Phenolic antioxidants from clonal oregano (Origanum vulgare) with antimicrobial activity against *Helicobacter pylori*," *Process Biochemistry*, vol. 40, no. 2, pp. 809–816, 2005.

[37] S. A. Fayed, "Antioxidant and anticancer activities of citrus reticulate (*petitgrain Mandarin*) and *Pelargonium graveolens* (*Geranium*) essential oils," *Research Journal of Agriculture and Biological Sciences*, vol. 5, no. 5, pp. 740–747, 2009.

[38] S. R. Zhuang, S. L. Chen, J. H. Tsai et al., "Effect of citronellol and the Chinese medical herb complex on cellular immunity of cancer patients receiving chemotherapy/radiotherapy," *Phytotherapy Research*, vol. 23, no. 6, pp. 785–790, 2009.

[39] S. Momtaz and M. Abdollahi, "An update on pharmacology of Satureja species; from antioxidant, antimicrobial, antidiabetes and anti-hyperlipidemic to reproductive stimulation," *International Journal of Pharmacology*, vol. 6, no. 4, pp. 346–353, 2010.

[40] K.-P. Hsu, S.-H. Tu, and Y.-C. Su, "Chemical composition and antimicrobial activity against food-borne pathogens of *calocedrus formosana* heartwood essential oil," *Natural Product Communications*, vol. 16, 2021.

[41] F. A. M. Monteiro, E. Muratov, A. Henrique, R. Bezerra, and M. T. Scotti, "Prediction of antifungal activity, cytotoxicity risks and molecular docking against," in *Proceedings of the International Conference on Multidisciplinary Sciences CHEMINFOUNC-01 Chemoinformatics Work*, 2019.

[42] M. S. S. Ribeiro, O. Freitas-Silva, I. M. Castro et al., "Efficacy of sodium hypochlorite and peracetic acid against *Aspergillus nomius* in Brazil nuts," *Food Microbiology*, vol. 90, Article ID 103449, 2020.

[43] A. El Barnossi, F. Moussaid, and A. Iraqi Housseini, "Tangerine, banana and pomegranate peels valorisation for sustainable environment: a review," *Biotechnology Reports*, vol. 29, Article ID e00574, 2021.

[44] L. de Sousa Eduardo, T. C. Farias, S. B. Ferreira, P. B. Ferreira, Z. N. Lima, and S. B. Ferreira, "Antibacterial activity and time-kill kinetics of positive enantiomer of α-pinene against strains of *Staphylococcus aureus* and *Escherichia coli*," *Current Topics in Medicinal Chemistry*, vol. 18, no. 11, pp. 917–924, 2018.

[45] R. Rahhal, H. E. L. Hajjouji, S. Gmouh, M. Hsaine, and H. Fougrach, "Chemical composition , antioxidant and antibacterial activities of the essential oils of *Juniperus phoenicea*," *Juniperus Thurifera and Juniperus Oxycedrus*, vol. 9, no. 3, pp. 190–198, 2019.

[46] A. Zeraib, M. Ramdani, L. Boudjedjou, P. Chalard, and G. Figuredo, "Characterization and chemosystematics of *Algerian thuriferous juniper* (*Juniperus thurifera* L.)," *Journal of Applied Botany and Food Quality*, vol. 87, pp. 249–255, 2014.

[47] F. Bahri, R. Harrak, N. Achak, and A. Romane, "Natural product research: formerly natural product letters chemical composition and antibacterial activities of the essential oils isolated from *juniperus thurifera* L. Var," *Natural Product Research*, vol. 27, pp. 1789–1794, 2012.

[48] S. T. Chang, S. Y. Wang, C. L. Wu, P. F. Chen, and Y. H. Kuo, "Comparison of the antifungal activity of cadinane skeletal sesquiterpenoids from Taiwania (Taiwania cryptomerioides hayata) heartwood," *Holzforschung*, vol. 54, no. 3, pp. 241–245, 2000.

[49] J. R. Nóbrega, D. D. F. Silva, F. P. d. Andrade Júnior et al., "Antifungal action of α-pinene against *Candida spp.* isolated from patients with otomycosis and effects of its association with boric acid," *Natural Product Research*, vol. 35, no. 24, pp. 6190–6193, 2021.

[50] Y. Shi, H. Si, P. Wang et al., "Derivatization of natural compound β-pinene enhances its *in vitro* antifungal activity against plant pathogens," *Molecules*, vol. 24, no. 17, p. 3144, 2019.

[51] M. E. Jemli, N. Khattabi, K. Lachqer et al., "Antifungal and insecticidal properties of *juniperus thurifera* leaves," *Natural Product Communications*, vol. 13, no. 8, Article ID 1934578X1801300, 2018.